

TCAD Parameters for 4H-SiC: A Review

Jürgen Burin ,¹ Philipp Gagg ,¹ Simon Waid,¹ Andreas Gsponer ,¹ and Thomas Bergauer ,¹

Institute of High Energy Physics, Austrian Academy of Sciences, Nikolsdorfer Gasse 18, 1050 Wien

(*e-mail: juergen.burin@oeaw.ac.at)

(Dated: 7 May 2025)

In this literature review we investigate the permittivity, density-of-state mass, band gap, impact ionization, charge carrier recombination, incomplete ionization and mobility in 4H silicon carbide. We provide a comprehensive overview over characterization methods, models and parameters to lower the entrance barrier for newcomers and allow a critical evaluation of common material property descriptions. We further highlight areas for future research by identifying gaps in the current knowledge base.

For each investigated property we found a large amount of models and parameter sets based on measurements, calculations or fittings. With literal and/or graphical comparisons we reveal qualitative good agreement but also flawed data values, misinterpretations of research results and inconsistencies among multiple investigations, even those directly referencing each other. We identify parameter variations, e.g., due to temperature, with high impact that are rarely considered in 4H-SiC analyses and common values that are based on old research of deviating materials or properties. We further show the slow accommodation of recent research results within the scientific community and reveal missing characterization data but also insufficient models in state-of-the-art technology computer aided design (TCAD) tools. Overall, our review enables scientifically based decisions on 4H-SiC material parameters and unravels the demand for further investigations to validate commonly used values, confirm hypothesis and cover additional dependencies.

Keywords: 4H-SiC, silicon carbide, material properties, TCAD simulations, simulation parameters, permittivity, density-of-states mass, band gap, impact ionization, charge carrier recombination, incomplete ionization, mobility, review

CONTENTS

Glossary	6
I. Introduction	10
II. Methodology	11
III. Silicon Carbide (SiC)	14
A. Brief history	14
B. Crystal structure & Polytypes	15
C. Anisotropy of 4H-SiC	16
IV. Permittivity	18
A. Introduction	19
1. Static and High-Frequency Relative Permittivity	20
2. Characterization Methods	20
B. Results & Discussion	21
1. Fundamental Values	21
2. Origin of Parameters	23
3. Literature Values	25
4. Temperature Dependency and Phonon Frequencies	27
V. Density-of-States Mass	29
A. Introduction	29
1. Effective Masses along Principal Directions	29
2. Density-of-States (DOS) Mass	30
3. Effective Conductivity Mass	31
4. Polaron Mass	32
5. Characterization Methods	32
B. Results & Discussion	33
1. Effective Mass along Principal Directions	33
2. Density-of-States Mass	36
3. Temperature Dependency	39

4. Origin of Parameters	40
5. Literature Values	42
VI. Band Gap	44
A. Introduction	44
1. Temperature Dependency	45
2. Doping Dependency	47
3. Methods	49
B. Results & Discussion	49
1. Temperature Dependency	53
2. Doping Dependency	56
3. Origin of Parameters	58
4. Literature Values	61
VII. Impact Ionization	65
A. Introduction	65
1. Anisotropy	67
2. Temperature Dependency	68
3. Methods	68
B. Results & Discussion	69
1. Impact Ionization Coefficients	69
2. Anisotropy	72
3. Temperature Dependency	74
4. Origin of Parameters	76
VIII. Charge Carrier Recombination	77
A. Introduction	79
1. Shockley-Read-Hall Recombination	80
2. Bimolecular Recombination	84
3. Auger Recombination	85
4. Analysis	86
5. Methods	88
B. Results & Discussion	89

1. SRH Lifetime	89
2. Doping Dependency of SRH Lifetime	90
3. Temperature Dependency of SRH Lifetime	95
4. Surface Recombination Velocity	99
5. Bimolecular Recombination	99
6. Auger Recombination	102
7. Origin of Parameters	104
IX. Incomplete Ionization	106
A. Introduction	108
1. Doping Dependency	109
2. Capture Cross Sections	111
3. Methods	111
B. Results & Discussion	112
1. Ionization Energy of Al	113
2. Ionization Energy of B	114
3. Ionization Energy of N	115
4. Ionization Energy of P	118
5. Capture Cross Sections	119
6. Values in Literature	119
7. Origin of Values	121
X. Mobility	123
A. Introduction	123
1. Low-Field Mobility	126
2. High-Field Mobility	129
3. Carrier-Carrier Scattering	130
4. Hall Scattering Factor	130
5. Methods	131
B. Results & Discussion	132
1. Hall Scattering Factor	132
2. Low-Field Mobility	133
3. High-Field Mobility	150

4. Carrier-Carrier Scattering	156
XI. Conclusion	157
Acknowledgments	159
Author Declarations	159
Conflict of Interest	159
Author Contributions	160
Data Availability Statement	160
A. Inaccuracies	160
1. Permittivity	160
2. DOS Mass	162
3. Band Gap	163
4. Impact Ionization	168
5. Charge Carrier Recombination	171
6. Incomplete Ionization	173
7. Mobility	175
References	179

GLOSSARY

General

T	temperature in K
e	elementary charge (1.602×10^{-19} C)
\hbar	reduced Planck constant (6.582×10^{-16} eV s)
k_B	Boltzmann constant (8.617×10^{-5} eV/K)
t	time
E	energy
F	electric field
m_0	electron rest mass
n, p	electron/hole concentration

Permittivity

ϵ_0	vacuum permittivity (8.854×10^{-12} F/m)
ϵ', ϵ''	real/imaginary part of the complex permittivity
$\epsilon_s, \epsilon_\infty$	static/optical relative permittivity
$\epsilon^\parallel, \epsilon^\perp$	permittivity parallel/perpendicular to c-axis
hf	photon energy
$\omega_{\text{LO}}, \omega_{\text{TO}}$	longitudinal/transversal optical phonon frequency

Density-of-States Mass

N_C, N_V	conduction/valence band density-of-states
$m_{\text{M}\Gamma}^*, m_{\text{MK}}^*, m_{\text{ML}}^*$	effective electron masses in the spatial directions \perp, \perp, \parallel to the c-axis
$m_{\text{TM}}^*, m_{\text{TK}}^*, m_{\text{TA}}^*$	effective hole masses in the spatial directions \perp, \perp, \parallel to the c-axis
$m_{\text{d}}^*, m_{\text{de}}^*, m_{\text{dh}}^*$	effective/electron/hole density-of-state mass
m_{c}^*	effective conductivity mass
$m_{\text{hh}}^*, m_{\text{lh}}^*$	heavy hole/light hole relative mass
m_p	polaron mass
α	Fröhlich constant
M_C	number of conduction band minima
z_x, n_x, η	temperature dependency parameters

Band Gap

E_g	band gap energy
E_{gx}	exciton band gap energy
E_x	free exciton binding energy
$\Delta E_{th}, \Delta E_{ph}$	bandgap variation due to thermal expansion/electron-phonon interaction
E_{CB}, E_{VB}	doping induced variation of conduction/valence band
E_{nc}, E_{nv}	donor induced variation of conduction/valence band
E_{pc}, E_{pv}	acceptor induced variation of conduction/valence band
E_{gn}, E_{gp}	donor/acceptor induced variation of the band gap
N_D^+, N_A^-	ionized donor/acceptor concentration
α, β, Θ, p	temperature dependency parameters
Δ	phonon dispersion
A, B, C	doping dependency parameters

Impact Ionization

N_D, N_A	donor/acceptor concentration
N_D^+, N_A^-	ionized donor/acceptor doping concentration
α, β	electron/hole impaction ionization coefficient
E_p	optical phonon energy
E_i	electron-hole pair ionization energy
$\langle E_i \rangle$	effective ionization threshold
λ	mean free path
a	impact ionization coefficient at $F = \infty$
b, m	field dependency parameters in Eq. (41)
c, d	temperature dependency parameters in Eq. (41)
γ	temperate scaling parameter
ω_{OP}	optical phonon energy

Charge Carrier Recombination

R, G	recombination/generation rate
$R_{SRH}, R_{bim}, R_{Auger}$	SRH/Bimolecular/Auger recombination rate
B	bimolecular recombination coefficient

C_n, C_p	electron/hole Auger recombination coefficients
τ_n, τ_p	electron/hole life time
$\tau_{SRH}, \tau_{bim}, \tau_{Auger}$	Shockley-Read-Hall/Bimolecular/Auger recombination lifetime
$\tau_{T0}, \tau_0, \tau_\infty$	lifetime at $T = T_0, T = 0 \text{ K}, T = \infty$
$\tau^{\text{ll}}, \tau^{\text{hl}}$	lifetime under low/high level injection
n_0, p_0	equilibrium electron/hole concentration
Δ_N, n_i	excess/intrinsic charge carrier concentration
E_t	trap energy level
E_i	effective Fermi level
E_g	band gap energy
E_C, E_V	conduction/valence band energy
E_{act}	activation energy in temperature scaling
v_{th}	thermal charge carrier velocity
s_n, s_p	electron/hole surface recombination velocity
g_t	trap degeneracy
σ	capture cross section
α, C	temperature dependency parameter
γ	doping dependency parameter

Incomplete Ionization

E_F	intrinsic Fermi energy
E_C, E_V	conduction/valence band energy
$E_{F,n}, E_{F,p}$	quasi Fermi energy for electrons/holes
$\Delta E_D, \Delta E_A$	donor/acceptor ionization energy
$\Delta E_{Dh}, \Delta E_{Dc}$	donor ionization energy at hexagonal/cubic lattice sites
$\Delta E_{Ah}, \Delta E_{Ac}$	acceptor ionization energy at hexagonal/cubic lattice sites
ΔE_0	ionization energy at zero doping
g_D, g_A	donor/acceptor degeneracy
n_i	intrinsic carrier concentration
n_0, p_0	equilibrium electron/hole concentration
N_D, N_A	donor/acceptor doping concentration
N_D^+, N_A^-	ionized donor/acceptor doping concentration
N_K	compensation carrier concentration
α, N_E, c	doping dependency parameter
σ	capture cross section

Mobility

σ	conductivity
ρ	resistivity
μ_n, μ_p	electron/hole majority carrier mobility
μ_{ccs}	carrier-carrier scattering mobility
μ_{min}, μ_{max}	mobility at zero/ ∞ doping concentration
μ_H	Hall mobility
v	charge carrier velocity
v_{sat}	saturation carrier velocity
$N_{ref}, N_{ref2}, \delta, \kappa$	doping dependency paramters
γ	temperature dependency parameter
β	scaling factor for high-field mobility
a, b, c	parameters for temperature scaling of β
r_H, R_H	Hall scattering factor/coefficient
n_H	Hall charge carrier count

I. INTRODUCTION

Silicon carbide (SiC) is a wide band gap semiconductor that enables the design of devices for high-voltage applications with low power losses and high power densities due to its favorable properties of high breakdown voltage, low leakage current, and fast switching speed¹. The inherent radiation hardness makes SiC also attractive for spacecraft, nuclear-medicine medical devices, and high-energy physics². To optimize device designs for these areas of application and decrease the number of design iterations, the materials parameters have to be known accurately. These commonly serve as input for *technology computer-aided design* (TCAD) simulations that predict the behavior of devices at an early development stage and allow insights into physical processes taking place inside devices, which is impossible with measurements. The accuracy and reliability of these simulations depend on the employed physical models and the provided material parameters.

For 4H-SiC, the most popular polytype in the industry, the main challenge when parameterizing a TCAD model is not the lack of parameters in the literature but the overwhelming amount. In the last 70 years, the physical properties of 4H-SiC were extensively measured and described by various approaches. This led to the essential problem of proper parameter selection: Finding, analyzing, and comparing the multitude of parameters is time-consuming, while assessing the accuracy of the available data is challenging. Consequently, parameters are often taken from secondary literature, thus passing them on in unverified reference chains. Unavoidable rounding and typographic mistakes in this process led to substantial parameter deviations over time. The resulting contradictions make it difficult to choose one option over the other, especially for newcomers.

To tackle these issues overview papers for the 4H-SiC properties permittivity³, density-of-states mass^{4–12}, band gap energy^{13–19}, impact ionization^{20–25}, charge carrier recombination^{26,27}, incomplete ionization^{6,7,28–34} and mobility^{6,15,16,18,21,22,35–38} were published. These, however, solely list values and parameters from an incomplete set of sources without addressing the following questions: How where the presented values characterized? What are the most commonly used values within the community? Are there additional descriptions/parameter sets and how do they compare against each other? Exist discrepancies among different models and can these be explained or is further research required? Where do we still lack information for proper approximations?

With this review, we aim to answer all these question by providing an overview of the existing literature on the material parameters permittivity, density-of-states mass, band gap, impact

ionization, charge carrier recombination, incomplete ionization and mobility. For each topic we (i) introduce the utilized mathematical models, (ii) list characterization methods, (iii) identify fundamental investigations, show the achieved model parameters and analyze inconsistencies over time, (iv) discuss the agreement among the models and comment on discrepancies, (v) depict the abundance of specific values in scientific publications and (vi) highlight shortcomings and propose areas for future research. These analyses provide newcomers a starting point on 4H-SiC, experienced users the possibility to evaluate their models/parameter sets and the community to plan future research goals.

This work is organized in the following fashion: In Section **II**, we introduce the general methods utilized in this review, followed by a description of (4H) silicon carbide in Section **III**. We then review the permittivity (Section **IV**), density-of-states mass (Section **V**), band gap (Section **VI**), impact ionization (Section **VII**), charge carrier recombination (Section **VIII**), incomplete ionization (Section **IX**) and mobility (Section **X**) before we conclude the paper in Section **XI**.

II. METHODOLOGY

Before we started this research we tried to gather the desired information with the help of artificial intelligence tools. These, however, only provided a very narrow range of publications for each topic and failed to properly extract the correct information. Consequently, we conducted the literature review by executing the tasks described in the sequel. The data, evaluation scripts and figures of this study are openly available in the repository [Data of 4H SiC TCAD Parameter Review³⁹](#).

Literature Review: To identify and acquire a comprehensive set of investigations we utilized scientific search engines and followed references respectively citations in suitable contributions. In total, we collected and analyzed 1041 scientific publications, but only included in the manuscript those who either (i) provided a theoretical description, (ii) conducted measurements, (iii) developed models, (iv) provided model parameters, (v) referenced previous results or (vi) simply named parameter values. The latter two were necessary to show the evolution of parameters when being referenced and which values are most commonly used. In a two step process the single contributions were first evaluated in isolation before we aggregated the extracted information by topic.

Data Extraction: Our initial belief that transferring parameter values is a straightforward task was quickly falsified. Understanding what the authors intended to say was often challenging and

required careful considerations. One common problem was that the data were presented in many shapes and formalisms and had to be converted to a common one. Accompanying information, such as temperature, doping concentration/type, or spatial direction, were difficult to grasp and demanded an analysis of the text. Thus, we concluded that an automated analysis was not feasible in this regard and transferred the data by hand, although this method is error prone.

Theoretical Background: For each topic we first compared the theoretical explanations, equations, and models described in the reviewed publications. This was sometimes surprisingly challenging because (i) fundamentally different values were denoted with the same symbol (e.g., the free and bound exciton binding energy in Section VI), (ii) parameters were declared ambiguously in various notations (see charge carrier recombination in Section VIII) and (iii) models were denoted by multiple names while being subsets of each other (see impact ionization in Section VII).

At the beginning of each section we summarized the relevant theoretical concepts in a concise introduction. We classified the differences among the models and merged, wherever possible, various approaches into a common description. For the latter, we aligned with state-of-the-art TCAD simulation tools.

We intend these summaries to result in a steep learning curve for newcomers, enabling them to easier comprehend the dedicated publications outside this review. Experienced readers might find the collection of the most important information in one place beneficial as a reference and to refresh their memory.

Symbol Definitions: Symbols are used with different meanings in the literature depending on the context. For example, α and β are commonly used to denote the impact ionization coefficients for electrons and holes (cp. Section VII), are parameters for the temperature-dependent band gap (cp. Section VI) and denote the 3C (β) and hexagonal (including 4H) (α) polytypes of SiC. To prevent ambiguities while sticking to the common literature, we defined the symbols for each topic separately in the glossary. Since the sections of this review are self-contained, we think that the risk of mix-ups is acceptable.

Characterization Methods: To reason about the reliability of TCAD parameters, it is essential to know how they were determined, i.e., the utilized characterization method. In this review, we encountered calculations, measurements, and fittings to existing data. A good mix among these is preferable to prohibit incorrect assumptions in the calculations or disturbances in the measurement setup that falsify the results. In this work, we simply list the found methods; for further details, we refer the interested reader to the specific publications or dedicated literature^{40,41}.

Data Analysis: As a first step of the analysis, we identified fundamental investigations, i.e., those that proposed parameter values for the first time. We documented the characterization method and further details, such as the value range used for fitting, spatial orientation, or doping concentration/type. For non-fundamental publications, we assumed that the provided values were referenced. We say “assume” because parameters were also stated without any further comment. Wherever possible, we inferred a relationship based on the used values and marked these as “guess” in the data.

A major challenge was to verify the referenced data, i.e., to compare citing and referenced publications. In the case of a mismatch, we noted the discrepancy in alphabetic order in the appendix (see Section A) and tried to find explanations, which included confusion of polytypes or spatial directions, erroneous theoretical concepts, rounding, and typographical errors. Instances where we were unsuccessful to resolve a mismatch are discussed in the text of the respective topic.

Origin Tracing: We mentioned that a proper understanding of how material parameters were derived is required to reason about their reliability. Unfortunately, fundamental investigations were not always referenced directly, resulting in long chains of citations, which we call “reference chains”. We wrote a Python script that explored these chains automatically and displayed the utilized values, which allowed us to investigate the changes introduced along the path.

Missing references could sometimes be inferred from the parameter values, but often, a unique mapping was not possible. We even encountered cases where the utilized values could not be traced back to any scientific publication, leaving the exact origin unknown. One possible explanation in such cases is that these value served as the default ones in simulation tools and were assigned within the respective company.

Presentation: For improved readability, we transformed the data into more comprehensible formats such as tables and figures, where we ordered the contributions in regard to their publication year to visualize changes over time. We also varied colors and line styles but solely for the purpose of increased readability. Self-written *Python* scripts automatized this task to reduce the chances of typographical errors.

For each topic, we summarized in a table the fundamental investigations together with their parameters. We chose this representation over a figure because the exact values decrease the effort to implement the respective model in the reader’s simulation. Complementary to the references provided by L^AT_EX, we labelled each paper with a unique badge of the form [XxxxYYZ], where Xxxx denotes the first four letters of the main author’s surname, YY, the last two digits of the

publication year and Z an optional letter to ensure the uniqueness of the label within this review. This scheme supports the reader in connecting the results of a single publication, reconstructing important relationships, and searching for a contribution throughout the document.

In addition to the parameter table, we showed the specific aspects of the models, e.g., temperature, doping, or field dependency graphically. All available parameter sets were combined in these plots to identify outliers and tendencies at the cost of readability. To identify every detail, we recommend the reader to zoom into the figures using the digital version of this review. Plotting each model ourselves had the side effect that, in rare cases, we identified incorrect parameters in the fundamental investigation and were able to suggest replacements. For further convenience  denotes plots for electrons and  those for holes.

The identified reference chains were also converted to a figure featuring the referenced parameter values. Since not all values in the literature were properly referenced and, thus, do not show up in the reference chain plot, we added a figure depicting the abundance of specific values. We allowed multiple publications from the same author to preserve a quantitative relation among values.

Discussion: Last but not least, we commented on trends and shortcomings in the data to highlight future avenues of research, which, hopefully, trigger a constructive reevaluation within the scientific community.

III. SILICON CARBIDE (SiC)

This section provides a historical introduction of silicon carbide in general and 4H in detail. We are also going to define the characteristics of this material that we require to model the material properties that are investigated in this review.

A. Brief history

The first-ever reference of silicon carbide (SiC) dates back to a report of a synthesized compound material containing silicon-carbon bonds by Berzelius in 1824⁴². Despite the initial interest in the material due to its diamond-like hardness, this makes it one of the earliest investigated semiconductor in history^{43–46}. Through mass-production, enabled by the Acheson process in 1892⁴⁷, it soon became a leading abrasive material^{43,48}. However, due to the poor quality of the crystalline

byproducts, only rudimentary insights into the outstanding physical and electrical properties of SiC, such as its electroluminescent nature^{43,49}, were possible. In 1905, Moissan reported the first natural occurrence of SiC, naming the mineral Moissanite⁵⁰.

After the invention of the Lely process in 1955, which enabled the synthesis of relatively pure single-crystalline SiC (mostly the polytype 6H)^{51,52}, scientific interest re-emerged. The semiconductor properties were heavily investigated in the subsequent decades^{43,53,54}, mainly focusing on its potential as blue LED and within high-temperature environments^{55,56}. In the 1970s, silicon based technologies surpassed SiC, which reduced research targeted at the latter to a minimum^{43,54,57}. Only in the late 1990s, following significant improvements in manufacturing by Tairov and Tsvektov (modified Lely method in 1981)^{58,59}, Barret (1991)⁶⁰, and Davis (1995)⁶¹, SiC became relevant again for the semiconductor industry^{43,54,62}.

Although today's electronics market is still dominated by Si, SiC has become increasingly interesting due to its higher band gap (compared to Si), which enables the development of devices with less power consumption, higher peak voltage, and higher temperature stability^{1,43,54}. After basic research into Schottky barrier diodes (SBDs), MOSFETs, and JFETs in the early 2000s and their respective first mass production only a decade later, SiC has rapidly evolved into a cornerstone of the high-power electronics industry^{1,54}. The following cost reduction and increasing accessibility of high-quality material quickly rekindled the interest of the high-energy physics (HEP) community in SiC (especially the 4H-SiC polytype) for particle detection. The primary goal has been to develop devices that fulfill the ever-growing demands for operation in high-luminosity and high-energy environments^{2,63}.

B. Crystal structure & Polytypes

SiC is a compound semiconductor formed by Si and C in equal parts, which both possess four valence electrons. Within a crystalline lattice, each Si-atom bonds with exactly four C-atoms and vice versa. The SiC crystal can arrange, at least theoretically, in infinitely many constellations^{43,57,64}. While the occurrence of a given compound in more than one crystal structure is defined as polymorphism, SiC itself is a prime example of a specialized form, called polytypism, where all stable phases (called polytypes) differ from each other in a specific way⁵⁷.

Each SiC polytype is constructed by stacking sheets of equal Si-C bilayers in a varying fashion upon each other. Thus, SiC polytypes are identical in two dimensions and only differ within the

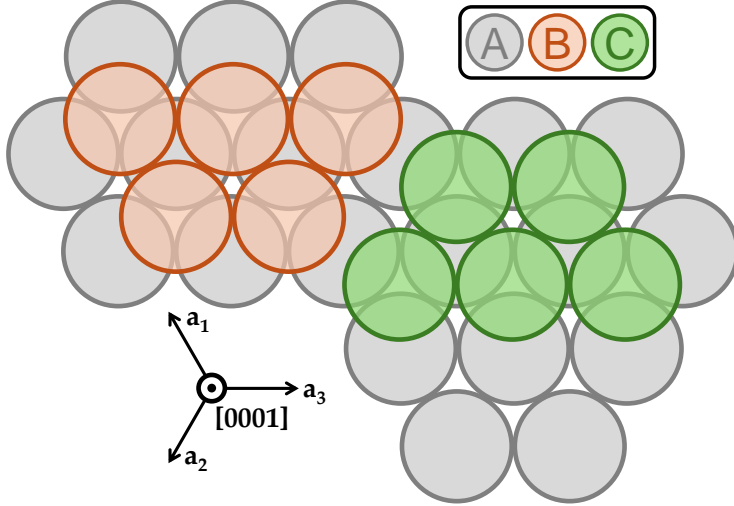


FIG. 1. The three possible occupation sites (*A*, *B*, and *C*) in a hexagonal close-packed system of Si-C bilayers stacked along the [0001] axis. a_1 , a_2 , and a_3 form base vectors with an angle of 120° that are consistent with the *Miller-Bravais notation*⁵⁷. Reproduced with permission from Fundamentals of Silicon Carbide Technology⁴³ (chap. 2). Copyright 2014, John Wiley & Sons Singapore Pte. Ltd.

dimension/axis perpendicular to the bilayer sheets (often referred to as the basal plane). This axis is known as the principal axis, *c*-axis, and [0001]-axis in literature^{3,43,48,57,63,64}.

In a hexagonal close-packed system, subsequent layers can not occupy the same lattice sites but have to alternate (see Fig. 1). The resulting stacking order of these three positional sites then defines the SiC polytype⁵⁷, which is named after two distinctive features: The number of layers until the respective stacking order repeats itself, and whether the emerging structure shows a cubic (C), hexagonal (H), or rhombohedral (R) symmetry^{43,57,63}. Besides the polytype 4H-SiC investigated in this review, the most prominent ones are 3C-SiC and 6H-SiC, whose stacking order and structure only differ slightly (see Fig. 2).

C. Anisotropy of 4H-SiC

Despite the infinite number of stacking variations, only 3C-SiC is isotropic in nature (cubic symmetry). Every other polytype features a certain degree of anisotropy, which denotes a directional dependence of material and electrical properties^{43,48,57}. Though this anisotropic nature can be simplified into two components, parallel and perpendicular to the *c*-axis, a very basic introduction regarding the complexity of the crystallographic structure of 4H-SiC is attempted. For more

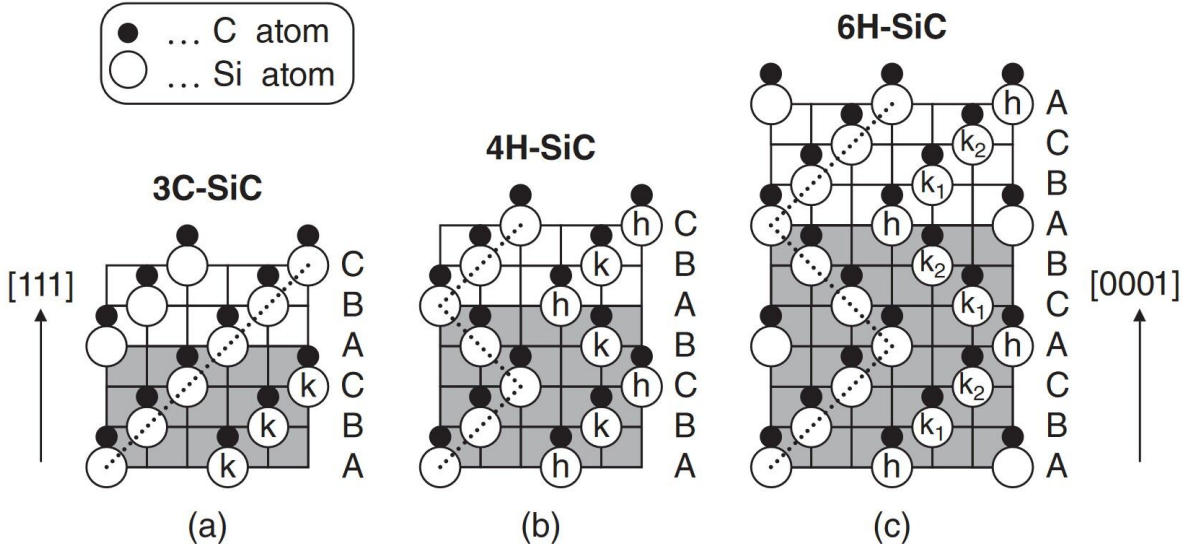


FIG. 2. Stacking structures of (a) 3C-SiC, (b) 4H-SiC, and (c) 6H-SiC along the principal axis. h and k denote whether the structure surrounding the lattice site is of cubic or hexagonal form. Gray layers highlight the name-giving number of stacks until the structure is repeated. Reproduced with permission from Fundamentals of Silicon Carbide Technology⁴³ (chap. 2). Copyright 2014, John Wiley & Sons Singapore Pte. Ltd.

detailed information, the reader is referred to the dedicated literature^{48,65,66}.

In the field of crystallography, structures are usually defined via a unit cell. Such a formation, often also called a primitive cell, represents the smallest repeating unit that still represents the full symmetry of the overlying crystal structure⁶⁷. In the case of 4H-SiC, the unit cell is of hexagonal type and consists of four Si and C atoms each. The given base vectors a_1 , a_2 , a_3 (forming a 120° angle between each other), and c form a Bravais lattice, while the so-called Miller-Bravais-notation is used to describe other important directions/axes and faces via a complex linear superposition (see Fig. 3)⁶⁷. For example, the (0001) -face and the opposite $(000\bar{1})$ -face are also often called the Si and C face⁶⁸, while the latter is also known as the basal plane⁴⁸. Considering common SiC-manufacturing methods, the (0001) -face (Si-face) is usually parallel to a wafer surface, implying that the c-axis ($[0001]$ direction) is perpendicular to it^{43,48,57,65,69}.

Within the unit cell characteristic points Γ , M , K and A were defined (see Fig. 4)^{70,71}, which are important in the context of energy band structures. From this definition, the following directions are derived:

- $\Gamma-A \rightarrow [0001]$ direction

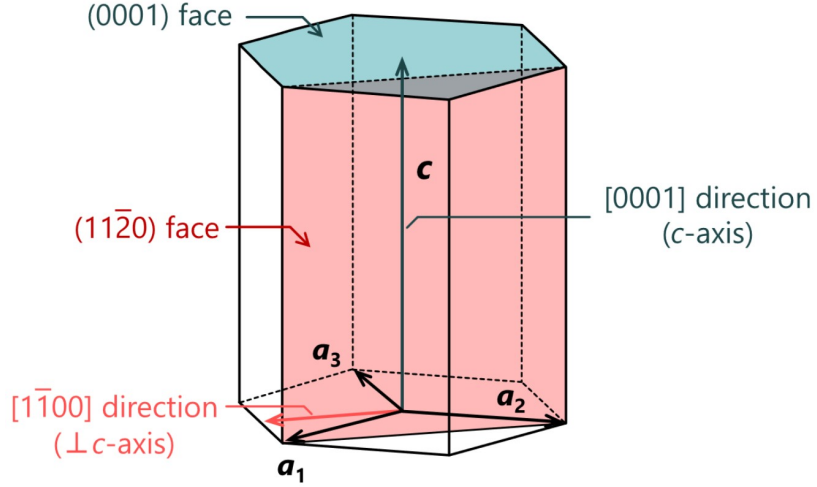


FIG. 3. 4H-SiC unit cell. a_1 , a_2 , a_3 , and c represent the base vectors of a Bravais lattice, while the [0001] and $[1\bar{1}00]$ direction, as well as the (0001) and $(11\bar{2}0)$ faces, are given in Miller-Bravais notation⁶⁷. Not shown, but often encountered within the literature, is the $[11\bar{2}0]$ direction, perpendicular to both the c -axis and $[1\bar{1}00]$ direction. Reproduced with permission from *Physica Status Solidi (b)* 260, 10 (2023)⁶⁹.

Copyright 2023, Wiley-VCH GmbH.

- Γ –M \rightarrow $[1\bar{1}00]$ direction
- Γ –K \rightarrow $[11\bar{2}0]$ direction

The anisotropic nature of 4H-SiC in simulations is usually handled in a much simpler way than the above definitions may indicate. In general, we differentiate two cases when discussing material and electrical parameters of 4H-SiC: A parallel and a perpendicular component with respect to the c -axis (or principal axis and [0001] direction)^{2,43,48,54,57,63,66,68}. These components will be denoted by \parallel and \perp throughout this work.

IV. PERMITTIVITY

The permittivity ϵ describes charge movement in response to internal/external potentials, how the latter are screened within a material⁷², the dielectric properties that influence electromagnetic wave propagation as well as their reflections on interfaces⁷³. In TCAD simulations, the main application of the permittivity is the Poisson equation⁷⁴, which describes the electric field induced by a charge. This is important, for example, to (i) calculate capacitances within a device, (ii) de-

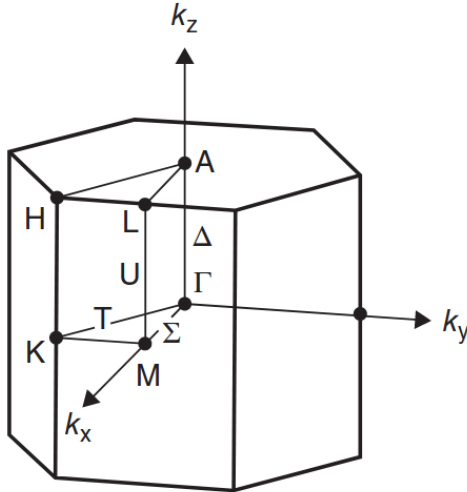


FIG. 4. Characteristic lattice locations of 4H-SiC within the unit cell. The included k_x , k_y , and k_z directions are according to Miller-Bravais notation. Reproduced with permission from Fundamentals of Silicon Carbide Technology⁴³ (chap. 2). Copyright 2014, John Wiley & Sons Singapore Pte. Ltd.

termine the doping concentrations of measured samples and (iii) investigate the impact of defects and traps.

All TCAD tools require a value input of the relative permittivity $\epsilon_r = \epsilon / \epsilon_0$, i.e., the ratio of ϵ to the vacuum permittivity $\epsilon_0 = 8.854 \times 10^{-12} \text{ F/m}$. Accurate values are important for two reasons: 1) Basic characteristics like the capacitance in response to an applied external voltage are often the foundation for more advanced investigations. Small errors in the beginning multiply, causing larger deviations down the line. 2) Depending on material and investigation, the amount of charge carriers can be very high ($10^{18}/\text{cm}^3$ and more), which amplifies any initial inaccuracy.

Our review shows that although fundamental investigations were published up to the present day, they rarely were referenced in the literature. Instead, the mainly deployed values trace back to a publication from the year 1970, which is itself based on measurements of the 6H-SiC polytype from 1944.

A. Introduction

The relative permittivity is a complex function of the frequency ω (see Eq. (1)). The real part ϵ' represents the energy stored in the material when exposed to an electric field, and the imaginary

part ϵ'' the losses, e.g., absorption and attenuation⁷³.

$$\epsilon_r^*(\omega) = \epsilon'(\omega) + i\epsilon''(\omega) \quad (1)$$

ϵ' and ϵ'' are tightly interconnected via the Kramers-Kronig (KK) relation³⁵ (see Eq. (2)). In TCAD simulations of semiconductor devices, ϵ'' is of low importance, while ϵ' is featured in the Poisson equation. Consequently, we will focus on ϵ' in the sequel.

$$\epsilon'(\omega) = 1 + \frac{2}{\pi} \int_0^\infty \frac{\omega' \epsilon''(\omega')}{\omega'^2 - \omega^2} d\omega' \quad (2a)$$

$$\epsilon''(\omega) = -\frac{2\omega}{\pi} \int_0^\infty \frac{\epsilon'(\omega')}{\omega'^2 - \omega^2} d\omega' \quad (2b)$$

1. Static and High-Frequency Relative Permittivity

Although investigations on the frequency-dependent ϵ' exist^{75–78}, we focus here on the static (ϵ_s) and high-frequency resp. optical (ϵ_∞) relative permittivity. The former is declared as $\epsilon_s = \epsilon'(\omega \rightarrow 0)$, while a definition for the latter is more complicated. ϵ_∞ denotes ϵ' at the end of the reststrahlen range towards higher frequencies, where the real part of the refractive index is null⁷⁹. In a publication that focused on optical high-frequency analysis⁸⁰, ϵ_∞ was even denoted as $\epsilon'(0)$, which must not be confused with ϵ_s . These inconsistencies were explained by Patrick and Choyke⁸¹ in the following fashion: “We shall use ϵ_∞ to denote the extrapolation … to zero frequency. This somewhat contradictory notation arose because ϵ_∞ , the “optical” dielectric constant, was often set … at a frequency much higher than the lattice frequency but low compared with electronic transition frequencies. In many substances no suitable frequency exists, and it is preferable to extrapolate optical data to zero frequency …”

Thus, ϵ_∞ is measured at frequencies well above the long-wavelength longitudinal optical (LO) phonon frequency ω_{LO} ³⁵. The latter is used in conjunction with the transversal optical (TO) phonon frequency ω_{TO} in the Lyddane-Sachs-Teller (LST) relationship⁸² to translate between ϵ_s and ϵ_∞ (see Eq. (3)).

$$\frac{\epsilon_s}{\epsilon_\infty} = \left(\frac{\omega_{LO}}{\omega_{TO}} \right)^2 \quad (3)$$

2. Characterization Methods

One possibility to determine the relative permittivity are calculations using the density functional theory (DFT) based local density approximation (LDA)^{7,80,83–88} or the effective mass

theory⁸⁹. These calculate the band structure and, thus, ϵ'' before transforming it into ϵ' using the Kramers-Kronig relations (Eq. (2)). Measurements use either some form of resonator (RES)^{77,78,90}, spectroscopy (SPEC)^{75,76,91}, spectroscopic ellipsometry (SE)^{92,93}, infrared ellipsometry (IRE)⁹⁴, the refractive index (RI)^{81,95,96} and a fitting to $\ln(J/F)$ ⁹⁷, with J the current density and F the field in a pin-diode. In two instances the transversal and longitudinal optical phonon frequencies were used in the Lyddane-Sachs-Teller relationship (Eq. (3))^{92,93}.

If ϵ'' is negligible, the permittivity can be computed from its tight relationship with the complex refractive index n^* , i.e., $n^*(E) = \sqrt{\epsilon_r(E)}$ ³⁵, with $E = \hbar\omega$. In four publications^{76,81,95,96} ϵ_∞ was fitted by the representation shown in Eq. (4), with hf being the photon energy, E_g an "average band gap" and ϵ_g proportional to the oscillator strength⁸¹. Six publications investigated the relative permittivity at mm-wave frequencies (MM) (10 GHz to 10 THz)^{90,98–102}, whose results got summarized by Li *et al.*⁷⁷ and Yanagimoto *et al.*¹⁰³.

$$n^2 = 1 + \frac{\epsilon_g}{1 - (hf/E_g)^2} \approx \epsilon_\infty + \epsilon_g \left(\frac{hf}{E_g} \right) \quad (4)$$

B. Results & Discussion

Publications had to be discarded for this review when no polytype was specified^{104–107} or powder material was investigated^{108,109}. Ivanov *et al.*⁸⁹ improved upon the value $\epsilon_s = 9.95$ ^{110,111} causing us to discard the outdated publications. For measurements at mm-wave frequencies, the data fluctuated, or solely single data points were provided. Since this makes an interpolation to zero frequency ($= \epsilon_s$) impossible we did not consider the respective data. We were unable to confirm some of the values referenced in the overview of high-frequency permittivities by Bechstedt *et al.*³ because we could not acquire the book by Bimberg¹¹². Out of 206 reviewed publications, only 179 provided a comprehensive set of data and were included in our analysis.

1. Fundamental Values

We found static relative permittivity (ϵ_s) values within 9.6 – 10.65 and high-frequency relative permittivity (ϵ_∞) within 6.25 – 7.61 (see Table I), whereas the direction parallel to the c-axis achieves larger values than the perpendicular ones. Wherever necessary, we calculated the relative permittivity according to $\epsilon_s = (\epsilon_s^\parallel (\epsilon_s^\perp)^2)^{\frac{1}{3}}$ resp. $\epsilon_\infty = (\epsilon_\infty^\parallel (\epsilon_\infty^\perp)^2)^{\frac{1}{3}}$ ^{70,117–120}, which was more often used than $\epsilon_s = (\epsilon_s^\parallel \epsilon_s^\perp)^{\frac{1}{2}}$ proposed by Ivanov *et al.*⁸⁹.

TABLE I. Fundamental investigations on permittivity. mark publications focused on 6H-SiC.

ref.	ϵ_s	ϵ_s^{\parallel}	ϵ_s^{\perp}	ϵ_{∞}	$\epsilon_{\infty}^{\parallel}$	$\epsilon_{\infty}^{\perp}$	method ^a	SiC	doping
[Patr70] ^{81a}	9.78 ^h	10.03	9.66	6.58 ^h	6.7	6.52	RI	6H	–
[Ikeda80] ^{95b}	9.94 ^h	10.32	9.76	–	–	–	RI	4H	–
[Chen94] ¹¹³	–	–	–	7.04 ^h	7.20	6.96	DFT-LDA	4H	–
[Nino94] ⁹²	9.83 ^h	9.98	9.76	6.62 ^h	6.67	6.59	SE	6H	–
[Hari95] ^{96c}	–	–	–	6.63 ^h	6.78 ^d	6.56 ^d	RI	4H	–
[Karc96] ⁸³	10.53 ^h	10.9	10.352	7.02 ^h	7.169	6.946	DFT-LDA	4H	–
[Well96] ⁸⁴	–	–	–	7.02 ^h	7.17	6.95	DFT-LDA	4H	–
[Adol97] ⁸⁵	–	–	–	7.56 ^h	7.61	7.54	DFT-LDA	4H	–
[Ahuja02] ⁸⁶	–	–	–	7.11 ^h	7.47	6.94	DFT-LDA	4H	n-type
[Peng04] ⁸⁷	–	–	–	6.31 ^h	6.44	6.25	DFT	4H	–
[Pers05] ¹¹⁴	9.73 ^h	9.94	9.63	6.47 ^h	6.62	6.40	DFT-LDA	4H	intrinsic
[Chin06] ⁸⁰	–	–	–	6.81	–	–	DFT-LDA	4H	intrinsic
[Dutt06] ⁹⁸	9.97 ± 0.02^e	–	–	–	–	–	MM	4H	high purity
[Ivan06] ⁸⁹	9.93 ± 0.01	–	–	–	–	–	EMT	4H	intrinsic
[Hart11] ⁷⁸	9.77 ^g	–	–	–	–	–	RES	4H	high purity
[Jone11] ⁹⁰	9.60 ^f	–	–	–	–	–	RES	4H	high purity
[Naft16] ⁷⁵	10.11 ^h	10.53 ^g	9.91 ^g	–	–	–	SPEC	4H	undoped
[Cout17] ⁸⁸	10.13 ^h	10.65	9.88	–	–	–	DFT-LDA	4H	–
[Tare19] ⁷⁶	–	–	–	6.587 ± 0.003	–	–	SPEC	4H	–
[Chen22] ⁹³	–	–	9.97	–	–	–	SE	4H	–
[Gao22a] ⁹¹	–	–	–	6.51	–	–	SPEC	4H	–
[Yang22a] ⁹⁷	10.21	–	–	–	–	–	$\ln(J/F)$	4H	p-type
[Li23] ⁷⁷	–	10.27 ± 0.03	–	–	–	–	RES	4H	high purity
[Li24b] ¹⁰¹	9.91 ^h	10.20 ± 0.05	9.77 ± 0.01	–	–	–	RES	4H	high purity
[Main24] ⁹⁴	–	–	–	–	–	6.40 ± 0.20	IRE	4H	–

^a fitted to refractive index values by Thibault¹¹⁵

^b fitted to refractive index values by Shaffer¹¹⁶ using 6H phonon frequencies

^c fitted to refractive index values by Shaffer¹¹⁶

^d referenced by Bechstedt *et al.*³ from [Bimb82]¹¹²

^e frequency range 131 – 145 GHz, for lower resp. higher frequencies $\epsilon_s = 9.74$ was achieved

^f calculated from refractive index n as $\epsilon_s = n^2$

^g wavelength and/or temperature dependent

^h $\epsilon_r = ((\epsilon_r^{\perp})^2 \epsilon_r^{\parallel})^{1/3}$

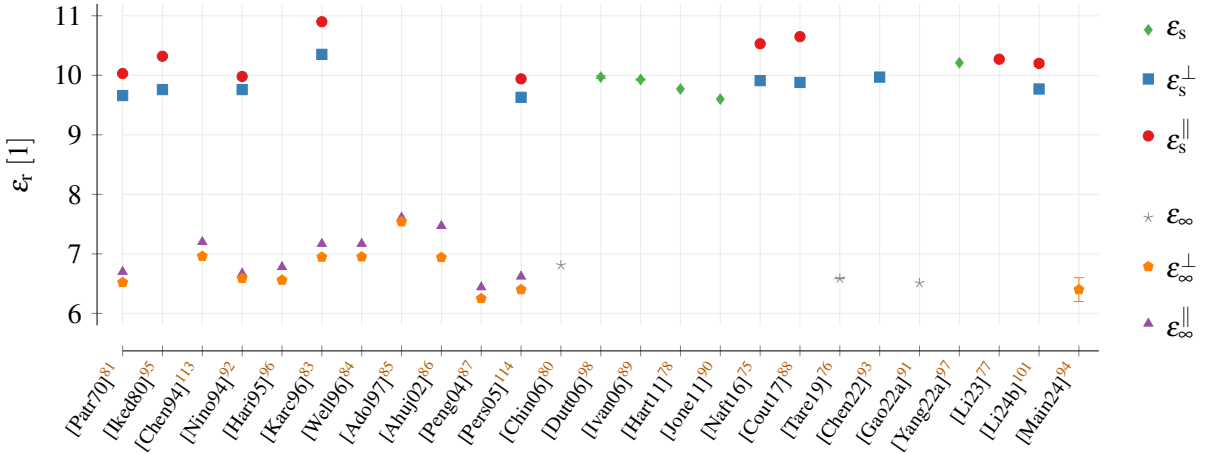


FIG. 5. Fundamental investigations on permittivity in chronological order.

Early investigations^{81,95,96} utilized Eq. (4) to extract the permittivity from varying refractive index data, some measured on 6H-SiC samples. After the year 1996 dominated calculations of ϵ_{∞} and past 2006 measurements of ϵ_s . Despite these different phases, we were unable to identify any trends over time (see Fig. 5). On the contrary: The 6H-SiC permittivity values are similar to 4H. This is underlined by the statements of Zollner *et al.*¹²¹ who stated that for energies below 3 eV their results are comparable to 6H values¹²².

2. Origin of Parameters

The primary source for 4H-SiC permittivity in literature is the investigation by Patrick and Choyke⁸¹ (see Fig. 6) based on 6H measurements published in 1944¹¹⁵. The usage of 6H values was justified in multiple publications^{6,118,126,127,139,141,144} by the unavailability of 4H specific parameters. The fact that this claim is repeated up to the year 2022⁹³ shows the high demand for a systematic parameter analysis. In the majority of cases, 6H values were, however, used for 4H analyses without further remark, which left the false impression of specific 4H parameters.

This unawareness of dedicated 4H-SiC permittivities is surprising, especially because Ikeda, Matsunami, and Tanaka⁹⁵ published corresponding values already in 1980. Based on measurements by Shaffer¹¹⁶ but using the phonon frequency of 6H, direction-dependent values for ϵ_s were, easy to overlook, added to a comment in the reference list. Interestingly, we encountered the proposed values on multiple occasions^{7,8,10,43,68,201} but never found a direction citation of that particular paper. Not even cross-references among the citing publications exist.

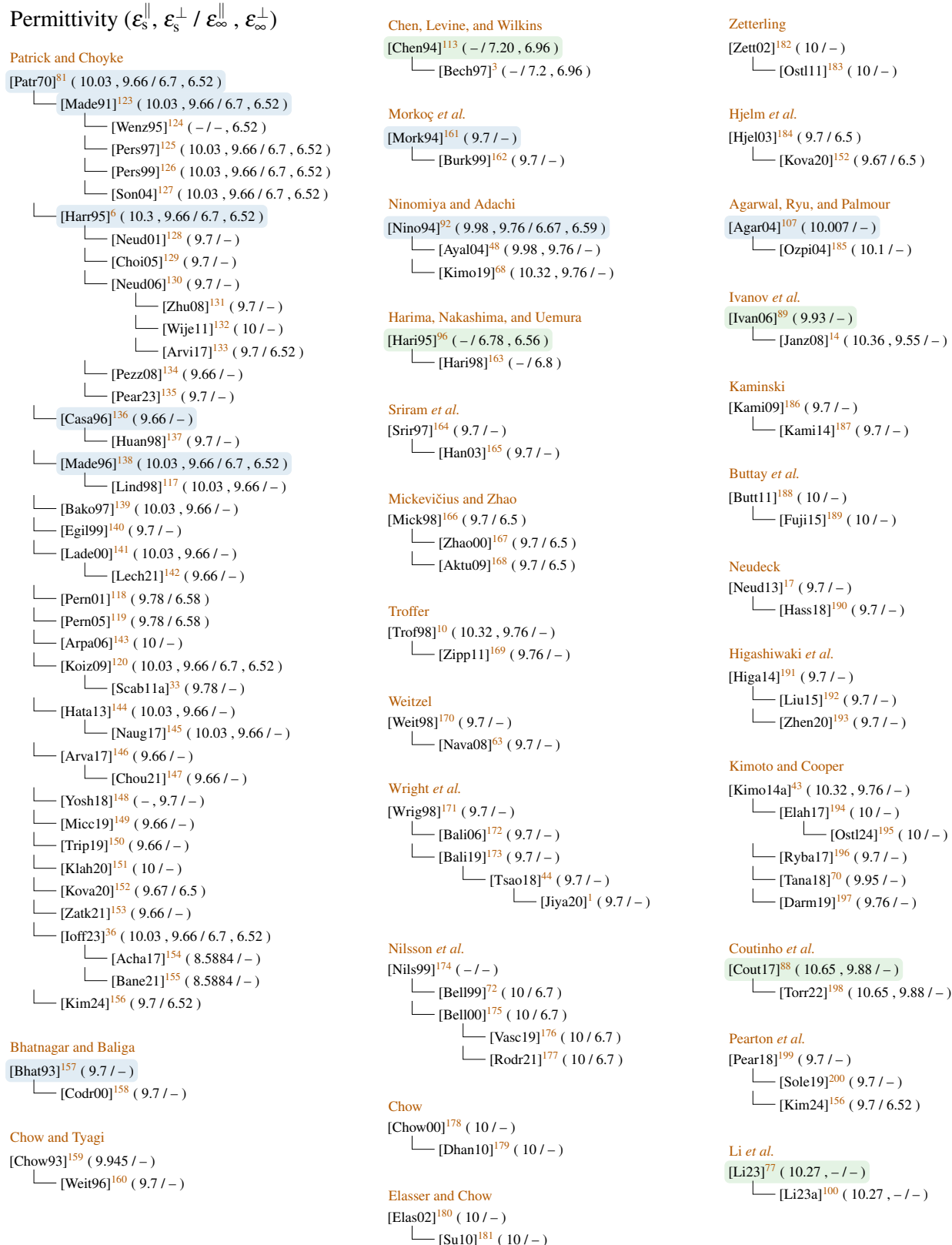


FIG. 6. Reference chains for the permittivity. A single value denotes ϵ_s respectively ϵ_{∞} without direction.

are investigations not focused on 4H-SiC and novel analyses on 4H-SiC.

The negligence of 4H-SiC permittivity investigations seems to be deeply rooted within the scientific community. Only 5 out of the 23 fundamental research articles were cited within the boundaries of this review. The fact that six got published after the year 2021 provides just a partial explanation. Although long reference chains (cp. Fig. 6) hide the fact that these are 6H-based values, we also found papers within the last five years referencing directly to Patrick and Choyke⁸¹. Another interpretation of these insights is that the permittivity has little impact in TCAD simulations, such that somewhat accurate 6H values are often sufficient. The difference is anyhow well within 5 %. Nevertheless, we highly encourage the scientific community to also adopt more recent permittivity evaluations on 4H-SiC in future publications, or at least clearly specify and comment on the usage of 6H parameter values.

3. Literature Values

We found evidence that the 6H values by Patrick and Choyke⁸¹ were used in 41 publication, either referenced directly or via intermediate publications. Thereby, the values were transformed by rounding, e.g., $9.66 \rightarrow 9.7 \rightarrow 10$ ^{128,143} (cp. Fig. 6), defining directional permittivities as effective ones, e.g., $\epsilon_s^\perp = 9.66 \rightarrow \epsilon_s = 9.7$ or $\epsilon_s^\parallel = 10.03 \rightarrow \epsilon_s = 10$, and mere typographical errors, e.g., turning 9.66 into 9.67¹⁵² (see Section A1 for a comprehensive analysis of all encountered inconsistencies). Over the years, these changes expanded the initial data set to such an extent that the majority of all values in literature are covered (see Figs. 7 and 8). Due to missing references, we cannot say for sure that all authors who picked the same value made their selection based on the same data. For example, values like $\epsilon_s = 9.7$ could be derived from both Patrick and Choyke⁸¹ and Ikeda, Matsunami, and Tanaka⁹⁵. In total, we found a direct connection of these two papers alone to the values deployed in 80 % of the investigated publications, which confirms again the negligence of 4H-SiC permittivity investigations.

In two cases, we had a hard time extracting and verifying permittivity results. Chow and Tyagi¹⁵⁹ specified the permittivity as a multiple of the permittivity in Si. For a comparison we picked $\epsilon_{sSi} = 11.7$ ³⁶. Challenging is $\epsilon_s = 8.5584$ ^{154,155}, according to the authors computed from $\epsilon_s^\perp = 9.66$ and $\epsilon_s^\parallel = 10.03$ ³⁶. We were not able to calculate this value analytically since the result is lower than both constituents. Only by adding the high-frequency relative permittivity to the mix we achieved a somewhat close value of 8.

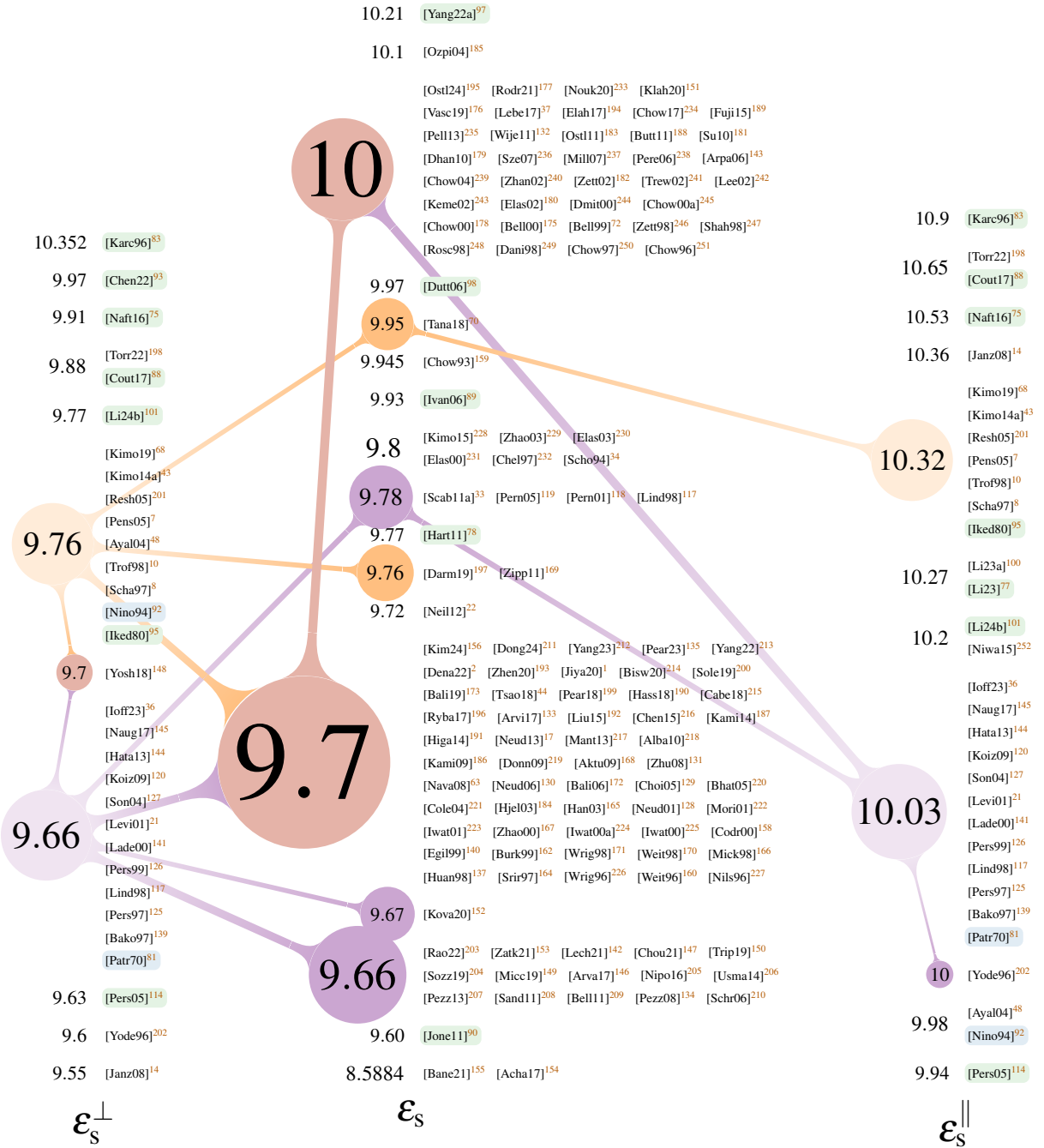


FIG. 7. Published values for the static permittivity. The size of values indicates the abundance in literature and connections that at least one direct reference was found. Brighter colors highlight the initial values. Publications are not focused on 4H-SiC and are novel analyses on 4H-SiC.

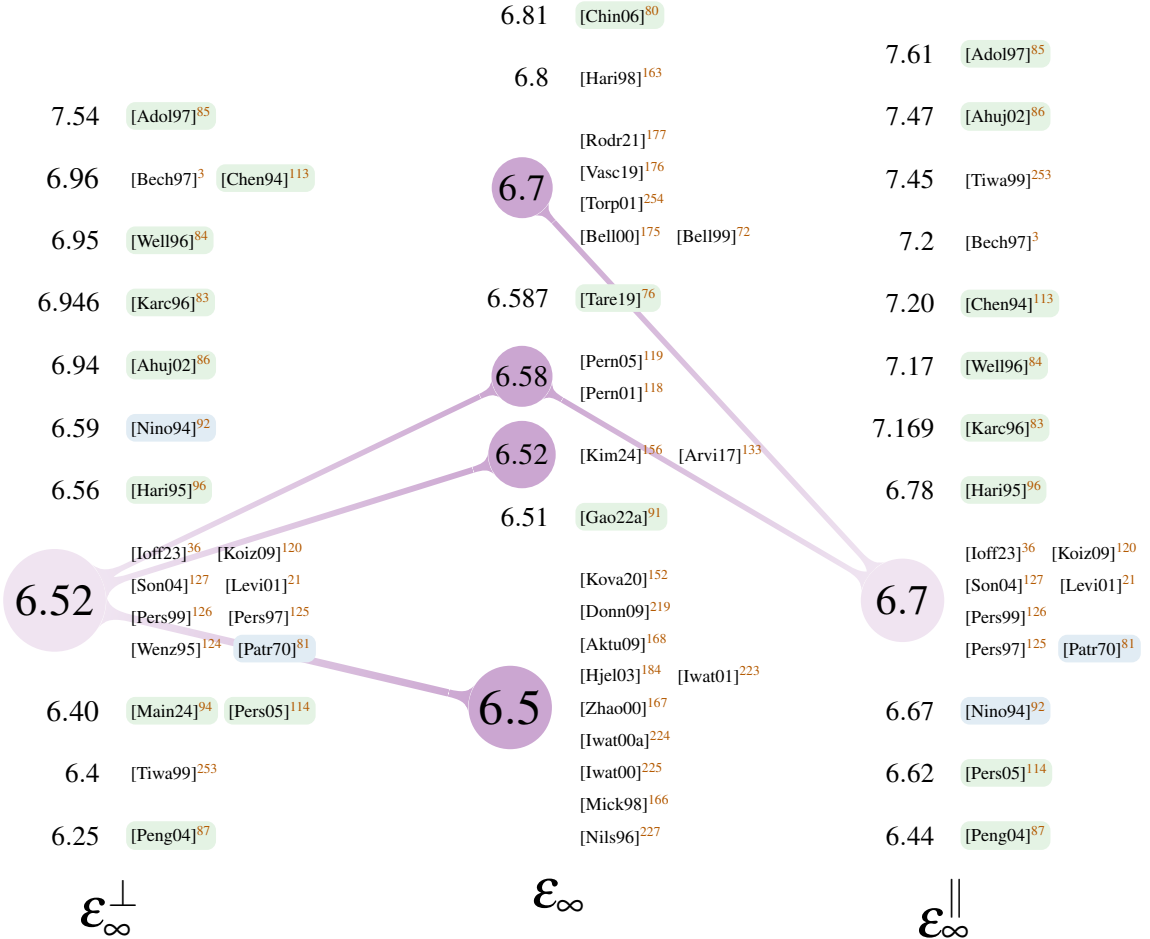


FIG. 8. Published values for the static permittivity. The size of values indicates the abundance in literature and connections that at least one direct reference was found. Brighter colors highlight the initial values. publications are not focused on 4H-SiC and are novel analyses on 4H-SiC.

4. Temperature Dependency and Phonon Frequencies

The static permittivity is temperature-dependent. Although TCAD tools do not support temperate-dependent permittivities by default, it is possible to cover these changes by custom code in the simulations. For a frequency around 40 GHz, Hartnett *et al.*⁷⁸ provided a polynomial approximation up to degree four (see Eq. 5). Cheng, Yang, and Zheng⁹³ approximated $\epsilon_s^\perp = 9.82 + 4.87 \times 10^{-4} T$ and Li *et al.*¹⁰¹ $\epsilon_s^\perp = 9.77 (1 + 6 \times 10^{-5} (T - 300 \text{ K}))$ and $\epsilon_s^\parallel = 10.2 (1 + 1 \times 10^{-4} (T - 300 \text{ K}))$. All these models show an increase of the permittivity with

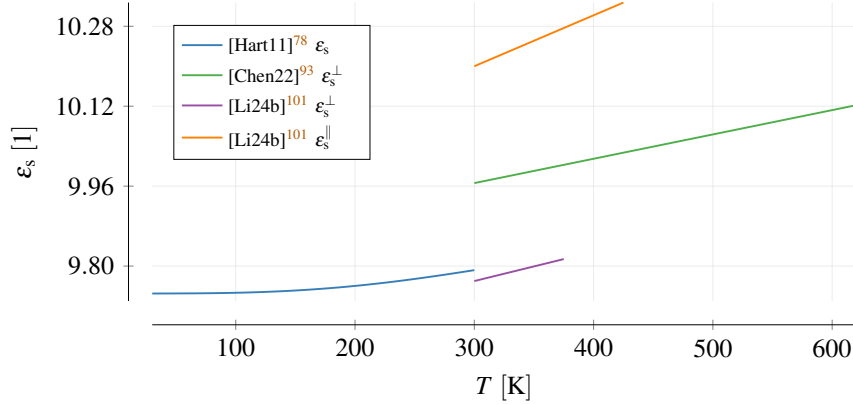


FIG. 9. Permittivity vs. temperature. The models are only shown in the interval used for characterization.

rising temperature (Fig. 9).

$$\begin{aligned} \epsilon_s(T) = & 9.7445 + 3.1862 \times 10^{-5} T - 6.3026 \times 10^{-7} T^2 \\ & + 5.9848 \times 10^{-9} T^3 - 8.2821 \times 10^{-12} T^4 \end{aligned} \quad (5)$$

While we investigated the permittivity, we encountered various values of the longitudinal (ω_{LO}) and transversal optical (ω_{TO}) phonon frequencies in 4H-SiC (see Table II). For ω_{LO} , we found values of 104 – 120 meV and 964 – 992 cm⁻¹. The two ranges do not fully overlap, as an energy of 104 meV translates to 838 cm⁻¹. For ω_{TO} the values of 95 – 100 meV and 776 – 798 cm⁻¹ match better. Due to the fact that this was not the result of a targeted search we do not claim completeness.

V. DENSITY-OF-STATES MASS

TCAD tools use effective masses to simplify the description of specific effects. Examples are tunneling masses, quantum well masses, effective mass at the contactor in a channel, thermionic relative masses, conductivity masses, and density-of-states masses. Detailed information on each can be found in the respective simulation framework manual. In this section we review the density-of-states (DOS) mass²⁶⁰, which is used in TCAD simulations, e.g., to calculate the charge carrier concentration or impact and incomplete ionization.

Overall, our review reveals that the majority of investigations on the density-of-states masses in 4H-SiC were conducted in a single decade between 1994 and 2004. The earliest studies in the 1970s were focused on measurements, while nowadays calculations are utilized predominantly. This led to the concerning circumstance that we were only able to identify two measurements

TABLE II. Phonon frequencies in 4H-SiC. No claim for completeness.

ref	ω_{LO}	ω_{LO}	$\omega_{\text{LO}}^{\parallel}$	$\omega_{\text{LO}}^{\perp}$	ω_{TO}	ω_{TO}	$\omega_{\text{TO}}^{\parallel}$	$\omega_{\text{TO}}^{\perp}$
	[meV]	[1/cm]	[1/cm]	[1/cm]	[meV]	[1/cm]	[1/cm]	[1/cm]
[Feld68] ²⁵⁵	–	967 – 971	–	–	–	–	–	–
[Neub71] ¹⁹	120 ^a	–	–	–	100	–	–	–
[Hari95] ⁹⁶	–	–	964.2	966.4	–	–	783	798
[Frei95] ²⁵⁶	104.1 ± 0.2	–	–	–	95	–	–	–
[Hari98] ¹⁶³	–	964	–	–	–	783	–	–
[Tiwa99] ²⁵³	–	–	967 ± 3	971	–	–	782	797
[Levi01] ²¹	104.2 ^b	–	–	–	–	–	–	–
[Sun11a] ²⁵⁷	–	984 ± 21	–	–	–	776.4 ± 1.0	–	–
[Arvi17] ¹³³	–	974	–	–	–	793	–	–
[Zhen19] ²⁵⁸	–	964	–	–	–	–	–	–
[Main24] ⁹⁴	–	–	–	992.1 ± 0.2	–	–	–	797.7 ± 0.3

^a corresponds to 29 THz, same value proposed in^{72,86,125,184,223,259}.

^b denoted as 6H by Neuberger¹⁹

for the hole DOS mass. The demand for a more thorough characterization is also fueled by the significant temperature dependency (the hole mass more than doubles between zero and 300 K) that was predicted by calculations but is rarely considered in literature.

A. Introduction

The density-of-states masses are calculated from the direction-dependent effective masses of electrons and holes, which are mathematically defined as the reciprocal of the second derivative of the spherically averaged dispersion relation¹¹⁷. The latter, also called conduction and valence band, are non-uniform in a semiconductor, resulting in deviating masses along each principal direction.

We start our analysis with a discussion of the direction-dependent masses and then show how the DOS (and also the conductivity) masses are derived. To increase readability the effective mass m is denoted relative to the free electron mass m_0 , i.e., $m^* = m/m_0$ ²⁶¹. For further information, the interested reader is referred to the dedicated literature^{4–8,35,114,127,262}.

1. Effective Masses along Principal Directions

For electrons, the masses are specified in the directions starting in the conduction band minimum at the M point^{5,48,263–265} (cp. Section III) towards the Γ , K and L point, denoted in the sequel as $m_{M\Gamma}^*$, m_{MK}^* and m_{ML}^* . The first two are perpendicular to the c-axis, the latter one parallel^{48,139,266,267}. In the M point, two conduction bands are very close together, such that both can influence the effective mass^{8,265}. Zhao *et al.*¹⁶⁷ even used three conduction bands. If not stated otherwise, we will focus solely on the lowest one within this paper.

The valence band maximum is in the Γ point^{10,48,139}. Consequently, the three relative hole masses are termed $m_{\Gamma M}^*$, $m_{\Gamma K}^*$ (perpendicular), and $m_{\Gamma A}^*$ (parallel), indicating the directions towards the M, K, and A point^{265,268}. Three separate bands meet at the Γ point^{127,139,263,268,269}. The two topmost are called heavy-hole (hh) and light-hole (lh), and the third one crystal split off (so)^{127,269}. Although all may influence the effective mass, often only a subset is used.

2. Density-of-States (DOS) Mass

The effective density-of-states is, for example, used to evaluate the electron and hole concentration. It is defined separately for conduction (N_C) and valence (N_V) band^{33,141,169,270–272} (see Eq. (6)) with M_C equal the number of conduction band minima in the first Brillouin zone²⁷¹.

$$N_C = 2 M_C \left(\frac{2\pi m_{de}^* k_B T}{h^2} \right)^{3/2} \quad (6)$$

$$N_V = 2 \left(\frac{2\pi m_{dh}^* k_B T}{h^2} \right)^{3/2}$$

m_{de}^* and m_{dh}^* denote the effective density-of-states masses, which are defined as the multiplicative average of the direction-dependent masses (see Eq. (7))^{7,127,139,140,262,272,273}.

$$m_{de}^* = (m_{de\perp}^* m_{de\parallel}^*)^{1/3} = (m_{M\Gamma}^* m_{MK}^* m_{ML}^*)^{1/3} \quad (7)$$

$$m_{dh}^* = (m_{dh\perp}^* m_{dh\parallel}^*)^{1/3} = (m_{\Gamma M}^* m_{\Gamma K}^* m_{\Gamma A}^*)^{1/3}$$

$$m_{de\perp}^* = \sqrt{m_{M\Gamma}^* m_{MK}^*}, \quad m_{de\parallel}^* = m_{ML}^*$$

$$m_{dh\perp}^* = \sqrt{m_{\Gamma M}^* m_{\Gamma K}^*}, \quad m_{dh\parallel}^* = m_{\Gamma A}^*$$

In this case m_{de}^* is called the *single valley* DOS electron effective mass^{7,48,140,144}, as the factor M_C is not considered. It is common, e.g., in some TCAD tools, to add M_C to the effective

mass^{35,139,218,274,275} (see Eq. (8)). In this review, we will only present the single valley values and highlight all publications where we found expressions including M_C .

$$m_{de}^* = (M_C^2 m_{de\perp}^* m_{de\parallel}^*)^{1/3} \quad (8)$$

In addition to the direction, the effective mass of the holes also has to combine multiple bands, i.e., the masses of heavy (m_{hh}^*) and light (m_{lh}^*) holes (see Eq. (9))^{117,119,236}.

$$m_{dh}^* = \left(m_{hh}^{*3/2} + m_{lh}^{*3/2} \right)^{2/3} \quad (9)$$

This expression is already a simplification because the energy differences among the bands also have to be considered^{139,276} (see Eq. (10)). ΔE_2 and ΔE_3 denote the energy difference to the highest band, which were determined as 9 meV¹³⁹ resp. 8.6 meV¹²⁵ for the second band and 73 meV¹³⁹, 77 meV²⁷⁷ resp. 72 meV²⁷⁶ for the third band.

$$m_h^*(T) = \left[m_{h1}^{*3/2} + m_{h2}^{*3/2} \exp\left(-\frac{\Delta E_2}{k_B T}\right) + m_{h3}^{*3/2} \exp\left(-\frac{\Delta E_3}{k_B T}\right) \right]^{2/3} \quad (10)$$

The changing amount of charge carriers with temperature can be compactly modeled by using a *thermal DOS effective mass*^{262,278}. There is no explicit form available but it was calculated by Wellenhofer and Rössler²⁶² (electrons and holes separately) and Tanaka *et al.*⁷⁰ (average effective mass). Later Schadt⁸, Hatakeyama, Fukuda, and Okumura¹⁴⁴ fitted the results from Wellenhofer and Rössler²⁶² with an equation used for silicon²⁷⁹ (see Eq. (11)).

$$m^*(T) = \left(\frac{z_0 + z_1 T + z_2 T^2 + z_3 T^3 + z_4 T^4}{1 + n_1 T + n_2 T^2 + n_3 T^3 + n_4 T^4} \right)^\eta \quad (11)$$

A temperature-dependent change according to Eq. (11) can be included in some of the modern TCAD tools, but we found no possibility of implementing Eq. (10). Not supported are also doping-dependent DOS masses³⁵, which were already shown for 6H-SiC²⁸⁰, but not yet for 4H.

3. Effective Conductivity Mass

We regularly encountered the conductivity mass in our review. Initially, we found it very challenging to distinguish it from the DOS mass, because both are calculated from the direction-dependent effective masses. Therefore, we decided to explicitly highlight the differences here.

The conductivity mass m_c^* is a simplification to model the mobility μ (see Section X) in 4H-SiC^{8,70,137,223–225,281–285} as shown in Eq. (12)⁵, with τ the charge carrier lifetime (see Section VIII).

$$\mu = \frac{e\tau}{m_c^* m_0}, \quad (12)$$

The differences to the DOS mass are seen in the definition of the conductivity mass, which is reciprocal (see Eq. (13))^{35,281,282,286}.

$$\begin{aligned} m_{ce}^* &= \frac{3m_{ce\perp}^* m_{ce\parallel}^*}{m_{ce\perp}^* + 2m_{ce\parallel}^*} \\ m_{ch}^* &= \frac{3m_{ch\perp}^* m_{ch\parallel}^*}{m_{ch\perp}^* + 2m_{ch\parallel}^*} \\ \frac{2}{m_{ce\perp}^*} &= \frac{1}{m_{MK}^*} + \frac{1}{m_{MG}^*}, \quad m_{ce\parallel}^* = m_{ML}^* \\ \frac{2}{m_{ch\perp}^*} &= \frac{1}{m_{TM}^*} + \frac{1}{m_{TK}^*}, \quad m_{ch\parallel}^* = m_{GA}^* \end{aligned} \quad (13)$$

Combining these definitions leads to condensed expressions for the conductivity mass we encountered regularly in literature (see Eq. (14))¹³⁷.

$$\begin{aligned} \frac{3}{m_{ce}^*} &= \frac{1}{m_{MG}^*} + \frac{1}{m_{MK}^*} + \frac{1}{m_{ML}^*} \\ \frac{3}{m_{ch}^*} &= \frac{1}{m_{TM}^*} + \frac{1}{m_{TK}^*} + \frac{1}{m_{GA}^*} \end{aligned} \quad (14)$$

4. Polaron Mass

In the Si-C bond of silicon carbide, carbon atoms are more electronegative than silicon ones, resulting in a partly ionic crystal¹²⁷. Within this surrounding, a charge carrier, together with its self-induced polarization, forms a quasiparticle, which is called a polaron²⁸⁷. This can also be described by longitudinal optical vibrations that generate an electric field along the direction of the vibration which interacts with the charge carriers^{127,261}. Effectively, the carrier is “dressed” by a charge leading to a deviating effective mass¹²⁵. The adapted mass m_p , called *polaron mass*, is slightly higher than the bare mass m and can be calculated according to Eq. (15)^{114,125,127}, where α is called the Fröhlich constant. If the CGS unit system is used^{287–289} the term $1/4\pi\epsilon_s$ of Eq. (16) has to be removed.

$$m_p = m \frac{1-8 \times 10^{-4} \alpha^2}{1-\alpha/6+3.4 \times 10^{-3} \alpha^2} \approx m \left(1 - \frac{\alpha}{6}\right)^{-1} \quad (15)$$

$$\alpha = \frac{1}{2} \left(\frac{1}{\epsilon_\infty} - \frac{1}{\epsilon_s} \right) \frac{e^2}{\hbar\omega_{LO}} \left(\frac{2m\omega_{LO}}{\hbar} \right)^{1/2} \frac{1}{4\pi\epsilon_s} \quad (16)$$

5. Characterization Methods

Effective masses were mainly determined by band structure calculations. The most commonly used approach is the density functional theory (DFT) using local density approximation (LDA)^{65,124,168,227,262,264–266,290}, projector augmented wave (PAW)^{268,291}, (full-potential) linearized augmented plane wave ((FP)LAPW)^{114,125,127,263,292}, (orthogonalized) linear combination of atomic orbital ((O)LCAO)^{80,293}, full-potential linear muffin-tin orbital method (FPLMTO)²⁹⁴ and hybrid pseudo-potential and tight-binding (HPT)²⁹⁵. Additional calculations feature empirical pseudo potentials (EPM)^{175,296} and RSP Hamiltonians (RSPH)²⁶⁹.

Published values also served as starting point for Monte Carlo (MC)^{168,227} simulations and genetic algorithm fittings (GAF)^{297,298} that condense multiple investigations into new parameter sets. For example, the data by Son *et al.*²⁹⁹ were refined by Nilsson, Sannemo, and Petersson²²⁷, whose results served as a starting point for a fitting by Mickevičius and Zhao¹⁶⁶. Similarly, Mikami, Kaneko, and Kimoto³⁰⁰ calculated the hole mass as the second derivative of the E-k dispersion by Persson and Lindefelt²⁶³.

The calculations are complemented by measurements of the infrared spectroscopic ellipsometry (IRSE)²⁵³, photoluminescence¹⁴⁰, infrared absorption (IR)²⁷¹, Raman scattering⁹⁶ and Hall effect^{120,283,301,302}. Also prominent are investigations based on optically detected cyclotron resonance (ODCR)^{261,285,299,303,304}, but in these cases, polaron masses were achieved.

B. Results & Discussion

In this section, we present and discuss the DOS mass values found in the literature. We discarded conductivity masses³⁰⁰, publications that did not clearly specify the SiC polytype³⁰⁵, the results by Son *et al.*²⁹⁹ because Son *et al.*¹²⁷ stated that the smaller values are due to “errors caused by a broad and asymmetric ODCR line shape with the peak position slightly shifted to lower magnetic fields” and the values by Bellotti⁷², which were later published again¹⁷⁵. Overall, 138 out of 153 collected publications were included in our analyses.

1. Effective Mass along Principal Directions

The relative masses in the principal directions (see Table III) are predominantly determined by calculations. Out of 21 publications, only two^{283,304} conducted measurements, and both fo-

TABLE III. Effective masses in principal directions. Multiple values for the same band are calculated by differing algorithms.  denotes measurements.

ref.	electron				hole				method	polaron
	m_{MF}^* [1]	m_{MK}^* [1]	m_{ML}^* [1]	band	m_{TM}^* [1]	m_{TK}^* [1]	m_{TA}^* [1]	band		
[Kack94] ²⁹⁰	0.62	0.13	0.39	–	4.23	2.41	1.73	hh	DFT-LDA	–
	–	–	–	–	0.45	0.77	1.73	lh	DFT-LDA	–
	–	–	–	–	0.74	0.51	0.21	so	DFT-LDA	–
[Karc95] ²⁶⁴	0.66	0.31	0.3	–	–	–	–	–	DFT-LDA	–
[Lamb95] ²⁹⁴	0.58	0.28	0.31	–	–	–	–	–	DFT-LDA	–
[Wenz95] ¹²⁴	0.6	0.28	0.19	–	–	–	–	–	DFT-LDA	–
[Kaec96] ⁶⁵	0.57	0.32	0.32	–	–	–	–	–	DFT-LDA	–
[Nils96] ²²⁷	0.43	0.43	0.28	1	–	–	–	–	DFT-LDA	–
	0.52	0.21	0.45	2	–	–	–	–	DFT-LDA	–
[Pers96] ²⁶³	0.57	0.28	0.31	–	–	–	–	–	DFT-LDA	–
[Volm96] ³⁰⁴	0.58 ± 0.01	0.31 ± 0.01	0.33 ± 0.01	–	–	–	–	–	ODCR	y
[Chen97] ²⁹⁵	1.2	0.19	0.33	–	–	–	–	–	DFT-LDA	–
[Pers97] ¹²⁵	0.57	0.28	0.31	1	–	–	–	–	DFT-LDA	–
	0.59	0.31	0.34	1	–	–	–	–	DFT-LDA	–
	0.61	0.29	0.33	1	–	–	–	–	DFT-LDA	y
	0.78	0.16	0.71	2	–	–	–	–	DFT-LDA	–
	0.8	0.18	0.75	2	–	–	–	–	DFT-LDA	–
	0.85	0.17	0.77	2	–	–	–	–	DFT-LDA	y
	–	–	–	–	0.7	3.04	1.64	1	DFT-LDA	–
[Pers98a] ^{277a}	–	–	–	–	0.6	0.34	1.64	2	DFT-LDA	–
	–	–	–	–	–	–	–	–	–	–
[Bell00] ¹⁷⁵	0.57	0.23	0.27	–	–	–	–	–	EPM	–
[Zhao00a] ²⁹³	0.62 ± 0.03	0.27 ± 0.02	0.31 ± 0.02	–	–	–	–	–	DFT-LDA	–
[Penn01] ²⁹⁶	0.60 ± 0.05	0.20 ± 0.02	0.36 ± 0.02	–	–	–	–	–	EPM	–
[Iwat03] ²⁶⁶	0.59	0.29	–	–	–	–	–	–	DFT-LDA	–
[Iwat03a] ²⁸³	0.58	0.3	–	–	–	–	–	–	Hall	–
[Dong04] ²⁶⁵	0.53	0.27	0.3	–	0.86	0.95	1.58	1	DFT-LDA	–
	–	–	–	–	0.55	0.52	1.32	2	DFT-LDA	–
	–	–	–	–	1.13	1.30	0.21	3	DFT-LDA	–
[Chin06] ⁸⁰	0.47	–	0.38	–	–	–	–	–	DFT-LDA	–
[Ng10] ²⁹⁷	0.66	0.31	0.34	–	–	–	–	–	GAF	–
[Kuro19] ²⁶⁸	0.54	0.28	0.31	–	0.54	0.54	1.48	–	DFT-LDA	–
[Lu21] ²⁹¹	0.54	0.3	–	–	2.77	1.82	1.52	–	DFT-LDA	–

^a fitted to^{125,263}

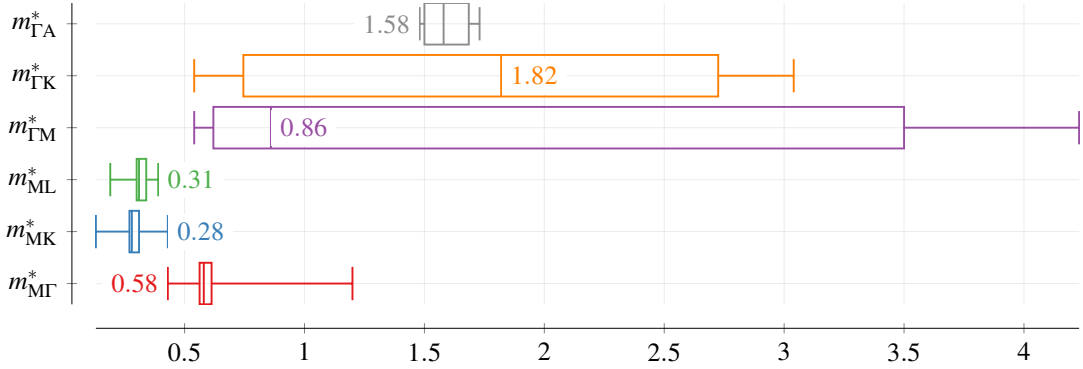


FIG. 10. Distribution of masses in principal directions. We only considered band 1 and values without further specifications. Shown are the 0th, 25th, 50th, 75th and 100th quartile. The mean value is added in numerical form.

cused solely on electrons. Consequently, calculations are, at the moment, the only source for hole masses. In literature, the hole bands are either denoted as heavy-hole (hh), light-hole (lh), and crystal split-off (so) or simply as 1, 2, 3. By comparison of the respective values, we are confident to say that $1 \equiv \text{hh}$, $2 \equiv \text{lh}$, and $3 \equiv \text{so}$.

We did not include the results by Pennington and Goldsman³⁰⁶, because (i) we were unable to retrace the stated effective masses of the second conduction band in the provided reference²⁹⁶ and (ii) two out of three values were identical to band 1, which contradicted other investigations of band 2. We also excluded the values $m_{MG}^* = 0.58$, $m_{MK}^* = 0.31$, $m_{ML}^* = 0.35$ ¹⁷⁵ because we were unable to acquire the referenced publication by Goano *et al.*³⁰⁷ to confirm them.

According to our statistical analysis (see Fig. 10) the electron masses in literature are clustered closely around the mean values of 0.58 (m_{MG}^*), 0.28 (m_{MK}^*) and 0.31 (m_{ML}^*) with few outliers, for example $m_{MG}^* = 1.2$ ²⁹⁵, $m_{MG}^* = 0.47$ ⁸⁰, $m_{MK}^* < 0.2$ ^{290,295} or $m_{ML}^* = 0.19$ ¹²⁴. Polaron masses deviate not distinguishable. For the second band m_{MG}^* and m_{ML}^* seem to increase while m_{MK}^* decreases, but for meaningful statement more information would be required. This is also the reason why we do not show any statistical analysis on band 2 here.

Although we only found five parameter sets for holes, the agreement among them is bad. Solely for $m_{\Gamma A}^*$ an acceptable spread around the mean of 1.58 was achieved. For $m_{\Gamma M}^*$ the oldest and newest investigation report values of 4.23²⁹⁰ and 2.77²⁹¹ while the remaining ones proposed $m_{\Gamma M}^* < 1$. We considered methodical or temperature differences to explain these discrepancies but were not successful in doing that.

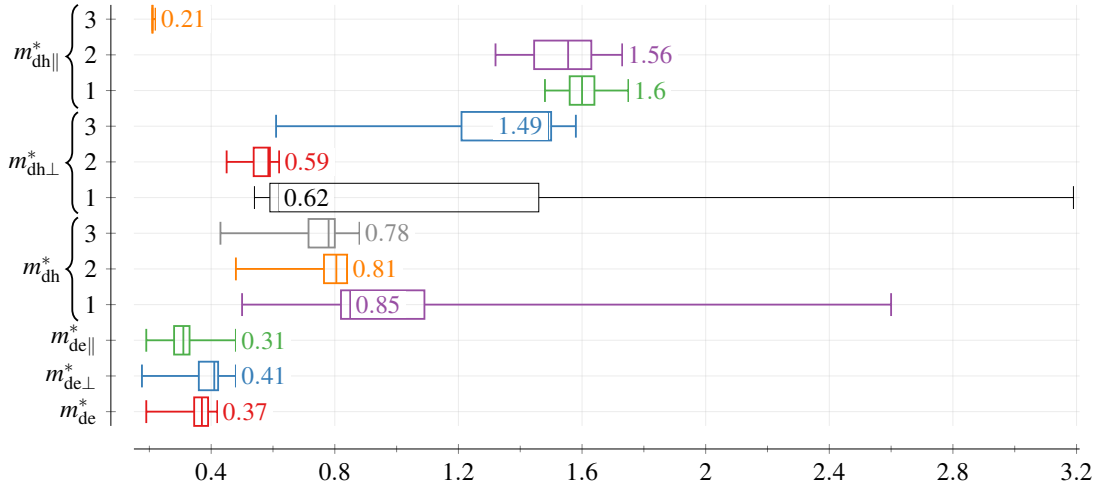


FIG. 11. Distribution of DOS masses. For electrons, we display band 1, and for holes, bands 1, 2, and 3. Shown are the 0th, 25th, 50th, 75th and 100th quartile. The mean value is added in numerical form.

Despite these discrepancies, the DOS masses are a relatively inactive field of research. From the 21 fundamental investigations 17 were conducted in the years 1994 to 2004. In contrast, we found only three papers on this topic within the last 15 years.

2. Density-of-States Mass

For the DOS masses we complemented values found in literature by those computed from the effective masses along the principal directions presented in the previous section using Eq. (7) (see Table IV and Table V). We also show parameters for a third conduction band by Zhao *et al.*¹⁶⁷, which is 2 eV above band 1 in the M-point. Again, the majority (31 out of 40) of the investigations were carried out in the years between 1993 and 2006, versus only five in the last 15 years. Calculations clearly dominate, but the amount of measurements increased significantly: We found eleven^{96,140,253,261,283,285,299,301,302,304} measurements for electrons but still only two^{120,261} for holes.

The statistical analysis shows a comparable distribution for electrons, but an improved variance for holes, especially for bands 2 and 3 (see Fig. 11). For $m_{dh\parallel}^*$ and $m_{dh\perp}^*$ the majority of scientific analyses deliver values < 1 and only few values bigger than 2. This suggest also a higher confidence in the lower masses for the principal directions discussed in the previous section. An exceptional agreement was reached for $m_{dh\parallel}^* = 0.21 \pm 0.01$ of the third band among five publica-

TABLE IV. DOS masses[1/2]. Multiple values for the same band are calculated by differing algorithms.

■ denotes measurements.

ref.	electron				hole				method	polaron
	m_{de}^* [1]	$m_{de\perp}^*$ [1]	$m_{de\parallel}^*$ [1]	band	m_{dh}^* [1]	$m_{dh\perp}^*$ [1]	$m_{dh\parallel}^*$ [1]	band		
[Loma73] ³⁰¹	0.20 ^a	0.21	0.19	—	—	—	—	—	Hall	—
[Loma74] ³⁰²	0.20 ^a	0.21	0.19	—	—	—	—	—	Hall	—
[Gotz93] ²⁷¹	0.19	0.176	0.224	—	—	—	—	—	IR	—
[Kack94] ²⁹⁰	0.31 ^a	0.28 ^b	0.39 ^c	—	2.60 ^a	3.19 ^b	1.73 ^c	hh	DFT-LDA	—
	—	—	—	—	0.84 ^a	0.59 ^b	1.73 ^c	lh	DFT-LDA	—
	—	—	—	—	0.43 ^a	0.61 ^b	0.21 ^c	so	DFT-LDA	—
[Hari95] ⁹⁶	0.35 ^a	0.30 ± 0.07	0.48 ± 0.12	—	—	—	—	—	Raman	—
[Karc95] ²⁶⁴	0.39 ^a	0.45 ^b	0.30 ^c	—	—	—	—	—	DFT-LDA	—
[Kord95] ²⁸⁵	—	0.42	—	—	—	—	—	—	ODCR	y
[Lamb95] ²⁹⁴	0.35 ^a	0.4	0.27	—	—	—	—	—	DFT-LDA	—
[Son95] ²⁹⁹	0.37 ^a	0.42	0.29 ± 0.03	—	—	—	—	—	ODCR	y
[Wenz95] ¹²⁴	0.32 ^a	0.41 ^b	0.19 ^c	—	—	—	—	—	DFT-LDA	—
[Kaec96] ⁶⁵	0.39 ^a	0.43 ^b	0.32 ^c	—	—	—	—	—	DFT-LDA	—
[Nils96] ²²⁷	0.37 ^a	0.43 ^b	0.28 ^c	1	—	—	—	—	DFT-LDA	—
	0.37 ^a	0.33 ^b	0.45 ^c	2	—	—	—	—	DFT-LDA	—
[Pers96] ²⁶³	0.37 ^a	0.40 ^b	0.31 ^c	—	—	—	—	—	DFT-LDA	—
[Volm96] ³⁰⁴	0.39 ^a	0.42 ^b	0.33 ^c	—	—	—	—	—	ODCR	y
[Bako97] ¹³⁹	—	—	—	—	0.84	—	—	1	—	—
	—	—	—	—	0.79	—	—	2	—	—
	—	—	—	—	0.78	—	—	3	—	—
[Chen97] ²⁹⁵	0.42 ^a	0.48 ^b	0.33 ^c	—	—	—	—	—	DFT-LDA	—
[Hemm97] ²⁷⁴	—	—	—	—	1 ^g	—	—	—	FIT	—
[Lamb97] ²⁶⁹	—	—	—	—	0.85 ^a	0.62	1.6	hh	RSPH	—
	—	—	—	—	0.84 ^a	0.62	1.55	lh	RSPH	—
	—	—	—	—	0.81 ^a	1.58	0.21	so	RSPH	—
[Pers97] ¹²⁵	0.37 ^a	0.40 ^b	0.31 ^c	1	0.82 ^a	0.59	1.56	1	DFT-LDA	—
	0.40 ^a	0.43 ^b	0.34 ^c	1	0.82 ^a	0.59	1.6	1	DFT-LDA	—
	0.39 ^a	0.42 ^b	0.33 ^c	1	0.82 ^a	0.59	1.56	2	DFT-LDA	y
	0.44 ^a	0.35 ^b	0.71 ^c	2	0.82 ^a	0.59	1.6	2	DFT-LDA	—
	0.48 ^a	0.38 ^b	0.75 ^c	2	0.78 ^a	1.49	0.21	3	DFT-LDA	—
	0.48 ^a	0.38 ^b	0.77 ^c	2	0.79 ^a	1.49	0.22	3	DFT-LDA	y

$$^a m_{de}^* = (m_{de\perp}^* m_{de\parallel}^*)^{1/3}$$

$$^b m_{de\perp}^* = \sqrt{m_{\text{MF}}^* m_{\text{MK}}^*}$$

$$^c m_{de\parallel}^* = m_{\text{ML}}^*$$

$$^d m_{dh}^* = (m_{dh\perp}^* m_{dh\parallel}^*)^{1/3}$$

$$^e m_{dh\perp}^* = \sqrt{m_{\text{TM}}^* m_{\text{TK}}^*}$$

$$^f m_{dh\parallel}^* = m_{\text{TA}}^*$$

^g fitted to [Pers96]²⁶³

TABLE V. DOS masses[2/2]. Multiple values for the same band are calculated by differing algorithms. █

denotes measurements.

ref.	electron				hole				method	polaron
	m_{de}^*	$m_{de\perp}^*$	$m_{de\parallel}^*$	band	m_{dh}^*	$m_{dh\perp}^*$	$m_{dh\parallel}^*$	band		
	[1]	[1]	[1]		[1]	[1]	[1]			
[Well97] ²⁶²	0.394	–	–	–	–	–	–	–	DFT-LDA	–
[Lind98] ¹¹⁷	–	–	–	–	1.7	–	–	–	DFT-LDA	–
	–	–	–	–	0.48	–	–	–	DFT-LDA	–
[Pers98a] ²⁷⁷	–	–	–	–	0.94	1.46 ^b	1.64 ^c	1	DFT-LDA	–
	–	–	–	–	0.84	0.45 ^b	1.64 ^c	2	DFT-LDA	–
	–	–	–	–	0.88	–	–	3	DFT-LDA	–
[Egil99] ¹⁴⁰	0.37	–	–	–	–	–	–	–	PL	–
[Pers99b] ²⁹²	–	–	–	–	0.85 ^a	0.62	1.61	1	DFT-LDA	–
	–	–	–	–	0.84 ^a	0.61	1.62	1	DFT-LDA	–
	–	–	–	–	0.78 ^a	0.56	1.52	2	DFT-LDA	–
	–	–	–	–	0.78 ^a	0.58	1.42	2	DFT-LDA	–
	–	–	–	–	0.78 ^a	1.5	0.21	3	DFT-LDA	–
	–	–	–	–	0.76 ^a	1.46	0.21	3	DFT-LDA	–
[Tiwa99] ²⁵³	0.36 ^a	0.36	0.36	–	–	–	–	–	IRSE	–
[Bell00] ¹⁷⁵	0.33 ^a	0.36 ^b	0.27 ^c	–	–	–	–	–	EPM	–
[Son00] ²⁶¹	0.39 ^a	0.45 ± 0.02	0.30 ± 0.02	–	0.91 ^a	0.66 ± 0.02	1.75 ± 0.02	–	ODCR	y
[Zhao00] ^{167g}	0.37 ^a	0.42	0.28	1	–	–	–	–	FIT	–
	0.44 ^a	0.35	0.71	2	–	–	–	–	FIT	–
	0.40 ^a	0.66	0.15	3	–	–	–	–	FIT	–
[Zhao00a] ²⁹³	0.37 ^a	0.41 ± 0.02	0.31 ^c	–	–	–	–	–	DFT-LDA	–
[Penn01] ²⁹⁶	0.34 ^a	0.35 ± 0.02	0.31 ± 0.05	–	–	–	–	–	EPM	–
[Iwat03] ²⁶⁶	–	0.41 ^b	–	–	–	–	–	–	DFT-LDA	–
[Iwat03a] ²⁸³	–	0.42 ^b	–	–	–	–	–	–	Hall	–
[Dong04] ²⁶⁵	0.35 ^a	0.38 ^b	0.30 ^c	–	1.09 ^a	0.90 ^b	1.58 ^c	1	DFT-LDA	–
	–	–	–	–	0.72 ^a	0.53 ^b	1.32 ^c	2	DFT-LDA	–
	–	–	–	–	0.67 ^a	1.21 ^b	0.21 ^c	3	DFT-LDA	–
[Chin06] ⁸⁰	–	–	0.38 ^c	–	–	–	–	–	DFT-LDA	–
[Aktu09] ¹⁶⁸	0.40	–	–	–	–	–	–	–	DFT-LDA	–
[Koiz09] ¹²⁰	–	–	–	–	0.5	–	–	–	Hall	–
[Ng10] ²⁹⁷	0.41 ^a	0.45 ^b	0.34 ^c	–	–	–	–	–	GAF	–
[Kuro19] ²⁶⁸	0.36 ^a	0.39 ^b	0.31 ^c	–	0.76 ^a	0.54 ^b	1.48 ^c	–	DFT-LDA	–
[Lu21] ²⁹¹	–	0.40 ^b	–	–	1.97 ^a	2.25 ^b	1.52 ^c	–	DFT-LDA	–

$$^a m_{de}^* = (m_{de\perp}^*{}^2 m_{de\parallel}^*)^{1/3}$$

$$^b m_{de\perp}^* = \sqrt{m_{\text{MI}}^* m_{\text{MK}}^*}$$

$$^c m_{de\parallel}^* = m_{\text{ML}}^*$$

$$^d m_{dh}^* = (m_{dh\perp}^*{}^2 m_{dh\parallel}^*)^{1/3}$$

$$^e m_{dh\perp}^* = \sqrt{m_{\text{TM}}^* m_{\text{TK}}^*}$$

$$^f m_{dh\parallel}^* = m_{\text{TA}}^*$$

$$^g \text{fitted to [Pers97]¹²⁵}$$

tions.

The presented values adhere to some restrictions. Schadt⁸ stated that they are only valid close to the band minimum/maximum as they are calculated there or at very low temperatures. Son *et al.*¹²⁷ claimed that if the polaron effect is added to the results from Persson and Lindefelt^{263, 292}, the values $m_{dh\perp}^* = 0.66$ and $m_{dh\parallel}^* = 1.76$ fit well to the results from ODCR measurements.

The value of M_C changed over the years. In early publications we encountered rather high values of $M_C = 12$ ^{271,308,309} or $M_C = 6$ ^{9,310,311}, but more recent publications agree upon $M_C = 3$ ^{7,8,21,33,36,117,139,141,144,169,205,223,274,277,278,312–314.}

In rare cases, the mathematical models to calculate the DOS masses (cp. Eq. (7)) differed. Pennington and Goldsman³⁰⁶ used $m_{de}^* = \sqrt{m_{MG}^* m_{MK}^*}$, which Tilak, Matocha, and Dunne³¹⁵ reused in combination with $m_{de\perp}^*$ calculated according to Eq. (7). This resulted in $m_{de}^* \approx m_{de\perp}^*$. Persson and Lindefelt²⁷⁷ included only one perpendicular mass into the calculation of the effective mass, i.e., $m_{de}^* = (m_{de\perp}^* m_{de\parallel}^*)^{1/3}$ and Gao *et al.*⁹¹ stated $m_{de}^* = m_{de\parallel}^*$. Ivanov, Magnusson, and Janzén¹¹¹ mixed parallel and perpendicular directions, i.e., $m_{de\perp}^* = \sqrt{m_{ML}^* m_{MK}^*} = 0.32$ resp. $m_{de\parallel}^* = m_{ML}^* = 0.58$. The authors referenced these equations³¹⁶ but we were unable to locate them there. Transformed to the set of equations used in this paper, we got $m_{de\perp}^* = 0.42$ and $m_{de\parallel}^* = 0.33$. A more comprehensive list of all inconsistencies we identified is presented in Section A 2.

3. Temperature Dependency

Wellenhofer and Rössler²⁶² and Tanaka *et al.*⁷⁰ calculated the temperature dependency of the DOS masses (see Fig. 12). Their results showed that the electron mass stays almost constant around 0.4 but predicted for m_{dh}^* an increase of more than 100 % in the range 0 – 200 K. This implies that parameters extracted from calculations at 0 K are quite inaccurate for simulations at 300 K. Despite these large variations, temperature is only occasionally considered in literature^{10,169}. Sozzi *et al.*²⁰⁴ ($m_{de}^* = 0.4$, $m_{dh}^* = 2.6$) and Luo and Madathil³¹⁷ ($m_{de}^* = 0.4$, $m_{dh}^* = 2.64$) extracted explicitly mass values at 300 K from the calculations. Rakheja *et al.*³¹⁸ claimed that the values they used were measured at 300 K, although the referenced investigation²⁶¹ was carried out at 4.4 K.

The result of the calculations by Wellenhofer and Rössler²⁶² can not be written in an implicit form, such that two fittings using Eq. (11) were proposed^{8,144}. The corresponding parameters are shown in Table VI. In Eq. (10) we introduced an approach proposed by Bakowski, Gustafsson,

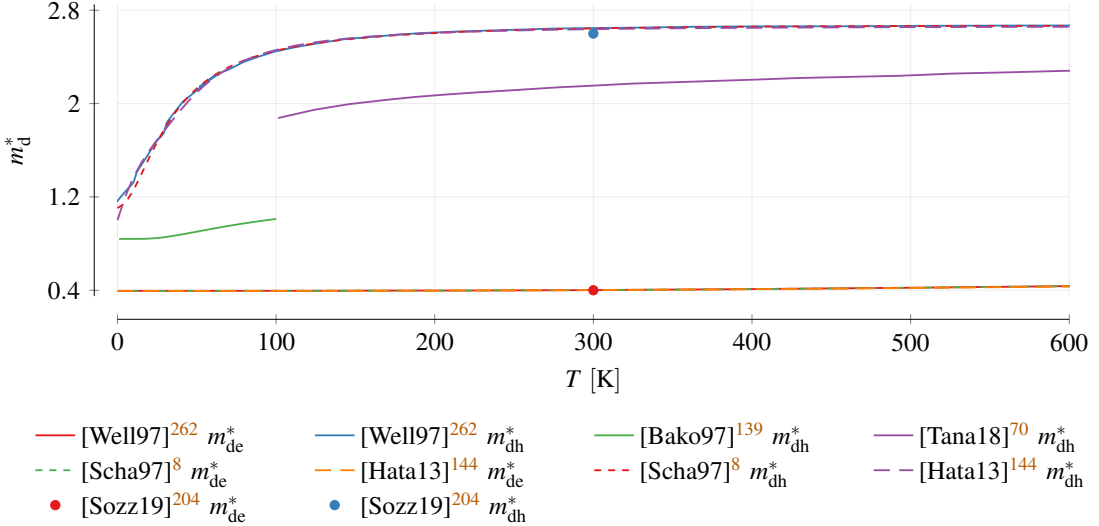


FIG. 12. Temperature dependency of the DOS mass. Dashed lines indicate fittings to the calculations by Wellenhofer and Rössler²⁶².

TABLE VI. Fitting parameters in Eq. (11) to calculations by Wellenhofer and Rössler²⁶².

ref.	mass	z_0	z_1	z_2	z_3	z_4	n_1	n_2	n_3	n_4	η
[Scha97] ⁸	m_{de}^*	0.3944	-6.822×10^{-4}	1.335×10^{-6}	3.597×10^{-10}	0	-1.776×10^{-3}	3.65×10^{-6}	0	0	1
[Scha97] ⁸	m_{dh}^*	1.104	1.578×10^{-2}	3.087×10^{-3}	-7.635×10^{-8}	0	1.387×10^{-2}	1.126×10^{-3}	0	0	1
[Hata13] ¹⁴⁴	m_{de}^*	0.394	0	3.09×10^{-8}	2.23×10^{-10}	-1.65×10^{-13}	0	0	0	0	1
[Hata13] ¹⁴⁴	m_{dh}^*	1	6.92×10^{-2}	0	0	1.88×10^{-6}	0	6.58×10^{-4}	0	4.32×10^{-7}	2/3

and Lindefelt¹³⁹ to combine the three valence bands in the Γ point, which also contained the temperature. Compared to the calculations by Wellenhofer and Rössler²⁶² m_{dh}^* increases only moderately for the coefficients $m_{\text{h1}} = 0.84$, $m_{\text{h2}} = 0.79$, $m_{\text{h3}} = 0.78$, $\Delta E_2 = 9$ meV and $\Delta E_3 = 73$ meV (see Fig. 12). We plotted the model only up to 100 K, because the authors remarked that the presented parameters are only valid for low temperatures. Almost the same values, i.e., $m_{\text{h1}} = 0.82$, $m_{\text{h2}} = 0.82$, $m_{\text{h3}} = 0.78$, $\Delta E_2 = 8.6$ meV and $\Delta E_3 = 72$ meV were reported by Persson and Lindefelt¹²⁵.

4. Origin of Parameters

For electrons (see Fig. 13) we identified the investigations by Götz *et al.*²⁷¹, Son *et al.*²⁹⁹, Persson and Lindefelt²⁶³, Volm *et al.*³⁰⁴, Persson and Lindefelt¹²⁵ and Wellenhofer and Rössler²⁶²

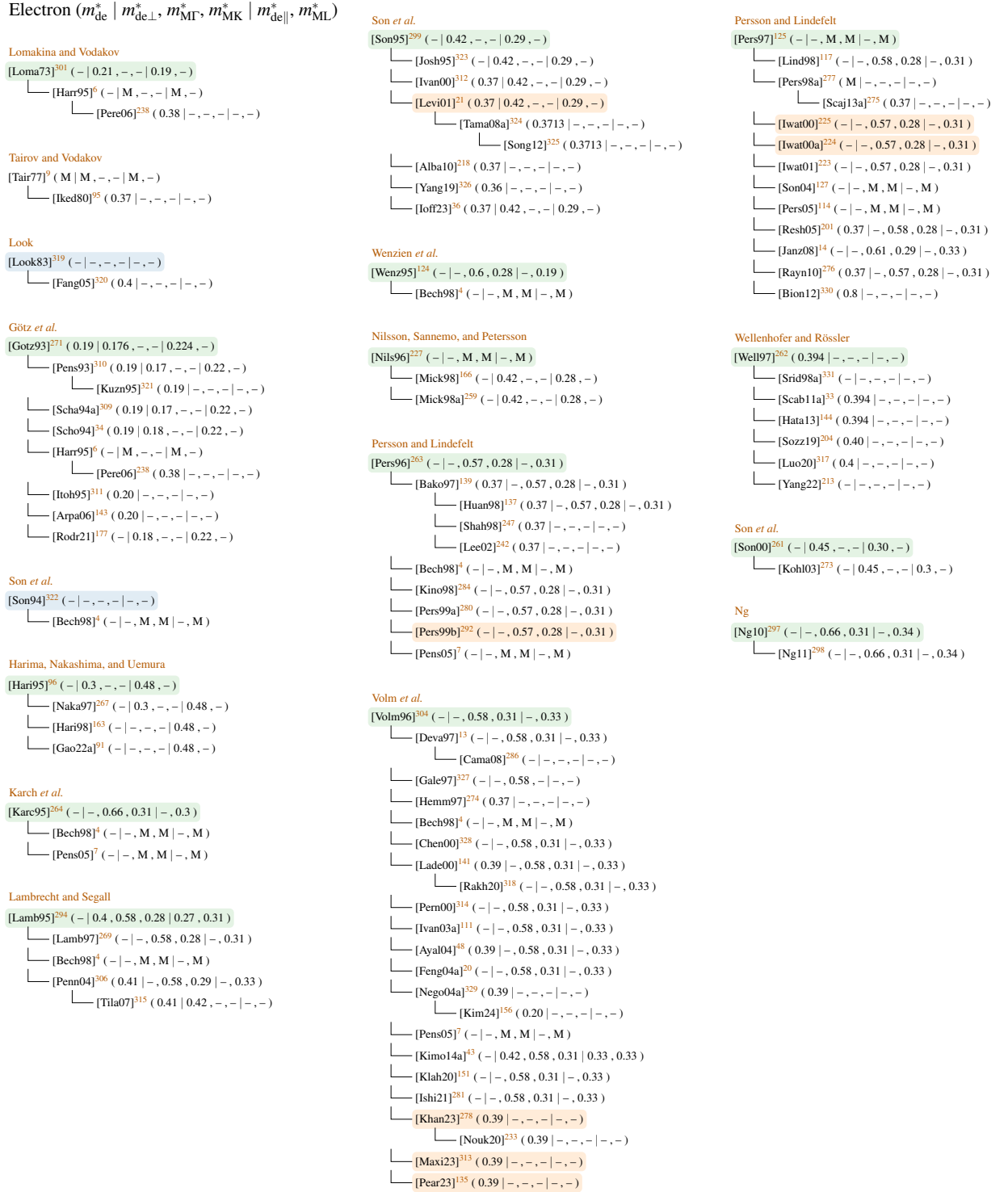


FIG. 13. Reference chain for electron DOS mass. ‘M’ denotes multiple values. ■ were not focused on 4H-SiC, ■ novel analyses on 4H-SiC and ■ shows connections we inferred based on the used data.

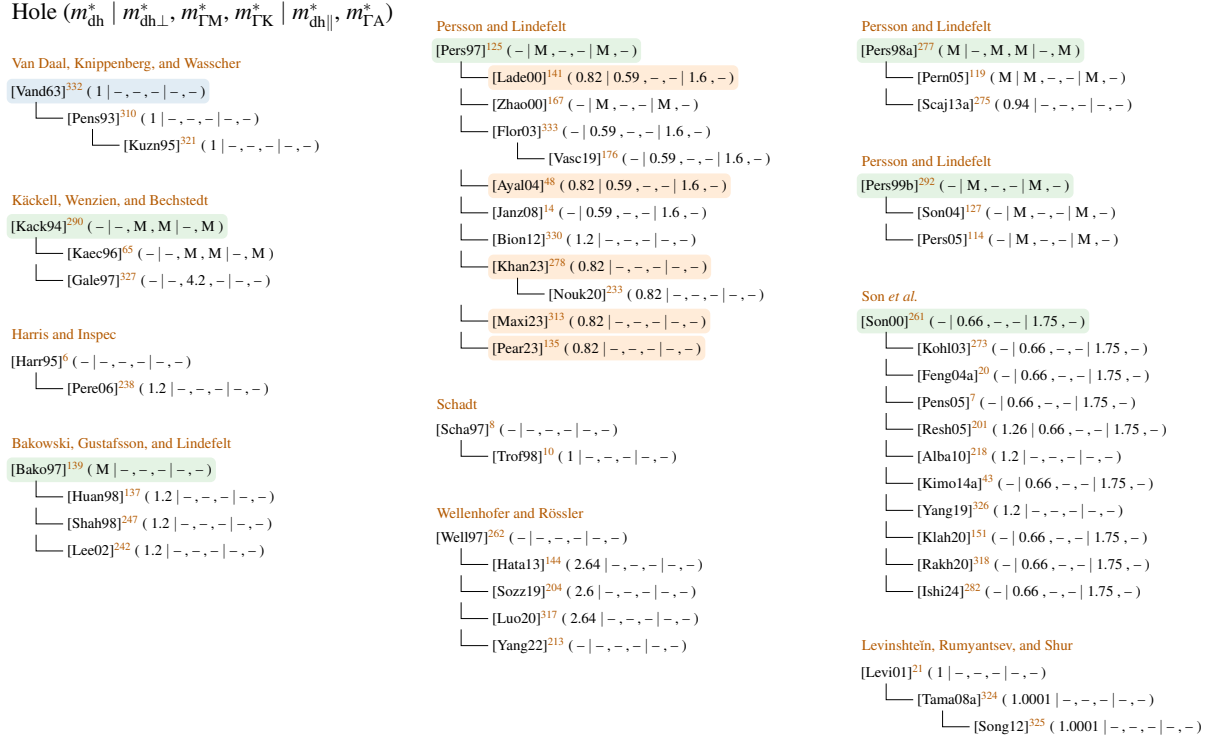


FIG. 14. Reference chain for hole DOS mass. ‘M’ denotes multiple values. █ were not focused on 4H-SiC, █ novel analyses on 4H-SiC and █ shows connections we inferred based on the used data.

as the most influential ones. Upon citation the values were transferred accurately: Solely the parameters proposed by Götz *et al.*²⁷¹ got rounded to two digits. Values were properly referenced, forcing us only occasionally to predict dependencies based on the utilized values and reference chains were found only to a level of two (one intermediate publication). The same statements can be made about hole masses (see Fig. 14), with the difference that only two publications, i.e., Persson and Lindefelt¹²⁵ and Son *et al.*²⁶¹, have more than four citations.

5. Literature Values

For a comprehensive overview of values utilized for m_{de}^* and m_{dh}^* we extended those we found in literature with computations based on fundamental values using Eq. (7) (see Fig. 15). For m_{de}^* we used only the first conduction band but for holes we merged the first two bands using Eq. (9).

For m_{de}^* we found dominantly values of 0.37 ± 0.05 , which matches the mean value of the fundamental studies. For holes the value spread is more significant. Although the majority of fundamental investigations (cp. Fig. 11) agree on values < 1 , e.g., 0.82 and 0.91, we found

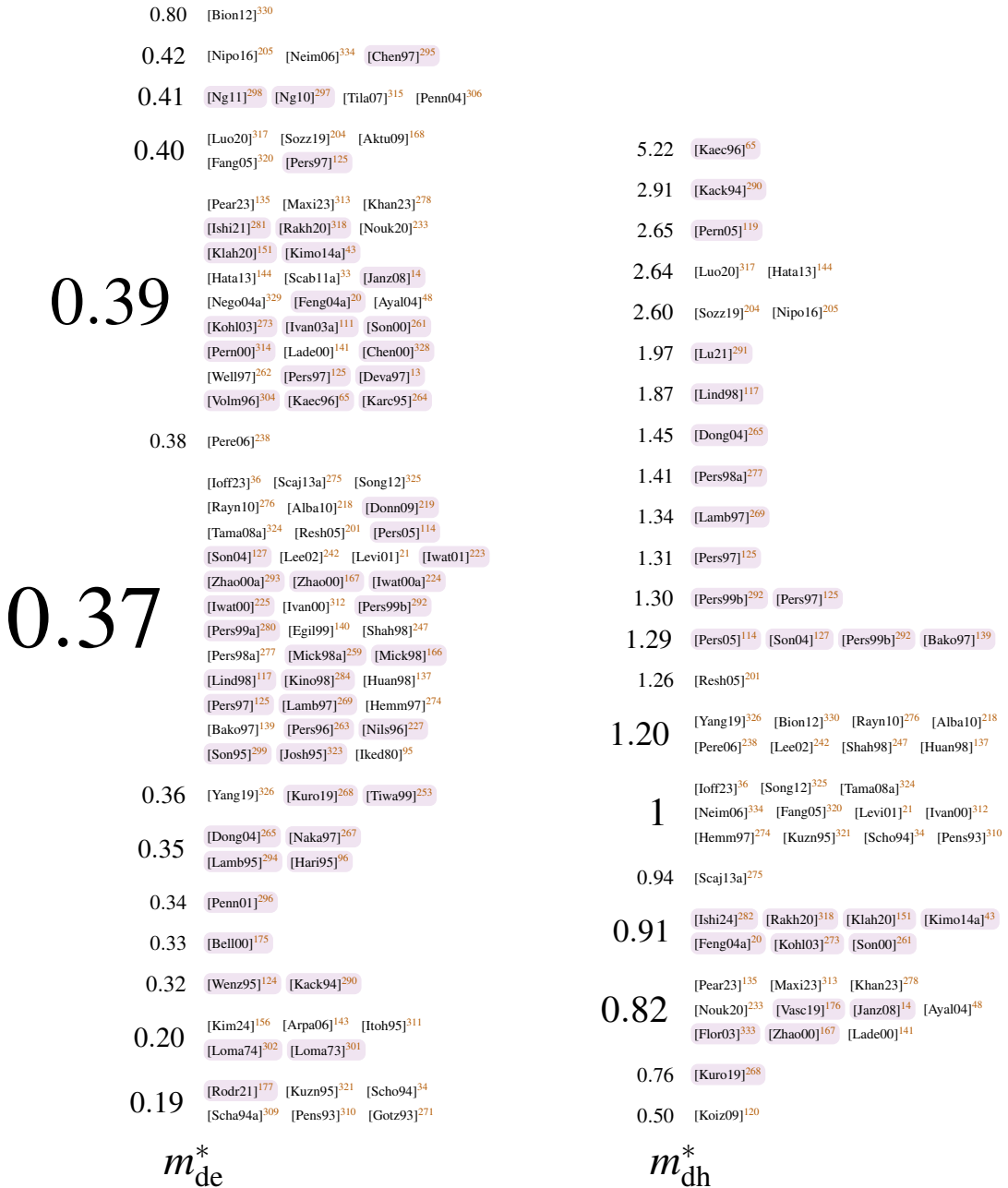


FIG. 15. Effective DOS masses. Size of values indicates abundance in literature. denotes values that we calculated from fundamental masses using Eqs. (7) and (9).

many values ≥ 1 . Possible explanations are high masses from calculations (colored background in the figure), confusions between direction-dependent and effective masses as well as temperature considerations ($m_{\text{dh}}^* = 2.64$ and 2.6).

The value $m_{\text{dh}}^* = 1.2$ has multiple origins: While Bakowski, Gustafsson, and Lindefelt ¹³⁹ derived it from the temperature dependent model at 300 K ^{137,242,247,276} some referenced it from Pers-

son and Lindefelt¹²⁵, where it was stated as m_{ML}^* in 6H³³⁰. A third possibility is that, based on the parameters by Son *et al.*²⁶¹ (cp. Fig. 14), the expression $m_{\text{dh}}^* = (m_{\text{dh}\perp}^* m_{\text{dh}\parallel}^*)^{1/3} = 1.26$ ²⁰¹ was used instead of $m_{\text{dh}}^* = (m_{\text{dh}\perp}^* m_{\text{dh}\parallel}^*)^{1/3} = 0.91$, which then may got rounded to $m_{\text{dh}}^* = 1.2$ ^{218,326}. The prominent value of $m_{\text{dh}}^* = 1$ was often provided without reference or explanation. Only Hemmingsson *et al.*²⁷⁴ fitted it to the calculations by Persson and Lindefelt²⁶³. Pensl *et al.*³³⁵ used the results by Van Daal, Knippenberg, and Wasscher³³², who investigated 6H-SiC.

VI. BAND GAP

The conductivity of a material depends, among others, on the number of free charge carriers, which possess a direction and a momentum-based energy. The physically allowed energy values are described in the *band diagram*: free electrons are located in the *conduction band* and free holes in the *valence band*. When an electron is excited from the valence to the conduction band, e.g., thermally or optically, it leaves a hole behind, such that in each band, a free charge carrier is created. If both bands touch, this generation process is simple, resulting in good conductivity, i.e., a conductor. A large forbidden energy region between the bands, called the *band gap*, makes transitions unlikely, leading to lower conductance, i.e., an insulator. Materials with intermediate band gaps are called *semiconductors*.

TCAD simulations use the band gap energy E_g to determine (i) the local carrier concentration, (ii) the electric currents and (iii) the barrier heights in Schottky contacts. In these cases, E_g is often located in exponent functions, which demands high accuracy to achieve a realistic description. In this section, we will therefore focus on band gap energies by extending previous analyses^{17–19}.

Our research revealed that the majority of the currently used values are, with high confidence, based on measurements conducted in the year 1964^{336–338}. However, these studies focused on the exciton band gap energy, which differs slightly from the band gap, at low temperatures. Coincidentally, recent measurements suggest that these values are reasonable for E_g at room temperature, although the uncertainty in the data is still big. Therefore, further investigations are required for confirmation.

A. Introduction

The band gap in 4H-SiC is measured between the top of the valence band in the Γ -point (see Section III) and the bottom of the conduction band in the M-point^{36,80,127}, making 4H-SiC an *indirect* semiconductor. Consequently, some transfer of moment, e.g., by a phonon, is required to raise an electron from the valence band maximum to the conduction band minimum. To create electron-hole pairs directly in the Γ -point, more than the band gap energy, i.e., the ionization energy, is required. Gsponer *et al.*³³⁹ provided an overview of ionization energies, whereat the authors extracted a value of (7.83 ± 0.02) eV from their own measurements.

The statement that electrons are lifted from the valence to the conduction is not completely accurate. Actually, the electron first forms an exciton by Coulomb interactions with the hole it left behind^{340–343}. This setup can be compared to the hydrogen atom but with larger radii due to the lower effective masses (cp. Section V). Additional energy has to be provided to inject the electron into the conduction band. Consequently, the band gap energy E_g is the sum of the energy required to generate the exciton, i.e., the *exciton band gap energy* E_{gx} , and the energy to free the electron from the exciton, i.e., the *free exciton binding energy* E_x (see Eq. (17))²¹⁸.

$$E_g = E_{gx} + E_x \quad (17)$$

An exciton is neutral and thus roams easily within the lattice, but it can achieve an energetically more favorable configuration by attaching itself to an impurity³⁴⁰. The energy reduction relative to E_{gx} is denoted as *bound* exciton binding energy^{53,95,151,271,285,308,340,344–348}, which depends on the impurity atom, the lattice site and the charge state³³⁷.

In our review, we found it quite challenging to distinguish the free and bound exciton binding energy, although they describe different processes and must not be confused. The main reasons were: (1) Both are denoted by the same symbol E_x . (2) They share similar values in the range of a few meV. (3) Publications often use only the term exciton binding energy.

The band gap energy is not constant. First and foremost, it varies among the polytypes of silicon carbide. It was empirically shown that the band gap scales linearly with the degree of hexagonality, i.e., the ratio of hexagonal to cubic lattice sites^{43,336,338,349} (4H-SiC has a hexagonality of 50 %³⁵⁰). In addition, the band gap shows a pressure³⁵, strain²⁶⁸, temperature and doping dependency. It is important to take these influences into account because shifting band edges can create potential barriers that then influence the carrier transport³⁵¹.

In this review, we describe changes in the band gap by Eq. (18). $E_g(T)$ denotes the temperature dependent variations and $\Delta E_g(N_D^+, N_A^-)$ the doping dependent ones, with N_D^+/N_A^- the concentration of ionized donors/acceptors (see also Section IX).

$$E_g(T, N_D^+, N_A^-) = E_g(T) - \Delta E_g(N_D^+, N_A^-) \quad (18)$$

1. Temperature Dependency

The temperature is equivalent to the amount of lattice vibrations in a material, which can cause a shift of the band energies and the electron-lattice interaction energy³⁵². Since these changes are not uniform for all bands, the effective band gap is altered³⁵³.

The temperature dependent band gap (see Eq. (19))³⁵ contains effects from thermal expansion ($\Delta E_{\text{th}}(T)$) and electron-phonon interaction ($\Delta E_{\text{ph}}(T)$). These effects are hard to separate in experiments³⁵; we only found one example⁹³ in literature where such distinction was made. In general, the models for $\Delta E_{\text{ph}}(T)$ are used to describe both with reasonable accuracy, because $\Delta E_{\text{th}}(T)$ has a much weaker impact³⁵⁴ and the scaling of both contributions is comparable³⁵⁵. Arvanitopoulos *et al.*¹⁴⁶ extended Eq. (19) by adding an additive term Δ_g^{Fermi} to account for carrier statistics. This is, however, only necessary for devices whose size is close to the de-Broglie wavelength.

$$E_g(T) = E_g(0) - \Delta E_{\text{th}}(T) - \Delta E_{\text{ph}}(T) \quad (19)$$

At high temperatures the band gap decreases linearly^{141,356,357} while for low temperatures non-linear, i.e., quadratic³⁵⁷ or plateau-like, behavior³⁵⁸ was observed. An empirical law to describe the temperature dependent band gap is the Varshni relation (see Eq. (20))³⁵⁹, with T_g as arbitrary characterization temperature. In this case, $E_g \propto T^2$ at low temperatures.

$$E_g(T) = E_g(T_g) + \alpha \left(\frac{T_g^2}{T_g + \beta} - \frac{T^2}{T + \beta} \right) \quad (20)$$

Two shortcomings of the Varshni relation were reported^{354,355,358}: First, available data sets can not be approximated simultaneously for low and high temperatures^{360,361}. For example, Pässler³⁶¹ tried to match the values from Choyke, Hamilton, and Patrick³³⁶ but achieved only unrealistic results. Second, it is impossible to correlate the parameters of the Varshni relation with physical mechanism-specific quantities. For example, β was said to be approximately the Debye temperature, but we even found negative values in the literature^{206,362,363}. For these reasons, Ščajev and

Jarašiūnas³⁶⁴ proposed a description that explicitly used the Debye temperature Θ_D (see Eq. (21)).

$$\begin{aligned} E_g(T) &= E_g(0) - a_D f_D(\Theta_D, T) \\ f_D(\Theta_D, T) &= \frac{18 k_B T^4}{\Theta_D^3} \int_0^{\Theta_D/T} (\exp(x) - 1)^{-1} x^3 dx \end{aligned} \quad (21)$$

Plateau-like behavior at cryogenic temperatures is achieved by physics-based models of Bose-Einstein type (see Eq. (22))^{358,365} with Θ_B as the mean frequency of the involved phonons and α_B as the strength of the electron-phonon interaction³⁵.

$$E_g(T) = E_B - \alpha_B \left(1 + \frac{2}{e^{\Theta_B/T} - 1} \right) \quad (22)$$

The rate of change of the band gap at low temperatures depends on the phonon dispersion Δ of a material³⁶¹. Eq. (20) is most accurate for $\Delta > 1$ ^{357,366} and Eq. (22) represents the lower limit ($\Delta \rightarrow 0$), most suitable for $\Delta < \frac{1}{3}$ ³⁶¹. Since the dispersion of most semiconductors is in the range of $0.3 - 0.6$ ³⁶¹ Pässler^{354,361} proposed the model shown in Eq. (23) with ε the entropy and Θ_p as the average phonon temperature.

$$\begin{aligned} E_g(T) &= E_g(0) - \frac{\varepsilon \Theta_p}{2} \left[\sqrt[p]{1 + \left(\frac{2T}{\Theta_p} \right)^p} - 1 \right] \\ p &\approx \sqrt{\frac{1}{\Delta^2} + 1} \end{aligned} \quad (23)$$

This model was subsequently extended by Pässler³⁵⁷ to cover a wider phonon dispersion (Δ) range and, thus, promises to bridge the gap between Eq. (20) and Eq. (22). Because this advanced description has not been adopted by the community yet, we will employ the more commonly used model described in Eq. (23) in this review.

2. Doping Dependency

Doping-dependent changes of the band gap are caused by many-body effects of free carriers, i.e., their interactions with dopants and with each other. These become dominant for small carrier-to-carrier distances³⁶⁷. Possible are interactions within a band, across bands, and with ionized dopants^{117,367,368}. These effects were investigated extensively on their own³⁶⁷ and were, for 4H-SiC, eventually merged by Lindefelt¹¹⁷ (see Eq. (24)) for ionized charge carrier concentrations (see Section IX) above a few $10^{18}/\text{cm}^3$ based on a similar analysis for silicon by Jain and Roulston³⁶⁸. $E_{(n/p)(c/v)}$ denotes the changes to the conduction (c) resp. valence (v) band due to

n- or p-type doping. With increasing doping concentrations, the conduction band energy level drops, i.e., $\Delta E_{\text{nc}} < 0$ and $\Delta E_{\text{pc}} < 0$, and the valence band energy level increases, i.e., $\Delta E_{\text{nv}} > 0$ and $\Delta E_{\text{pv}} > 0$. To correctly account for the overall reduction of the band gap, also called *band gap narrowing*, in Eq. (18), the factors concerning the conduction band are subtracted in the first line of Eq. (24). The term C_{pv} was added later in an extension proposed by Persson, Lindefelt, and Sernelius¹²⁶.

$$\begin{aligned}
\Delta E_{\text{g}}(N_{\text{D}}^{+}, N_{\text{A}}^{-}) &= \Delta E_{\text{VB}} - \Delta E_{\text{CB}} \\
&= \Delta E_{\text{nv}}(N_{\text{D}}^{+}) + \Delta E_{\text{pv}}(N_{\text{A}}^{-}) - \Delta E_{\text{nc}}(N_{\text{D}}^{+}) - \Delta E_{\text{pc}}(N_{\text{A}}^{-}) \\
\Delta E_{\text{nc}}(N_{\text{D}}^{+}) &= A_{\text{nc}} \left(\frac{N_{\text{D}}^{+}}{10^{18}} \right)^{1/3} + B_{\text{nc}} \left(\frac{N_{\text{D}}^{+}}{10^{18}} \right)^{1/2} < 0 \\
\Delta E_{\text{nv}}(N_{\text{D}}^{+}) &= A_{\text{nv}} \left(\frac{N_{\text{D}}^{+}}{10^{18}} \right)^{1/4} + B_{\text{nv}} \left(\frac{N_{\text{D}}^{+}}{10^{18}} \right)^{1/2} > 0 \\
\Delta E_{\text{pc}}(N_{\text{A}}^{-}) &= A_{\text{pc}} \left(\frac{N_{\text{A}}^{-}}{10^{18}} \right)^{1/4} + B_{\text{pc}} \left(\frac{N_{\text{A}}^{-}}{10^{18}} \right)^{1/2} < 0 \\
\Delta E_{\text{pv}}(N_{\text{A}}^{-}) &= A_{\text{pv}} \left(\frac{N_{\text{A}}^{-}}{10^{18}} \right)^{1/3} + B_{\text{pv}} \left(\frac{N_{\text{A}}^{-}}{10^{18}} \right)^{1/2} + C_{\text{pv}} \left(\frac{N_{\text{A}}^{-}}{10^{18}} \right)^{1/4} > 0
\end{aligned} \tag{24}$$

We found publications that grouped the contributions to the band gap narrowing by doping type and, occasionally, also merged the parameters and the denominator 10^{18} . This description is often referred to as Jain-Roulston model³⁶⁸ (see Eq. (25)). The correlations among the parameters of Eqs. (24) and (25) result to $A_{\text{xc}}^{\text{j}}/A_{\text{xc}} = 10^{-6}$, $A_{\text{xc}}^{\text{j}}/A_{\text{xv}} \approx 3.162 \times 10^{-5}$ and $B_{\text{xy}}^{\text{j}}/B_{\text{xy}} = 10^{-9}$ with $x \in \{\text{n}, \text{p}\}, y \in \{\text{c}, \text{v}\}$. For better comparison, we transferred all parameters of Eq. (25) to their respective counterparts in Eq. (24), except the sum of B_{xy} , which could not be separated.

$$\begin{aligned}
\Delta E_{\text{g}}(N_{\text{D}}^{+}, N_{\text{A}}^{-}) &= \Delta E_{\text{gp}}(N_{\text{A}}^{-}) + \Delta E_{\text{gn}}(N_{\text{D}}^{+}) \\
\Delta E_{\text{gn}}(N_{\text{D}}^{+}) &= -A_{\text{nc}}^{\text{j}} (N_{\text{D}}^{+})^{1/3} + (B_{\text{nv}}^{\text{j}} - B_{\text{nc}}^{\text{j}}) (N_{\text{D}}^{+})^{1/2} + A_{\text{nv}}^{\text{j}} (N_{\text{D}}^{+})^{1/4} \\
\Delta E_{\text{gp}}(N_{\text{A}}^{-}) &= -A_{\text{pc}}^{\text{j}} (N_{\text{A}}^{-})^{1/3} + (B_{\text{pv}}^{\text{j}} - B_{\text{pc}}^{\text{j}}) (N_{\text{A}}^{-})^{1/2} + A_{\text{pv}}^{\text{j}} (N_{\text{A}}^{-})^{1/4}
\end{aligned} \tag{25}$$

An alternative approach to describe the doping dependency is the Slotboom model (see Eq. (26)), which was originally developed for Si. N denotes the sum of all dopants and $N_{\text{n,p}}$ a reference concentration. Ruff, Mitlehner, and Helbig³⁶⁹ proposed parameters for 6H before Lades¹⁴¹ fitted Eq. (26) to the results of Eq. (24).

$$\Delta E_{\text{g}} = C_{\text{n,p}} \left(\ln \left(\frac{N}{N_{\text{n,p}}} \right) + \sqrt{\left(\ln \left(\frac{N}{N_{\text{n,p}}} \right) \right)^2 + G} \right) \tag{26}$$

Finally, the band gap reduction can also be interpreted as renormalization due to electron-electron interactions alone, which Schubert³⁶⁷ described by Eq. (27).

$$\Delta E_g = \frac{e^2}{4\pi\epsilon r_s} \quad (27)$$

The screening radius r_s depends on the charge carrier concentration n and is given by the Debye and Thomas-Fermi radii for the non-degenerate (see Eq. (28)) and degenerate (see Eq. (29)) case³⁶⁷.

$$\Delta E_g = \frac{e^3 \sqrt{n}}{4\pi\epsilon^{3/2} \sqrt{k_B T}} \quad (\text{Debye, non-degenerate}) \quad (28)$$

$$\Delta E_g = \frac{e^3 \sqrt{m_{de}^* (3n)^{1/3}}}{4\pi^{5/3} \epsilon^{3/2} \hbar} \quad (\text{Thomas-Fermi, degenerate}) \quad (29)$$

State-of-the-art TCAD tools only support Eqs. (20), (24) and (26) out of the box, although some feature the possibility to write custom code for band gap narrowing. Eq. (25) is only partially supported, which can cause problems if solely the sum $(B_{nv}^j - B_{nc}^j)$ respectively $(B_{pv}^j - B_{pc}^j)$ is provided in the literature.

3. Methods

Appropriate methods to determine the band gap were partially discussed by De Napoli² and Nava *et al.*⁶³. One possibility are measurements, e.g., transmission spectroscopy (TS)^{86,93}, spectroscopic ellipsometry⁹⁴, photo absorption (PA)^{336,337,360,370}, optical admittance (OA)³⁷¹, exciton electroabsorption (EE)³⁴⁸, free carrier absorption (FCA)³⁵⁶, free exciton luminescence (FEL)³⁴⁷, photoluminescence (PL)^{285,346,372}, photoconductivity (PC)³⁷³, transient absorption spectrum (TAS)³⁷⁴, optical absorption spectrum (OAS)³⁷⁵ and wavelength-modulated absorption (WMA)^{151,376}. Sometimes, the results of multiple measurements are combined to improve the accuracy⁵³. Stefanakis and Zekentes¹⁵ stated that the free carrier absorption method overestimates the band gap while optical absorption studies deliver more accurate results.

Calculations are a common alternative and include empirical pseudopotentials (EP)^{175,377-379}, density functional theory based local density approximation (DFT-LDA)^{80,125,127,198,265,268,291,293,295,380}, rectangular barriers of finite height (RB)³⁸¹ and estimations based on the crystal hexagonality (HEX)³³⁸. Available results in literature were approximated by fitting (FIT)^{21,43,141,142,144} and genetic algorithm fitting (GAF)²⁹⁷.

B. Results & Discussion

In the time span from the early 1960s until today, we identified 51 fundamental investigations. Out of those were 21 measurements, 20 calculations, 6 fittings to existing data and 4 models whose origin could not be determined (see Tables VII and VIII). Seven out of the 51 fundamental investigations were published within the last five years, showing that research on the band gap is still very active.

Ivanov *et al.*³⁷³ conducted the only measurement of the band gap energy E_g at temperatures below 5 K, who extracted a value of ≈ 3.285 eV. This is consistent with the analysis by Galeckas *et al.*³⁵⁶ who measured the absorption coefficient down to 50 K and then added measurement values taken at 2 K by Sridhara, Devaty, and Choyke³⁸⁸ to extrapolate $E_g(0) = 3.285$ eV. At slightly elevated temperatures Miller *et al.*³⁷⁵ ((3.378 ± 0.001) eV at 15 K) and Ewvaraye, Smith, and Mitchel³⁷¹ ((3.41 ± 0.03) eV at 40 K) achieved higher values for the band gap.

An explanation for this lack of data on E_g is the fact the exciton band gap E_{gx} was mainly determined for low temperatures. We found seven investigations that agreed remarkably well on $E_{gx}(0) = 3.265$ eV (see Fig. 16 for a statistical representation). Grivickas *et al.*³⁶⁰ predicted $E_{gx}(0) = 3.267$ eV by combining measurements down to 100 K with the low-temperature results by Itoh, Kimoto, and Matsunami³⁴⁶. The authors thereby shifted the latter, which predicted $E_{gx}(4.25) = 3.265$ eV³⁴⁶, by 2 meV to achieve a better match with their own results.

The free exciton binding energy E_x was extracted either directly from measurements^{347,348,360,373} or calculated by using the reduced mass of the electron-hole pair m_{red} and the permittivity ϵ in the hydrogen model shown in Eq. (30)^{151,343}.

$$E_x = \frac{m_{\text{red}} e^4}{2 \hbar^2 \epsilon^2} \quad (30)$$

The values of E_x range from 10 – 40 meV, whereas Devaty and Choyke¹³ argued that 10 meV³⁴⁷, which denote the activation energy for thermal quenching of free excitons, is too low to be the free exciton binding energy. Two out of five investigations propose an average value of 20 meV, which would match the observation of $E_{gx} = 3.265$ eV and $E_g = 3.285$ eV below five Kelvin.

At room temperature, measurements were only conducted for E_g . The spread of values is, compared to E_{gx} at low temperatures, big (cp. Fig. 16). Single measurements, such as the investigation by Ahuja *et al.*⁸⁶ with an uncertainty of 98 meV, showed variations in the range of a few %. Even the latest three results published in the last seven years propose values of (3.26 ± 0.04) eV. A possible explanation are doping-dependent band gap variations. Therefore, we ordered the results by

TABLE VII. Band gap energies and temperature dependency fittings according to Eq. (20) [1/2].

indicates research not focused on 4H-SiC and  calculations.

ref.	band gap				temperature dep.		range [K]	method
	E_g [eV]	E_{gx} [eV]	E_x [meV]	T_g [K]	α [eV/K]	β [K]		
[Choy57] ^{370 a}	–	–	–	–	3.3×10^{-4}	–	300 – 710	PA
[Choy64] ³³⁶	–	3.263 ± 0.003	–	4	–	–	–	PA
[Choy64a] ^{337 b}	–	3.265	–	4.7	–	–	–	PA
[Zanm64] ³³⁸	–	3.23	–	300	–	–	–	HEX
[Jung70] ³⁷⁸	2.8	–	–	0	–	–	–	EP
[Dubr75] ³⁴⁸	–	–	20.0 ± 1.5	2	–	–	–	EE
[Dubr77] ³⁸¹	3.2	–	–	0	–	–	–	RB
[Ikeda80b] ³⁴⁷	–	3.2639	10	77	–	–	–	FEL
[Gavr90] ³⁸²	2.89	–	–	0	–	–	–	DFT-LDA
[Back94] ³⁷⁷	3.28	–	–	0	–	–	–	EP
[Park94] ³⁸³	2.14	–	–	0	–	–	–	EP
[Kord95] ²⁸⁵	–	3.265	–	4.2	–	–	–	PL
[Wenz95] ¹²⁴	3.56	–	–	0	–	–	–	DFT-LDA
[Evwa96] ³⁷¹	3.41 ± 0.03	–	–	40	–	–	–	OA
[Itoh96] ^{346 b}	–	3.265	–	4.25	–	–	–	PL
[Kaec96] ⁶⁵	2.18	–	–	0	–	–	–	DFT-LDA
[Chen97] ²⁹⁵	3.27	–	–	0	–	–	–	DFT-LDA
[Pers97] ¹²⁵	2.9	–	–	0	–	–	–	DFT-LDA
[Vanh97] ³⁷⁹	3.28	–	–	0	–	–	–	EP
[Ivan98] ³⁷²	–	3.266	–	2	–	–	–	PL
[Bell00] ¹⁷⁵	3.05	–	–	0	–	–	–	EP
[Lade00] ^{141 d}	–	3.265	40	0	3.3×10^{-4}	1050	4 – 200	FIT
	–	3.265	40	0	3.3×10^{-2}	1×10^5	4 – 600	FIT
	–	3.342	40	0	3.3×10^{-4}	0	300 – 700	FIT
[Mill00] ³⁷⁵	3.378 ± 0.001	–	–	15	–	–	–	OAS
[Srid00] ³⁷⁶	–	3.267	–	2	–	–	–	WMA
[Zhao00a] ²⁹³	3.11	–	–	0	–	–	–	DFT-LDA
[Levi01] ^{21 c}	3.23	–	–	300	6.5×10^{-4}	1300	0 – 800	FIT
[Ahuj02] ⁸⁶	3.260 ± 0.098	–	–	300	–	–	–	TS

^a according to the shown band gap, the data are for 21R but others¹³⁹ denote them as 6H^b solely measurement for lowest temperature shown^c model fitted to results by Choyke⁵³^d model fitted to 6H-SiC results by Choyke and Patrick³⁸⁴

TABLE VIII. Band gap energies and temperature dependency fittings according to Eq. (20) [2/2].

indicates research not focused on 4H-SiC and  calculations.

ref.	band gap				temperature dep.		range	method
	E_g [eV]	E_{gx} [eV]	E_x [meV]	T_g [K]	α [eV/K]	β [K]		
[Gale02] ³⁵⁶	3.285	–	–	0	3.5×10^{-4}	1100	0 – 650	FCA
	3.2625	–	–	300	2.4×10^{-4}	0	300 – 650	FCA
[Ivan02] ³⁷³	3.285	–	20.5 ± 1.0	2	–	–	–	PC
[Shal02] ³⁸⁵	3.18	–	–	300	–	–	–	PL
[Dong04] ²⁶⁵	2.194	–	–	0	–	–	–	DFT-LDA
[Son04] ¹²⁷	3.35	–	–	0	–	–	–	DFT-LDA
[Bala05] ^{362 a}	3.26	–	–	300	4.15×10^{-4}	–131	–	–
[Chin06] ⁸⁰	2.433	–	–	0	–	–	–	DFT-LDA
[Griv07] ³⁶⁰	–	3.267	30 ± 10	0	–	–	0 – 500	PA
[Tama08a] ^{324 a}	3.23	–	–	300	7.036×10^{-4}	1509	–	–
[Ng10] ²⁹⁷	3.28	–	–	0	–	–	–	GAF
[Khal12] ^{386 a}	3.285	–	–	0	2.206×10^{-2d}	1×10^5	–	–
[Hata13] ^{144 c}	3.285	3.265	–	0	9.06×10^{-4}	2030	0 – 800	FIT
[Kimo14a] ^{43 c}	–	3.265	–	2	8.2×10^{-4}	1800	0 – 800	FIT
[Stef14] ^{15 b}	3.285	–	–	0	3.3×10^{-4}	240	–	–
[Fang18] ³⁷⁴	3.22	–	–	300	–	–	–	TAS
[Yama18] ³⁸⁰	3.12	–	–	0	–	–	–	DFT-LDA
[Kuro19] ²⁶⁸	3.15	–	–	0	–	–	–	DFT-LDA
[Klah20] ¹⁵¹	–	3.2659	40	1.4	–	–	–	WMA
[Lech21] ^{142 a}	3.265	–	–	0	10.988×10^{-3}	32 744.3	–	FIT
[Lu21] ²⁹¹	3.17	–	–	0	–	–	–	DFT-LDA
[Chen22] ⁹³	3.28	–	–	300	5.27×10^{-4}	0	300 – 620	TS
[Huan22b] ³⁸⁷	3.18	–	–	0	–	–	–	DFT-LDA
[Torr22] ¹⁹⁸	3.17	–	–	0	–	–	–	DFT-LDA
[Main24] ⁹⁴	3.30 ± 0.02	–	–	300	–	–	–	SE

^a origin of Varshni parameters unknown^b values referenced from a TCAD tool manual, no corresponding scientific publication found^c model fitted to results by Choyke⁵³^d this parameter is negative in the paper, leading to an increasing band gap with temperature^e model fitted to results by Miller *et al.*³⁷⁵

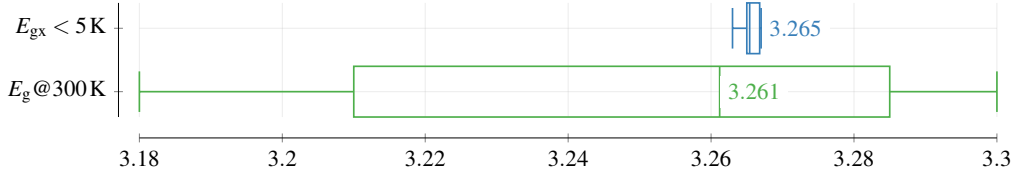


FIG. 16. Statistical analysis of band gap measurements. Shown are the 0th, 25th, 50th, 75th and 100th quartile. The mean value is added in numerical form.

the utilized n-type doping concentration in Table IX. However, no clear tendency could be identified, meaning that future research is required to converge on a common value or find a suitable explanation for the deviations.

TABLE IX. Measurements of E_g at 300 K ordered by the utilized n-type doping concentration.

ref.	dopant	doping conc.	band gap	
			[1/cm ³]	[eV]
[Chen22] ⁹³	–	–		3.28
[Gale02] ³⁵⁶	N	$(7 - 40) \times 10^{14}$		3.2625
[Shal02] ³⁸⁵	N	1×10^{16}		3.18
[Fang18] ³⁷⁴	–	1.1×10^{18}		3.22
[Main24] ⁹⁴	–	3.7×10^{18}		3.30 ± 0.02
[Ahuj02] ⁸⁶	–	7×10^{18}		3.260 ± 0.098

Compared to measurements, the results achieved by calculations are in less agreement. The values for $E_g(0)$, which is the only quantity that was calculated in the past, show a much larger spread with occasionally more than 100 meV lower values than measurements. Even the latest five publications published in the past seven years do not show an improvement in this regard because the proposed values of $E_g = (3.15 \pm 0.03)$ eV are way below the measurements of $E_g(2) \approx 3.285$ eV³⁷³.

We only found one publication that described the anisotropy³⁶⁰ of the band gap. The results revealed uniform exciton (band gap) energies for fields parallel resp. perpendicular to the c-axis.

1. Temperature Dependency

We found four measurement campaigns on the temperature dependency of the band gap in 4H-SiC^{93,337,356,360}. Additional models^{21,43,141,144} were developed by fitting to data published in

the 1960s^{53,336,337} (see Tables VII and VIII). Since the development of dedicated temperature-dependent models only started in the 2000s, earlier publications were forced to rely on models developed for 6H-SiC^{139,389}. However, in 2004⁴⁸ and even in 2015³⁹⁰, 6H based models were still in use for 4H-SiC, showing the importance of a comprehensive literature overview on this topic.

Some of the proposed model parameters^{15,142,324,362,386} could not be related to any scientific publication, but in some cases to default values of prominent TCAD simulation suites¹⁵. Although Tamaki *et al.*³²⁴ provided a reference¹³⁶, we were unable to reproduce their parameters. The model by Khalid, Riaz, and Naseem³⁸⁶ is extraordinary, as it has a positive temperature dependency, i.e., an increase of the band gap with temperature is predicted. In our opinion, the chances are high that this was a typographical error, and we corrected the value for this review.

In the analyzed publications, the model in Eq. (20) is predominantly used to describe the temperature dependency. The respective parameters are shown in Tables VII and VIII. We did not include $\alpha = 3.2 \times 10^{-4}$ eV/K and $\beta = 565$ K presented by Grivickas *et al.*³⁶⁰, because the sole purpose of these values was to highlight the bad fit to the experimental data. Nevertheless, they still got referenced by Levcenco *et al.*³⁹¹. The model introduced in Eq. (23) was utilized only once by Grivickas *et al.*³⁶⁰ with the parameters shown in Eq. (31). The model proposed by Ščajev and Jarašiūnas³⁶⁴ (see Eq. (21)) used the parameters shown in Eq. (32), which were fitted to data by Miller *et al.*³⁷⁵.

$$\Theta_p = 450\text{K} , \varepsilon = 3 \times 10^{-4}\text{eV/K} , p = 2.9 \quad (31)$$

$$E_g(0) = 3.3762\text{eV} , a_D = 1.31 , \Theta_D = (1000 \pm 50)\text{K} \quad (32)$$

For an easier comparison, we plotted all the measurements and models presented earlier (see Fig. 17). The fittings^{21,43,392} to the data by Choyke⁵³ are all very similar, so we only show two out of the three explicitly. Clearly observable is the similarity of these models with the one proposed by Tamaki *et al.*³²⁴, suggesting that also the latter was fitted to Choyke⁵³. Similarly, the parameters provided by Lechner¹⁴² reproduce the fitting from Lades¹⁴¹ (4 – 600 K), causing us to not show the former. The results by Ščajev and Jarašiūnas³⁶⁴ are not shown as they are identical to those by Miller *et al.*³⁷⁵.

We identified some confusion between E_g and E_{gx} in the literature. For example, some authors^{15,21,142,324} stated that they describe E_g but the values agree more to E_{gx} . The model by Khanna²⁷⁸ matches E_g at low temperatures, but at around 200K, it is equal to E_{gx} and follows that value from there onward. The fitting by Balachandran, Chow, and Agarwal³⁶² is only feasible

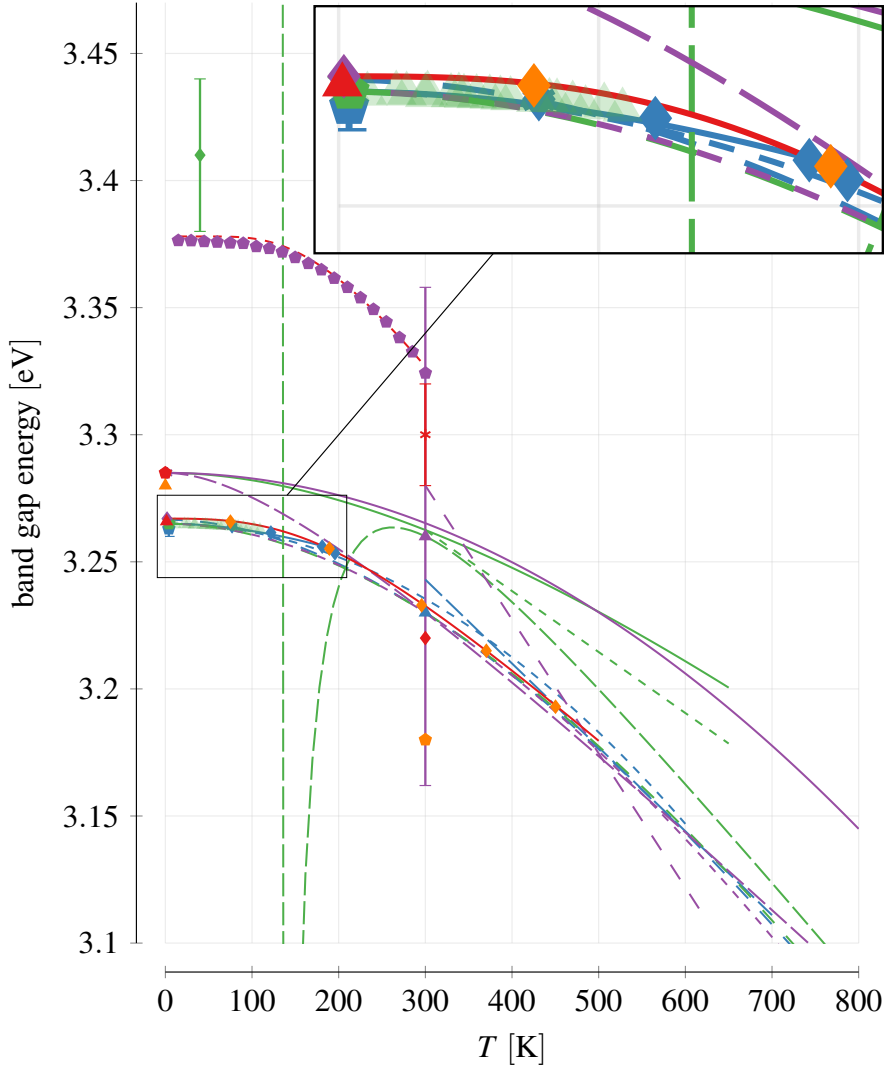


FIG. 17. Band gap measurements and models. The latter are only shown in the interval used during characterization, with their corresponding equations referenced at the end of each entry.

for $T \geq 300$ K as it has a singularity at 131 K. Newer models, e.g., the one by Cheng, Yang, and Zheng⁹³, suggested a steeper slope, actually crossing the traces of E_{gx} with E_g .

The plateau described by Eq. (23) is barely visible, showing that the deviations are only subtle. Lades¹⁴¹ approximated the shape with the Varshni model by just fitting it in a very narrow temperature range. The phonon dispersion of 4H-SiC $\Delta = 0.29$ ³⁶⁰ is rather low, which would actually indicate that Eq. (22) is the most suitable; however, Eq. (23) seems to be accurate as well. Even more, Stefanakis and Zekentes¹⁵ compared the single models and identified Eq. (20) as the most suitable one.

Miller *et al.*³⁷⁵ is the only publication we found that used Eq. (22). The authors also proposed a second fitting (see Eq. (33)) with the difference that the exponent -1 was missing. Due to unreasonable results, we consider this a typographical error that we corrected in this review. The values achieved with $E_g(0) = (3.378 \pm 0.001)$ eV, $\kappa = 0.345 \pm 0.031$ and $\theta_E = 613 \pm 23$ were equal to those by Eq. (22) so we do not show them explicitly.

$$E_g(T) = E_g(0) - \kappa (\exp(\theta_E/T) - 1)^{-1} \quad (33)$$

In the figure, the tremendous spread of measurement values for $E_g(300)$ is visible. Clearly, no conclusive statements can be made based on these data, highlighting the need for further detailed analyses. It would also be possible to use $E_g = E_{gx} + E_x$ for this purpose. However, we did not find any investigations of E_x with increasing temperature.

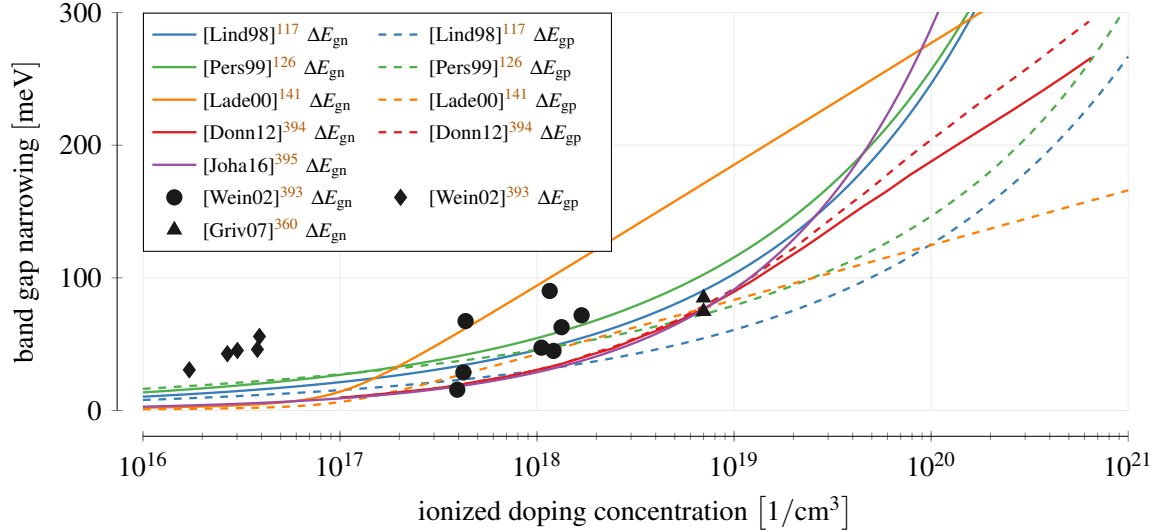
2. Doping Dependency

We encountered two fittings for the doping-dependent narrowing model in Eq. (24) (see Table X), which are solely based on calculations. Measurement results are available^{360,393}, but due to their sparsity (see Fig. 18), they are not suitable to verify the calculations. The models predict an increasing rate of change with doping concentration, whereas the narrowing induced by n-type doping is bigger than the one by p-type doping. The additional parameters proposed by Persson, Lindefelt, and Sernelius¹²⁶ only led to small differences.

Lindefelt¹¹⁷ highlighted that the valence band displacement is larger than the one of the conduction band (see Fig. 19). In their model, this is consistent for both doping types. Other publications distributed the band gap narrowing equally across valence and conduction band¹⁴⁶ or chose a contribution of $|\Delta E_c| / |\Delta E_g| = 0.7$ ³⁹⁴. The model predictions are right in the middle of these

TABLE X. Parameters for ionized dopants induced band gap narrowing in Eq. (24).

ref.	method	n-type				p-type				
		A_{nc} [meV]	B_{nc} [meV]	A_{nv} [meV]	B_{nv} [meV]	A_{pc} [meV]	B_{pc} [meV]	A_{pv} [meV]	B_{pv} [meV]	C_{pv} [meV]
[Lind98] ¹¹⁷	calculation	-15	-2.93	19	8.74	-15.70	-0.39	13	1.15	-
[Pers99] ¹²⁶	calculation	-17.91	-2.20	28.23	6.24	-16.15	-1.07	-35.07	6.74	56.96


 FIG. 18. Doping induced band gap narrowing due to n- (E_{gn}) and p-type (E_{gp}) doping. Black dots denote measurements.

two cases, i.e., around a value of 0.6.

For the Slotboom model, that is used by various publications^{48,141,142}, we found one set of parameters¹⁴¹ (see Table XI). In contrast to the other models, the band gap narrowing is linear in the semi-logarithmic plot (see Fig. 18). Up to a doping concentration of $10^{20}/\text{cm}^3$, the predictions for p-type doping-induced narrowing are comparable to the earlier model, but for n-type doping, they are up to 100 % higher.

The band gap narrowing according to Eq. (29) is also shown because it is occasionally used in literature^{15,394}. Stefanakis and Zekentes¹⁵ used a slightly different form of the Thomas-Fermi radius shown in Eq. (34) with n_0 as the equilibrium carrier density.

$$\Delta E_g = \frac{e^2}{4\pi\epsilon_0\epsilon_s} \left(\frac{3n_0e^2}{2\epsilon_0 E_F} \right)^{1/2} \quad (34)$$

Unfortunately we were unable to reproduce the results achieved by this formalism in the mentioned publications so we extracted the curves from Donnarumma, Palankovski, and Selberherr³⁹⁴. Jo-

TABLE XI. Parameters for ionized dopants induced band gap narrowing Slotboom model.

ref.	type	<i>C</i>	<i>N</i>	<i>G</i>
		[eV]	[1/cm ³]	[1]
[Lade00] ¹⁴¹	n	2×10^{-2}	10^{17}	0.5
	p	9×10^{-3}	10^{17}	0.5

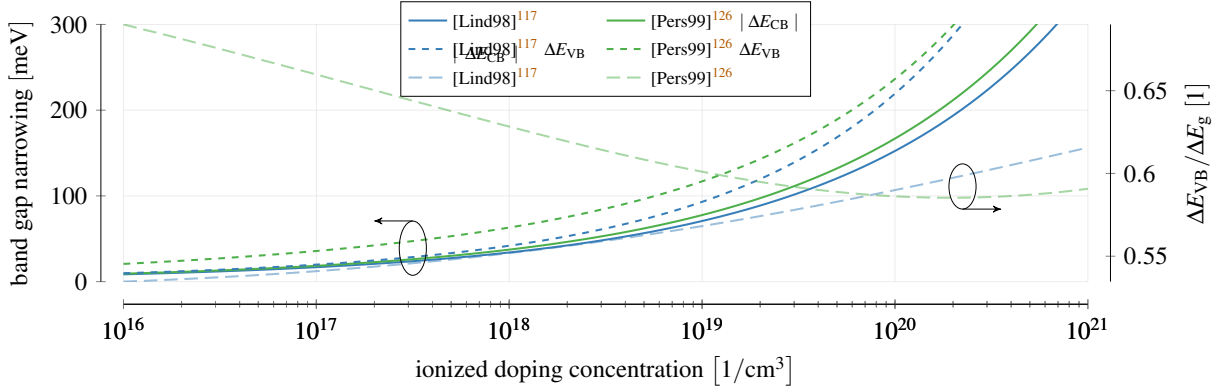


FIG. 19. Doping induced band gap narrowing. The changes to the conduction and valence band are shown for both dopants.

hannesson and Nawaz³⁹⁵ used the Debye radius from Eq. (28) scaled by 3/4, based on the calculations by Lanyon and Tuft³⁹⁶.

Miller *et al.*³⁷⁵ analyzed semi-insulating and doped 4H-SiC (without providing further details such as the doping concentration) with the surprising result that the band gap for the latter is bigger. Fang *et al.*³⁷⁴ only registered a band gap narrowing of 10 meV, which is explainable by the employed doping concentrations of $1.1 \times 10^{18}/\text{cm}^3$ and $9.1 \times 10^{18}/\text{cm}^3$.

3. Origin of Parameters

Tracing parameters back to their origin was a challenging task because frequently references were missing. From the ones that were stated and some that we inferred based on the used values, we concluded that the most influential publications are from 1964 by Choyke, Hamilton, and Patrick³³⁶ and Choyke, Patrick, and Hamilton³³⁷ (see Fig. 20). The outcome of more recent measurements was not yet adopted in the scientific community.

Through reference chains, the values previously found in low-temperature measurements were altered. Already in 1970 Junginger and Van Haeringen³⁷⁸ rounded the values of $E_{\text{gx}} = 3.263\text{ eV}$

Band Gap (E_g , E_{gx} , T)

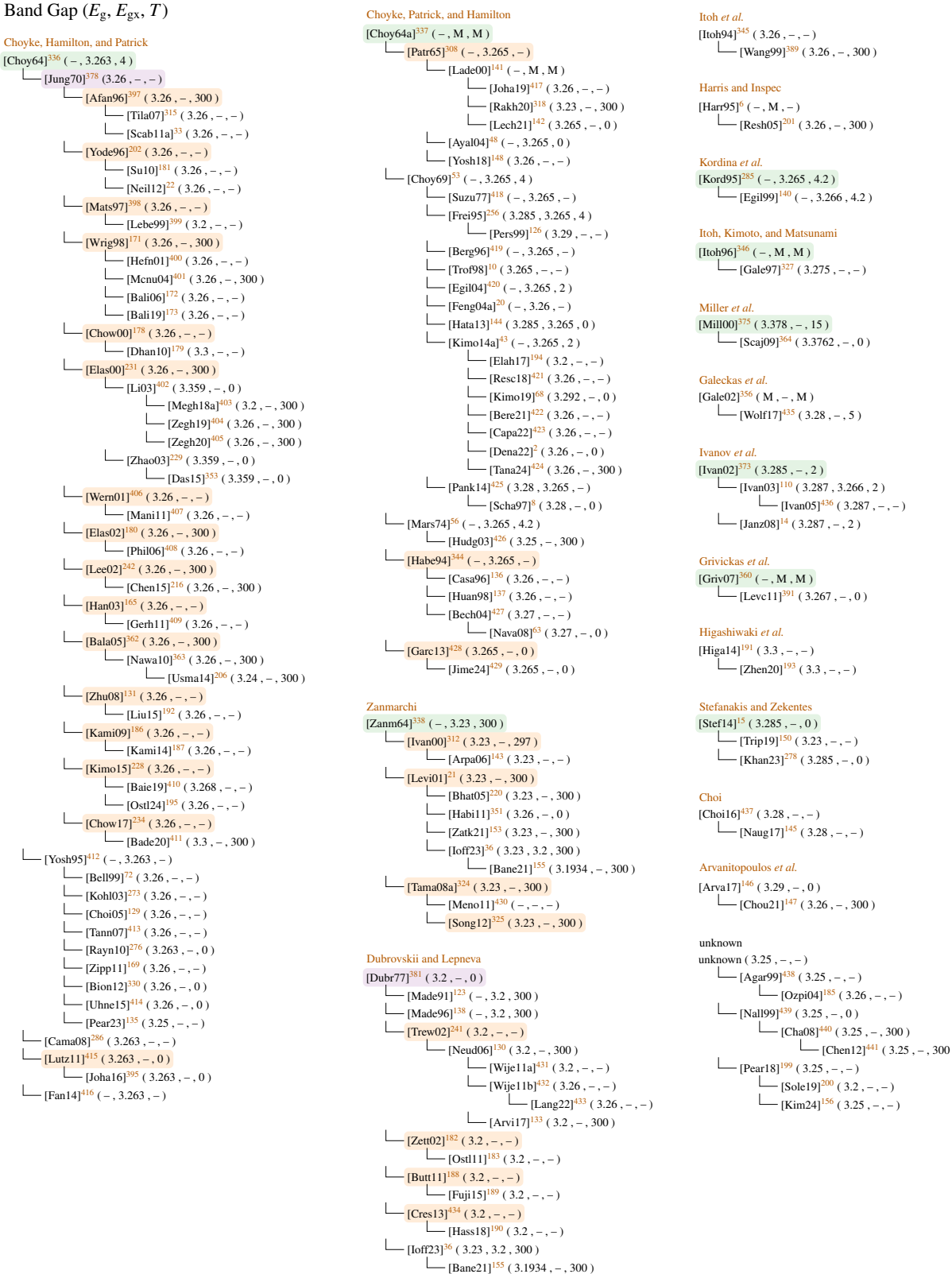


FIG. 20. Reference chain for band gap energies. are fundamental investigations, calculations and connections predicted from the used values.

to $E_g = 3.26\text{ eV}$, i.e., changing both value and meaning. This was not the only time that we found such a change in literature^{2,72,129,169,273,330,413,414,417,421–423}, sometimes even extended by a change of the temperature to 300 K. We also found evidence that $E_g = 3.26\text{ eV}$ was turned into $E_g = 3.3\text{ eV}$ ¹⁷⁹ or $E_g = 3.2\text{ eV}$ ³⁹⁹. The latter was also derived from $E_g = 3.25\text{ eV}$ ²⁰⁰ and proposed by Dubrovskii and Lepneva³⁸¹ based on measurements, although some references^{36,123,138} interpreted it as exciton band gap energy. The value $E_{gx} = 3.23\text{ eV}$ was first introduced by Zanmarchi³³⁸, but we were unable to find a direct connection to $E_g = 3.23\text{ eV}$. Rakheja *et al.*³¹⁸ used this value based on the models proposed by Lades¹⁴¹, but we were unable to reproduce it. We only achieved $E_g = 3.23\text{ eV}$ by using the 2H band gap from Persson and Lindefelt¹²⁵ and scaling it with temperature. $E_g = 3.25\text{ eV}$ was derived once from $E_{gx} = 3.265\text{ eV}$ ⁴²⁶ and once from $E_{gx} = 3.263\text{ eV}$ ¹³⁵, but no temporal coherent connections could be found. We thus summarized publications featuring this value in the figure under the reference *unknown*.

Sometimes it is beneficial to look at the missing data to reason about the validity of certain values: We did not find a single measurement that proposed a band gap energy at room temperature of either $E_g = 3.2\text{ eV}$, 3.23 eV or $E_g = 3.25\text{ eV}$. These values were exclusively extracted from models that were characterized by low-temperature measurements of E_g and sometimes even E_{gx} , as we showed in the previous section. The only exception is $E_g = 3.26\text{ eV}$, which was derived by Ahuja *et al.*⁸⁶. However, the uncertainty of 98 meV stated by the authors is so big that it also contains all other energy values mentioned so far.

The main source for the free exciton binding energy is the analysis by Dubrovskii and Sankin³⁴⁸ from 1975 (see Fig. 21). Results based on 6H are available^{442,443} but were rarely utilized. The overall amount of references in regard to E_x is very limited: the latest ones we found were from the year 2014.

The most commonly used temperature scaling factor $\alpha = 3.3 \times 10^{-4}\text{ eV/K}$ (see Fig. 22) was determined by Choyke and Patrick³⁷⁰ in 1957 for an undefined polytype of SiC. Bakowski, Gustafsson, and Lindefelt¹³⁹ and Yoshida⁴¹² argued that it was 6H but the shown absolute band gap energy ($\approx 2.9\text{ eV}$ at 0 K) indicates a different polytype. Despite that, a wide range of 4H-SiC fittings up to this day utilize this value, implying that 4H and 6H share the same temperature dependency²²⁹. The also popular $\alpha = 6.5 \times 10^{-4}\text{ eV/K}$ was proposed by Levenshtein, Rumyantsev, and Shur²¹ based on a fitting to the low-temperature measurements by Choyke⁵³ (basically the same data as in Choyke, Patrick, and Hamilton³³⁷). Therefore, most of the parameters for the temperature dependency are based on data from the 50s and 60s.

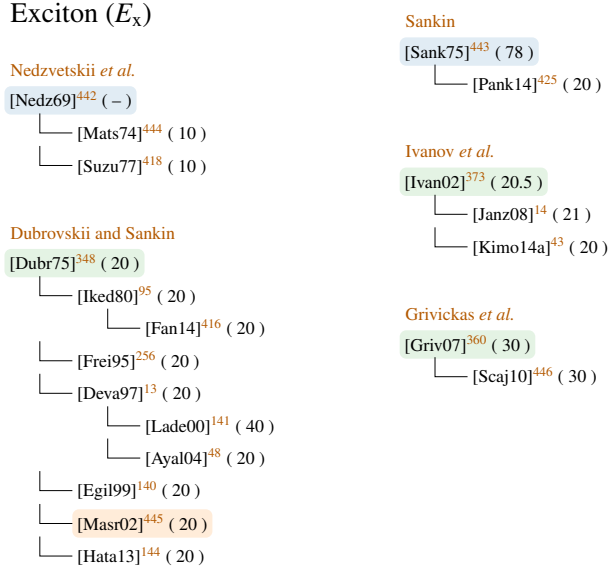


FIG. 21. Reference chain of the free exciton binding energy E_x . indicates values that were not determined for 4H-SiC, fundamental investigations and connections predicted from the used values.

In contrast to the band gap energy, more recent models for the temperature dependency were also utilized in the literature. In some occasions, we were again either unable to identify the measurements used for the model fitting^{324,362} or the models were based on the same old data^{43,144}.

In regard to variations caused by doping, the publication by Lindefelt¹¹⁷ is the most referenced (see Fig. 23) one. Its values were transferred in most cases without changes, although the usage of Eq. (25) made a direct comparison of the parameters challenging. For example, B_{nc} and B_{nv} resp. B_{pc} and B_{pv} got merged^{207,218,404,405} but also A_{pc} and C_{pv} ⁴⁴⁸. Occasionally, we identified typographical mistakes, which we documented together with all other detected inconsistencies in Section A 3.

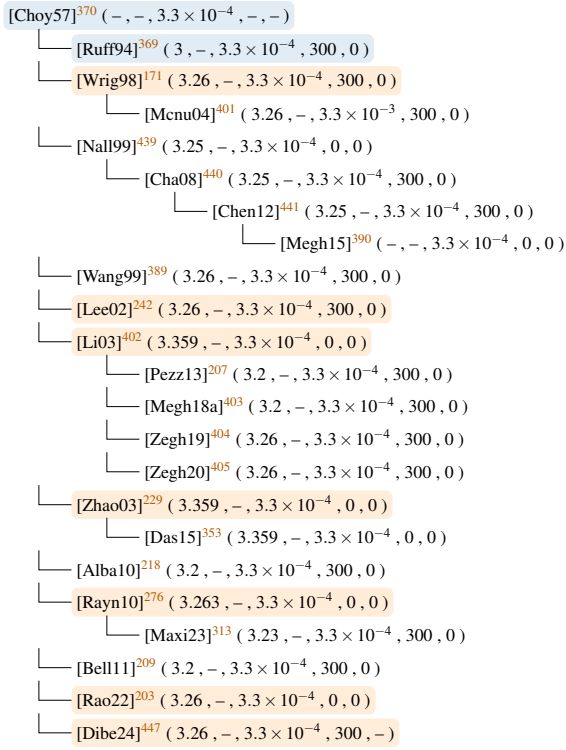
4. Literature Values

In the previous section, we discussed the changes to measurement results along reference chains. Together with models that utilize various combinations of energy values and temperature scaling factors, these lead to many (exciton) band gap energy values in literature (see Fig. 24).

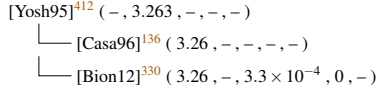
The majority of calculations for E_g at 0 K reported rather low values. In our opinion, the origin of this discrepancy is not well understood because recent investigations also predicted values of

Varshni (E_g , E_{gx} , α , T_g , β)

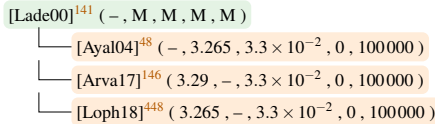
Choyke and Patrick



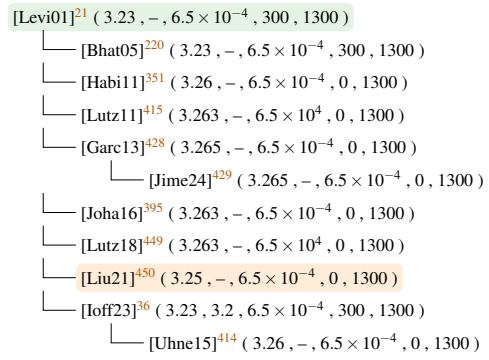
Yoshida



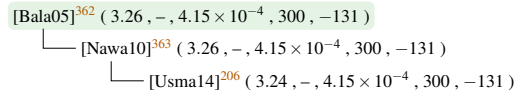
Lades



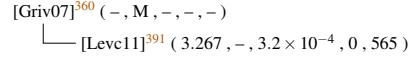
Levinshtein, Rumyantsev, and Shur



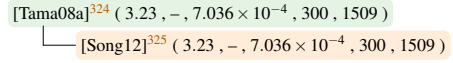
Balachandran, Chow, and Agarwal



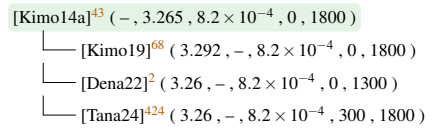
Grivickas et al.



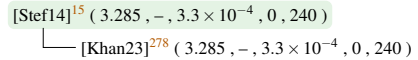
Tamaki et al.



Kimoto and Cooper



Stefanakis and Zekentes



Passler (E_{gx} , ε , Θ_p , p)

Grivickas et al.

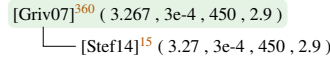


FIG. 22. Reference chain for the temperature dependency of the band gap. indicates values that were not determined for 4H-SiC, are fundamental investigations and connections predicted from the used values.

Lindefelt ($A_{\text{nc}} / A_{\text{nv}}$) [$B_{\text{nc}} / B_{\text{nv}}$] { $A_{\text{pc}} / A_{\text{pv}}$ } | $B_{\text{pc}} / B_{\text{pv}}$ | (C_{pv})

Lindefelt

[Lind98]¹¹⁷ ($-1.5 \times 10^{-2} / 1.9 \times 10^{-2}$) [$-2.93 \times 10^{-3} / 8.74 \times 10^{-3}$] { $-1.57 \times 10^{-2} / 1.3 \times 10^{-2}$ } | $-3.87 \times 10^{-4} / 1.15 \times 10^{-3}$ | (-)
 └── [Levi01]²¹ ($-1.5 \times 10^{-2} / 1.9 \times 10^{-2}$) [$-2.93 \times 10^{-3} / 8.74 \times 10^{-3}$] { $-1.57 \times 10^{-2} / 1.3 \times 10^{-2}$ } | $-3.87 \times 10^{-4} / 1.15 \times 10^{-3}$ | (-)
 └── [Well01]⁴⁵¹ (- / -) [- / -] { - / - } | - / - | (-)
 └── [Cha08]⁴⁴⁰ ($-1.5 \times 10^{-2} / 1.9 \times 10^{-2}$) [$-2.93 \times 10^{-3} / 8.74 \times 10^{-3}$] { - / - } | - / - | (-)
 └── [Chen12]⁴⁴¹ ($-1.5 \times 10^{-2} / 1.9 \times 10^{-2}$) [$-2.93 \times 10^{-3} / 8.74 \times 10^{-3}$] { - / - } | - / - | (-)
 └── [Alba10]²¹⁸ ($-1.5 \times 10^{-2} / 1.9 \times 10^{-2}$) [1.7×10^{-2}] { $-1.57 \times 10^{-2} / 1.3 \times 10^{-2}$ } | 1.54×10^{-2} | (-)
 └── [Zhan10]⁴⁵² ($-1.5 \times 10^{-2} / 1.9 \times 10^{-2}$) [$-2.93 \times 10^{-3} / 8.74 \times 10^{-3}$] { - / - } | - / - | (-)
 └── [Bell11]²⁰⁹ ($-1.5 \times 10^{-2} / 1.9 \times 10^{-2}$) [1.17×10^{-2}] { $-1.57 \times 10^{-2} / 1.3 \times 10^{-2}$ } | 1.54×10^{-3} | (-)
 └── [Habi11]⁵⁵¹ ($-1.5 \times 10^{-2} / 1.9 \times 10^{-2}$) [$-2.93 \times 10^{-3} / 8.74 \times 10^{-3}$] { $-1.57 \times 10^{-2} / 1.3 \times 10^{-2}$ } | $-3.87 \times 10^{-4} / 1.15 \times 10^{-3}$ | (-)
 └── [Buon12]⁶⁶ ($-1.5 \times 10^{-2} / -1.9 \times 10^{-2}$) [$-2.93 \times 10^{-3} / -8.74 \times 10^{-3}$] { - / - } | - / - | (-)
 └── [Pezz13]²⁰⁷ ($-1.5 \times 10^{-2} / 1.9 \times 10^{-2}$) [1.17×10^{-2}] { $-1.57 \times 10^{-2} / 1.3 \times 10^{-2}$ } | 1.54×10^{-3} | (-)
 └── [Stef14]¹⁵ ($-1.5 \times 10^{-2} / 1.9 \times 10^{-2}$) [$-2.93 \times 10^{-3} / 8.74 \times 10^{-3}$] { $-1.57 \times 10^{-2} / 1.3 \times 10^{-2}$ } | $-3.87 \times 10^{-4} / 1.15 \times 10^{-3}$ | (-)
 └── [Megh18a]⁴⁰³ ($-1.5 \times 10^{-2} / 1.9 \times 10^{-2}$) [1.17×10^2] { $-1.57 \times 10^{-2} / 1.3 \times 10^{-2}$ } | 1.54×10^{-3} | (-)
 └── [Zegh19]⁴⁰⁴ ($-1.5 \times 10^{-2} / 1.9 \times 10^{-2}$) [1.17×10^{-2}] { $-1.57 \times 10^{-2} / 1.3 \times 10^{-2}$ } | 1.54×10^{-3} | (-)
 └── [Zegh20]⁴⁰⁵ ($-1.5 \times 10^{-2} / 1.9 \times 10^{-2}$) [1.17×10^{-2}] { $-1.57 \times 10^{-2} / 1.3 \times 10^{-2}$ } | 1.54×10^{-3} | (-)
 └── [Ioff23]³⁶ ($-1.5 \times 10^{-2} / -1.9 \times 10^{-2}$) [$-2.93 \times 10^{-3} / -8.74 \times 10^{-3}$] { $-1.57 \times 10^{-2} / -1.3 \times 10^{-2}$ } | $-3.87 \times 10^{-4} / -1.15 \times 10^{-3}$ | (-)
 └── [Maxi23]³¹³ ($-1.5 \times 10^{-2} / 1.9 \times 10^{-2}$) [$-2.93 \times 10^{-3} / 8.74 \times 10^{-3}$] { $-1.57 \times 10^{-2} / 1.3 \times 10^{-2}$ } | $-3.87 \times 10^{-4} / 1.15 \times 10^{-3}$ | (-)

Persson, Lindefelt, and Sernelius

[Pers99]¹²⁶ ($-1.791 \times 10^{-2} / 2.823 \times 10^{-2}$) [$-2.2 \times 10^{-3} / 6.24 \times 10^{-3}$] { $-1.615 \times 10^{-2} / -3.507 \times 10^{-2}$ } | $-1.07 \times 10^{-3} / 6.74 \times 10^{-3}$ | (5.696×10^{-2})
 └── [Nipo16]²⁰⁵ (- / -) [- / -] { - / - } | - / - | (-)
 └── [Loph18]⁴⁴⁸ ($-1.791 \times 10^{-2} / 2.823 \times 10^{-2}$) [$-2.2 \times 10^{-3} / 6.24 \times 10^{-3}$] { $-7.311 \times 10^{-2} / 3.507 \times 10^{-2}$ } | $-1.07 \times 10^{-3} / 6.74 \times 10^{-3}$ | (-)

Slotboom ($C_{\text{n}} / N_{\text{n}}$) ($C_{\text{p}} / N_{\text{p}}$) (G)

Lades

[Lade00]¹⁴¹ ($2 \times 10^{-2} / 1 \times 10^{17}$) ($9 \times 10^{-3} / 1 \times 10^{17}$) (5×10^{-1})
 └── [Ayal04]⁴⁸ ($2 \times 10^{-2} / 1 \times 10^{17}$) ($9 \times 10^{-3} / 1 \times 10^{17}$) (5×10^{-1})
 └── [Lech21]⁴² ($2 \times 10^{-2} / 1 \times 10^{17}$) (- / -) (5×10^{-1})

FIG. 23. Reference chain for the doping dependency of the band gap. If solely a single value is shown for parameter B then the publication only provided $B_{\text{xc}} + B_{\text{xc}}$. are fundamental investigations and connections predicted from the used values.

(3.15 ± 0.03) eV. Models and measurements < 5 K derived higher values, starting at 3.25 eV up to > 4 eV. These extreme values often indicate that the respective parameters were fitted to 300 K because the model in Eq. (20) is not able to simultaneously describe the band gap at low and high temperatures. We identified value clusters for $E_g(0)$ at 3.26 eV, 3.263 eV, 3.265 eV and 3.285 eV, but also at 3.359 eV. The latter is achieved for $E_g(300) = 3.26$ eV and $\alpha = 3.3 \times 10^{-4}$ eV/K. The other values overlap, in large parts, with measurements of E_{gx} .

At room temperature the most commonly used values for E_g include 3.2 eV, 3.23 eV and 3.26 eV. We already showed direct connections between these values and the exciton band gap

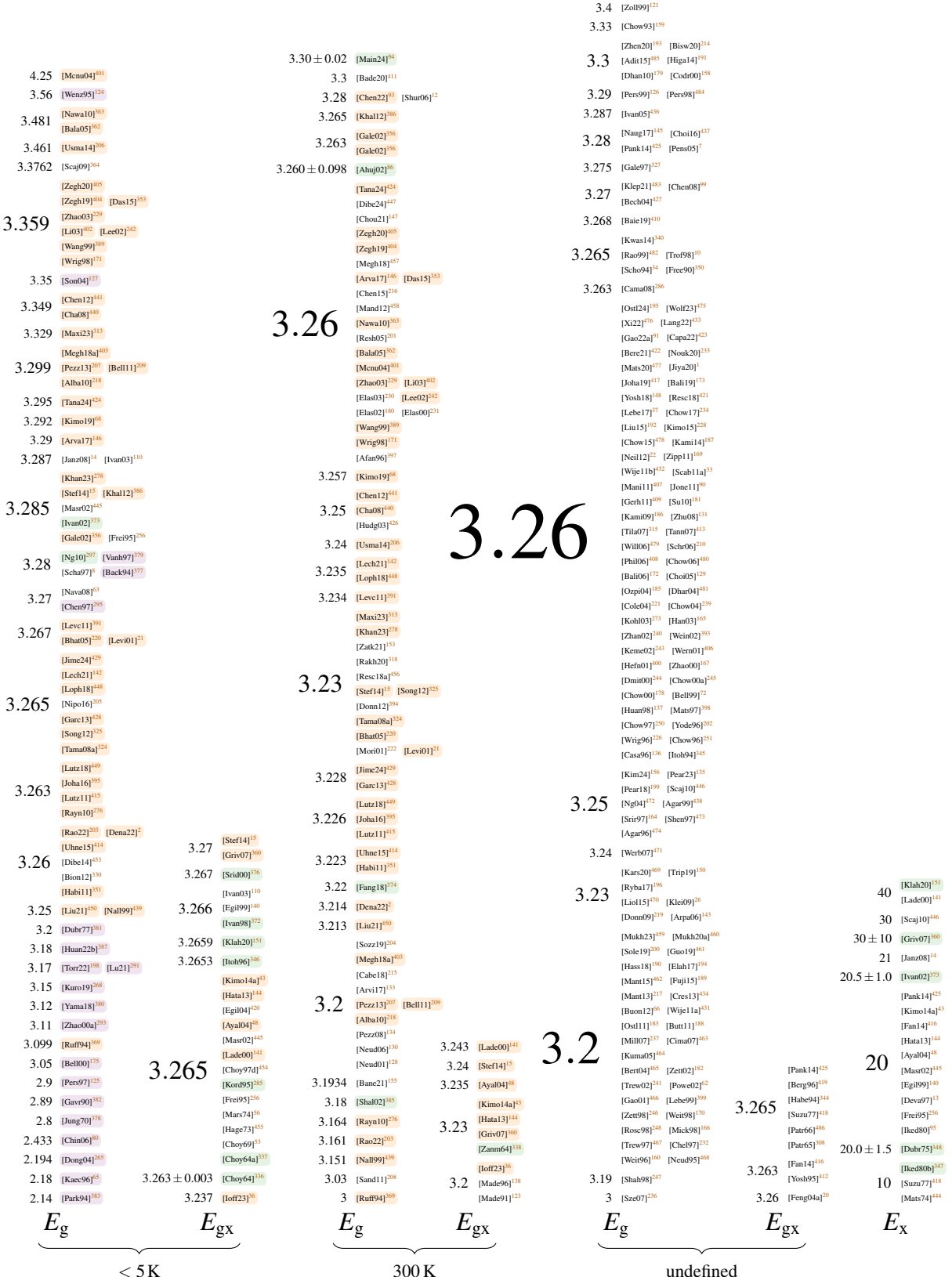


FIG. 24. Values for band gaps at varying temperatures. values correspond to calculations, ones to measurements and ones are values calculated from models.

at low temperatures, which means that a large share of currently used values denote a different quantity at a deviating temperature.

The investigated publications largely agree upon $E_x \approx 20\text{ meV}$, but we found only a single usage of this value in the last decade. The same statement can be made about the exciton band gap energy, which is seemingly pushed out of focus of the community. For a precise discussion of band gap parameters, the knowledge about the existence and the influence of excitons is indispensable and needs to be reintroduced.

VII. IMPACT IONIZATION

An electric field accelerates free charge carriers. When their kinetic energy exceeds the *ionization energy* of the material, the charge carrier is able to generate an excessive electron-hole pair. This process is called *impact ionization* and is sometimes deliberately used, e.g., in avalanche diodes, to increase the responsiveness of a detection device³⁵. However, in most devices, it is an undesired effect causing breakdown and destruction. Consequently, impact ionization simulations are crucial to identify and subsequently guard the unsafe operation regions of a device.

The amount of generated electron-hole pairs via impact ionization differs between holes and electrons and depends on conditions such as field strength and the spatial direction. Of special importance is the temperature dependency, as a fraction of the deposited energy during impact ionization is transferred to the lattice, increasing its temperature. If the impact ionization is enhanced with rising temperature, a self-amplifying process can be started, eventually destroying the device thermally (thermal runaway).

Our review shows that most of the existing models agree upon the relevant parameters and also, that the impact ionization decreases with temperature. However, many small inaccuracies were discovered (mostly typographical errors and confusion of units), causing big differences in the results. The focus of past research primarily focused on the direction parallel to the c-axis, although the parameters for the electron indicate an anisotropy that has to be considered.

A. Introduction

TCAD tools describe impact ionization described via a charge carrier generation rate (see Eq. (35)^{66,139}) with J_n/J_p and v_n/v_p being current and velocity respectively, while n and p denote

parameters representing either electrons or holes.

$$G_{II} = \frac{1}{q} (\alpha J_n + \beta J_p) = \frac{1}{q} (\alpha n v_n + \beta p v_p) \quad (35)$$

The impact ionization coefficients for electrons (α) and holes (β) represent the number of electron-hole pairs a single charge carrier can generate per unit length when moving in an electric field F (see Eq. (36))³⁵. In the sequel, we will introduce some of the models to describe α and β . For further details, the interested reader is deferred to the dedicated literature^{20,22,35,487,488}.

$$\alpha = \frac{1}{n} \frac{dn}{dx} 1/\text{cm} \quad , \quad \beta = \frac{1}{p} \frac{dp}{dx} 1/\text{cm} \quad (36)$$

The still very popular empirical Chynoweth's law (see Eq. (37))^{489,490}, also called Van Overstraeten-de Man model⁴⁹¹, was published in the late 1950s and based upon the same formalism to model impact ionization in gases.

$$\alpha, \beta(F) = a \exp \left[-\frac{b}{F} \right] \quad (37)$$

At the time of publication, this empirical fitting was the only possibility to describe the charge carrier multiplication at low electric fields. A physical explanation was only available for high field strengths (see Eq. (38))⁴⁹², which utilizes the optical phonon energy (E_p), the mean free path (λ), and the ionization energy (E_i).

$$\alpha, \beta(F) = \frac{eF}{E_i} \exp \left[-\frac{3E_p E_i}{(eF\lambda)^2} \right] \quad (38)$$

In 1961 Shockley⁴⁹³ modeled the low-field impact ionization coefficient according to Eq. (39). The term preceding the exponential is equal to Eq. (38) and denotes how often a carrier's kinetic energy can reach the ionization energy E_i (generate an excessive electron-hole pair) per unit length. The exponential scales this value by the chance of an uninterrupted acceleration, which is characterized by the mean free path λ . This model is therefore called Shockley's "lucky electron"⁴⁹⁴.

$$\alpha, \beta(F) = \frac{eF}{E_i} \exp \left[-\frac{E_i}{eF\lambda} \right] \quad (39)$$

The close relationship between Eq. (37) and Eq. (39) ($a = eF/E_i$, $b = E_i/e\lambda$) finally enabled a physics based calculation of parameters a and b ⁴⁹⁵.

The models in Eq. (38) and Eq. (39) were combined in Baraff's theory⁴⁹⁶ in 1962, which resulted in $\alpha, \beta \propto \exp[-b/F]$ for low fields and $\alpha, \beta \propto \exp[-c/F^2]$ for high ones. It was later extended by Thornber⁴⁹⁷ to the expression shown in Eq. (40)⁴⁸⁷ with $\langle E_i \rangle$ the effective ionization

threshold⁴⁸⁷ and $E_{k_B T}$ the energy due to thermal effects²³³. For the ionization energy E_i originally a value of $3/2 E_g$ ²³³ $\approx 4.89 \text{ eV}$ ³⁵⁶ at 300 K (E_g the band gap; see Section VI) was assumed. Recent measurements, however, revealed for 4H-SiC values in the range of $7.28 - 8.6 \text{ eV}$ ^{339,428,498-504}.

$$\alpha, \beta(F) = \frac{eF}{\langle E_i \rangle} \exp \left[-\frac{\langle E_i \rangle}{[(eF\lambda)^2/3E_p] + eF\lambda + E_{k_B T}} \right] \quad (40)$$

We also encountered variations of Eq. (40): Konstantinov *et al.*⁴⁹⁴ removed everything but the high-field part for α , while Kyuregyan⁵⁰⁵ proposed a transformation that used only three condensed parameters. As Baraff's theory failed to satisfy all demands⁵⁰⁶, Okuto and Crowell⁵⁰⁷ extended Eq. (41) by adding the electric field as a multiplicative factor, an exponential parameter m and a temperature dependency via c and d (see Eq. (41)). The simplified version with $c = d = n = 0$ is often referred to as Selberherr model⁴⁸⁸. All investigated publications use $n = 0$ (Biondo *et al.*³³⁰ stated $n = 1$, but the result did only match when we set $n = 0$), so we will not consider this parameter in the sequel.

$$\alpha, \beta(F) = a\{1 + c(T - 300)\} F^n \exp \left[-\left(\frac{b\{1 + d(T - 300)\}}{F} \right)^m \right] \quad (41)$$

To enable calculations we found models for the impact ionization coefficients using a power law, i.e., $\alpha, \beta \propto F^A$ ^{415,508,509}. We also encountered descriptions based on multi-stage⁵¹⁰ and inelastic collision events¹⁵⁴, which are not yet supported by TCAD tools. Banerjee¹⁵⁵ proposed a slightly deviation equation (see Eq. (42)), whose predictions deviated from the remaining results. Therefore we did not include it in our analysis.

$$\begin{aligned} \alpha &= \left(\frac{F}{a_n} \right) \exp \left(-\frac{b_n}{F^2} \right) \\ \beta &= \left(\frac{F}{7} \right) \exp \left[-\frac{1}{a_n F^2 + b_n F} \right] \end{aligned} \quad (42)$$

TCAD tools also support more advanced models, including a sophisticated temperature dependency in Eq. (41)⁵¹¹ and the consideration of the initial location of the impact carrier (Lackner model)⁴⁹⁵. We found, however, no application to 4H-SiC so far.

1. Anisotropy

Impact ionization is anisotropic in 4H-SiC. The breakdown field perpendicular to the c-axis, i.e., in $[1\bar{1}\bar{2}0]$ direction, was reported to be $80 - 85 \%$ ⁵¹², 75% ⁵¹³ respectively $50 - 60 \%$ ⁵¹⁴ to

that parallel to the c-axis, i.e., in [0001] direction. Nevertheless, Bhargav and Gurugubelli⁵¹⁵ pointed out that this discrepancy becomes less pronounced at high fields due to the dominant hole coefficient along the c-axis.

Multiple approaches to deal with direction-dependent impact ionization were developed: (i) Hatakeyama⁵¹⁶ developed a formalism (already available in modern TCAD tools) that combines measurements along the principal axis to predict the impact ionization coefficient in any desired direction. (ii) Jin *et al.*⁵¹⁷ reused available parameters but introduced a new approach to calculate the “driving force” by considering the field direction for constant carrier temperature. (iii) Nida and Grossner⁵¹⁸ adapted the field strength to an effective $F^* = (m_d^*/m_F)^{1/2}F$, with m_F the effective masses along the direction of F and m_d^* the density-of-states effective mass (see Section V).

2. Temperature Dependency

To depict the changing behavior with temperature, the dedicated parameters in Eq. (41) were commonly used, whereas Niwa, Suda, and Kimoto⁵¹⁹ extended its capabilities by providing a second-degree polynomial in T for a_p . In contrast, Hamad *et al.*⁵²⁰ extracted parameter values for eight temperatures independently.

A different approach applied the multiplicative factor γ shown in Eq. (43)⁵²¹ to the parameters a and b of Eq. (37)^{48,141,439,516,522}, with T_0 being a reference temperature (usually 300 K), T_L the lattice temperature and ω_{OP} the optical phonon energy. We are confident that ω_{OP} corresponds to the longitudinal optical phonon energy ω_{LO} (see Section IV) due to matching values.

$$\gamma = \frac{\tanh\left(\frac{\hbar\omega_{OP}}{2k_B T_0}\right)}{\tanh\left(\frac{\hbar\omega_{OP}}{2k_B T_L}\right)} \quad (43)$$

Finally, Nida and Grossner⁵¹⁸ scaled the mean free path in Eq. (40) by $\sqrt{\gamma}$ and the ionization energy by the ratio of the band gap at the lattice temperature T_L and 300 K.

3. Methods

To measure the impact ionization coefficients, an equal amount of charge carriers is generated in a space charge region, either by (pulsed) electron (electron beam induced current (EBIC))⁵²³ or optical beams (optical beam induced current (OBIC))^{494,519,520,524–530}. Defects have a significant

impact on the measured coefficients, such that EBIC is used to extract parameters at defect-free regions¹⁷³.

The charge carrier generation is executed at varying field strengths. Recording the respective terminal currents enables a comparison against the no-field current and, thus, the determination of the effective amplification. The readout of the current can be executed in DC mode^{494,524}, which complicates the elimination of leakage current⁵²³, AC mode^{523,527,528}, or both combined^{525,526}. Additional challenges are the selection of suitable test structures, (e.g., p-n/n-p diodes or pnp/npn transistors) and the proper separation of electron and hole multiplication phenomena. For further information, the interested reader is referred to the dedicated literature^{494,505,519,527,529,531}.

Monte Carlo simulations were also used to investigate impact ionization. Some authors extracted the impact coefficients as the reciprocal of the average scattering distance^{532,533} while others solely presented simulated values without fitting them to any of the earlier presented model^{166–168,175,184,534–539}. Further investigations focused on non-localized models^{540,541} and the impact of defects⁵⁴² in the presence of a magnetic field^{543,544}.

We found multiple fittings of Eq. (41) to the OBIC results by Konstantinov *et al.*⁴⁹⁴ (FO-BIC)^{129,155,173,222,229,545–547}, who originally used Eq. (40), and to the Monte Carlo results by Nilsson *et al.*⁵³⁶ (FMC)^{330,548}.

B. Results & Discussion

In the sequel, we present the results of our research on impact ionization. We did not include the parameters provided by Banc *et al.*⁵⁴⁹, as the authors focused on transistor channels. We also discarded publications that did not clearly specify the used polytype of SiC^{550–553}, as well as those solely investigating the deviations of the breakdown voltage^{472,554–557}.

A common figure of merit for impact ionization in literature is the critical electric field strength. We found values in the range of 2 – 3 MV/cm^{7,128,165,180,182,199,202,406,558}, and dependencies on the doping concentration^{12,68,173,252,400,415,494,513,523,530,559–562}. These values are, most commonly, determined for uniformly doped non-punch-through diodes using power law approximations of the impact coefficients⁵²³. Consequently, such values have to be corrected according to the actual structure and doping level^{252,563}. For example, over short distances, a higher field is required to achieve breakdown and vice versa. Therefore, the product of distance and field is a more important parameter for impact ionization than the critical electric field alone.

In TCAD simulations the critical electric field is automatically achieved based on the provided impact ionization coefficients, so we will not present these results in detail here.

1. Impact Ionization Coefficients

The earliest investigations on 4H-SiC impact ionization were published by Konstantinov *et al.*⁴⁹⁴ and Raghunathan and Baliga⁵²³. The proposed values, however, differed by almost one order of magnitude, forcing authors to consciously use 6H based values³⁸⁹. Manifold explanations were provided for this discrepancy: Bellotti⁷² reported that Konstantinov *et al.*⁴⁹⁴ used non-defect-free material, explaining the higher coefficients through defect-assisted ionization. Nilsson *et al.*⁵³⁶ stated that the techniques used by Raghunathan and Baliga⁵²³ are considered more accurate and Bertilsson, Nilsson, and Petersson⁵⁴⁸ argued that the deviations could be explained by the anisotropy of the impact ionization coefficients, which the author later revoked⁴⁶⁵. Feng and Zhao²⁰ concluded that the results by Raghunathan and Baliga⁵²³ deviated from practical results because a large share of the intrinsic defects was simply missed due to the focused beam that was used in the analysis.

While early Monte Carlo simulations^{175,536,548,571} supported the results by Raghunathan and Baliga⁵²³, more advanced simulation models⁵³³ and additional measurements showed a better agreement with Konstantinov *et al.*⁴⁹⁴. The results of the latter were, in hindsight, more commonly accepted within the community, which is also highlighted by seven different fittings (see Table XII and Table XIII).

We discovered multiple issues regarding these fittings: (i) The commonly used $m = 1$ in Eq. (41) is unable to match the curvature of the original data. Therefore, proper model selection in regard to the expected field strengths is key to avoid unacceptable discrepancies. (ii) Brossetlard⁵⁴⁶, Bellone and Di Benedetto⁵⁴⁷, and Raynaud *et al.*²⁷⁶ derived the same parameters, but their prediction for electrons is based on a faulty assumption. Raynaud *et al.*²⁷⁶ described the procedure as fitting the holes and then using $\beta/\alpha = 40$, but⁴⁹⁴ used this value only in an intermediate calculations, whereas the final results revealed a non-constant relationship of β/α . For this reason, the predictions of α by the stated authors are too low. (iii) Although Baliga¹⁷³ stated to use the results by Konstantinov *et al.*⁴⁹⁴, the model approximates the measurements by Hatakeyama *et al.*⁵¹⁴ much better.

In general, the literature is dominated by measurements (see Table XII and Table XIII). Since

TABLE XII. Fundamental parameters for Eq. (41). Single values indicate that the crystal direction was not specified. A dash represents 1 for m and 0 otherwise.  marks fittings to the OBIC results by Konstantinov *et al.*⁴⁹⁴ and  fittings to the MC investigation by Nilsson *et al.*⁵³⁶.

ref.	electron							hole							method			
	a_{\parallel} [10 ⁶ /cm]	a_{\perp}	b_{\parallel} [MV/cm]	b_{\perp}	c	d	m	F region	a_{\parallel} [10 ⁶ /cm]	a_{\perp}	b_{\parallel} [MV/cm]	b_{\perp}	c	d	m	F region		
	[1]								[1]									
[Ragh99] ⁵²³	–	–	–	–	–	–	–	–	3.09	17.9 ± 0.4	–3.46	–	–	–	–	2.5 – 3.2	EBIC	
[Bert00] ⁵⁴⁸	0.4	48	15	–	–	–	1.15	2 – 4	1.8	45	15	–	–	–	–	2 – 4	FMC	
[Sher00] ^{545a}	–	–	–	–	–	–	–	–	5.18	–	14	–	–	–	–	1.5 – 10	FOBIC	
[Mori01] ²²²	1.69	–	9.69	–	–	–	1.6	2.5 – 10	3.32	–	10.7	–	–	–	–	1.1	1.5 – 10	FOBIC
[Ng03] ⁵²⁶	1.98	–	9.46	–2.02 ^b	–	1.42	1.8 – 4	–	4.38	–	11.4	–0.91 ^b	–	–	1.06	1.8 – 4	OBIC	
[Zhao03] ²²⁹	7.26	–	23.4	–	–	–	–	2.5 – 10	6.85	–	14.1	–	–	–	–	1.5 – 10	FOBIC	
[Bros04] ⁵⁴⁶	0.408	–	16.7 ^c	–	–	–	–	1.25 – 3	16.3	–	16.7	–	–	–	–	1 – 3	FOBIC	
[Hata04] ⁵¹⁴	176	21	33	17	–	–	–	–	2 – 5	341	29.6	25	16	–	–	–	2 – 5	OBIC
[Choi05] ¹²⁹	16.5	–	25.8	–	–	–	–	2.7 – 5	5.5	–	13.5	–	–	–	–	–	1.5 – 4	FOBIC
[Loh08] ⁵²⁵	2.78	–	10.5	–	–	1.37	1.25 – 5	–	3.51	–	10.3	–	–	–	1.09	1 – 5	OBIC	
[Loh09] ⁵⁶⁴	–	–	–	–	–	–	–	–	3.321	–	10.385	–2.78	0.48 ^d	1.09	1.33 – 2	OBIC		
[Nguy11] ⁵²⁷	0.46	–	17.8	–	–	–	–	2 – 2.7	15.6	–	17.2	–	–	–	–	1.5 – 2.7	OBIC	
[Bion12] ^{530e}	0.325	–	17.1	–32.9	–	–	–	2 – 4	3.25	–	17.1	–32.9	–	–	–	2 – 4	FMC	
[Gree12] ⁵³¹	0.019	–	2.888	–	–	4.828	1.8 – 2.5	–	6 ^f	–	13.87 ^f	–	–	0.96	1.6 – 4	OBIC		
[Nguy12] ⁵²⁸	3.36	–	22.6	–	–	–	–	1.5 – 4.8	8.5	–	15.97	–	–	–	–	1.5 – 4.8	OBIC	
[Song12] ^{525g}	3.78	–	10.5	–1.47	–	1.37	1.25 – 5	–	4.51	–	10.5	–1.56	–	1.1	1 – 5	FIT		
[Sun12] ⁵³³	1.803	–	13.52	–	–	1.2	2 – 5	–	1.861	–	9.986	–	–	1.11	1.5 – 4	MC		
[Bell14] ⁵⁴⁷	0.407	–	16.7	–	–	–	–	2.5 – 10	16.3	–	16.7	–	–	–	–	1.5 – 10	FOBIC	
[Niwa14] ⁵¹⁹	8190	–	39.4	–	–	–	–	2.2 – 2.7	4.513	–	12.82	x ^h	1.38	–	1.4 – 2.5	OBIC		
[Hama15] ⁵²⁰	0.99	–	12.9	–	–	–	–	2.5 – 7	1.61	–	11.5	–	–	–	–	2.5 – 7	OBIC	
[Niwa15] ⁵²²	0.143	–	4.93	–	– ⁱ	– ⁱ	2.37	2.2 – 3.3	3.14	–	11.8	–	6.3 ⁱ	1.23 ⁱ	1.02	1 – 2.35	OBIC	
[Shar15] ⁵⁶⁵	186	–	28	–	–	–	–	–	301	–	20.5	–	–	–	–	–	DIV	
[Kyur16] ^{505j}	38.6 ± 15.0	–	25.6 ± 0.1	–	–	–	–	1.2 – 5	5.31 ± 0.30	–	13.10 ± 0.01	–	–	–	–	1 – 5	FIT	
[Zhan18] ⁵⁶⁶	1.31	–	13	–1.47	–	–	–	–	2.98	–	13	–1.56	–	–	–	–	–	
[Bali19] ¹⁷³	313	–	34.5	–	–	–	–	2 – 5	8.07	–	15	–	–	–	–	1.1 – 4	FOBIC	
[Zhao19] ⁵³⁰	0.339	–	5.15	–	–	–	2.37	2.4 – 3.2	3.56	–	11.7	–	6.19	1.15	1.02	1 – 2.5	OBIC	
[Stef20] ⁵²⁹	–	6.4	–	12.5	–	–	–	1.6 – 2	–	6	–	13.3	–	–	–	1.5 – 2	OBIC	
[Chea21] ^{532k}	0.932	–	7.19	–	–	1.95	2 – 10	–	1.75	–	6.56	–	–	1.45	1.6 – 10	MC		
[Stef21] ²⁴¹	2.8	–	20.7	–	–1 ^m	–0.29 ^m	–	1.25 – 10	2.5	–	12.1	–	1.74 ^m	0.59 ^m	–	1.25 – 10	FIT	
[Kita24] ⁵¹²	–	6.91	–	14.4	3.75	0.657	–	1.6 – 2.1	–	34.6	–	17.5	4.39	0.604	–	1.6 – 2.1	OBIC	

^a same values achieved as 6H investigation by Ruff, Mitlehner, and Helbig³⁶⁹

^b provided by Cha *et al.*⁵⁶⁷

^c changed value $b_p = 1.67 \times 10^5$ V/cm to $b_p = 1.67 \times 10^7$ V/cm as the results were too high

^d we changed $b_p = 8.9 \times 10^6 – 4.95 \times 10^3 T$ to $8.9 \times 10^6 + 4.95 \times 10^3 T$ to match the plots in the paper

^e we changed m from 2 to 1 and n from 1 to 0 to match the specified reference⁵³⁶

^f we changed $a_p = 6 \times 10^4$ /cm to 6×10^6 /cm and $b_p = 1.387 \times 10^6$ V/cm to 1.387×10^7 V/cm to fit plots

^g fitted to results by Loh *et al.*⁵²⁵

^h $a_p = 3.94 \times 10^6 – 1.96 \times 10^4 T + 71.7 T^2$

ⁱ different values suggested by Steinmann *et al.*⁵⁶⁸

^j values achieved by averaging of^{472,494,519,524–526,531,564}

^k a and b presumably stated in 1/m and MV/m in paper, converted to 1/cm and MV/cm

^l values fitted to^{175,369,494,525,526,528,530,569,570}

TABLE XIII. Fundamental parameters for Eq. (40).

ref.	dir	electron					hole					method
		$\langle E_i \rangle$	λ	E_p	$E_{k_B T}$	F region	$\langle E_i \rangle$	λ	E_p	$E_{k_B T}$	F region	
		[eV]	[Å]	[meV]	[meV]	[MV/cm]		[eV]	[Å]	[meV]	[meV]	[MV/cm]
[Kons97] ^{494a}		10	29.9	120	0	2.5 – 10	7	32.5	120	0	1.5 – 10	OBIC
[Nida19] ^{518b}		10.61	27	120	$k_B T$	1 – 10	10.87	39.49	85	$k_B T$	1 – 10	FIT
[Nouk20] ^{233c}	–	7.5	10	92.5	14.4	0.9 – 10	6.62	4.8	9	102	0.9 – 10	FIT
[Stei23] ^{568d}	–	10.6	27	95	$k_B T$	1 – 10	10.9	62	95	$k_B T$	1 – 10	FETIV
		10.6	27	87	$k_B T$	1 – 10	10.9	80	87	$k_B T$	1 – 10	FETIV

^a only high field asymptotics (without linear term in denominator) used for α

^b fitting to^{252,494,516,523,525}

^c $3/2 E_g$ instead of $\langle E_i \rangle$ used in the exponential, fitting to^{252,518,524–526,569}

^d parameters by Nida and Grossner⁵¹⁸ used as starting point

2008, multiple studies on the impact ionization of 4H-SiC, twelve of them within the last decade, were published, demonstrating an active area of research. By comparing the models with the plots in the respective papers, we identified inaccuracies in five out of 33 investigations, including errors in presented parameter values^{531,532,546} and equations^{330,564} (see footnotes of Table XII). Section A 4 presents a more comprehensive listing of encountered inaccuracies.

The measurements are complemented by the investigation of Stefanakis *et al.*²⁴, who provided fittings to Monte Carlo simulations^{175,570} and to existing 4H-SiC models^{494,525,526,528,530,569} (as well as 6H³⁶⁹), by enforcing $m = 1$ in Eq. (41). Based on these fittings the authors achieved a “global fit” model. Nouketcha *et al.*²³³ used a genetic algorithm to fit to multiple sources^{252,518,524–526,569}, and Nida and Grossner⁵¹⁸ fitted their model to values from^{252,494,516,523,525}. Kyuregyan⁵⁰⁵ calculated the average of available parameter values without conducting any fitting. According to the authors, this is supposed to remove statistical inaccuracies and uncertainties introduced by the characterization methods. Song *et al.*³²⁵ fitted to Loh *et al.*⁵²⁵, who in turn fitted high-field values from Ng *et al.*⁵²⁶ and low-field ones of own measurements.

Vastly deviating parameter values in Eq. (41) can lead to similar results, because a and b compensate each other. For an efficient comparison it is thus crucial to plot the models. The impact ionization coefficients for electrons (see Fig. 25) show a spread of more than one order of magnitude, whereas deviations increase for low fields. Zhang and You⁵⁶⁶ resp. Sharma, Hazdra, and Popelka⁵⁶⁵ predicted higher values than most other models and Biondo *et al.*³³⁰, Bellone and

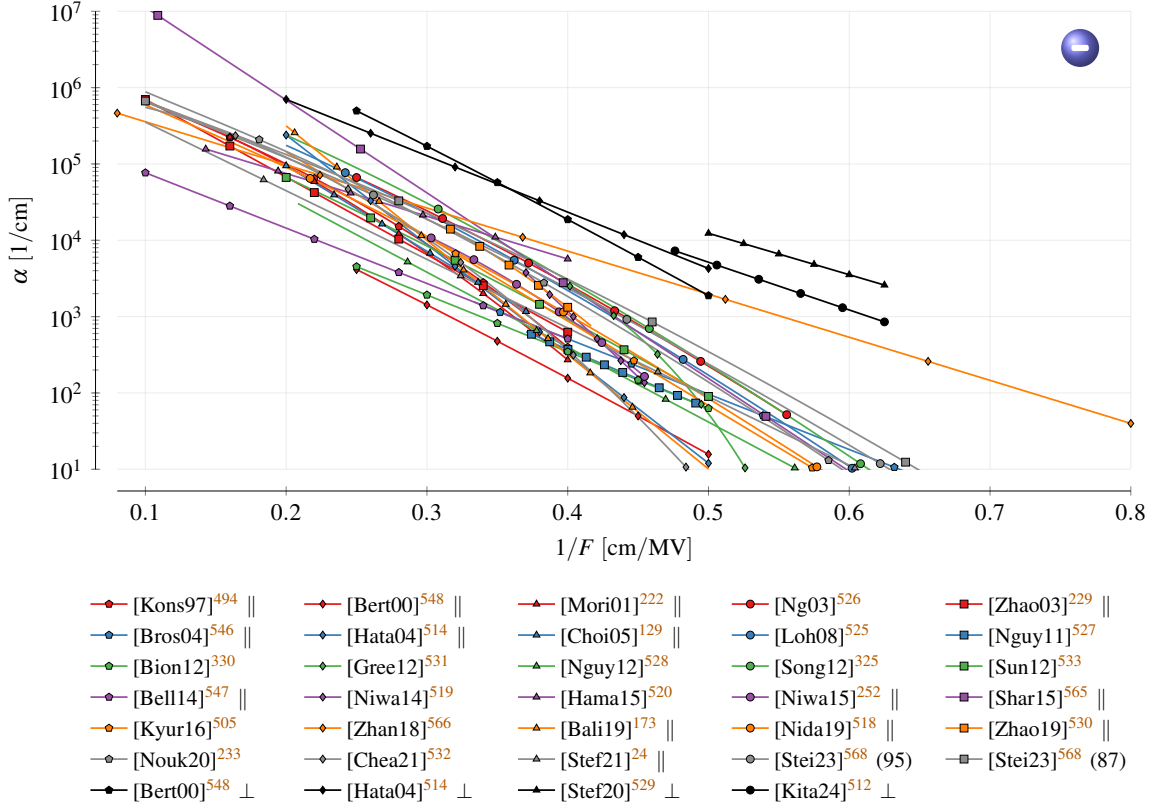


FIG. 25. Impact ionization coefficient for electrons. Each model is limited to the interval used for characterization. To distinguish the models proposed by [Stei23]⁵⁶⁸, we added (E_p).

Di Benedetto⁵⁴⁷, Bertilsson, Nilsson, and Petersson⁵⁴⁸ lower ones. Hatakeyama *et al.*⁵¹⁴ modeled the increase of α with the electric field steeper than the majority in literature.

For holes (see Fig. 26) the spread in values is much smaller, especially close to a field strength around 2 MV/cm. Nevertheless, the results of Steinmann *et al.*⁵⁶⁸ at low fields are several orders of magnitude higher than the average value in literature, while the results by Raghunathan and Baliga⁵²³, Biondo *et al.*³³⁰ and Bertilsson, Nilsson, and Petersson⁵⁴⁸ are around one order of magnitude lower. In fact, the latter match the impact ionization coefficient of electrons so well that they got occasionally interpreted as α^{525} . Similar to electrons, Hatakeyama *et al.*⁵¹⁴ predicted a much steeper increase with field strength, leading to higher than average values (comparable to Sharma, Hazdra, and Popelka⁵⁶⁵).

In contrast to Silicon, 4H-SiC shows higher hole than electron current amplification (i.e., $\beta > \alpha^{35,245,572}$), which is attributed to discontinuities in the electron spectrum²²⁷. Consequently, the Shockley approximation of the “lucky electron” can only be applied to holes, as the electron’s

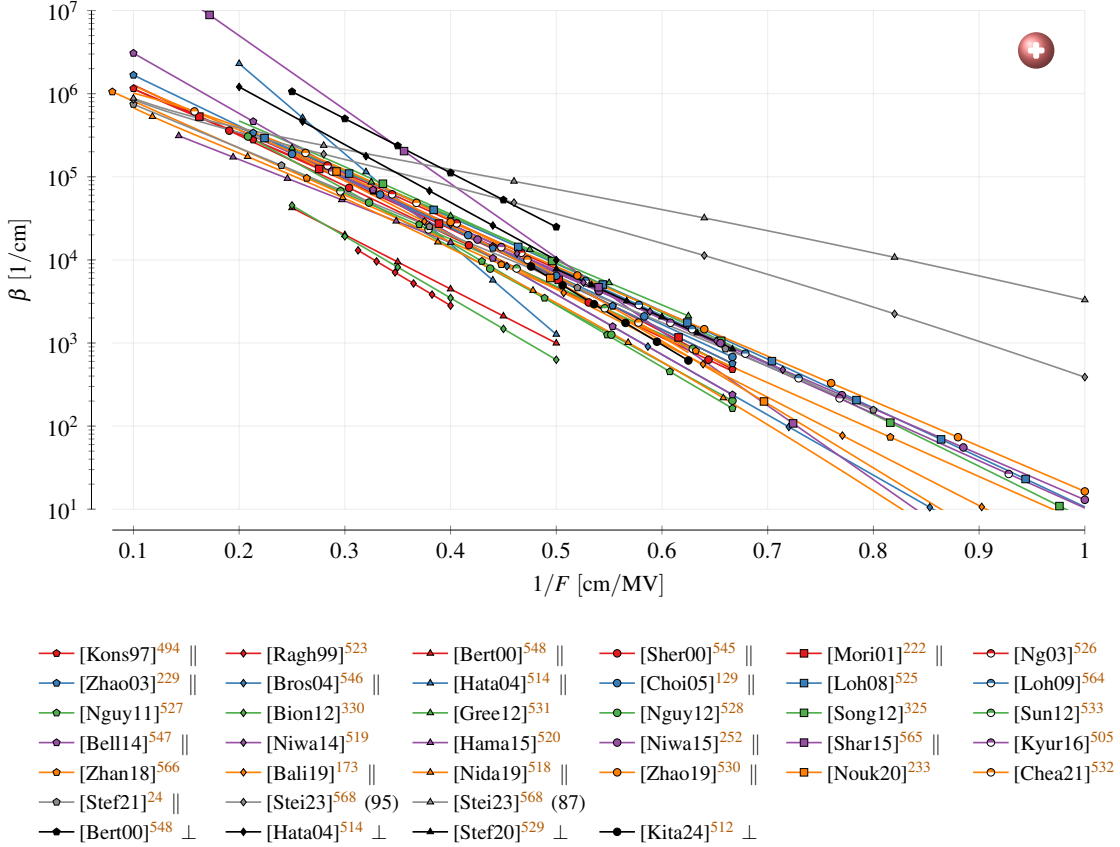


FIG. 26. Impact ionization coefficient for holes. Each model is limited to the interval used for characterization. To distinguish the models proposed by [Stei23]⁵⁶⁸, we added (E_p).

energy is prohibited to continuously increase⁴⁹⁴. For this reason, Konstantinov *et al.*⁴⁹⁴ only used the high-field part for α .

2. Anisotropy

As outlined earlier, the breakdown field in $[1\bar{1}20]$ is lower than in $[0001]$ direction, meaning that the respective impact ionization coefficient values ought to be higher. Already in the year 2000, Nilsson *et al.*⁵³⁶ proposed a non-constant relationship between the single directions, though early simulations/calculations did not manage to depict this correctly⁵⁴⁸, using constant factors instead. We found $\beta_{\perp}/\beta_{\parallel} = 25$ and $\alpha_{\perp}/\alpha_{\parallel} = 120^{548}$, as well as $\alpha_{\perp}/\alpha_{\parallel} = 1/3.5^{139,141}$, whereas the latter was most likely derived for 6H.

In Table XII we denoted the directions only in clearly distinguishable cases, though it is safe to assume that all investigations concentrated on the direction parallel to the c-axis⁵¹⁵. We found

only five exceptions^{424,512,514,529,548}: Tanaka and Kato⁴²⁴ conducted Monte Carlo simulations to show that the impact ionization coefficient for holes perpendicular to the c-axis is only slightly higher than parallel to it (see Fig. 26). The results by Stefanakis *et al.*⁵²⁹ even shows an overlap of the coefficients perpendicular and parallel to the c-axis.

For electrons the perpendicular coefficients turned out to be approximately one order of magnitude higher than the parallel ones. In fact, the values of α_{\perp} are comparable to β_{\parallel} ⁴²⁴, implying that electrons have to be carefully considered in breakdown analyses as well. The low value of α parallel to the c-axis was explained by the discontinuities in the conduction band^{424,494,513}, making it difficult for electrons to gain enough energy⁴²⁴. Nevertheless, more information is required for definite statements.

3. Temperature Dependency

Temperature analyses are rare in the literature. Some of the available data were even proposed by other authors years after the original publication, e.g., by Cha and Sandvik⁴⁴⁰, or by Steinmann *et al.*⁵⁶⁸, who fitted the linear and quadratic temperature coefficients of the breakdown voltage.

Nida and Grossner⁵¹⁸ presented the high-temperature evolution of selected models, though well outside of their experimental temperature range. The proposed calculations require a band gap model, whereas we picked the one from Galeckas *et al.*³⁵⁶ (see Section VI). Hatakeyama⁵¹⁶ used the temperature scaling shown in Eq. (43) (multiplication with γ), which can also be found in additional publications^{141,210,522}. We only show this temperature scaling for electrons, as it was not specified for holes explicitly. Hatakeyama⁵¹⁶ noted that for a good fit $\omega_{\text{OP}} = 190 \text{ meV}$ had to be used, thereby contradicting experimental results of $\omega_{\text{LO}} = 120 \text{ meV}$. Nallet *et al.*⁵²² used $\hbar\omega_{\text{OP}} = 90 \text{ meV}$ with $T_0 = 600 \text{ K}$.

All models we found predicted a decreasing hole impact ionization coefficient with increasing temperature (see Fig. 27), matching reports of a direct relationship between breakdown voltage and temperature^{440,573}. Consequently, thermal runaway is prevented. Steinmann *et al.*⁵⁶⁸ provided a fitting to their own measurements for the model by Niwa, Suda, and Kimoto²⁵² with the parameters shown in Eq. (44). We do not explicitly plot this fitting, as it is very close to the original model. Extraordinary is the model by Biondo *et al.*³³⁰, who proposed a value of $c_p = -32.9 \times 10^{-3} / \text{K}$ (comparable to Loh *et al.*⁵⁶⁴), leading to $\beta = 0$ at $\approx 330 \text{ K}$. We are unsure about the origin of the underlying data, as the reference used for fitting⁵³⁶ did not provide a temperature analysis.

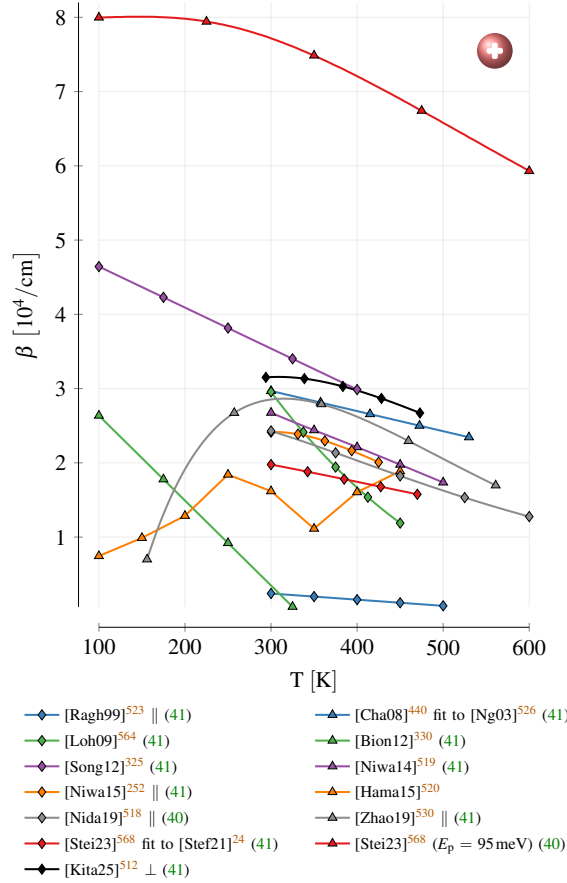


FIG. 27. Temperature dependence of the hole impact ionization coefficient at $1/F = 0.4\text{cm/MV}$. The references in bracket denote the used models.

Similarly Song *et al.*³²⁵ denoted Loh *et al.*⁵²⁵ as source, who also did not provide the respective data. Hamad *et al.*⁵²⁰ fitted the model shown in Eq. (41) at various temperatures, which explains the weird shape of the plot.

$$c_p = 2.05 \times 10^{-3}/\text{K} \quad , \quad d_p = 0.65 \times 10^{-3}/\text{K} \quad (44)$$

An exception to the general statement of decreasing impact coefficient with temperature is the model by Zhao, Niwa, and Kimoto⁵³⁰. However, the indicated increase within the range from 150 – 300 K is not supported by the plots shown in the very same publication.

The results for electrons (see Fig. 28) are comparable to those for holes, in that α approximately halves between 100 K and 600 K. Kimoto *et al.*⁵⁵⁹ assigned the discontinuities in the conduction band, called “minigaps” in the paper, as the reason for the low-temperature dependence of α .

The only exception are the fittings of Steinmann *et al.*⁵⁶⁸ to Niwa, Suda, and Kimoto²⁵² and Stefanakis *et al.*²⁴, who reported an increase of α . The model for the former only delivered

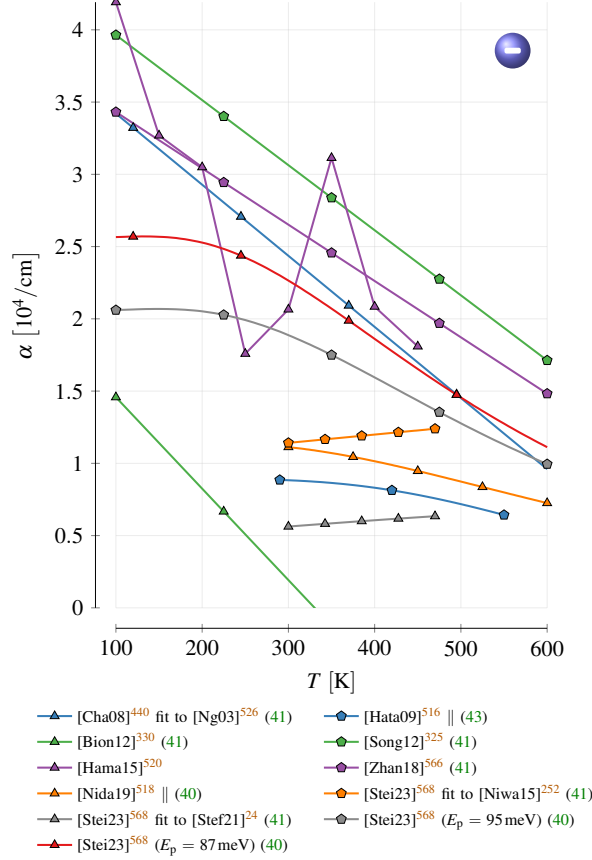


FIG. 28. Temperature dependence of the electron impact ionization coefficient at $1/F = 0.3 \text{ cm/MV}$. The references in bracket denote the used models.

reasonable results after we changed $d_n = -0.72 \times 10^{-3}/\text{K}$ to $d_n = -0.72 \times 10^{-6}/\text{K}$. Calculations by Tanaka and Kato⁴²⁴ also predicted an increase of α due to a small Brillouin zone width and narrow bandwidth of the $E - k$ dispersion in the conduction band. Comparable to holes, Biondo *et al.*³³⁰ proposed the same high value for c_n , leading to $\alpha = 0$ at $\approx 330 \text{ K}$. In the plot, we also added the temperature modeling by the γ factor (see Eq. (43)), showing a decline with increasing temperature. Niwa, Suda, and Kimoto²⁵² did not detect any changes of α with temperature.

4. Origin of Parameters

The majority of the currently utilized impact ionization coefficients are based on 4H measurements (see Fig. 29). Care has to be taken, especially for publications prior to the year 2000, as those are often based on 6H-SiC^{139,369,550,574}. The main reason is that 4H values were not available or simply³⁸⁹ because available fittings from Konstantinov *et al.*⁵²⁴, Raghunathan and Baliga⁵⁶⁹

deviated, resulting in an inconclusive picture. Nevertheless, the respective values often found their way in later 4H-SiC publications^{22,141,171,220,226}.

The most influential publication was published by Hatakeyama *et al.*⁵¹⁴ but also the one by Konstantinov *et al.*⁴⁹⁴ was extensively used for fittings. In total, twelve fundamental investigations were referenced at least once in literature.

During our analyses, we discovered some inconsistencies: The results from Bakowski, Gustafsson, and Lindefelt¹³⁹ were changed by Lades¹⁴¹ who calculated the parameters at 273 K and introduced a typographical error for the hole coefficient a , which was stated as $3.24 \times 10^6/\text{cm}$ instead of $2.24 \times 10^6/\text{cm}$. Nallet *et al.*⁴³⁹ used 6H values of β proposed by Raghunathan and Baliga⁵⁶⁹ for both electrons and holes. Surprisingly, multiple authors^{207,439,575} followed that example. Fig. 29 indicates incorrect values for b_p in publications referencing [Ragh99]⁵²³. This is not the case, because Raghunathan and Baliga⁵²³ proposed a temperature dependent value of $b_p = 3.09 \text{ MV/cm}$, which we adopted in this review, and $b_p = (3.25 \pm 0.30) \times 10^6 \text{ MV/cm}$, which was also used in literature. Khalid, Riaz, and Naseem³⁸⁶ correctly referenced $m = 2$ from Biondo *et al.*³³⁰ but, as our analyses showed, this value is unreasonable. Section A 4 presents a more comprehensive listing of encountered inaccuracies.

VIII. CHARGE CARRIER RECOMBINATION

In a semiconductor electron-hole pairs are continuously created, for example due to thermal processes, and annihilated by recombination. In thermal equilibrium these process are balanced, resulting in the electron (n_0) and hole (p_0) equilibrium carrier concentrations that satisfy the condition $n_0 p_0 = n_i^2$, with n_i being the intrinsic carrier concentration.

In TCAD tools the equilibrium state is not explicitly modeled, only how the semiconductor returns to it. The deviation of the charge carriers to n_0 and p_0 is denoted as excess carrier, non-equilibrium, generated^{587,588} or solely carrier concentration³³⁴ Δ_N and its rate of change includes diffusion (D equals the ambipolar diffusion coefficient), recombination (R) and generation (G) (see Eq. (45)^{374,589,590}). The latter can be caused for example by impact ionization, which we already investigated in Section VII, or optical generation.

$$\frac{d\Delta_N}{dt} = D \frac{d^2\Delta_N}{dx^2} - R + G \quad (45)$$

In this section we are going to review charge carrier recombination. Accurate models enable

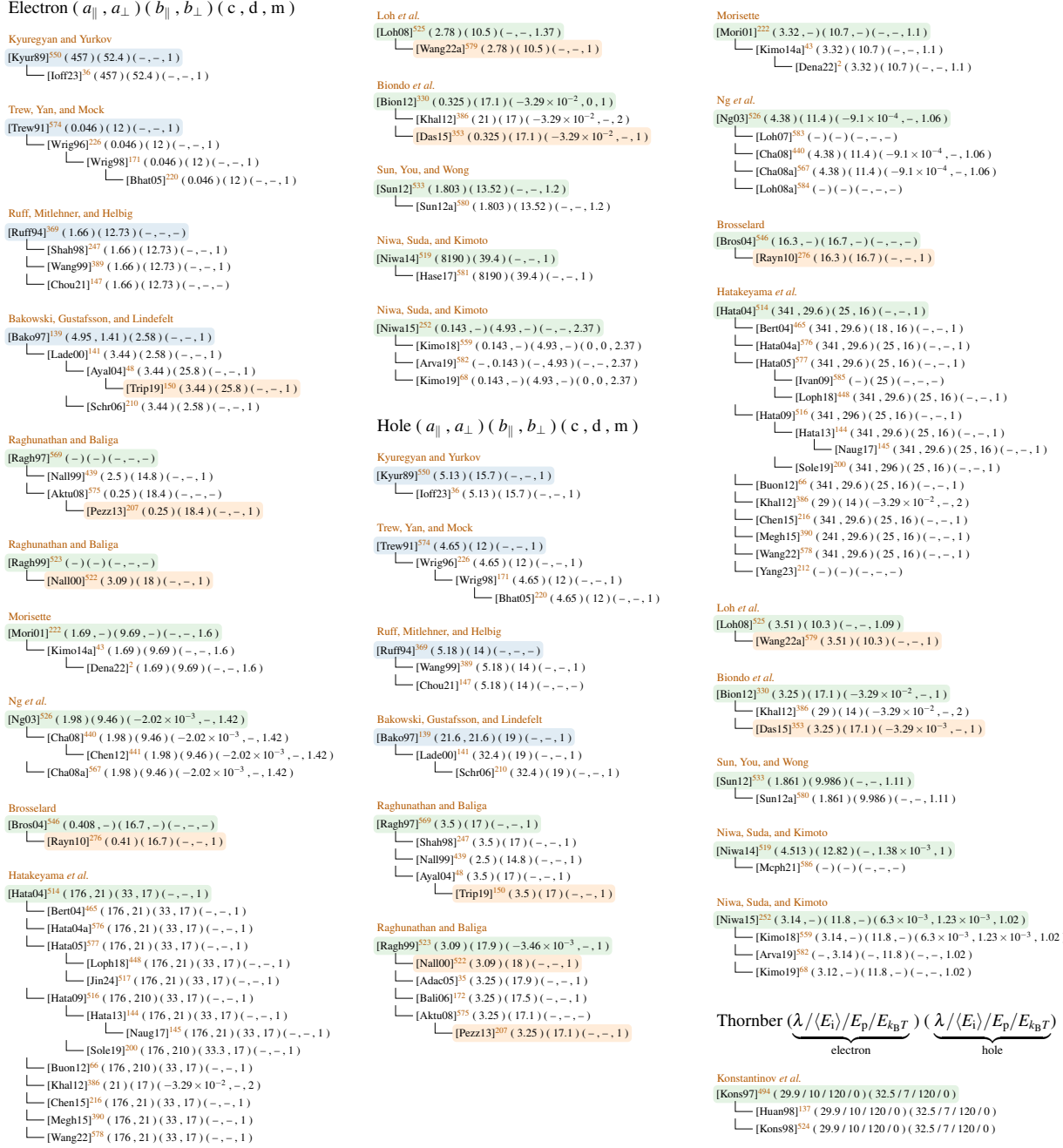


FIG. 29. Reference chain for impact ionization parameters. are not focused on 4H-SiC, while are novel analyses on 4H-SiC, and indicates an educated guess on the reference based on the given values in cases the source is not explicitly stated in the publication. The values for a and b were scaled by 1×10^6 for improved readability.

high-resolution charge carrier concentrations over time, which influence the conductivity and internal electric fields. We focused our investigation on minority charge carriers, i.e., electrons in p-type and holes in n-type material, because these are the most common ones found in literature.

Our analyses revealed that the lifetime, i.e., the average time between two recombination events, depends on Δ_N , the temperature and the doping concentration. We found measurements that proposed values in a range of four orders of magnitude, but we were unable to identify a clear trend with time or measurement technique. Therefore, we conclude a strong dependency on the quality of the device. Less and even contradicting data is available for temperature and doping related changes of the recombination rate, calling for further investigations in the future.

A. Introduction

The decline of charge carriers towards their equilibrium values n_0 resp. p_0 is described by the recombination rate R^{591} , which includes the trap-assisted Shockley-Read-Hall (R_{SRH}), the bimolecular (R_{bim}) and the Auger (R_{Auger}) recombination rate³²⁷ (see Eq. (46)^{326,374,446,592,593}). An alternative representation is to use lifetimes τ_x , which denote the average time between two recombination events (see Eq. (47)²¹⁸).

$$R = R_{SRH} + R_{bim} + R_{Auger} \quad (46)$$

$$= \frac{\Delta_N}{\tau_{SRH}} + \frac{\Delta_N}{\tau_{bim}} + \frac{\Delta_N}{\tau_{Auger}} = \frac{\Delta_N}{\tau_r} \quad (47)$$

The individual contributions to the recombination will be investigated separately in the sequel. For a comprehensive description the interested reader is referred to the dedicated literature^{236,341,592,594}.

1. Shockley-Read-Hall Recombination

The term R_{SRH} denotes the successive capturing of a hole and an electron in a trap level with energy E_t inside the band gap^{592,595}, sometimes also called monomolecular recombination³²⁷. The following expressions were introduced to describe this process (see also Fig. 30)^{596–598}: *electron capture* denotes the transition of an electron from the conduction band into the trap and *electron emission* the reverse process. Similarly, during *hole capture* a hole rises from the valence band to the trap level, i.e., an electron drops from the trap into the valence band, and *hole emission* denotes

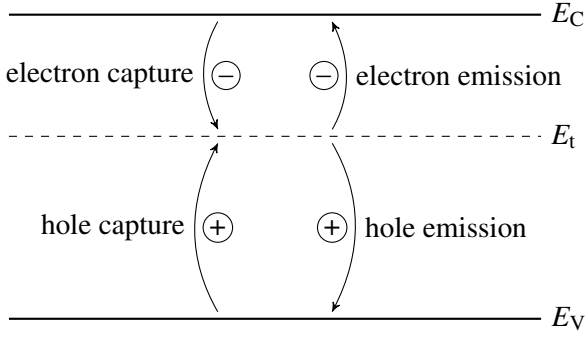


FIG. 30. Capture and emission of charge carriers described by R_{SRH} . E_t denotes the trap level energy.

the reverse case. In any capture event the electron, thus, loses energy, while in any emission event it gains some. The electron/hole *capture cross sections* quantify the possibility to capture an electron/hole⁵⁹⁹, but they can also describe the thermal emission rate e (see Eq. (48)⁶⁰⁰) with E_a the defect activation energy.

$$e = \sigma \gamma T^2 \exp\left(-\frac{E_a}{k_B T}\right) \quad (48)$$

The energy released/consumed during these transitions is exchanged with lattice vibrations (phonons)⁵⁹², whereat different phonon interactions are distinguished, e.g., multi- or cascade-phonon interaction^{594,601}. Among these the capture cross section and their respective temperature dependencies differ⁵⁹⁷.

The recombination rate R depends on the material quality⁵⁹²: Structural defect positions⁶⁰² can cause a decrease of R but certain impurities or damages in the lattice, which are called effective “lifetime killers”⁶⁰³, lead to a steep increase. The recombination even varies across a single wafer. Typically it is smallest in the middle where the best growth conditions are available^{604–617}, but also in thick 4H-SiC layers variations were reported⁶¹⁸. Lots of effort was undertaken to refine growth conditions in order to achieve cleaner samples^{326,613,615,616,619–636}.

An accurate description of R_{SRH} requires detailed information about energy level, type (acceptor or donor) and cross section of the defects in the device. We encountered a large amount of investigations targeting this topic^{31,48,66,133,139,146,172,209,218,220,362,637–649,2,6,13,20,88,140,144,197,271,295,328,344,371,409,416,454,455,650–661,14,36,43,68,95,110,223,228,274,345,417,436,469,559,623–625,662–674,21,26,120,123,141,166,192,291,301,302,321,340,399,402,415,444,448,457,483,675–684,7,8,12,114,118,119,128,130,135,201,207,248,280,310,318,363,425,482,484,565,617,685–693,10,28,131,132,148,150,169,182,198,204,254,414,418,600,630,694–704}, which makes a comprehensive analysis

within this review infeasible. Instead, we refer the interested reader to the report by Gaggl *et al.*⁷⁰⁵, who investigated defects in 4H-SiC and developed a TCAD model for it. In regard to recombination, the most important ones are called $Z_{1/2}$ and $EH_{6/7}$ ^{27,698,703,706} and, presumably, denote different charge states of a carbon vacancy⁶⁴⁶.

The Shockley-Read-Hall recombination includes a bulk (R_{SRH}^b) and surface (R_{SRH}^s) contribution. Both occur simultaneously and are therefore often hard to separate^{592,707}. Nevertheless, we will describe them in isolation in the sequel.

a. Bulk Recombination Rate Shockley and Read⁵⁹⁶, Hall⁷⁰⁸ first described the recombination rate of the bulk mathematically in 1952 (see Eq. (49)^{146,341,415,488,596,598,708}). $\tau_{n,p}$ denotes the electron resp. hole lifetime, $\sigma_{n,p}$ the electron resp. hole cross section, N_t the trap concentration, $v_{\text{th}} = \sqrt{3k_B T/m_d^*}$ ^{272,598} the thermal velocity and g_t the trap degeneracy factor. The latter is often neglected as it is usually one⁶⁶. Shockley and Read⁵⁹⁶ stated that the trap energy level (E_t) is an effective one that they calculated from the trap level and the degeneracies of the empty (w_p) and full (w) trap, i.e., $E_t = E_t(\text{true}) + k_B T \ln(w_p/w)$. TCAD tools accept either the lifetimes $\tau_{n,p}$ or the cross sections $\sigma_{n,p}$, but they do not consider the degeneracy factor yet.

$$R_{\text{SRH}}^b = \frac{np - n_i^2}{\tau_p(n + n_1) + \tau_n(p + p_1)} \quad (49)$$

$$n_1 = \frac{1}{g_t} N_C \exp\left(-\frac{E_C - E_t}{k_B T}\right) \quad (50)$$

$$p_1 = g_t N_V \exp\left(-\frac{E_t - E_V}{k_B T}\right) \quad (51)$$

$$n_i = \sqrt{n_1 p_1} = \sqrt{N_C N_V} \exp\left(-\frac{E_C - E_V}{2k_B T}\right) = \sqrt{N_C N_V} \exp\left(-\frac{E_g}{2k_B T}\right) \quad (52)$$

$$\tau_{n,p} = (\sigma_{n,p} v_{\text{th}} N_t)^{-1} \quad (53)$$

p_1 and n_1 can also be described by the intrinsic carrier concentration and an effective Fermi level E_i (see Eq. (54)^{218,242,601}). E_i , which was defined in one case as the mid gap energy level³³⁰, differs from the intrinsic Fermi level E_F that defines the actual carrier concentration $n = N_C \exp[(E_F - E_C)/k_B T]$ and $p = N_V \exp[(E_V - E_F)/k_B T]$.

$$\begin{aligned} n_1 &= \frac{1}{g_t} n_i \exp\left(-\frac{E_t - E_i}{k_B T}\right) \\ p_1 &= g_t n_i \exp\left(-\frac{E_i - E_t}{k_B T}\right) \end{aligned} \quad (54)$$

The SRH carrier lifetime changes with the doping concentration $N_{A,D}$ ⁷⁰⁹. On the one hand dopants are defects (see Section IX), i.e., recombination centers, whose impact on the recom-

bination is described with Eq. (49)³¹⁸. On the other hand the doping process introduces additional damage⁴⁸⁸ that lowers the lifetime according to the empirical Scharfetter relation (see Eq. (55))^{146,209,369,488,601,710–714}. Shao *et al.*⁷¹⁵ recently provided a detailed analysis on the change of the lifetime for various relations of donor and acceptor concentrations.

$$\tau = \frac{\tau_{\max}}{1 + \left(\frac{N_A + N_D}{N_{\text{ref}}}\right)^{\gamma}} \quad (55)$$

The defect induced lifetime reduction was determined in more simplistic fashions as well, e.g., $\tau(\mu\text{s}) = 1.5 \times 10^{13} / N_{\text{VC}}$ ^{706,716} and $\tau(\mu\text{s}) = 1.8 \times 10^{13} / N_{\text{VC}}$ ⁵⁵⁹ for carbon vacancies, and $\tau(\mu\text{s}) = 1.6 \times 10^{13} / N_{Z_{1/2}}$ ^{43,717} and $\tau(\mu\text{s}) = 2 \times 10^{13} / N_{Z_{1/2}}$ ⁶²⁶ for the $Z_{1/2}$ defect, with N_x the respective concentration⁷¹⁸.

At high temperatures the energetic charge carrier has to approach the center of the defect more closely to be captured⁷¹³. Consequently, the lifetime increases with temperature^{612,629,632,719–722}, which was analyzed by Udal and Velmre⁷²³. The cross section changes in the order of T^{-x} ⁷²⁴, which leads, in conjunction with the change of the thermal velocity according to \sqrt{T} , to a power law description⁷¹⁶. TCAD tools use the model shown in Eq. (56)^{725–727}, whereat τ_{T0} denotes the lifetime at some reference temperature T_0 .

$$\tau_{\max} = \tau_{T0} \left(\frac{T}{T_0}\right)^{\alpha} \quad (56)$$

Because this approximation predicts $\tau_{\max} \rightarrow 0$ for $T \rightarrow 0$ a modified approach shown in Eq. (57) was proposed³¹⁸. By comparison we find $\tau_0 = \tau_{T0}/2$ at $T = T_0$ and $\tau_{\max} = \tau_0$ at $T = 0\text{K}$.

$$\tau_{\max} = \tau_0 \left(1 + \left(\frac{T}{T_0}\right)^{\alpha}\right) \quad (57)$$

We also found an exponential description (see Eq. (58))⁷²³ for the temperature dependency of τ , with E_{act} being an activation energy and τ_{∞} the lifetime for $T \rightarrow \infty$.

$$\tau_{\max} = \tau_{\infty} \exp\left(-\frac{E_{\text{act}}}{k_B T}\right) \quad (58)$$

Since the meaning of τ_{∞} is hard to grasp, it can be replaced by $\tau_{T0} \exp(E_{\text{act}}/k_B T_0)$ ^{43,728}, with τ_{T0} the lifetime at $T = T_0$. For $E_{\text{act}} = 0.105\text{eV}$ and $T_0 = 300\text{K}$ we get $\exp(E_{\text{act}}/k_B T_0) = 57.9$, which was sometimes stated explicitly^{43,728}. A similar model shown in Eq. (59)⁵⁸⁹ approaches a value of $51\tau_0$ for $T \rightarrow \infty$.

$$\tau_{\max} = \tau_0 \left(1 + \frac{100}{1 + \exp(E_{\text{act}}/k_B T)}\right) \quad (59)$$

The lifetimes in Eq. (58) and Eq. (59) stall for high temperatures, which makes them only suitable for temperatures between 300 – 500 K⁷²³. The model shown in Eq. (60)^{142,439} circumvents this problem.

$$\tau_{\max} = \tau_{T_0} \exp^{C\left(\frac{T}{T_0} - 1\right)} \quad (60)$$

A recent investigation by Lechner¹⁴² identified an increase of the lifetime up to a temperature between 600 – 700 K followed by a decrease at higher ones. Based on the research by Schenk⁷²⁷ the author proposed the fitting shown in Eq. (61)¹⁴².

$$\tau_{\max} = \tau_{T_0} \left(\frac{T}{T_0} \right)^{T_{\text{coeff}}} \exp \left[-\alpha_{\tau} \left(\frac{T}{T_0} - 1 \right)^{\beta_{\tau}} \right] \quad (61)$$

In state-of-the-art simulation tools only Eq. (56) and Eq. (60) are included.

b. Surface Recombination Rate Surface recombination includes mechanisms that occur on surfaces or interfaces. The primary causes are imperfections or impurities at the transition between two materials. This includes many different surface types and thus also effects, such as semiconductor-oxide or semiconductor-semiconductor and oxides across these. The share of the surface recombination on the overall recombination rate decreases with the thickness of the samples, because the ratio of surface to bulk volume decreases⁷¹⁸.

The boundary condition of the diffusion defines the surface recombination (see Eq. (62))^{729–732}. For the interested reader Mao *et al.*⁵⁹⁰ presented a fantastic review on the causes, characterization methods and possible countermeasures of surface recombination and Gulbinas *et al.*⁷²⁹ a theoretical analysis.

$$D \frac{d\Delta_N(\mathbf{x}, t)}{d\mathbf{x}} = S_0 \Delta_N(\mathbf{x}, t) \quad (62)$$

Despite the tight connection between diffusion and surface recombination, TCAD tools model the latter by the SRH formalism. The sole difference to the bulk recombination rate is that instead of lifetimes the *surface recombination velocities* $s_{n,p}$ (see Eq. (63)^{66,341,488,592}) that depend on the interface trap density N_{it} are used.

$$R_{\text{SRH}}^s = \frac{(n_s p_s - n_i^2)}{(n_s + n_i)/s_p + (p_s + p_i)/s_n} \quad (63)$$

$$s_n = \sigma_{ns} v_{\text{th}} N_{\text{it}} \quad (64)$$

$$s_p = \sigma_{ps} v_{\text{th}} N_{\text{it}} \quad (65)$$

TCAD tools expect s_n and s_p as inputs. Their dependency on the crystal faces^{610,707,730–732} is not included in state-of-the-art simulation tools yet. Some provide the possibility to model a doping dependency but we found no reliable data for 4H-SiC in literature.

The surface recombination velocity depends on the surface quality and the neighboring material. Therefore, many studies sought to improve the material quality^{551,587,707,729,733–739} by varying growth mechanisms or by irradiation⁶⁶². Even an elaborate model using trap regions inside the band gap was developed^{397,740,741}.

Kato *et al.*⁷³¹ and Klein *et al.*⁷¹⁸ described the temperature dependency of the surface recombination velocity, which is modeled by Eq. (66)^{742,743}. $-E_{bb}$ denotes the band bending near the surface that leads to accumulation of charge carriers of one type at the surface while repelling the other^{625,743}.

$$s_{\text{eff}}(T) = s_{\infty} \exp\left(\frac{-E_{bb}}{k_B T}\right) \quad (66)$$

2. Bimolecular Recombination

The term R_{bim} denotes the recombination rate due to the interaction of two particles, which can be described by Eq. (67)^{415,488} with B the bimolecular recombination coefficient^{218,374}.

$$R_{\text{bim}} = B(np - n_i^2) \quad (67)$$

In literature, bimolecular recombination is sometimes reduced to the radiative band-to-band recombination process emitting a photon⁴⁴⁶. However, in the indirect semiconductor 4H-SiC (see Section VI) it is less important, because a phonon always has to absorb the momentum of the charge carrier^{218,374,589,597,611}. Besides radiative recombination, R_{bim} also includes (i) recombinations between donor-acceptor pairs (DAP)^{326,744} (ii) the recombination of a charge carrier from the conduction/valence band and an unionized dopant (e.g., e-A)^{424,744} and (iii) the recombination of excitons (see Section VI)⁴⁴⁶.

Trap-assisted Auger recombination (TAA)⁷⁴⁵ is also a bimolecular process but it is handled in differing fashions in the literature. TAA denotes the process when an electron (hole) interacts with a trap (capture resp. emission) and the additional/missing energy is exchanged with a particle of the same kind. In the past, authors included this process in the bimolecular recombination coefficient^{91,327,446,746}, the Auger process^{201,747} and SRH^{594,745,748}. The latter is the only option to model TAA in existing TCAD tools, but we were unable to find suitable values for 4H-SiC.

We found additional trap-assisted Auger processes that have to be handled with care: Lin-nros⁷⁴⁶ remarked that the excitonic Auger capture process described by Hangleiter⁵⁹⁵ is “markedly different” from TAA and should be regarded as an alternative explanation for multi-phonon/SRH recombination. Booker *et al.*⁶⁴⁶ reported a trap-Auger mechanism using a neutral EH_{6,7} trap that contains two electrons. When a hole recombines with one of the electrons, the excessive energy is transferred to the other electron and ejects it to the conduction band. Finally, Takeshima⁷⁴⁹ described a phonon-assisted Auger recombination process.

3. Auger Recombination

At last, the term R_{Auger} , also called Auger recombination “(first discovered in atomic systems by Pierre Auger; soft g, please, the gentleman is French not German!)”⁵⁹⁴, denotes a three particle interaction where the excessive resp. missing energy and momentum is taken from/transferred to a third particle (either hole or electron). This process is an intrinsic property of the material⁵⁹² and dominates for high excessive charge carrier densities. It is described by Eq. (68)^{146,415,488,750} where C_n denotes the energy transfer to an electron and C_p the transfer to a hole³²⁷.

$$R_{\text{Auger}} = (C_n n + C_p p)(np - n_i^2) \quad (68)$$

We found several approaches to model the temperature dependency^{360,632} of the parameters. Galeckas *et al.*³²⁷ proposed an exponential correlation according to Eq. (69).

$$C_n + C_p = \gamma_{30} \exp\left(-\frac{\alpha(T - 300\text{K})}{k_B T}\right) \quad (69)$$

Ščajev and Jarašiūnas⁵⁸⁹ explained their deviating results by the fact that Galeckas *et al.*³²⁷ did not consider the in-depth profile. For an improved coverage the authors developed the model in Eq. (70), with $B_{\text{CE}}(T) \propto T^{-1.5}$ the Coulomb enhancement coefficient and a_{SC} the screening parameter.

$$C(T, \Delta_N) = \left(C_0 + \frac{B_{\text{CE}}(T)}{\Delta_N}\right) / \left(1 + \frac{\Delta_N}{a_{\text{SC}} \times T}\right)^2 \quad (70)$$

Ščajev *et al.*⁴⁴⁶ mentioned a more simplistic relationship of $C \propto \Delta_N^{-0.3}$ due to the screening of the Coulomb enhancement coefficient, and Tanaka, Nagaya, and Kato⁷⁴⁷ $C \propto \Delta_N^{-0.68}$. The differences may be explainable by the deviating fitting procedures.

In rare cases researchers even reused the formalism to describe the temperature induced changes of the Auger recombination coefficients in Silicon (see Eq. (71))^{448,566}.

$$C_{n,p} = \left(A_{n,p} + B_{n,p} \left(\frac{T}{T_0} \right) + D_{n,p} \left(\frac{T}{T_0} \right)^2 \right) \left[1 + H_{n,p} \exp \left(-\frac{n,p}{N_{0n,p}} \right) \right] \quad (71)$$

4. Analysis

In the sequel we want to analyze the presented equations and extract further useful information. Some reader might have noticed that all recombination rates contain the multiplicative factor shown in Eq. (72) with Δ_n, Δ_p the excessive carrier concentrations for electrons resp. holes. Recall that $n = n_0 + \Delta_n$, $p = p_0 + \Delta_p$ and $n_i = n_0 p_0$.

$$(np - n_i^2) = (n_0 + \Delta_n)(p_0 + \Delta_p) - n_0 p_0 = n_0 \Delta_p + p_0 \Delta_n + \Delta_n \Delta_p \quad (72)$$

For a device without traps, i.e., $\Delta_p = \Delta_n = \Delta$, and for low-level (ll, $\Delta \ll n_0, p_0$) resp. high-level (hl, $\Delta \gg n_0, p_0$) injections the models can be simplified^{236,341,415,592,746}, which provides useful insights on how to interpret measurements results⁵⁹². After a short calculation we get, due to $R = \Delta_N / \tau_r$ (see Eq. (47)), for low-level injections the results shown in Eq. (73) and high-levels the results in Eq. (74).

$$\tau_{SRH}^{ll} = \frac{\tau_p(n_0 + n_1) + \tau_n(p_0 + p_1)}{n_0 + p_0} \quad (73a)$$

$$\tau_{bim}^{ll} = \frac{1}{B(n_0 + p_0)} \quad (73b)$$

$$\tau_{Auger}^{ll} = \frac{1}{(C_n n_0 + C_p p_0)(n_0 + p_0)} \quad (73c)$$

$$\tau_{SRH}^{hl} = \tau_p + \tau_n \quad (74a)$$

$$\tau_{bim}^{hl} = \frac{1}{B\Delta} \quad (74b)$$

$$\tau_{Auger}^{hl} = \frac{1}{(C_n + C_p)\Delta^2} \quad (74c)$$

At high-injection levels $\tau_{SRH} = \tau_p + \tau_n$ (also called ambipolar lifetime^{43,485,751}) and τ_{Auger} solely provide the sum of electron and hole lifetimes. Separate measurements are only possible at low-injection levels and with doped semiconductors, i.e., either $n_0 \gg p_0, p_1, n_1$ or $p_0 \gg n_0, n_1, p_1$. In that case one of the summands can be ignored.

For doped semiconductors we can rewrite the high-level injection results from Eq. (74) as shown in Eq. (75)^{218,327,374,415,446,592–594,657,746}, which highlights that the introduced recombination terms actually represent a polynomial approximation of the recombination rate up to degree three in respect to the excess carrier concentration. If no excess charge carriers exist, i.e., $\Delta = 0$, no recombination is considered ($R = 0$). For low excess charge carrier densities the SRH term dominates while for high densities the Auger process is most important.

$$\begin{aligned} R = \Delta \tau^{-1} &= \Delta(\tau_{\text{SRH}}^{-1} + \tau_{\text{bim}}^{-1} + \tau_{\text{Auger}}^{-1}) \\ &= A\Delta + B\Delta^2 + C\Delta^3 \end{aligned} \quad (75)$$

All these simplifications are only valid for $\Delta \geq 0$. If $(np - n_i^2) < 0$ the recombination rate becomes negative, meaning that according to Eq. (45) charge carriers are generated. The corresponding rate of change can be described by using the so-called generation lifetime τ_g ^{27,341,415,591,752}. Such a reversal is not meaningful for the bimolecular recombination because the respective generation demands incoming photons⁵⁹¹. TCAD tools provide for this purpose dedicated optical generation mechanism, meaning that bimolecular recombination is deactivated for $(np - n_i^2) < 0$.

Impact ionization (see Section VII) is often stated as the inverse of Auger recombination^{236,601,753}, implying that it also gets deactivated if too few charge carriers are present. However, Selberherr⁴⁸⁸ stated that there is a difference: While impact ionization requires high current densities the inverse process of the Auger recombination only requires high charge carrier concentrations with negligible current flow. Despite these facts, R_{Auger} gets deactivated in TCAD tools when it drops below zero by default, but some allow to explicitly enable it for this case.

5. Methods

The recombination lifetime was measured either optically or electrically. Commonly used optical techniques include photoluminescence decay (PLD)^{612,669,709}, (transient) (time-resolved) free carrier absorption ((T)(TR-)FCA)^{275,327,446,589,593,611,620,746,754,755}, electron beam induced current (EBIC)⁶¹⁹, time-resolved photoinduced absorption (TRPA)³²⁷, time-resolved photoluminescence (TRPL)^{590,611,613,617,627,630–632,698,703,718,756}, time-resolved transient absorption (TRTA), longitudinal optical phonon-plasmon coupling (LOPC)^{757,758}, transient absorption spectroscopy (TAS)³⁷⁴, four wave mixing (FWM)³³⁴, low-temperature photoluminescence (LTPL)^{709,714}, capacitance transient (C-t)⁵⁵¹, differential transmittivity (DT)⁷¹⁴ and (microwave) photoconductance

decay ((μ)-PCD)^{478,559,587,588,590,604,606,611,616,621–626,628,629,634,657,707,731,737,759–763}. Hirayama *et al.*⁷⁶⁴ described a two-photon absorption (TPA) process to determine the lifetime in a specific depth of the sample.

Electrical measurements included reverse recovery (RR)^{558,723,765,766}, thyristor turned off gate current (TTOGC)⁷²⁰, short-circuit current/open-circuit voltage decay (SCCVD/ OCVD)^{201,218,716,721,767–770}, diode current density (DCD)^{16,453,581,771}, bipolar transistor emitter current (BTEC)⁷⁷² and diode forward voltage degradation (DFVD)⁷⁷³. Also utilized were fittings to measurement (FIT)^{206,313,394} or simulations (SIM)⁷²².

The achieved lifetime values depend on the utilized method²⁰¹. It has to be assured that the same quantity is measured, and that injection level and temperature are taken into account²⁰¹. For example, Kato, Mori, and Ichimura⁷⁷⁴ claimed that μ -PCD tends to overestimate the carrier lifetimes in high injection conditions and Tawara *et al.*⁶⁹⁸ that μ -PCD achieves longer lifetimes than the ones by TRPL. Deviations might also result from improper measurement setups: OCVD is limited to low and high injection regions²¹⁸. Levinstein *et al.*⁷⁷⁵ even argued that RR and OCVD measurement may provide incorrect results³⁹⁴. For more detailed information, e.g., which carrier lifetime is extracted from the decay time for high and low injection by each measurement technique, the interested reader is referred to the dedicated literature^{43,611}.

It is important to consider the impact of the surface recombination R_{SRH}^s as well⁶¹¹, because samples with a thickness in the range of mm or even cm would be required³⁴¹ to extract R_{SRH}^b directly⁵⁹². In the optimal case R_{SRH}^s is determined separately^{558,718,761,765}, but that is not always practical⁶¹¹.

B. Results & Discussion

In the sequel the results of our analyses will be presented, whereas we will not distinguish the different faces inside the crystal^{631,731}. We did not include values when solely the effective lifetime was proposed^{471,609,752} or if it was not possible to clearly distinguish τ_n and τ_p ^{446,757,759,760}. We also removed the values by Kato *et al.*⁷⁷⁶ who investigated the recombination at specific crystal stacking faults or dislocations, because the achieved lifetimes were a lot lower than all other values we gathered. We discarded the investigation by Grivickas *et al.*⁶²⁰ because no concrete values were mentioned.

TABLE XIV. Electron lifetime results. Column *inj.* denotes the carrier injection level, i.e., low (ll) resp. high (hl), and column *excess* the exact amount. A y in column *impr.* highlights that the shown value is the highest lifetime achieved in an optimization process.

ref.	τ_n	dop	conc.	T	inj.	Δ_N	impr.	method
	[μs]		[1/cm ³]	[K]		[1/cm ³]		
[Agar01] ⁷²⁰	0.6	p	7×10^{14}	293	hl	-	-	TTOGC
[Ivan06a] ⁷²²	0.066	p	2×10^{17}	300	-	-	-	SIM
[Alba10] ²¹⁸	0.008	-	2.04×10^{17}	300	-	-	-	OCVD
[Haya11] ⁵⁸⁷	1.3	Al	9×10^{14}	-	ll	1.5×10^{14}	y	μ -PCD
[Haya11a] ⁵⁸⁸	1.6	p	9×10^{14}	300 – 525	ll	1.5×10^{14}	y	μ -PCD
[Haya12] ⁶²¹	1.7	p	5.6×10^{14}	-	ll	1×10^{15}	y	μ -PCD
[Okud13a] ⁶²⁸	0.31	Al	1×10^{18}	300	-	9.1×10^{15}	-	μ -PCD
[Dibe14] ⁴⁵³	0.001	-	-	-	hl	-	-	DCD
[Okud14] ⁶²⁹	10	Al	2×10^{14}	300	-	3.6×10^{16}	y	μ -PCD
[Liau15] ⁷¹⁴	0.02	Al	1×10^{17}	300	hl	-	-	DT
[Okud16] ⁷⁶²	12	Al	1×10^{15}	300	-	3.6×10^{14}	y	μ -PCD
[Hase17] ⁵⁸¹	0.4	p	8×10^{14}	-	-	-	-	DCD
[Kato20] ⁷³¹	1.2	Al	6×10^{14}	300	ll	-	y	μ -PCD
[Koya20] ⁷⁷³	0.13	p	1×10^{19}	-	-	-	-	DFVD
[Maxi23] ^{313a}	6	-	-	-	-	-	-	FIT
[Zhan23a] ⁶¹⁶	3.14	Al	2×10^{14}	300	-	-	y	μ -PCD

^a value fitted to measurements by Kimoto *et al.*⁵⁵⁹

1. SRH Lifetime

We identified 16 investigations of the electron lifetime τ_n in 4H-SiC (see Table XIV) and 62 of τ_p (see Table XV and Table XVI). The first scientific reports were published in the late 1990s and up to the present day this is an active research topic. Despite the wide range of values, we still encountered the relation $\tau_n = 5\tau_p$ ^{16,210,229,247,369,389,402,417,452,777}, which was originally used for Si and more recently $\tau_n = \tau_p$ ^{29,203,207,324,386,439,778,779}. Based on our results the latter seems more reasonable.

The shown tables represent already a simplification, because many publications include values

TABLE XV. Hole lifetime results [1/2]. Column *inj.* denotes the carrier injection level, i.e., low (ll) resp. high (hl), and column *excess* the exact amount. A y in column *impr.* highlights that the shown value is the highest lifetime achieved in an optimization process.

ref.	τ_p [μs]	dop	conc. [1/cm ³]	T [K]	inj.	Δ_N [1/cm ³]	impr.	method
[Kord96] ⁶¹²	2.1	n	-	300	-	-	-	PLD
[Gale97] ³²⁷	0.26	N	5×10^{15}	-	hl	-	-	TRPA
[Neud98] ⁵⁵⁸	0.7	N	$(2 - 4) \times 10^{16}$	-	-	-	-	RR
[Gale99a] ⁶⁰⁸	0.5	N	$< 1 \times 10^{16}$	-	-	-	-	FCA
[Ivan99] ⁷²¹	0.6	n	6×10^{14}	293	hl	-	-	OCVD
	3.8	n	6×10^{14}	550	hl	-	-	OCVD
[Kimo99] ⁷⁶⁵	0.33	N	5×10^{14}	-	-	-	-	RR
[Udal00] ⁷⁶⁶	0.052	n	$(0.9 - 2.6) \times 10^{15}$	-	-	-	-	RR
[Cheo03] ⁵⁵¹	1	N	$(1 - 1.8) \times 10^{16}$	300	-	-	-	Ct
[Dome03] ⁷⁷²	0.0035	n	8.6×10^{15}	-	hl	-	-	BTEC
[Zhan03] ⁷⁰³	0.3	n	$(1 - 200) \times 10^{14}$	-	-	-	-	TRPL
[Levi04] ⁷⁶⁹	1.55	n	3×10^{14}	293	hl	-	-	OCVD
[Tawa04] ⁶⁹⁸	0.26 – 6.8	n	$(1.8 - 34) \times 10^{14}$	300 – 500	-	$(1.1 - 4.2) \times 10^{15}$	-	TRPL
[Resh05] ²⁰¹	1	n	7×10^{15}	-	-	-	-	OCVD
[Huh06] ⁶⁶⁹	0.5	n	1×10^{14}	-	ll	1×10^{13}	-	PLD
[Ivan06b] ⁷⁶⁸	3.7	n	2×10^{14}	300	hl	-	-	OCVD
[Jenn06] ⁶¹⁹	15.5	N	5×10^{15}	-	-	-	-	EBIC
[Neim06] ³³⁴	0.012	N	1×10^{16}	-	-	-	-	FWM
[Dann07] ⁶⁵⁷	2.5	N	1.5×10^{15}	300	hl	$(2 - 20) \times 10^{16}$	y	μ -PCD
[Stor07] ⁶³⁰	0.218	N	5×10^{15}	300	-	-	y	TRPL
[Udal07] ⁷²³	0.0044	n	7×10^{15}	297	-	-	-	RR
[Kimo08] ⁶²⁵	8.6	n	$(1 - 2) \times 10^{15}$	-	ll	5×10^{12}	-	μ -PCD
[Stor08] ⁶³¹	0.99	n	1×10^{14}	300	-	-	y	TRPL
[Hiyo09] ⁶³⁴	1.62	N	$(1 - 5) \times 10^{15}$	-	hl	$(2 - 20) \times 10^{16}$	y	μ -PCD
[Resh09] ⁷⁶⁷	2.13	n	$(1 - 1.2) \times 10^{15}$	-	hl	-	-	OCVD
[Alba10] ²¹⁸	1.5×10^{-5}	-	2.21×10^{17}	300	-	-	-	OCVD
[Jara10] ⁷⁸⁰	0.8	n	4×10^{14}	300	-	$(1 - 100) \times 10^{17}$	-	FCA
[Kimo10] ⁶²⁶	9.5	n	$(0.9 - 1) \times 10^{15}$	-	hl	$(5 - 50) \times 10^{15}$	y	μ -PCD
[Kimo10a] ⁷³⁷	13.1	N	7×10^{14}	-	hl	$(5 - 50) \times 10^{15}$	y	μ -PCD
[Klei10] ⁷¹⁸	>100	N	$< 1 \times 10^{16}$	222	ll	2×10^{14}	-	TRPL
[Miya10] ⁷⁶¹	18.5	N	7×10^{13}	-	ll	3×10^{12}	-	μ -PCD

TABLE XVI. Hole lifetime results [2/2]. Column *inj.* denotes the carrier injection level, i.e., low (ll) resp. high (hl), and column *excess* the exact amount. A y in column *impr.* highlights that the shown value is the highest lifetime achieved in an optimization process.

ref.	τ_p [μs]	dop	conc. [1/cm ³]	T [K]	inj.	Δ_N [1/cm ³]	impr.	method
[Haya11a] ⁵⁸⁸	4.6	n	1.2×10^{15}	300 – 525	ll	1.5×10^{14}	y	μ -PCD
[Donn12] ^{394a}	0.24	N	1×10^{16}	-	-	-	-	FIT
[Ichi12] ⁶²²	33.2	N	$(3 - 8) \times 10^{14}$	-	-	$(1 - 10) \times 10^{15}$	y	μ -PCD
[Kawa12] ⁶²⁴	6.5	n	1×10^{16}	300	-	1×10^{16}	y	μ -PCD
[Lilj13] ⁶¹³	1.6	N	3×10^{15}	300	ll	-	y	TRPL
[Miya13] ⁶²⁷	13	N	$(2 - 3) \times 10^{14}$	300	-	-	y	TRPL
[Scaj13] ⁵⁸⁹	0.55	n	4×10^{14}	-	ll	-	-	FCA
[Dibe14] ⁴⁵³	0.01	-	-	-	hl	-	-	DCD
[Usma14] ^{206b}	1.3	n	2×10^{14}	-	-	-	-	FIT
[Chow15] ⁴⁷⁸	2.5	n	2.5×10^{14}	300	hl	-	-	μ -PCD
[Kaji15] ⁶²³	21.6	N	2×10^{14}	-	-	1×10^{14}	y	μ -PCD
[Suva15] ⁷⁵⁴	0.35	N	8×10^{15}	-	hl	6×10^{17}	-	FCA
[Puzz16] ⁷⁷¹	1	n	3×10^{15}	400	-	-	-	DCD
[Sait16] ⁷⁶³	26	n	1×10^{14}	300	-	1.8×10^{17}	-	μ -PCD
[Stre16] ⁷⁸¹	$(22.5 \pm 7.5) \times 10^{-3}$	n	1.5×10^{15}	300	-	-	-	EBIC
[Tawa16] ⁶³²	0.3	N	7.7×10^{17}	300	ll	-	-	TRPL
[Tsuc16] ⁷⁵⁶	2.6	n	1.4×10^{14}	-	-	-	-	TRPL
[Ayed17] ⁶⁰³	20	N	1×10^{15}	-	-	-	y	-
[Lilj17] ⁷⁰⁹	3.5	N	1.3×10^{15}	300	ll	-	-	PLD
[Fang18] ³⁷⁴	$(11 \pm 3) \times 10^{-3}$	N	9.1×10^{18}	300	-	-	-	TAS
[Kimo18] ⁵⁵⁹	110	n	1×10^{14}	-	-	$(1 - 10) \times 10^{14}$	y	μ -PCD
[Cui19] ⁶⁰⁴	1.05	N	2×10^{13}	300	-	4×10^{16}	-	μ -PCD
[Mura19] ⁶¹⁷	9.9	N	1×10^{15}	293	ll	-	-	TRPL
[Kato20] ⁷³¹	0.7	N	$(1 - 10) \times 10^{15}$	300	ll	-	y	μ -PCD
[Naga20] ⁵⁹³	10	N	1×10^{18}	293	hl	1.5×10^{18}	-	TR-FCA
[Sapi20] ⁷¹⁶	19	n	1×10^{16}	300	hl	-	-	OCVD
[Erle21] ⁶⁰⁶	5	N	$(5 - 10) \times 10^{14}$	-	ll	-	-	μ -PCD
[Mura21] ⁷⁴⁴	0.14	N	2×10^{17}	293	ll	7×10^{14}	-	TRPL
[Meli22a] ⁷⁵⁸	$(1.63 \pm 0.18) \times 10^1$	n	5×10^{13}	-	hl	$(5.2 - 6.6) \times 10^{17}$	y	LOPC
[Maxi23] ^{313c}	2	-	-	-	-	-	-	FIT
[Kato24] ⁷⁰⁷	4.5	n	1×10^{15}	300	-	$(5 - 50) \times 10^{15}$	-	μ -PCD
[Sozz24] ⁷⁷⁰	6.09	n	1.5×10^{14}	298	hl	4×10^{17}	-	OCVD

^a value fitted to results by Galeckas *et al.*³²⁷

^b value fitted to forward current measurements by Ryu *et al.*⁷⁸²

^c value fitted to measurements by Kimoto *et al.*⁵⁵⁹

for multiple operating conditions, i.e., temperature, doping concentration and excess carrier concentration. For example Hayashi *et al.*⁵⁸⁸ provided measurements for various injection levels and two temperatures (300 K and 525 K). In these cases we only selected the highest lifetime for the table.

The measurements show no difference between τ_n and τ_p , which both decrease with increasing doping density (see Fig. 31). However, the reported values differ by up to four orders of magnitude for a constant doping concentration. To investigate this circumstance we scaled the maker size with the excess carrier concentration, because for a high level only the sum $\tau_n + \tau_p$ is achieved^{669,754} (cp. Eq. (74)). Consequently, we expected that the lifetime increases when going from low to high injection level, until it eventually starts to decrease when the bimolecular or Auger recombination become dominant. This effect was explicitly shown in literature^{587,588,621,707}. In addition, Kimoto *et al.*⁷⁸³ stated in 2016 that the injection-level dependence of SRH lifetimes is not known in SiC, calling for further research, Tawara *et al.*⁶³² experienced a lifetime decrease eventually approaching a constant value and Ščajev and Jarašiūnas⁵⁸⁹ concluded that the lifetime is almost injection level independent. Our analysis agrees mostly with the latter, because we were unable to identify any clear tendency in the data.

The lifetime values that were referenced in literature (see Fig. 32) also show a big spread, with values ranging from 15 ns to 39.5 ms, but similar values for τ_n and τ_p . Compared to other topics investigated in this review lifetimes are rarely referenced, which highlights the impact of the material quality and the necessity for device specific measurements.

2. Doping Dependency of SRH Lifetime

We could solely identify parameter sets for the Scharfetter relation in Eq. (55) (see Table XVII) that were fitted to suitable measurements. Liaugaudas *et al.*⁷¹⁴ conducted their own differential transmittivity measurements and Maximenko³¹³ fitted to the results of the μ -PCD measurements by Kimoto *et al.*⁵⁵⁹. These are the only ones that distinguished between electrons and holes. For early publications no 4H-SiC values were available, so Ruff, Mitlehner, and Helbig³⁶⁹ settled for a combination of Silicon based values gathered from various sources. In other cases^{29,129} we were unable to retrace the origin of the values, although often explicit references were provided.

We discovered in two cases a mix-up of doping and excess charge carrier concentration during fitting. While both lead to a decrease in lifetime with increasing concentration (as we will show

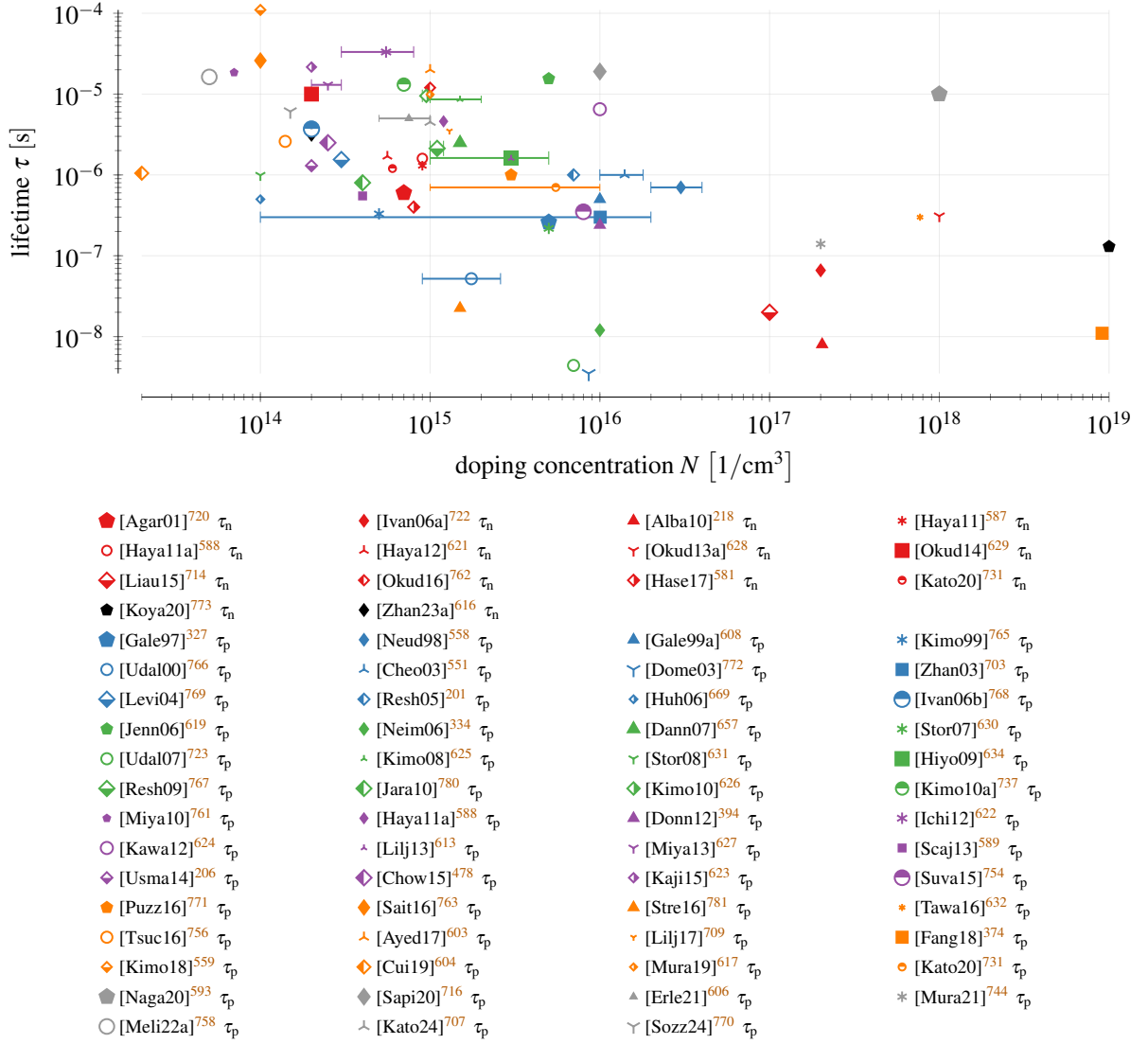


FIG. 31. Measurements of the minority charge carrier lifetime for the respective doping densities. The mark size indicates the excess carrier concentration. We picked an intermediate size if no data were available. We excluded the results by Albanese²¹⁸ for τ_p because the value was very low and distorted the plot.

later) the underlying physical processes are fundamentally different. While more doping results in an increased amount of recombination centers, more excess charge carriers lead to a higher contribution of bimolecular and Auger recombination. Although the Scharfetter relation only covers the former Nallet *et al.*⁴³⁹ and Donnarumma, Palankovski, and Selberherr³⁹⁴ fitted the lifetime versus the excess charge carrier concentration. Despite this discrepancy we included the respective results to paint a more complete picture but highlighted them accordingly.

The fittings predict that τ_p starts to decrease for doping concentration $> 10^{14}/\text{cm}^3$ and τ_n only

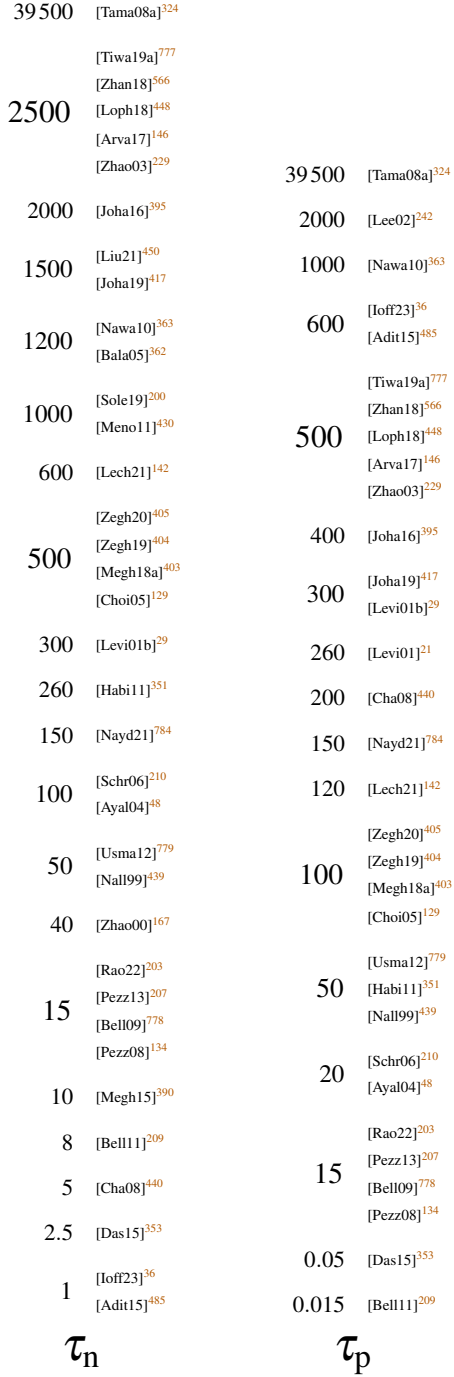


FIG. 32. Lifetime values referenced in literature in [μs].

after a concentration of $10^{18}/\text{cm}^3$ is exceeded. The rate of change is thereby higher for τ_n . The only exception of this observation is the fitting of τ_n by Kimoto *et al.*⁵⁵⁹, which matches the fittings of τ_p from various authors well. To resolve this disagreement and to confirm our hypothesis further measurements would be necessary in the future. The remaining models agree either more to the

TABLE XVII. Parameters for doping dependency according to the Scharfetter relation in Eq. (55).  are investigations not focused on 4H-SiC,  are fittings to doping variations and  fittings to varying excess carrier concentrations (not covered by this model). The last column denotes the source for the fitting data.

ref.	electrons		holes		quantity	fit to
	N_{ref} [1/cm ³]	γ [1]	N_{ref} [1/cm ³]	γ [1]		
[Ruff94] ^{369 a}	3×10^{17}	0.3	3×10^{17}	0.3	–	–
[Nall99] ⁴³⁹	1×10^{16}	1	1×10^{16}	1	excess	[Gale97] ³²⁷
[Levi01b] ²⁹	7×10^{17}	1	7×10^{17}	1	–	–
[Choi05] ^{129 b}	5×10^{16}	1	5×10^{16}	1	–	–
[Donn12] ³⁹⁴	2×10^{18}	1.9	2×10^{18}	1.9	excess	[Gale98] ⁷⁸⁵
	4×10^{18}	1.4	4×10^{18}	1.4	excess	[Neim06] ³³⁴
[Liau15] ⁷¹⁴	5×10^{18}	1.2	–	–	doping	–
[Lech21] ^{142 c}	7×10^{16}	1	7×10^{16}	1	–	–
[Maxi23] ³¹³	5×10^{15}	0.55	5×10^{15}	0.67	doping	[Kimo18] ⁵⁵⁹

^a based on data for Silicon

^b no data found in provided reference⁶, according to Albanese²¹⁸ based on Silicon

^c default values from TCAD tool

electron or hole behavior. Solely the Silicon based model ([Ruff94]³⁶⁹) shows a very slow decrease and thus can not be assumed accurate for 4H-SiC.

3. Temperature Dependency of SRH Lifetime

We found various fantastic investigations on the temperature dependent lifetime^{707,731}; one even distinguished between surface and bulk lifetime⁷¹⁸. Excess charge carriers in the range $1 \times 10^{16} - 1 \times 10^{19}/\text{cm}^3$ were investigated⁴²⁴, with the conclusion that the temperature behavior depends on the excess carrier concentration⁷⁸⁰.

In the literature predominantly the power law description of Eq. (56) was used (see Table XVIII). The values for the exponent α thereby commonly vary between 1 and 2. Udal and Velmre⁷²³ stated a fitting in two regions, as the lifetime started to increase faster above 700 K based on charge carrier lifetimes that the authors extracted from reverse recovery measurements by Boltovets *et al.*⁷³⁹. Sapienza *et al.*⁷¹⁶ achieved $\alpha = 1.5$ which is exactly the value expected

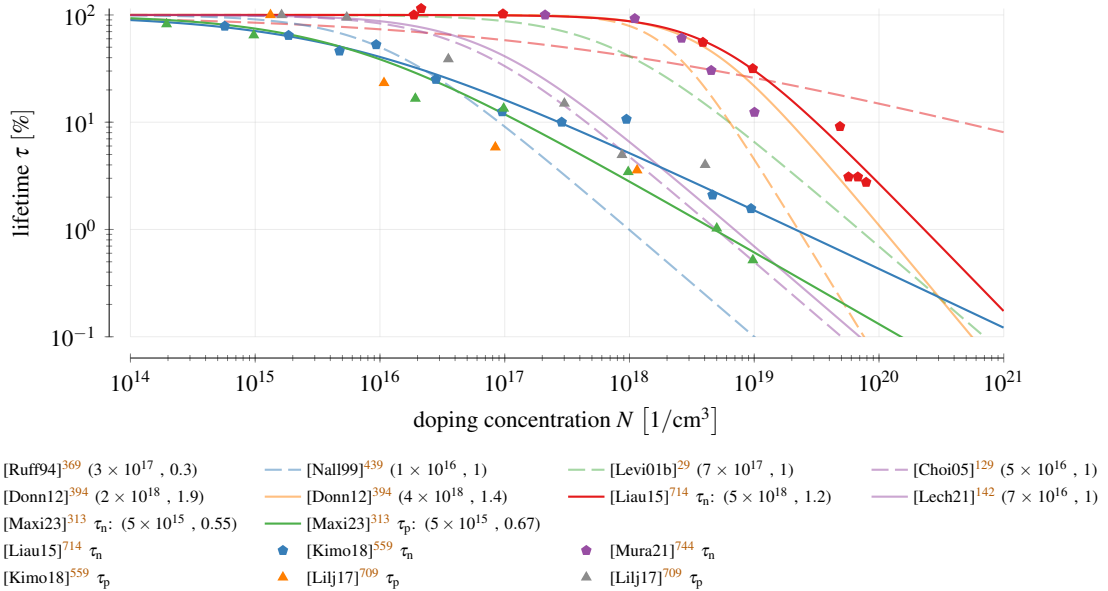


FIG. 33. Doping dependency according to the Scharfetter relation in Eq. (55). In brackets are the values for (N_{ref}, γ) . Only one graph is shown if electron and hole parameters are equal (see Table XVII). Solid non-opaque lines represent fittings to suitable 4H-SiC measurement data.

for Coulomb-attractive charge recombination centers⁷²³.

The origin for the value $\alpha_{n,p} = 5$ ^{206,362,363} is unclear. Although we stated Balachandran, Chow, and Agarwal³⁶² here we were not able to find a measurement that derived these values. We suspect that these were default values of a TCAD tool but we could not even confirm that. In the same sense we were not able to pinpoint the origin of the value $C = 2.55$ ⁴³⁹ for Eq. (60). Although Lechner¹⁴² provided a reference⁷⁸⁶ we were not able to find anything in there either.

For the exponential based approaches the value of E_{act} was chosen between 110 – 125 meV and for Eq. (61) Lechner¹⁴² proposed a variety of parameters. We calculated the average from the single sets and achieved the values shown in Eq. (76).

$$T_{\text{coeff}} = 0.666, \quad \alpha_{\tau} = 0.06385, \quad \beta_{\tau} = 5.716 \quad (76)$$

A comparison of the single models (see Fig. 34) shows a consistent increase of the lifetime with temperature. We added some temperature measurements and scaled them such that the room temperature values are around the arbitrary value of 1 μs . We had to dismiss the values by Lophitis *et al.*⁴⁴⁸ because the authors only showed the parameters but not the according equations. We also do not show the results by Puzzanghera and Nipoti⁷⁷¹, who derived solely minor deviations around the room temperature value.

TABLE XVIII. Temperature dependency of the lifetime. If only one value for $\alpha_{n,p}$ is stated no charge carrier specification was made in the publication. Column *conf.* shows the confidence interval and *equ.* the model.

ref.	α_n	α_p	T_0	E_{act}	C	conf.	equ.	method
	[1]	[1]	[K]	[eV]	[1]	[K]		
[Kord96] ^{612 a}	–	1.72	300	–	–	300 – 500	(56)	PLD
[Ivan99] ^{721 c}	–	–	–	0.11	–	300 – 500	(58)	OCVD
[Nall99] ^{439 b}	–	–	300	–	2.55	–	(60)	–
[Udal00] ⁷⁶⁶	–	2.2	300	–	–	200 – 450	(56)	RR
[Agar01] ^{720 c}	–	–	–	0.12	–	300 – 500	(58)	TTOGC
[Bala05] ³⁶²	5	–	300	–	–	–	(56)	–
[Levi05] ^{719 c}	–	–	–	0.08	–	300 – 550	(58)	–
[Ivan06a] ^{722 d}	–	–	–	0.105	–	300 – 500	(58)	SIM
[Udal07] ⁷²³	–	1.9	300	–	–	300 – 700	(56)	RR
	–	4.4	300	–	–	700 – 1000	(56)	RR
[Scaj13] ⁵⁸⁹	–	–	–	0.125	–	70 – 1000	(59)	FCA
[Dibe14] ⁴⁵³	2.15	–	300	–	–	250 – 500	(56)	DCD
[Chow15] ^{478 e}	1.2	–	300	–	–	300 – 525	(56)	μ -PCD
[Rakh20] ³¹⁸	–	8	450	–	–	100 – 700	(57)	–
	–	14	530	–	–	100 – 700	(57)	–
[Sapi20] ⁷¹⁶	1.5	–	300	–	–	300 – 450	(56)	OCVD
[Tian20] ¹⁶	1.84	1.84	300	–	–	300 – 573	(56)	DCD
[Maxi23] ^{313 f}	1.72	1.72	300	–	–	–	(56)	FIT
[Sozz24] ⁷⁷⁰	1.7	–	298	–	–	300 – 450	(56)	OCVD

^a fitting provided in citing articles, Sapienza *et al.*⁷¹⁶ fitted $\alpha = 1.9$

^b default value in simulation tool, according to Lechner¹⁴² based on the research from Grasser *et al.*⁷⁸⁶

^c fitting by Udal and Velmre⁷²³

^d fitting by Tamaki *et al.*⁷²⁸

^e fitting by Sapienza *et al.*⁷¹⁶

^f fitted to results by Kimoto *et al.*⁵⁵⁹

Some trajectories^{16,313,453,716,722,770} can be inferred from the existing results and are not explicitly shown to improve visibility. For Eq. (56) a higher value of α leads to a steeper increase, comparable to a higher value of E_{act} in Eq. (58). Different shapes are predicted by Eq. (57), which shows an increases steepness at high temperatures, and Eq. (61), with the eventual decrease of the

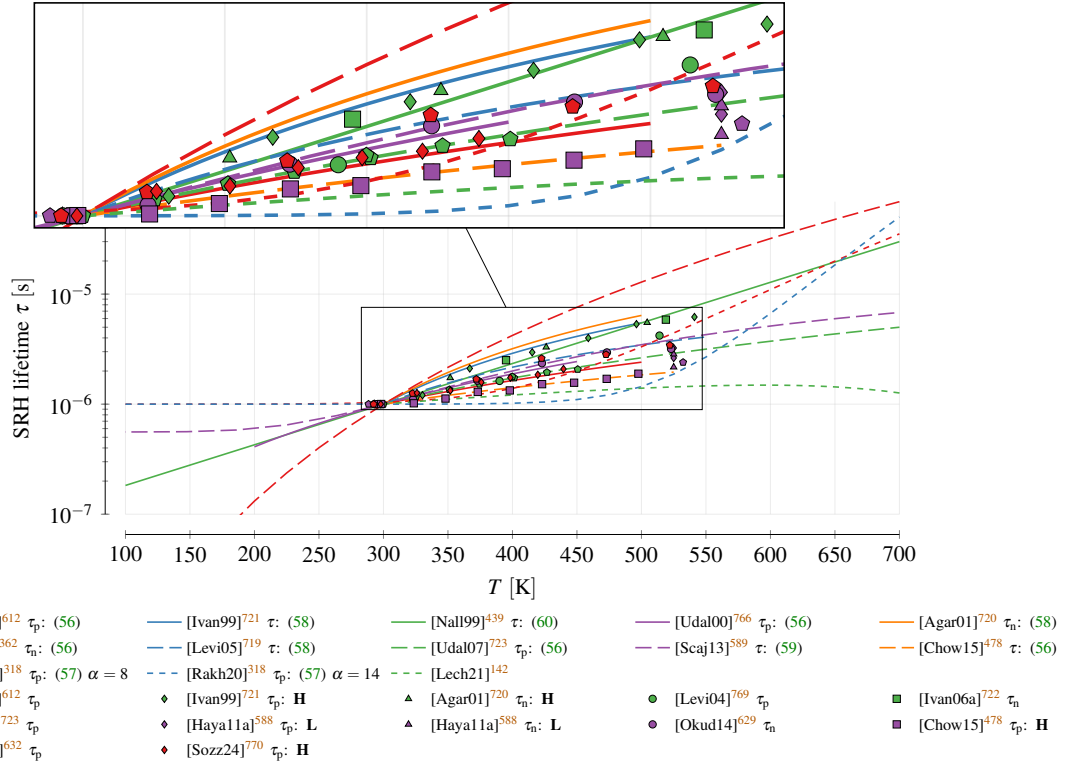


FIG. 34. Temperature Dependency of the SRH lifetime. Models are calibrated to hit $1\ \mu\text{s}$ at 300 K. Measurement results are scaled such that $1\ \mu\text{s}$ at (296 ± 4) K is achieved. **H** denotes high level injection and **L** low level one.

lifetime at high temperatures.

We want to remind the reader that temperature changes depend on the doping concentration⁷⁴⁴. In addition, the measured value, e.g., the sum of hole and electron lifetime for high level injection⁴⁷⁸, can have a differing temperature dependency. Sapienza *et al.*⁷¹⁶ compared various sources in this respect^{147,612,723}.

4. Surface Recombination Velocity

The surface recombination velocity is, as the name indicates, not a bulk property but depends on many parameters such as crystal faces, i.e., Si-, C-, a- or m-face^{731,732}, interface treatment and the resulting interface traps⁷⁸⁷. For these reasons we will only roughly cover this topic. Ščajev *et al.*⁴⁴⁶, Gulbinas *et al.*⁷²⁹, Mori, Kato, and Ichimura⁷³² published interesting analyses of the surface recombination velocity for the interested reader.

In general, the surface recombination velocity has to be determined for each sample separately,

due to its wide range of dependencies. It scales with temperature^{718,731} and depends on the injection level^{341,446,707}, which was explained by a possible band banding near the interface⁶²⁵. Suitable values in literature were mainly based on dedicated investigations (see Table XIX) or were simply assumed, e.g., $s = 2.2 \times 10^5 \text{ cm/s}$ ⁷³⁸ and $s = 1 \times 10^3 \text{ cm/s}$ ⁶²².

To determine the surface recombination velocity complementary measurement methods to the ones mentioned in Section VIII A 5 were used, for example colinear pump probe (CPP)⁷²⁹, non-equilibrium free-carrier density (NFCD)³⁶⁰, the current density (CD)^{734,789} or reverse recovery (RR)⁷⁶⁵. A common method to extract⁷²⁹ and sometimes even eliminate^{558,761} the surface recombination was to vary the thickness of the device, but an effective bulk lifetime of more than 1 μs can only be measured directly within epitaxial layers thicker than 100 μm ⁴³. Kimoto, Miyamoto, and Matsunami^{765,790} varied the radius and extracted s_n from the change of lifetime versus the perimeter/area ratio.

Due to the numerous growth parameters⁷⁸⁸ a wide range of growth optimizations and surface treatments were proposed. While mechanically polishing surfaces leads to an increased roughness (high velocities)⁶¹¹, more recent experiments achieved velocities of $< 200 \text{ cm/s}$, indicating high surface qualities. The amount of publications in the last years also indicates an active research community.

Publications referencing other investigations often combine multiple values to achieve reasonable values, e.g., $s = (1 - 100) \times 10^3 \text{ cm/s}$ ^{21,36}, $s = 2 \times 10^3 \text{ cm/s}$ ⁴¹⁷, $s = 1 \times 10^4 \text{ cm/s}$ ⁷¹⁴, $s = 1 \times 10^3 \text{ cm/s}$ ^{593,747}, $s = 4 \times 10^4 \text{ cm/s}$ ⁵⁸⁹ and $s_n = s_p = 1 \times 10^5 \text{ cm/s}$ ⁷⁷², whereat 4H and 6H are fairly similar in this regard⁶⁰⁸.

5. Bimolecular Recombination

All studies regarding the bimolecular coefficient B achieved a value of $(1.5 \pm 0.5) \times 10^{-12} \text{ cm}^3/\text{s}$ (see Table XX) despite the comments that the parameters by Galeckas *et al.*³²⁷ were just an estimation³⁶. Exceptions were the investigation by Neimontas *et al.*³³⁴, whose value is one order of magnitude bigger, and Murata *et al.*⁷⁴⁴, who achieved 3-4 times higher values. We also found publications^{589,593,731} that only used the radiative component with a value of $(1 - 3) \times 10^{-14} \text{ cm}^3/\text{s}$ ²⁷⁵. The rather high values of B compared to the radiative part was explained by the additionally included trap-assisted Auger^{327,364} and electron-acceptor (e-A) recombination⁷⁴⁴.

Little data about the temperature dependency of B is available. Tawara *et al.*⁶³² presented

TABLE XIX. Surface recombination velocity. A *y* in column *impr.* indicates that the velocities represent the end of an optimization process.

ref.	<i>s</i> [cm/s]	<i>s_n</i> [cm/s]	<i>s_p</i> [cm/s]	type ^a	impr.	method
[Gale97] ³²⁷	–	–	$4 \times 10^4 / 1 \times 10^4$	S/I	–	FCA
[Neud98] ⁵⁵⁸	–	–	5×10^4	M	–	RR
[Gale99a] ⁶⁰⁸	–	–	$(5 - 8) \times 10^3$	S	y	FCA
[Kimo99] ⁷⁶⁵	–	–	5×10^4	M	–	CD
[Gale01] ⁶⁰⁹	$(5 - 500) \times 10^3$	–	–	S	y	TA
[Cheo03] ⁵⁵¹	–	–	1 – 1000	S	y	Ct
[Huh06] ⁶⁶⁹	–	–	2.50×10^3	S	–	TRPL
[Ivan06a] ⁷²²	4200	–	–	M	–	CD
[Neim06] ³³⁴	–	–	$(4 \pm 1) \times 10^4$	S	–	FWM
[Griv07] ³⁶⁰	1×10^4	–	–	S	–	NFCD
[Klei08] ⁶¹¹	–	–	$(5 - 500) \times 10^3$	S	y	TFCA
[Klei10] ⁷¹⁸	–	–	400 – 6940	S	–	TRPL
[Scaj10] ⁴⁴⁶	$(2 - 13) \times 10^3$	–	–	S	–	FCA
[Gulb11] ⁷²⁹	–	$(1.5 - 3) \times 10^4$	$(1 - 100) \times 10^4$	S	y	CPP
[Pour11] ⁷⁸⁸	–	1.07×10^3	$(1.07 - 57) \times 10^3$	S	y	FCA
[Kato12] ⁷³⁰	–	–	$(1 - 2) \times 10^3$	S	y	μ -PCD
[Mori14] ⁷³²	–	–	1500 – 7500	S	y	μ -PCD
[Suva15] ⁷⁵⁴	–	–	$(3.5 - 200) \times 10^4$	S/I	y	FCA
[Asad18] ⁷³⁴	$(6 - 120) \times 10^5$	–	–	M	y	CD
[Ichi18] ⁷³⁶	–	300 – 6000	200 – 2500	S	y	μ -PCD
[Kato20] ⁷³¹	–	400 – 1950	150 – 750	S	y	μ -PCD
[Xian21] ⁷⁸⁹	$((6.0 \pm 0.7) - 58 \pm 5) \times 10^5$	–	–	M	y	CD
[Kato24] ⁷⁰⁷	–	–	100 – 2500	S	y	μ -PCD

^a mesa structure (M), surface (S) or interface (I)

TABLE XX. Fundamental investigations of the bimolecular recombination parameter.

ref.	B [cm ³ /s]	T [K]	Δ_N [1/cm ³]	method
[Gale97] ³²⁷	1.50×10^{-12}	300	$1 \times 10^{16} - 1 \times 10^{19}$	FCA
[Neim06] ³³⁴	$(3 \pm 1) \times 10^{-11}$	–	$1 \times 10^{16} - 2 \times 10^{19}$	FWM
[Jara10] ⁷⁸⁰	$(1.2 \pm 0.4) \times 10^{-12}$	300	$1 \times 10^{17} - 1 \times 10^{19}$	FCA
[Tawa16] ⁶³²	1.3×10^{-12}	300	$4 \times 10^{14} - 1 \times 10^{16}$	TRPL
	0.94×10^{-12}	523	$4 \times 10^{14} - 1 \times 10^{16}$	TRPL
[Mura21] ^{744 a}	5.6×10^{-12}	293	7×10^{14}	TRPL
	4.5×10^{-12}	523	7×10^{14}	TRPL
[Tana23a] ⁷⁵⁵	$< 2 \times 10^{-12}$	–	$2 \times 10^{18} - 1 \times 10^{19}$	FCA

^a includes electron acceptor recombination

measurements for six different temperatures and concluded that the value stayed constant. If one would, however, ignore the data point at the lowest temperature, a decrease with temperature could be inferred. Ščajev *et al.*²⁷⁵ stated that the radiative recombination coefficient doubles in the range of 10 – 1000 K, which could also lead to an increase of B . Jarašiūnas *et al.*⁷⁸⁰ proposed an empirical equation for the temperature dependent coefficient (see Eq. (77)), which shows a decrease with increasing temperature. For higher confidence in the results further investigations would be necessary.

$$B(T) = 1.1 \times 10^{-12} \text{ cm}^3/\text{s} + T^{-4} \times 1.7 \times 10^{-4} \text{ K}^4 \text{ cm}^3/\text{s} \quad (77)$$

Tanaka, Nagaya, and Kato⁷⁴⁷ noted that for the investigation of excess carrier dependent Auger coefficients, which will be presented in the sequel, the characterization of $B(\Delta_N)$ is essential and thus will be one topic of their future research.

6. Auger Recombination

Galeckas *et al.*³²⁷ conducted in 1997 the first research on Auger coefficients in 4H-SiC and provided separate values for electrons (C_n) and holes (C_p). Despite this early availability 4H investigations^{48,142} still used values based on 6H⁷⁹¹ and even³⁵³ based on Silicon^{247,369}. Zhao

TABLE XXI. Auger recombination parameters.

ref.	C_n [cm ⁶ /s]	C_p [cm ⁶ /s]	T [K]	method	Δ_N [1/cm ³]
[Gale97] ³²⁷	$(5 \pm 1) \times 10^{-31}$	$(2 \pm 1) \times 10^{-31}$	300	FCA	$2 \times 10^{18} - 2 \times 10^{19}$
[Griv07] ³⁶⁰	2×10^{-30}	–	75	FCA	1×10^{16}
[Scaj10] ⁴⁴⁶		$(7 \pm 4) \times 10^{-31}$	298	FCA	$1 \times 10^{18} - 3 \times 10^{18}$
		$(0.8 \pm 0.2) \times 10^{-31}$	298	FCA	$1 \times 10^{19} - 1 \times 10^{20}$
[Scaj13] ⁵⁸⁹	$(5 \pm 1) \times 10^{-31}$	–	FCA	1×10^{17}	
[Tawa16] ⁶³²	1.6×10^{-30}	–	300	TRPL	$3 \times 10^{17} - 7 \times 10^{18}$
	0.44×10^{-30}	–	523	TRPL	$3 \times 10^{17} - 7 \times 10^{18}$
[Tana23] ^{747 a}	7.4×10^{-19}	$\Delta_N^{-0.68}$	–	FCA	$5 \times 10^{18} - 1 \times 10^{20}$
[Tana23a] ⁷⁵⁵	$< 3 \times 10^{-31}$	–	FCA	$2 \times 10^{18} - 1 \times 10^{19}$	

^a added measurements by Ščajev *et al.*⁴⁴⁶ to characterization

*et al.*¹⁶⁷ simply assumed $C_n = C_p = 1 \times 10^{-28}$ cm⁶/s, which is nearly three orders of magnitude larger than the measured values.

The next fundamental characterization we found after this initial work was conducted one decade later by Grivickas *et al.*³⁶⁰. From then onward new values were published on shorter intervals, up to this day (see Table XXI). However, these only proposed combined coefficients or considered just one charge carrier. For the results presented by Tawara *et al.*⁶³² we concluded from the description of samples and measurement (low injection and highly n-doped material) that C_n was determined.

The achieved values are in the range of $(1 - 11) \times 10^{-31}$ cm⁶/s, with the exceptions of Grivickas *et al.*³⁶⁰ and Tawara *et al.*⁶³², who derived parameters up to 2×10^{-30} cm⁶/s. A possible explanation is a dependency on the excess charge carrier density Δ_N , which was first discussed by Ščajev *et al.*⁴⁴⁶, who denoted $C \propto \Delta_N^{-0.3}$. In recent days Tanaka, Nagaya, and Kato⁷⁴⁷ achieved $C \propto \Delta_N^{-0.68}$ and explained the deviation by deviating estimation methods, differences in the samples and a Δ_N -dependency of the bimolecular coefficient B . Possible is also a doping material dependency because Murata *et al.*⁷⁴⁴ reported that Auger recombination was not important for an Aluminum doping concentration of 1×10^{19} /cm³ but considerable for a Nitrogen doping in the

TABLE XXII. Parameters for Auger model shown in Eq. (71)

ref	type	A [cm ⁶ /s]	B [cm ⁶ /s]	D [cm ⁶ /s]	H	N_0 [1/cm ³]	T_0 [K]
. [Loph18] ⁴⁴⁸	τ_n	6.7×10^{-32}	2.45×10^{-31}	-2.2×10^{-32}	3.47	10^{18}	300
	τ_p	7.2×10^{-32}	4.5×10^{-33}	2.63×10^{-32}	8.26	10^{18}	300
[Zhan18] ⁵⁶⁶	τ_n	5×10^{-31}	2.45×10^{-31}	-2.2×10^{-32}	0	—	—
	τ_p	9.9×10^{-32}	4.5×10^{-33}	2.63×10^{-32}	0	—	—

mid $1 \times 10^{18} / \text{cm}^3$ range.

The value from Ščajev and Jarašiūnas⁵⁸⁹ presented in the table corresponds to the temperature-independent unscreened phonon-assisted coefficient. The authors combined the decrease of the Auger coefficient with rising excess carrier concentration, which they attributed to the screening of the carrier-phonon interaction by free carriers, with a temperature dependency (see Eq. (70)) using the parameters shown in Eq. (78). We found this kind of description only once again in literature⁹¹ but two instances based on the description of Si (see Eq. (71))^{448,566}. The respective parameters are shown in Table XXII, which we encountered also as default value for Si in some TCAD simulation suites.

$$\alpha = 0.45 \text{ meV/K} \quad (78a)$$

$$B_{CE}(T) = 3.5 \times 10^{-9} T^{-3/2} \text{ cm}^3/\text{s} \quad (78b)$$

$$a_{SC} = 7.8 \times 10^{16} \text{ K/cm}^3 \quad (78c)$$

Dedicated 4H-SiC models and measurements predict a decrease of C with increasing temperature (see Fig. 35), which confirms the prediction that Auger recombination is not significant for power devices operated at high temperatures Bellone *et al.*²⁰⁹. In contrast, the models that were developed for Silicon predict an increase of C .

Finally, we combine all contributions to the lifetime into one plot, showing the lifetime over the excess carrier concentration (see Fig. 36). For the SRH lifetimes we added all measurements that clearly specified the excess carrier concentrations. In this log-log representation changes of the bimolecular and Auger coefficients only cause a horizontal shift while the derivative (-1 for bimolecular; -2 for Auger, except for Δ_N -dependent models) stays constant. The higher the value of τ_{SRH} the earlier and more pronounced is the impact of the bimolecular recombination. A

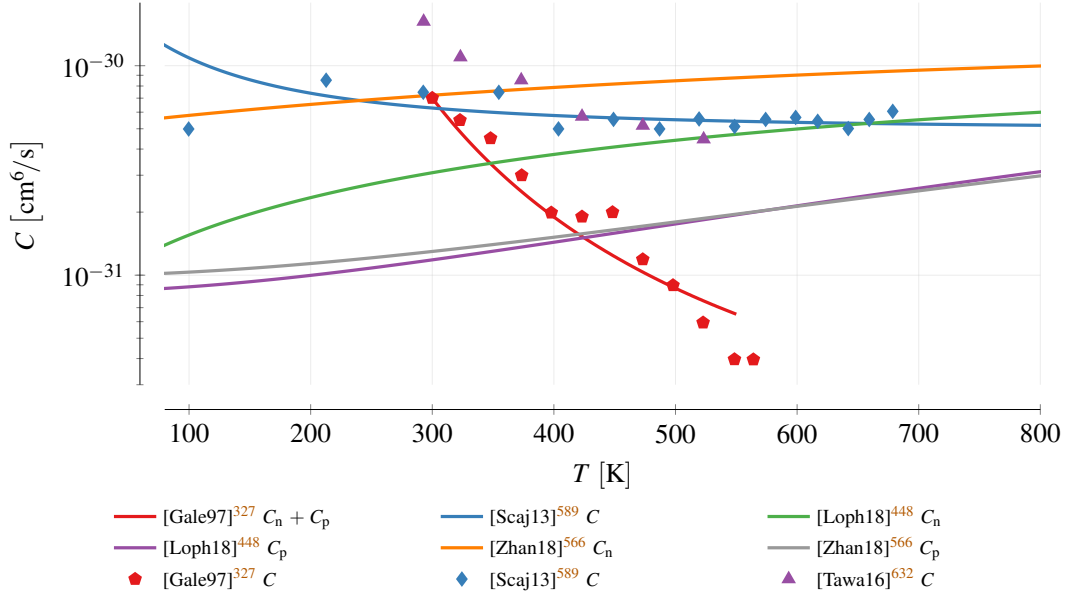


FIG. 35. Temperature dependency of the Auger recombination coefficients C_n and C_p for $\Delta_N = 2.5 \times 10^{18}/\text{cm}^3$.

decrease due to Auger recombination only becomes significant for $\Delta_N > 10^{18}/\text{cm}^3$.

At the moment we are unable to explain the lifetime measurements in regions where bimolecular resp. Auger recombination should be the limiting factors. To explain these deviations we scaled, wherever possible, the marker size with the reported doping concentration, because according to Eq. (55) the lifetime should decrease with increasing doping. However, the data did not show such a behavior. Exceptional in our opinion is also the Δ_N -dependent model of Tanaka, Nagaya, and Kato⁷⁴⁷ that uses $C \propto \Delta_N^{-0.68}$ because the slope in the log-log plot is equal to the bimolecular coefficient B . At high concentrations of Δ_N the model by Ščajev and Jarašiūnas⁵⁸⁹ even predicts a constant Auger contribution.

7. Origin of Parameters

The doping dependency of 4H-SiC is predominantly modeled by the Silicon based values by Ruff, Mitlehner, and Helbig³⁶⁹ (see Fig. 37). While some publications are well aware that Silicon data are used^{48,66,740} this information seemingly was lost over the years. More recent investigations that were focused on 4H-SiC were almost never referenced. In regard to the temperature dependency the most influential publication is the one by Kordina *et al.*⁶¹². In total five funda-

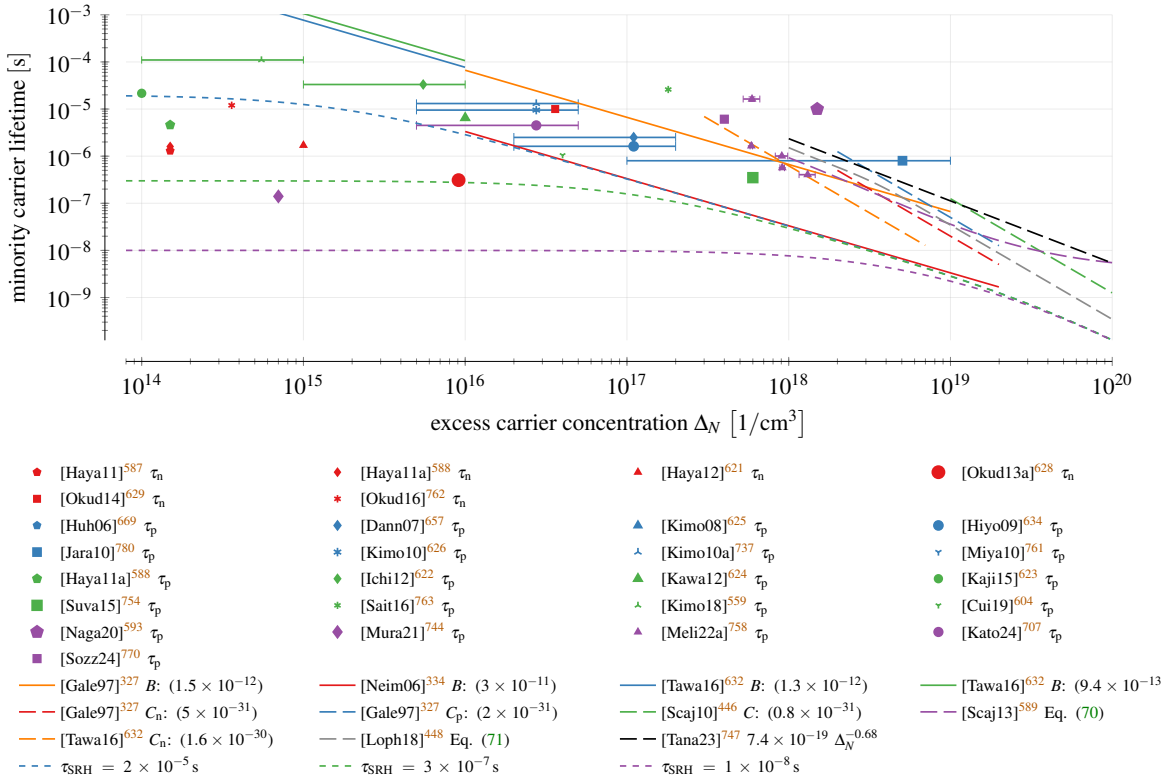


FIG. 36. Charge carrier lifetime considering the contributions of SRH, bimolecular (solid lines) and Auger (long dashed lines). The overall recombination lifetime τ_r (dashed line) is shown for three values of $A = (\tau_{SRH})^{-1}$, $B = 3 \times 10^{-11} \text{ cm}^3/\text{s}$ ³³⁴ and $C = 5 \times 10^{-31} \text{ cm}^6/\text{s}$ ³²⁷ in Eq. (75). The marker size scales with the doping concentration. We picked an intermediate size if no data were available.

mental investigations on 4H-SiC were referenced in literature.

For bimolecular and Auger recombination the main source in literature is the publication by Galeckas *et al.*³²⁷ (see Fig. 38). Additional fundamental investigations^{446,589,755,780} are referenced as well. Despite the large amount of references, the coefficients were transferred in almost all cases truthfully. This is extraordinary when we compare it against other topics investigated within this review. All the inconsistencies we encountered for charge carrier recombinations are presented in Section A 5.

IX. INCOMPLETE IONIZATION

To build electronic devices it is indispensable to utilize doping, i.e., to introduce impurity atoms during or even after the growth process. These so-called dopants add energy levels near the con-



FIG. 37. Reference chain for doping and temperature dependency of the SRH lifetime. are fundamental investigations, research not focused on 4H and connections predicted from the used values.

duction (n-type doping) respectively valence band (p-type doping) such that free charge carrier are already available at moderate temperatures. Unintentional impurities, often referred to as traps or defect (centers), distinguish from dopants mainly due to their generally higher ionization energy, but their description in TCAD tools is similar. Consequently, the boundary between traps and dopants is continuous.

We found several overviews on the most common doping elements and their respective activation energies in 4H-SiC^{6,7,20,21,28,30–32,114,128,130,131,179,182,228,340,399,415,425,449,656}. In addition, ab initio calculations by Miyata, Higashiguchi, and Hayafuji⁷⁹⁶ identified Arsenic⁷⁹⁷, Gallium⁷⁹⁸ or Antimony as fitting based on their energy level. Krieger *et al.*⁷⁹⁹ investigated group IV elements, Feng and Zhao²⁰, Huang *et al.*⁶⁶⁸ focused on Tantalum and Chromium and Dalibor *et al.*⁶⁵⁵, Dalibor and Schulz⁶⁵⁶ on Vanadium. The activation rates⁸⁰⁰ or the impact of hydrogen⁶⁶⁷ prevented so far the deployment of these dopants.

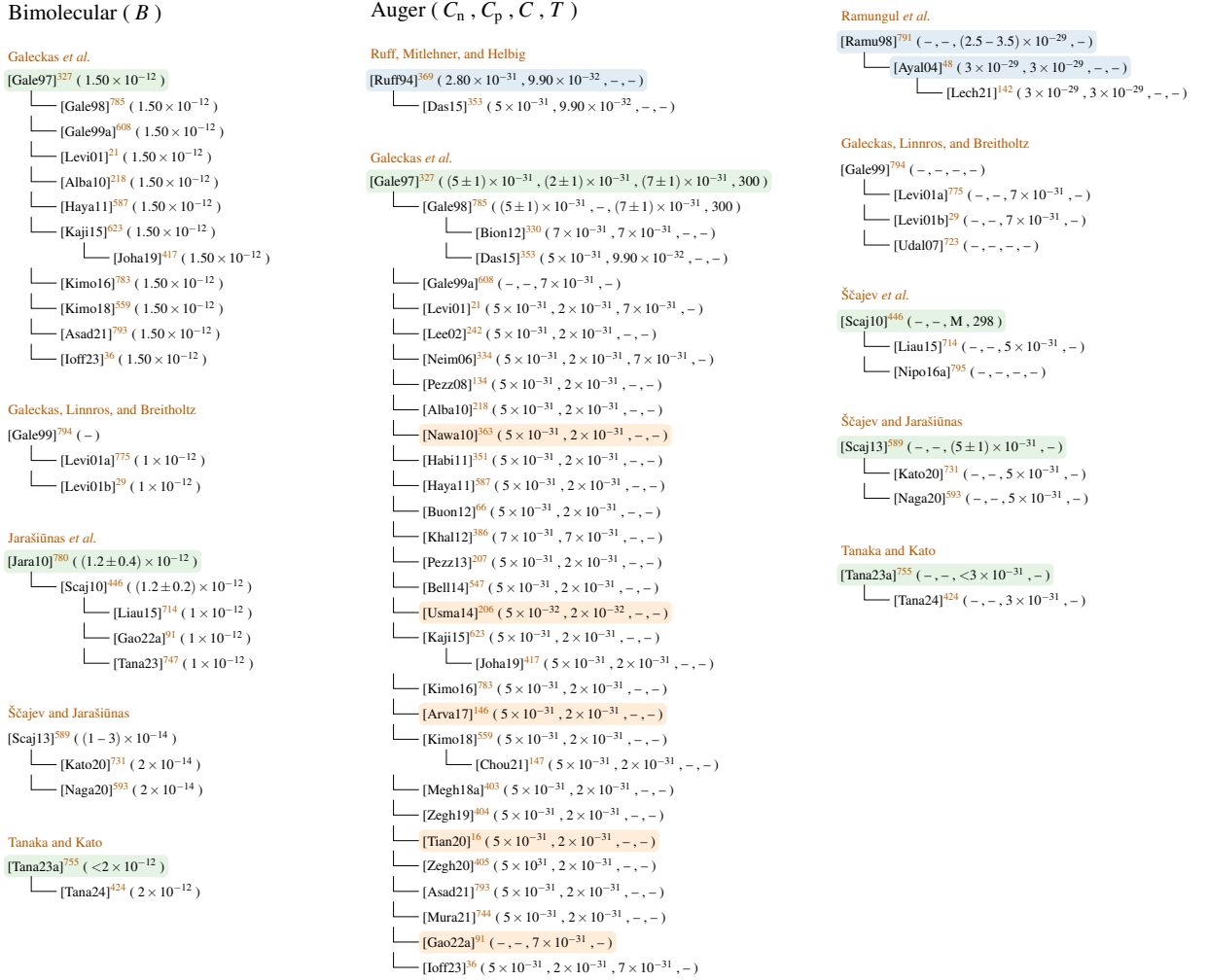


FIG. 38. Reference chain for bimolecular and Auger charge carrier recombination. are fundamental investigations, research not focused on 4H and connections predicted from the used values.

Due to the wide band gap of 4H-SiC the difference between the doping energy level and the conduction resp. valence band, i.e., the dopant activation energy, is large compared to the thermal energy. Consequently, the often used assumption of full ionization is not applicable. Quite the opposite: incomplete ionization has to be considered to accurately predict the amount of free charge carriers and, thus, a realistic conductivity^{801,802}. Scaburri³³ and Schöner³⁴ provided an overview of various physics-based models to describe incomplete ionization.

In this section we will review measurements, models and TCAD parameters used to described the amount of ionized dopants and their respective ionization energies depending on temperature and doping concentration. We focus on the four most common doping species in 4H-SiC^{33,218,803}: Aluminum and Boron for p-type resp. Nitrogen and Phosphorous for n-type doping. We limit

ourselves to simple models that use a single energy level per lattice site (cubic or hexagonal; cp. Section III), because elaborate descriptions³¹⁰ would be necessary to cover changes due to the binding type or the dopant location^{198,427,678,692,802}.

Our review revealed that Aluminum and Nitrogen were primarily investigated in the past, while Boron and Phosphorous received less attention. The energy levels introduced by donors are “shallower” (less activation energy) than those by acceptors. For the latter we found even deeper energy levels that accompany the doping process and that were occasionally considered the activation energy. For Nitrogen further measurements at high doping densities are required to fit the available doping dependency models.

A. Introduction

The amount of ionized donors (N_D^+) and acceptors (N_A^-) can be determined by the Fermi-Dirac distribution^{236,351,414,415,804}, also known as steady-state Gibbs distribution⁸⁰² (see Eq. (79)). N_A resp. N_D are the active acceptor resp. donor concentrations, E_A resp. E_D the acceptor resp. donor energy levels and $E_{F,n}$ resp. $E_{F,p}$ the electron resp. hole Fermi levels.

$$\begin{aligned} N_D^+ &= \frac{N_D}{1 + g_D \exp\left(\frac{E_{F,n} - E_D}{k_B T}\right)} \\ N_A^- &= \frac{N_A}{1 + g_A \exp\left(\frac{E_A - E_{F,p}}{k_B T}\right)} \end{aligned} \quad (79)$$

g_D resp. g_A denote the degeneracy of the energy levels²⁷⁰, which was also modeled as $G_A(T)$ and $G_D(T)$ ^{7,8,10,33,118,683,805} by adding a temperature dependency. The latter was based on the ionization energy or the energy separation of excited states using varying models, whereat TCAD tools provide at the moment sole the scaling shown in Eq. (80), with $\Delta E_D = E_C - E_D$ resp. $\Delta E_A = E_A - E_V$ the ionization energies of donors and acceptors relative to the conduction (E_C) and valence band (E_V). Since the degeneracy factor is still the only parameter here we are not going to discuss this temperature dependency any further.

$$G_{A,D}(T) = g_{A,D} \exp\left(\frac{\Delta E_{A,D}}{k_B T}\right) \quad (80)$$

If solely the Boltzmann statistics are considered, Eq. (79) can be simplified to the expression shown in Eq. (81)^{33,48,66,144,182} with N_C resp. N_V the effective density of states in the conduction

resp. valence band (see Section VI). This representation is often preferred in TCAD simulation tools, because these commonly operate on charge carrier concentrations.

$$\begin{aligned} N_D^+ &= \frac{N_D}{1 + g_D \frac{n}{n_1}}, & n_1 &= N_C \exp\left(-\frac{\Delta E_D}{k_B T}\right) \\ N_A^- &= \frac{N_A}{1 + g_A \frac{p}{p_1}}, & p_1 &= N_V \exp\left(-\frac{\Delta E_A}{k_B T}\right) \end{aligned} \quad (81)$$

The carrier concentration can be eliminated completely by using the neutrality equation³³ shown in Eq. (82) .

$$N_D^+(E_F) + p(E_F) = N_A^-(E_F) + n(E_F) \quad (82)$$

If we assume a highly donor doped material ($p(E_F)$ can be neglected) and no compensation ($N_A^-(E_F) = 0$) the expression for N_D^+ in Eq. (81) can be inserted into Eq. (82) resulting in a quadratic equation whose solution is shown in Eq. (83)^{218,242,246,369,404,405,700}. For a highly acceptor doped material an according expression is achieved. The calculations of Scaburri³³ interfered with our analyses, because the author presented on page 22 an expression for n that (i) is not required for the calculation and that (ii) we did not find in the cited publication²⁷⁰. We solely achieved the shown result when we calculated $1/n$ and used in one occasion the wrong parameter.

$$N_D^+ = N_D \frac{-1 + \sqrt{1 + 4 g_D \frac{N_D}{N_C} \exp\left(\frac{\Delta E_D}{k_B T}\right)}}{2 g_D \frac{N_D}{N_C} \exp\left(\frac{\Delta E_D}{k_B T}\right)} \quad (83)$$

The ionization energy of a dopant is not constant but can vary due to band gap narrowing effects, which we discussed in Section VI, and a doping dependency. The latter will be discussed in the sequel.

1. Doping Dependency

The changing potential energy of charge carriers in the vicinity of ionized atoms, which effectively shielding them⁸⁰⁶, was provided as explanation for the doping dependency of the ionization energy. The Pearson-Bardeen⁸⁰⁶ expression shown in Eq. (84) models the decrease of ΔE .

$$\Delta E(N) = \Delta E_0 - \alpha N^{1/3} \quad (84)$$

Schöner³⁴ proposed a more physics based approach shown in Eq. (85) with f being a dimensionless factor that denotes the interaction strength with ionized acceptors and donors. Several other

approaches to model the decrease of the ionization energy, e.g., due to interactions with a neighboring ionized dopant of the same kind, a local potential variation due to interaction with charged donors and acceptors⁸⁰⁷ and an extension of the latter in regard to the temperature dependency⁸⁰⁸, were also discussed^{33,34,809}. These were, however, not applied to 4H-SiC in the literature and are thus not considered in this review.

$$\Delta E(N) = \Delta E_0 - f \frac{q^2}{4\pi\epsilon_s\epsilon_0} N^{1/3} \quad (85)$$

We found some disagreement on what kind of dopants should be used for parameter N in Eq. (84). We found the sum of donors and acceptors $N_A + N_D$ ^{66,144}, the respective doping concentration (N_A or N_D)^{119,133,672,683,810,811} and the ionized dopants⁷⁰. Kajikawa⁸¹² argued that the compensating dopant concentration N_K , i.e., donors for the acceptor levels and vice versa, have the bigger impact and should be used instead of the overall donor and acceptor concentrations. This is supported by Scaburri³³ who used $N = N_D - N_K$ and approaches that proposed to include N_K into the factor α ^{33,813,814}.

Altermatt, Schenk, and Heiser⁸¹⁵, Altermatt *et al.*⁸¹⁶ proposed the logistic equation shown in Eq. (86) as an alternative to Eq. (84). For $N = N_E$, which denotes a reference concentration, the ionization energy dropped to half its initial value ΔE_0 . Darmody and Goldsman¹⁹⁷ argued that with Eq. (84) it is possible to shift the dopant level into the conduction/valence band and thus ionize all dopants immediately, which is neither physically reasonable nor possible with Eq. (86). Despite these arguments, the described approach has not yet found its way into the major simulation tools.

$$\Delta E(N) = \frac{\Delta E_0}{1 + (N/N_E)^c} \quad (86)$$

Dopants have differing ionization energies depending on whether they are located in a hexagonal or a cubic lattice site⁹⁵ (see Section III). Consequently Eq. (81) has to be adapted to the expression shown in Eq. (87)^{144,797} with ΔE_{Dc} and ΔE_{Dh} the cubic resp. hexagonal ionization energies for donors and ΔE_{Ac} and ΔE_{Ah} for acceptors.

$$\begin{aligned} N_D^+ &= \frac{\frac{1}{2}N_D}{1 + g_D \frac{p}{N_C} \left(\frac{\Delta E_{Dh}}{k_B T} \right)} + \frac{\frac{1}{2}N_D}{1 + g_D \frac{p}{N_C} \left(\frac{\Delta E_{Dc}}{k_B T} \right)} \\ N_A^- &= \frac{\frac{1}{2}N_A}{1 + g_A \frac{p}{N_V} \left(\frac{\Delta E_{Ah}}{k_B T} \right)} + \frac{\frac{1}{2}N_A}{1 + g_A \frac{p}{N_V} \left(\frac{\Delta E_{Ac}}{k_B T} \right)} \end{aligned} \quad (87)$$

The factors 1/2 denote that both lattice sites are equally probable⁴⁸. In TCAD simulations it is often the case that these separate values are merged to an effective energy level, ending up once

again in a description as shown in Eq. (81)^{66,139,220,369,449}. Lades¹⁴¹ and Ayalew *et al.*⁶⁴² reported on the consequences of such simplifications.

2. Capture Cross Sections

For more accurate approximation of dynamic processes around the dopant, i.e., (de)trapping of charge carriers, the electron and hole cross sections are required (see Section VIII). The larger the cross section the easier a charge carrier can transition to the dopant energy level. We found multiple descriptions in literature that differ in their temperature scaling⁵⁹⁷. The multi-phonon capture model is independent of temperature^{34,817–819} and the cascade capture model, which Kaindl *et al.*⁸²⁰ credited a better fit, is proportional to T^{-2} ^{34,331,821,822} (also [78Aba] in Schöner³⁴). Kuznetsov and Zubrilov³²¹ used a scaling with T^{-3} . In TCAD tools deviating subsets of these models are supported.

3. Methods

The most commonly method to determine the ionization energy of dopants in literature is to fit the neutrality equation, i.e., for p-type doping shown in Eq. (88), to Hall measurements of the conductivity or charge carrier concentration for varying temperature^{133,271,454,650,670,673,674,812,823–825 8,10,118–120,301,314,331,335,482,678,680,684,688,690,697,699,700,798,811,826–836}. Due to the anisotropy of the Hall effect it is possible to achieve direction dependent ionization energies⁸.

$$p + N_K = \frac{N_A}{1 + \frac{g_{AP}}{N_V} \exp\left(\frac{\Delta E_A}{k_B T}\right)} \quad (88)$$

Other electrical measurement methods include the fitting to the activation ratio of Hall measurements⁸³⁷, free carrier concentration spectroscopy (FCCS)^{672,683,838}, (thermal)^{371,839–841} admittance spectroscopy (AS)^{8,10,201,331,674,798,811,820}, electron spin resonance (ESR)⁸⁴², deep level transient spectroscopy (DLTS)^{8,321,703,843}, thermally stimulated current (TSC)^{458,685} and minority carrier transient spectroscopy (MCTS)⁷⁰³, which are often combined with Hall measurements for more accurate results. Troffer¹⁰ noted that DLTS is more sensitive but admittance spectroscopy allows to depict time constants below 1 μ s.

These electrical methods are complemented by optical ones, e.g., (fourier transform infrared) photothermal ionization spectroscopy (PTIS)³²⁸, donor-acceptor pair (DAP) luminescence^{13,95,110,436},

free to acceptor (FTA) spectroscopy⁹⁵, infrared absorption (IA)²⁷¹, photoluminescence (PL)^{418,444,455,674,696}, time-resolved spectroscopy (TRS)⁴⁵⁵ or delay measurements (DM)⁴⁵⁵. In these cases electrons are empowered and the resulting photon emission is recorded. The latter can be caused by transitions among dopants (traps) or between dopants (traps) and the conduction/valence band⁸. Different methods lead to slightly deviating results, even when applied to the same device²⁷¹. Also possible are calculations, e.g., Faulkner model (FM) calculations¹¹¹, density functional theory (DFT)^{291,796}, effective mass approximation (EMA)²⁹⁵, first principles calculations (FPC)^{198,667,668} or *ab initio* supercell calculations (AISC)⁸⁴⁴. Finally, some authors defined a value range based on measurements in literature^{48,141,218}, calculated an average value⁶⁸², fitted to existing data^{142,144,197} or to the upper concentration limit of a dopant (UCLF)⁸¹⁰.

B. Results & Discussion

In the sequel we are going to present measurements and models for the ionization energies ΔE_D resp. ΔE_A . To depict reported measurement results we occasionally dropped uncertainties and replaced the sometimes stated free exciton binding energy E_x by 20 meV (see Section VI). We had to discard publications that described the samples solely as “high purity” or “unintentional doped”^{418,444,454,696} and the data by Laube *et al.*⁸⁴⁵, which were superseded by a publication of the same authors⁶⁷⁸. We mark results for the hexagonal lattice site by a trailing h and result for the cubic one by a trailing c . In the literature the latter is often denoted by the letter “k”, which, most probably, corresponds to the german word “kubisch” for cubic. In fact, some of the literature is written in german^{8,10}, posing a considerable barrier for the international community.

In the theoretical analysis of the previous section we showed that the incomplete ionization is dominated by two parameters: the degeneracy factor and the ionization energy. For the former commonly the values $g_A = 4$ (spin up and spin down plus two valence bands) and $g_D = 2$ (spin up and down)^{8,16,34,48,66,139,141,142,144,203,209,236,325,351,386,402,404,405,448–450,452,482,690,801,804,846} were used. We also found $g_D = 6$ ¹⁰, a spin degeneracy of $g_D = 4$ for Phosphorous^{33,845}, $g_A = g_D = 3$ ^{362,363}, $g_A = 2$ ⁴⁸⁴, $g_A = g_D = 2$ ⁸⁴⁷ and $g_k = 6$ resp. $g_h = 2$ for the cubic resp. hexagonal site of Nitrogen³¹⁴.

Many fundamental studies and measurements of incomplete ionization were published over more than five decades. The acquired data do not converge on single values but shows deviations of up to $\pm 20\%$. This spread did not improve with high-quality samples: Even as we limited our

analysis to the last two decades we achieved the same spread. The fact that values for hexagonal and cubic lattice sites are often used without appropriate notation adds to this uncertainty and leads to confusions and errors. These are most striking for Boron, where the deep level is approximately twice the shallow one.

1. Ionization Energy of Al

For Aluminum we found measurements and models in a time span of almost three decades (see Fig. 39), which qualitatively agree on a value of (225 ± 25) meV at low doping. This value is almost tenfold the thermal voltage at room temperature ($k_B \times 300\text{K} = 26\text{ meV}$). Most models show a noticeable change in the energy level for doping concentrations bigger than $10^{18}/\text{cm}^3$.

Eq. (84) was almost exclusively used to approximate the measurements. Achatz *et al.*⁸¹⁰ a critical aluminum concentration of $8.7 \times 10^{20}/\text{cm}^3$ for the doping-induced metal-insulator transition to set $\Delta E_A = 0$ (Kimoto and Cooper⁴³ predicted for the solubility limit $1 \times 10^{21}/\text{cm}^3$). In contrast Darmody and Goldsman¹⁹⁷ used the logistic equation in Eq. (86) that shows a slower decrease of ΔE_A below 100 meV. Aluminum is the only material where we encountered this model with the parameters shown in Eq. (89).

$$\Delta E_0 = 214.86\text{ meV} \quad , \quad N_E = 8.12 \times 10^{19}/\text{cm}^3 \quad , \quad c = 0.632 \quad (89)$$

To properly describe the measurements of low-doped and compensated devices a second energy level denoted with letter d in the figure is required¹¹⁹. The origin of this deep level is still discussed in literature: Matsuura *et al.*^{683,838} were not able to provide any explanation, Weiße *et al.*⁸¹¹ suspected excited states of the aluminum ground state and Pernot, Contreras, and Camassel¹¹⁹, Smith, Evvaraye, and Mitchel⁸³⁹ described them as the cubic lattice site, which contradicts, however, several other investigations^{119,436,839}. Although Smith, Evvaraye, and Mitchel⁸³⁹ stated that for higher concentrations only the hexagonal site is measured we show the data as they were published. An exception are the values by Saks *et al.*⁸³¹: The authors did not specify the lattice site but Pernot, Contreras, and Camassel¹¹⁹ later denoted them as cubic.

The values of ΔE_0 for the fittings according to Eq. (84) are within (220 ± 20) meV, with the exception of Schöner³⁴ and Koizumi, Suda, and Kimoto¹²⁰, who proposed slightly higher values (see Table XXIII). For α the values agree upon $(3.2 \pm 1.7) \times 10^{-5}$ meV cm. This is confirmed by a statistical analysis (see Fig. 40), which reveals that 75 % of all proposed values for α are below

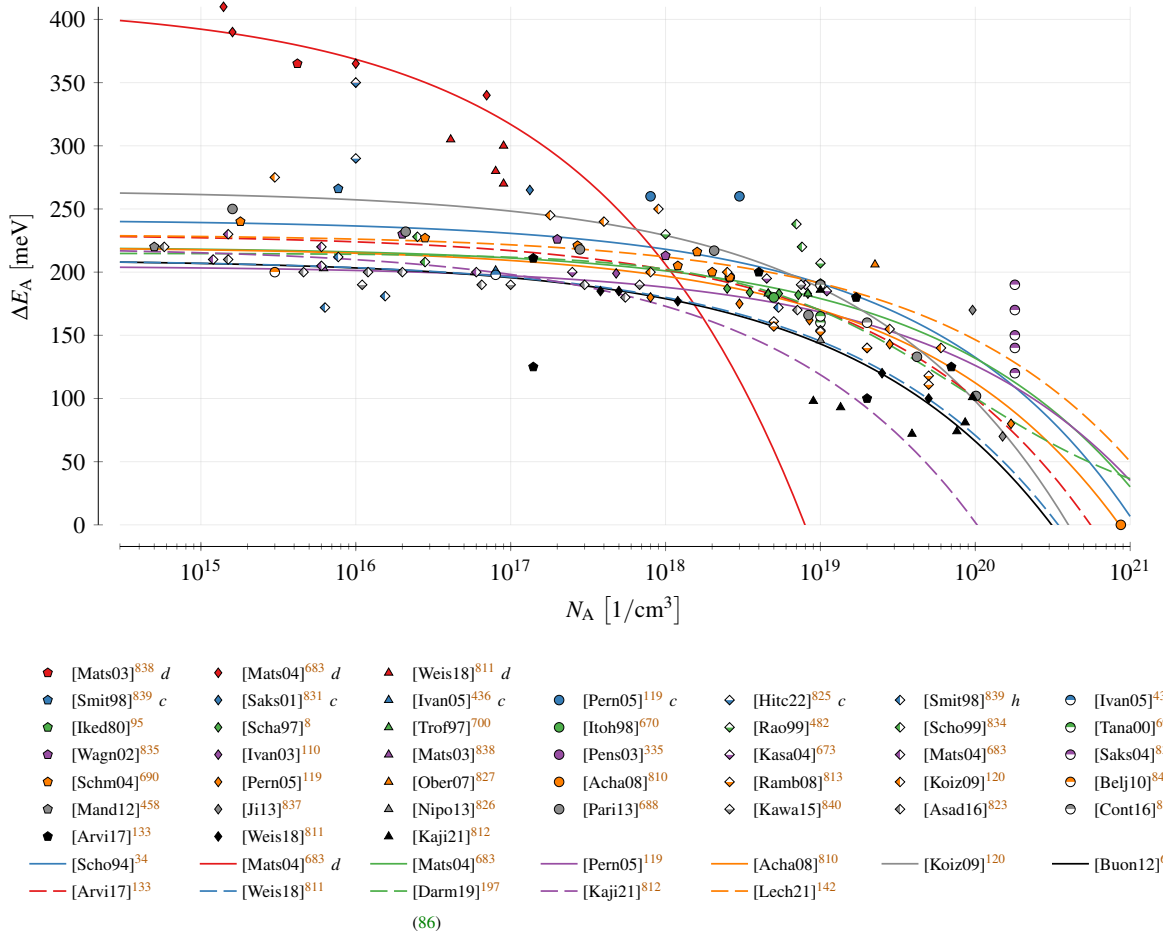


FIG. 39. Ionization energy of Aluminum. Marks refer to measurements and lines to fittings. The letter *d* after the reference indicates a deep level whose origin is still discussed (see text).

$$3.2 \times 10^{-5} \text{ meV cm.}$$

2. Ionization Energy of B

We found only a few measurements for Boron in the range of 285 – 332 meV that date back to the last millennium (see Fig. 41). We suspect the main cause in the deep D-center^{10,197,198,848} that comes with a Boron doping. It introduces an efficient recombination center with an ionization energy of 495 – 630 meV^{10,13,95,321,331,703}. Deák *et al.*⁸⁴⁹ calculated that the shallower Boron level corresponds to a hydrogen assisted incorporation at the Silicon site while the deeper is located at a carbon vacancy⁸⁵⁰. The lack of hydrogen during an implantation leads to more deep levels but in chemical vapor deposition (CVD) growth more shallow ones are observed. Nevertheless, in certain publications^{13,36,95,123,340,416,418,661} and simulation tools the D-center serves as the Boron

TABLE XXIII. Changing ionization energy of acceptors with doping (Eq. (84)). Column N denotes the interpretation of factor N : active dopants (dop), all dopants (tot), compensating ones (comp) or simply a fitting (fit). The site denotes besides hexagonal and cubic also a combined effective energy level (eff) and the deep level for Aluminum (deep).

ref.	method	N	site	ΔE	α
				[meV]	[meV cm]
Acceptor					
[Tama08a] ³²⁴	–	dop	–	191	3×10^{-5}
Aluminum					
[Scho94] ³⁴	Hall	dop	–	241.6 ± 4.8	2.35×10^{-5}
[Mats04] ⁶⁸³	FCCS	dop	–	220	1.9×10^{-5}
			deep	413	2.07×10^{-4}
[Pern05] ¹¹⁹	Hall	dop	–	205	1.7×10^{-5}
[Acha08] ⁸¹⁰	UCLF	dop	–	220	2.32×10^{-5}
[Koiz09] ¹²⁰	Hall	dop	–	265	3.6×10^{-5}
[Buon12] ⁶⁶	–	tot	eff	210	3.1×10^{-5}
[Arvi17] ¹³³	Hall	dop	–	230 ± 10	$(2.8 \pm 0.3) \times 10^{-5}$
[Weis18] ⁸¹¹	Hall AS	dop	–	210	3×10^{-5}
[Kaji21] ⁸¹²	HC	comp	–	220	4.7×10^{-5}
[Lech21] ¹⁴²	FIT	tot	–	230	1.8×10^{-5}
Boron					
[Lech21] ¹⁴²	FIT	tot	–	345	3.1×10^{-5}
t.w.	FIT	fit	–	311	1.41×10^{-5}

ionization energy.

Due to the fact that only a single fitting according to Eq. (84) was available for Boron¹⁴² we used all the available data to generate an additional one (t.w.). Both fittings show a decrease of the ionization energies for $N_A > 10^{17}/\text{cm}^3$ and a solubility limit at or above $10^{20}/\text{cm}^3$. This is in contradiction to the value of $2 \times 10^{19}/\text{cm}^3$ reported by Kimoto and Cooper⁴³.

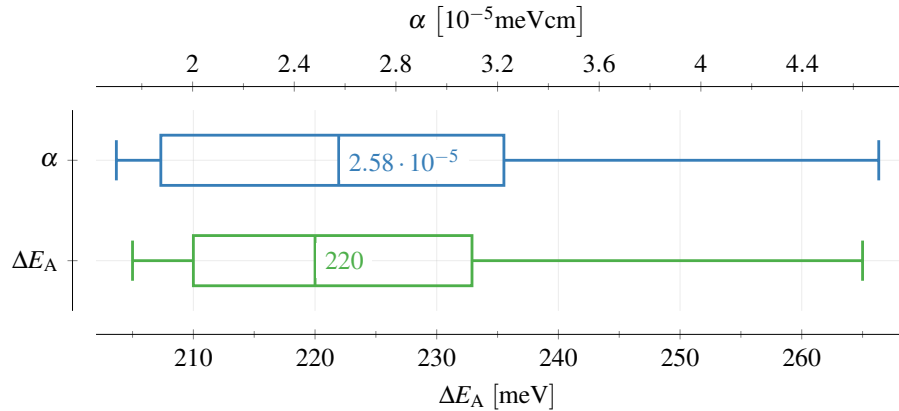


FIG. 40. Statistical analysis of Aluminum doping dependency models. Shown are the 0th, 25th, 50th, 75th and 100th quartile. The mean value is added in numerical form.

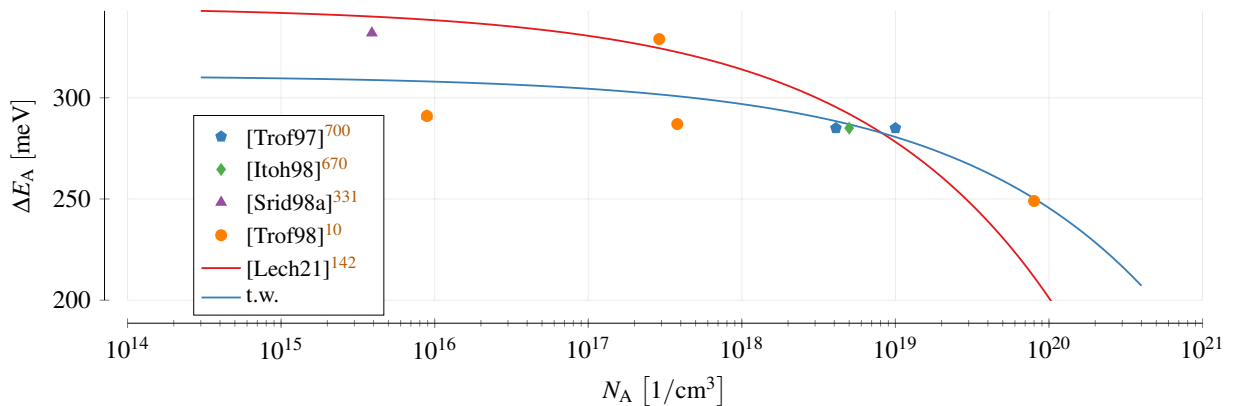


FIG. 41. Ionization energy of Boron. We added a fitting to all available data points (t.w.).

3. Ionization Energy of N

For the n-type donor Nitrogen almost all publications distinguish between cubic and hexagonal site (see Fig. 42), but one can observe a discrepancy in the data, especially towards higher doping concentrations. Due to the high solubility limit ($1 \times 10^{19}/\text{cm}^3$ for annealing at 1700 K, up to $3 \times 10^{20}/\text{cm}^3$ for annealing at 2500 K^{68,123,425,436,850}, $2 \times 10^{21}/\text{cm}^3$ ⁴³) these results might still be realistic, but further investigations at doping concentrations beyond $10^{19}/\text{cm}^3$ would be required.

The measurements still show that the ionization energy of the cubic lattice site lies within a range of 80 – 130 meV, which is bigger than the energy for the hexagonal lattice site in a range of 30 – 80 meV at low to moderate doping concentrations. Gorban *et al.*⁸⁵¹ used this circumstance to predict E_{Dc} based on $E_{\text{Dh}} = 66 \text{ meV}$ ⁹⁵.

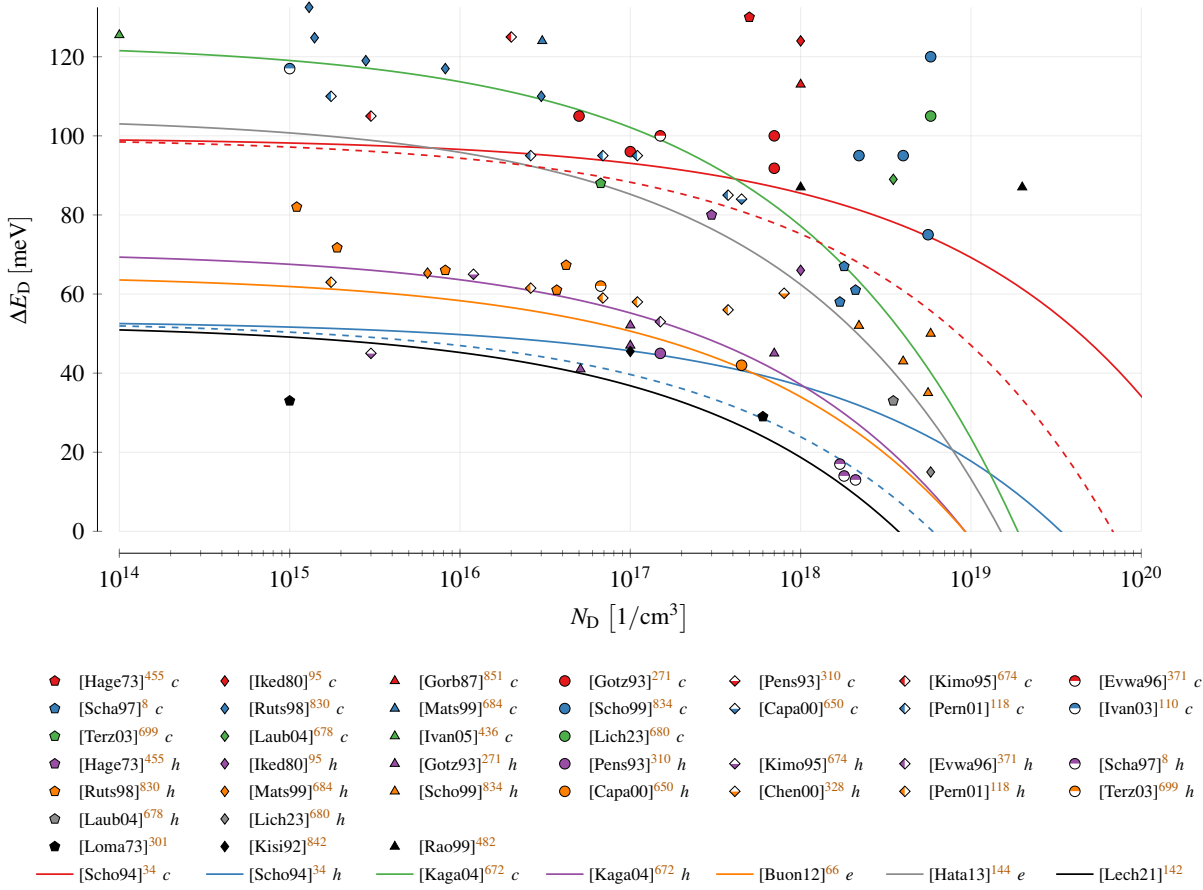


FIG. 42. Ionization energy of Nitrogen. Dashed lines represent the maximum value of α for Schöner³⁴.

For Nitrogen only fittings according to Eq. (84) are available. Kagamihara *et al.*⁶⁷² provided a fitting for both hexagonal and cubic lattice site, which were combined by Hatakeyama, Fukuda, and Okumura¹⁴⁴ to an effective ionization energy model. Buono⁶⁶ also proposed an effective level but the respective values are surprisingly low. This can be explained by the selection of $\Delta E_0 = 65$ meV, which was determined by Bakowski, Gustafsson, and Lindefelt¹³⁹ based on the values from Götz *et al.*²⁷¹. The latter extracted this ionization level value for a doping concentration of $1 \times 10^{17}/\text{cm}^3$ resp. $1 \times 10^{18}/\text{cm}^3$, where a deviation from the low-doping levels has to be expected (cp. Fig. 42). In Eq. (84), however, ΔE_0 denotes the ionization energy at zero doping causing the predicted values to be too low.

The detailed model parameters are shown in Table XXIV. Schöner³⁴ conducted multiple fittings using different models, whose ionization energies were all within 53.3 ± 10.5 for the hexagonal and 99.6 ± 8.3 for the cubic lattice sites. One approximation used Eq. (85) with $\epsilon_s = 9.8$ and $f = 1.12 \pm 0.88$ for cubic lattice sites and $f = 0.96 \pm 0.70$ for hexagonal ones. The values for α

TABLE XXIV. Changing ionization energy of donors with doping (Eq. (84)). Column N denotes the interpretation of factor N : active dopants (dop), all dopants (tot), compensating ones (comp) or simply a fitting (fit). The site denotes besides hexagonal and cubic also a combined effective energy level (eff).

ref.	method	N	site	ΔE [meV]	α [meVcm]
Donor					
[Tama08a] ³²⁴	–	dop	–	66	1.9×10^{-5}
Nitrogen					
[Scho94] ³⁴	Hall	dop	hex	53.3 ± 10.5	$(1.65 \pm 1.29) \times 10^{-5}$
			cubic	99.6 ± 8.3	$(1.41 \pm 1.03) \times 10^{-5}$
[Kaga04] ⁶⁷²	FCCS	dop	hex	70.9	3.38×10^{-5}
			cubic	123.7	4.65×10^{-5}
[Buon12] ⁶⁶	–	tot	eff	65	3.1×10^{-5}
[Hata13] ¹⁴⁴	FIT	tot	eff	105	4.26×10^{-5}
[Lech21] ¹⁴²	FIT	tot	–	52.5	3.38×10^{-5}
Phosphorous					
t.w.	FIT	fit	hex	57	9.54×10^{-6}
			cubic	113	1.26×10^{-5}

deviate by up to a factor of three, resulting in shallower and steeper approximations (cp. Fig. 42). Compared to Aluminum the values of α are higher, indicating a more rapid decline with increasing doping concentration.

4. Ionization Energy of P

Compared to Nitrogen a less measurements are available for Phosphorous (see Fig. 43), all roughly two decades old. Again, hexagonal and cubic lattice site were always distinguished, but this time the values are much more concise. The cubic lattice site showed again the higher values around (100 ± 20) meV while the hexagonal ionization energy was determined within (55 ± 5) meV. These values are by a factor two to six smaller than the energies we found for the p-type doping. Consequently, more free electrons can be expected for an equivalent n-type doping.

Due to the lack of fittings according to Eq. (84) we used the available data to generate one

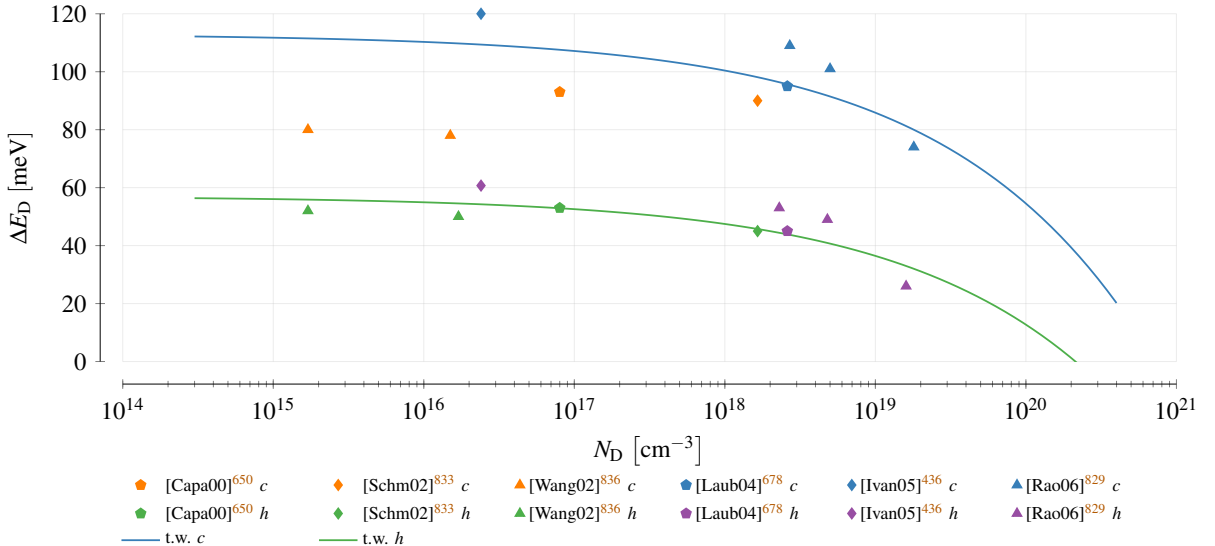


FIG. 43. Ionization energy of Phosphorous.

ourselves. For the cubic site we excluded the results by Wang, Bhat, and Chow⁸³⁶ as the measured values had to be considered outliers in respect to the remaining data. The achieved models agree quite well with the solubility limits we found in literature. ($6 \times 10^{18}/\text{cm}^3$ for annealing at 1700 K, up to $2 \times 10^{20}/\text{cm}^3$ for annealing at 2500 K^{68,123,425,436,850}, $1 \times 10^{21}/\text{cm}^3$ ⁴³). The exact parameters are shown in Table XXIV.

5. Capture Cross Sections

For 4H-SiC various models with varying temperature dependencies were published at the end of the last century (see Table XXV). Since then we only found data for Aluminum, whereat for n-type doping only one investigation Kaindl *et al.*⁸²⁰ could be acquired.

The ionization energy in column ΔE shows large variations, even among the same temperature dependency models. This is also the case for the cross section σ , which refers to the charge carrier in the energetically closer band (conduction or valence) because the interaction with the other band is significantly lower^{10,820}. Differences of more than five orders of magnitude were encountered.

6. Values in Literature

Ionization energies collected from overviews or TCAD simulations (see Fig. 44) show a wide range of values for each dopant. These are, however, well within the boundaries of the fundamental

TABLE XXV. Dopants and their respective cross sections with the charge carriers in the energetically closer band (conduction or valence). Different temperature dependencies are indicated in the column T^α .

ref.	method	site	T^α	ΔE [meV]	σ [cm ²]
Nitrogen					
[Kain99] ⁸²⁰	AS	cubic	T^0	77	7.92×10^{-15}
			T^{-2}	90	3.57×10^{-10}
Aluminum					
[Kuzn95] ³²¹	DLTS		T^{-3}	229	8×10^{-13}
[Scha97] ⁸	Hall AS DLTS		T^0	164 – 179	$(2.2 – 7.6) \times 10^{-13}$
			T^{-2}	189 – 202	$(1.7 – 5.6) \times 10^{-12}$
[Kain99] ⁸²⁰	AS		T^0	189	2.58×10^{-13}
			T^{-2}	208	2.57×10^{-8}
[Resh05] ²⁰¹	AS		T^0	185	1×10^{-14}
			T^{-2}	210	1×10^{-13}
[Belj10] ⁸⁴¹	AS		T^0	200	1×10^{-12}
[Mand12] ⁴⁵⁸	TSC		T^0	220	1×10^{-16}
[Kawa15] ⁸⁴⁰	AS		T^0	190	1.4×10^{-13}
[Kato22] ⁸⁴³	DLTS		T^0	120 – 170	$(1 – 100) \times 10^{-17}$
Boron					
[Srid98a] ³³¹	Hall AS		T^0	259 – 262	–
			T^{-2}	284 – 295	–
[Trof98] ¹⁰	Hall AS		T^0	292	6×10^{-15}
			T^{-2}	314	5×10^{-14}
[Kain99] ⁸²⁰	AS		T^0	312	2.1×10^{-14}
			T^{-2}	375	9.69×10^{-9}
[Zhan03] ⁷⁰³	DLTS MCTS		T^0	230 – 280	$(2 – 30) \times 10^{-14}$

investigations we identified. An exception are the values of the D-center for Boron, that was specified in eleven publications as the ionization energy. Interestingly, we were unable to identify clear favorites for each dopant. Instead, several values are utilized equally often. Only for Al the value $\Delta E_A = 191$ meV has a slight edge.

In some cases the dopant was not clearly specified: Instead only the acceptor and donor energy levels were stated (see Fig. 45). While the acceptor values clearly correspond to Aluminum the n-type values could belong to both Nitrogen and Phosphorous.

7. *Origin of Values*

Due to missing references it is often impossible to retrace where and how the used ionization energies were determined. Nevertheless, we tried to create reference chains for n-type (see Fig. 46) and p-type (see Fig. 47) doping and inferred missing connections based on the used values. On the bright sight, we rarely encountered 6H values^{318,669}, although they seem to match 4H ones^{146,448,802}.

The ionization energy for Nitrogen was often referenced from the publications by Ikeda, Matsunami, and Tanaka⁹⁵, Götz *et al.*²⁷¹ and Ivanov, Henry, and Janzén⁴³⁶ while the energy for Phosphorous goes regularly back to the investigations by Capano *et al.*⁶⁵⁰ and Ivanov, Henry, and Janzén⁴³⁶. The latter reported $E_{Dc} = 60.7$ meV and $E_{Dh} = (120 \pm 20)$ meV, i.e., $E_{Dc} < E_{Dh}$, which contradicts every other measurement we found. In fact, all papers^{43,228,803,809} that referenced Ivanov, Henry, and Janzén⁴³⁶ changed the values to $E_{Dh} = 60.7$ meV and $E_{Dc} = (120 \pm 20)$ meV so we assumed a typographical issue in the paper.

Twelve fundamental investigations were referenced for n-type ionization energies, which is a lot more compared to other topics we studied in this review. The concrete values were, in general, transferred correctly, but in some cases the information regarding cubic or hexagonal lattice site was dropped. Ikeda, Matsunami, and Tanaka⁹⁵, Troffer *et al.*⁷⁰⁰, Lades¹⁴¹, Ivanov, Henry, and Janzén⁴³⁶ and Koizumi, Suda, and Kimoto¹²⁰ represent the main sources for the ionization energies of Aluminum and Boron, whereat overall thirteen different fundamental investigations were at least once referenced.

For the parameters to model the doping dependency according to Eq. (84) we only found two (n-type) respectively three (p-type) fundamental investigations that were referenced (see Fig. 48). An unfortunate typographical error occurred in Song *et al.*³²⁵, who changed the acceptor ionization

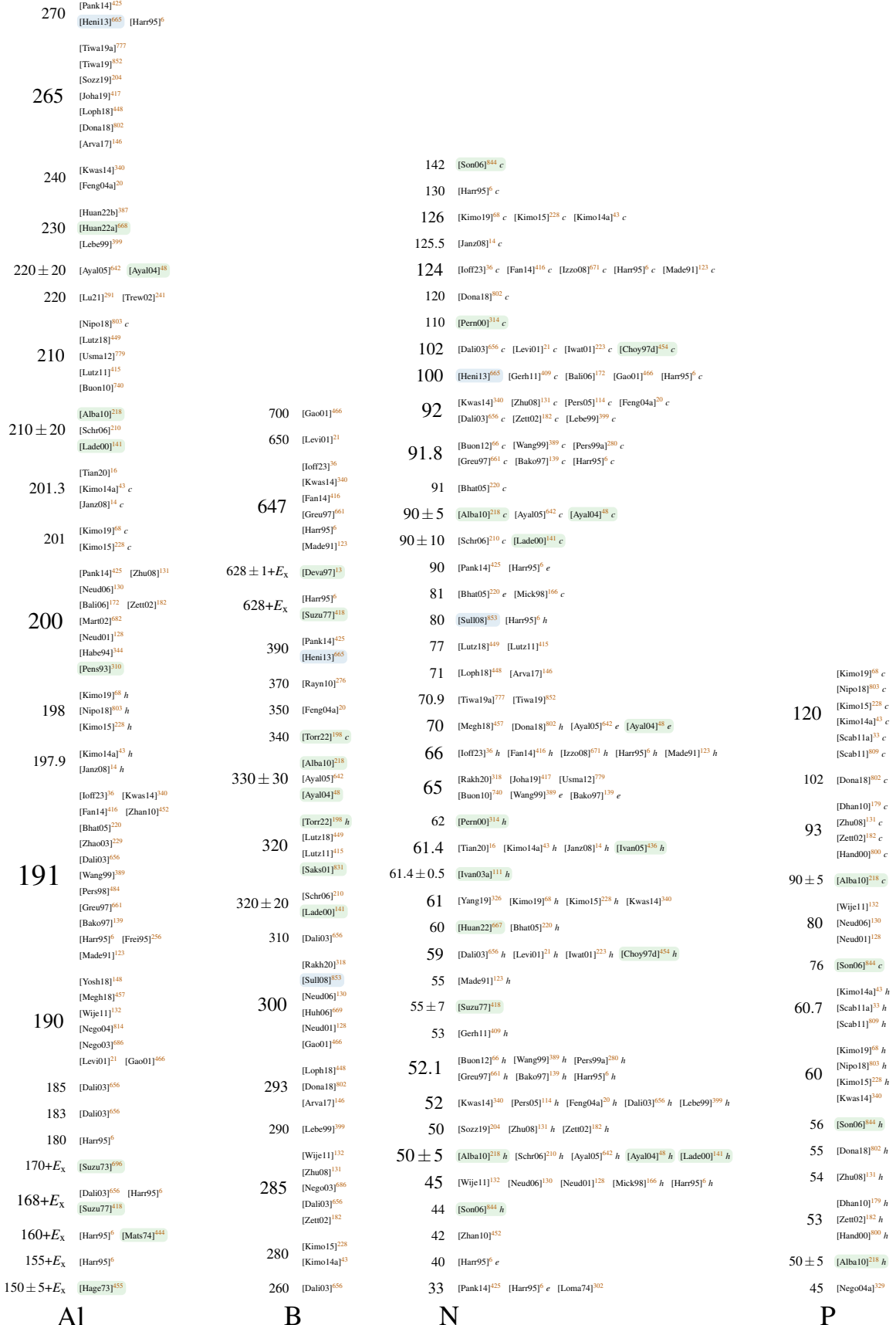


FIG. 44. Energy levels for each investigated dopant. ■ are fundamental investigations and ■ research not focused on 4H. *h*, *c* and *e* denote hexagonal, cubic and effective lattice sites respectively.

A1

B

N

P

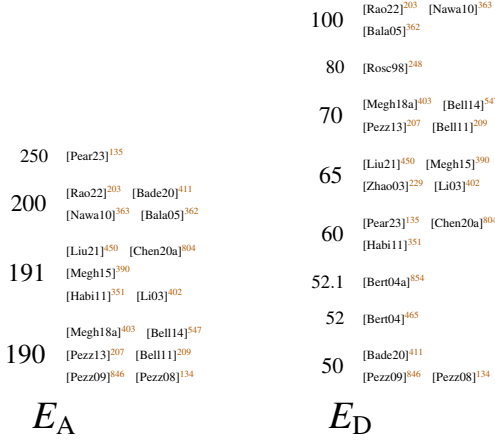


FIG. 45. Energy levels used in literature for acceptors and donors without specification of dopant.

energy from 191 meV³²⁴ to 19 meV. In terms of charge carrier densities this results in a huge difference. The incorrect value was later referenced by Khalid, Riaz, and Naseem³⁸⁶, which shows the importance of referencing the original research results. A comprehensive listing of all inconsistencies for incomplete ionization can be found in Section A 6.

X. MOBILITY

Charge carrier mobilities (μ_n for electrons; μ_p for holes) of a material determine its conductivity σ (see Eq. (90); n and p are the free electron/hole concentrations), which influences all transient processes. Surfaces, inversion channels in MOS structures and the bulk¹⁴² may have different mobilities, whereat we will investigate in this review solely the latter. We, thereby, extend the analysis of measurements by Darmody and Goldsman¹⁹⁷ and the summaries of mobility models published by Neila Inglesias²², Stefanakis and Zekentes¹⁵ and Tian *et al.*¹⁶.

$$\sigma = e(n\mu_n + p\mu_p) \quad (90)$$

Overall, our analyses reveal many investigations targeted toward the mobility. The change with doping concentration is well covered, however, for holes a large spread of values is apparent. More problematic is the temperature dependency, because only few models predict a decrease of the mobility at low temperatures, as observed in measurements. A better agreement is visible in the high-field regime, but only few values of the hole saturation velocity exist. Except for one publication, all indicate a decrease of the velocity with temperature. For carrier-carrier scattering only a single publication could be identified in literature.

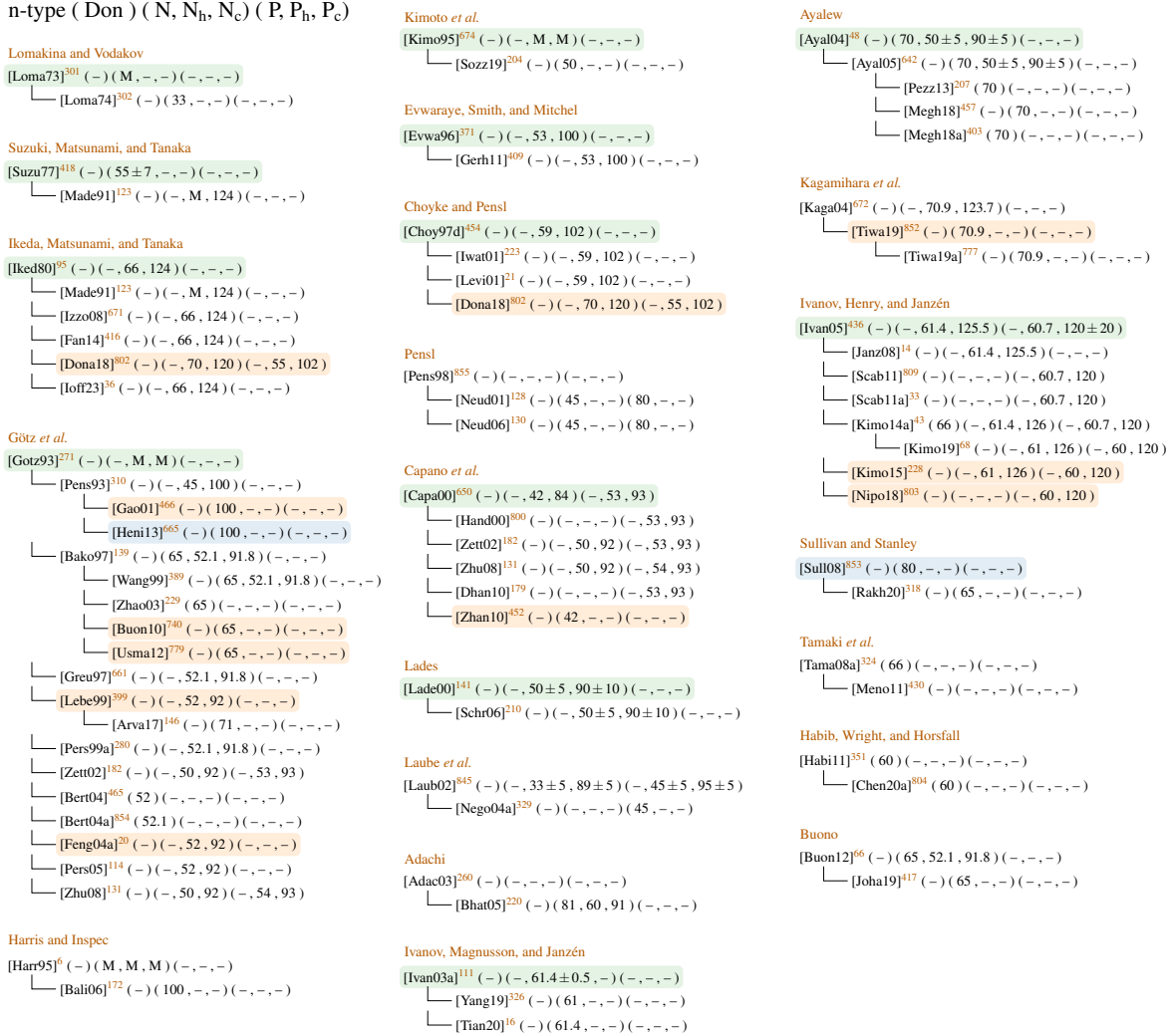


FIG. 46. Reference chain for n-type doping. are fundamental investigations, research not focused on 4H and references we inferred based on the used data.

A. Introduction

Charge carriers in 4H-SiC accelerate along an electric field F until they are “scattered”, i.e., they drastically change their velocity and/or direction by interacting with other particles. Theoretical analyses investigated the individual contributions in detail^{22,35,118–120,314,488,856}. In this context, the mobility defines the average time between two scattering events¹⁴¹ and thus provides a link between charge carriers and scattering processes⁹³. The most prominent processes for 4H-SiC are (i) phonon, i.e., acoustic phonon, (non-)polar optical phonon, zero and first order optical intervalley phonon, (ii) defect, i.e., ionized and neutral impurity, and (iii) carrier-carrier scattering^{35,119,120,281,623,857}. An overall mobility is derived by combining the individual contributions

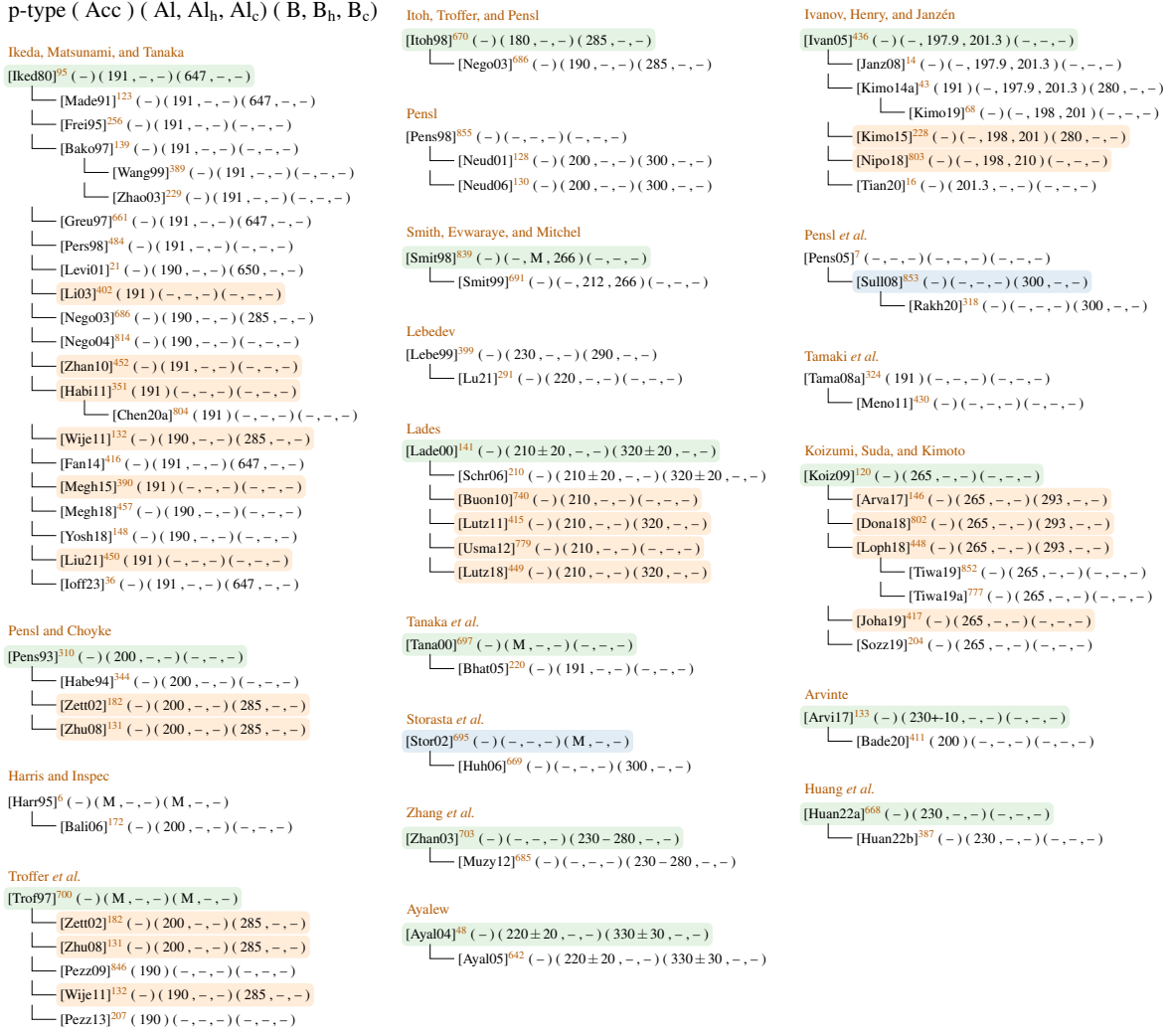


FIG. 47. Reference chain for p-type doping. ■ are fundamental investigations, ■ research not focused on 4H and ■ references we inferred based on the used data.

using the Matthiessen rule^{35,43,48} (see Eq. (91)), such that the lowest value dominates.

$$\frac{1}{\mu} = \sum_i \frac{1}{\mu_i} . \quad (91)$$

Due to the various scattering processes, the mobility depends on several material parameters such as doping concentration³⁵³, degree of compensation⁴¹⁵, spatial direction^{96,223,225}, temperature³⁵³ and whether majority or minority charge carriers³⁵ are described. For holes even the separate valence bands (heavy-hole, light-hole, split-off; see Section V)^{35,119,167} have to be considered.

In the past years, hopping conduction⁸⁵⁸, also denoted as nearest-neighbor-hopping (NNH)^{859,860} or variable-range-hopping (VRH)⁸⁵⁹, was investigated in 4H-SiC. This process denotes the tun-

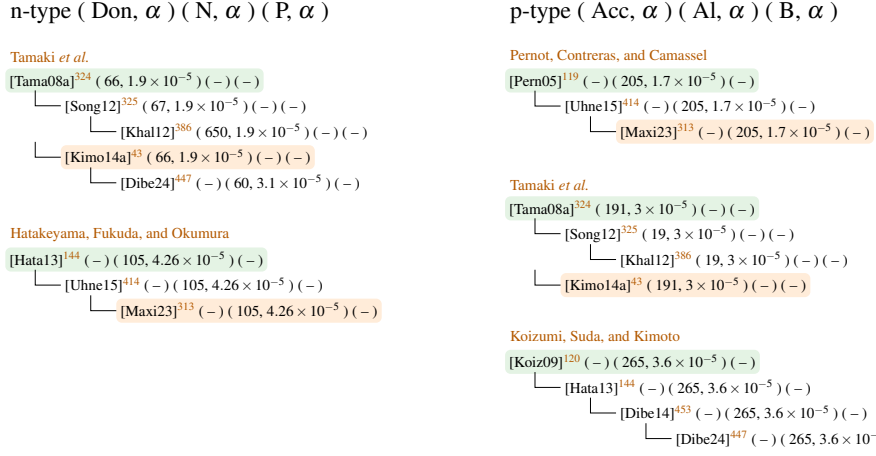


FIG. 48. Reference chain for doping dependency modeling. are fundamental investigations, research not focused on 4H and references we inferred based on the used data.

neling of charge carriers bound to a dopant from one impurity to the next, possibly alternated by conventional drifting phases in the bands. This effect was described at temperatures below 100 K⁸¹² and at very high doping concentrations^{156,859}, whereat Darmody and Goldsman¹⁹⁷ calculated the critical limit to $N_{\text{crit}} \approx 1 \times 10^{20}/\text{cm}^3$. Since this is a relatively new effect the available information are very limited, so we will not further consider it in this review.

In TCAD tools high detailed descriptions are not convenient¹²⁰. Instead, empirical models describe the mobility in the low- and high-field region, which we will elaborate in the sequel.

1. Low-Field Mobility

At low electric fields the carrier velocity v and the electric field strength F are directly related via the mobility μ (see Eq. (92))³⁸. The latter depends on phonon and impurity scattering²¹⁰, meaning that both temperature and doping concentration have to be included in the same model.

$$v = \mu(N, T)F \quad (92)$$

Each dopant in 4H-SiC represents a coulomb scattering center¹⁷³ that causes the charge carrier mobility to decrease. Caughey and Thomas⁸⁶¹ mathematically described this effect by Eq. (93). μ_{min} can be interpreted as the mobility for very high doping where impurity scattering is dominant^{15,22} and μ_{max} the highest possible mobility at low doping, i.e., when lattice (phonon) scattering is dominant^{15,22,142}. N_{ref} denotes the doping concentration where the mobility is exactly in

between those values^{38,415} and δ how quickly the transition from one to the other occurs. Arora, Hauser, and Roulston⁸⁶² later simplified the model by replacing the expression $\mu_{\max} - \mu_{\min}$ by μ_0 ¹³⁷.

$$\mu(N) = \mu_{\min} + \frac{\mu_{\max} - \mu_{\min}}{1 + (N/N_{\text{ref}})^{\delta}} \quad (93)$$

There is some disagreement in literature (discussed by Vasilevskiy *et al.*⁸⁶³) whether N denotes all dopants^{15,48,66,68–70,120,137,139,144–146,166,238,281,282,387,401,440,565,714,863–865} or just the ionized ones^{70,158,330,392,402,452,457,814,857}. An argument to use all dopants was that this model is just a fit^{15,16} or that also scattering on neutral dopants decreases the mobility^{120,144}. Roschke and Schwierz³⁸ stated that using something different than the absolute doping for N did not improve the results but led to convergence issues.

Masetti, Severi, and Solmi⁸⁶⁶ extended the model by an additive term that leads to a further reduction of the mobility at high doping densities (see Eq. (94))⁸⁶⁷. We found only one instance⁵⁶⁶ where this model was used; other publications referencing this model^{142,439} chose $\mu_1 = 0$ leading to the description in Eq. (93).

$$\mu(N) = \mu_{\min} + \frac{\mu_{\max} - \mu_{\min 2}}{1 + (N/N_{\text{ref}})^{\delta}} - \frac{\mu_1}{1 + (N_{\text{ref}2}/N)^{\kappa}} \quad (94)$$

The mobility scaling with temperature depends on the dominant scattering mechanism^{120,281}, whereat each has its own temperature dependency⁶⁸. Acoustic phonon scattering showed a decrease $\propto T^{-1.5}$ ^{34,141,813,828,864,868} and optical-mode phonons $\propto T^{-2.5}$ ¹⁴¹. A reduction $\propto T^{-2.6}$ was attributed to nonpolar optical phonon scattering^{120,868}, but Adachi³⁵ stated a dependency according to $T^{-1.5}$ for this process. Ionized impurities scale with $T^{3/2}$ ^{34,281,714,813,828}, neutral impurities with T^0 ^{34,35,281,714}, Coulomb scattering with T^1 and phonon scattering with T^{-1} ⁴²².

Phonon scattering dominates in hot samples because more phonons are generated^{173,271,353}, and (un)ionized impurity scattering at low temperatures^{68,869}. The exact amount of “low temperature” in this context increases with the doping concentration, i.e., more dopants lead to an earlier impact of impurity scattering. According to the temperature dependencies mentioned before, the mobility thus rises in cold samples with temperature before it decreases in phonon-dominated temperature regimes¹²⁰.

These dependencies are added to Eq. (93) by scaling the single parameters with temperature (see Eq. (95)^{144,218}). We listed all scaling parameters we found in literature, although some of them are redundant ($\gamma_{NN\text{ref}} = -\delta\gamma_{\text{ref}}$). In most publications only a subset of these parameters is used⁸⁷⁰, whereat differing origins were stated. Referenced were, among others, the publications

by Mohammad *et al.*⁸⁷¹ and Sotoodeh, Khalid, and Rezazadeh⁸⁷² but also the description *Masetti model*^{353,402} was used, although the second additive term in Eq. (94) was missing.

$$\theta = \theta_{300} \left(\frac{T}{300} \right)^\zeta \quad (95)$$

$$(\theta, \zeta) \in [(\mu_{\min}, \gamma_{\min}), (\mu_{\max}, \gamma_{\max}), (\mu_0, \gamma_0), (N_{\text{ref}}, \gamma_{\text{ref}}), (\delta, \gamma_\delta), ((N/N_{\text{ref}})^\delta, \gamma_{\text{NNref}})] \quad (96)$$

The temperature-dependent mobility can be properly described by the approach in Eq. (95) if the parameters are carefully determined, e.g., as done by Hatakeyama, Fukuda, and Okumura¹⁴⁴. In most cases (details follow in Section XB), however, the decrease of μ at low temperatures is not properly covered making these approximations only adequate for high temperatures⁸⁷³. As a workaround Schröder²¹⁰ defined on page 668 equations below/above 200K with deviating temperature scalings, but only provided parameters for Si.

We found various additional models to describe the temperature and doping dependencies of the mobility in 4H-SiC. Rambach, Bauer, and Ryssel^{813,813,828} proposed a more inclusive approach based on the doping dependent parameters $\delta(N_A)$, $N_{\text{ref}}(N_A)$, $\gamma_{\min}(N_A)$ and $N = p(T, N_A, N_K)$. In another model for $T > 250$ K the exponential parameter ζ had the same structure as Eq. (93) (see Eq. (97) and Eq. (98))^{672,683}.

$$\mu(T, N) = \mu(300, N) \left(\frac{T}{300} \right)^{\beta(N)} \quad (97)$$

$$\beta(N) = \beta_{\min} + \frac{\beta_{\max} - \beta_{\min}}{1 + (N/N_p)^\eta} \quad (98)$$

La Via *et al.*⁶⁷⁹ used the phenomenological function shown in Eq. (99) to model the increasing mobility due to ionized impurity scattering at low temperature ($T^{3/2}$) and an adjustable decrease for high temperatures. This description was further simplified by Mitchel *et al.*⁸⁷⁴, who just used $\mu(T) = A T^{-n}$.

$$\mu(T) = \left(\frac{A}{T^{3/2}} + \frac{B}{T^{-n}} \right)^{-1} \quad (99)$$

Uhnevionak⁴¹⁴ found discrepancies between simulated and measured MOSFET currents with varying temperature. To better match the bulk-phonon scattering, the author split μ_{\max} into two additive parts with separate temperature scaling factors (see Eq. (100)).

$$\mu_{\max} \left(\frac{T}{300} \right)^{\gamma_{\max}} = \mu_{\max 1} \left(\frac{T}{300} \right)^{\gamma_{\max 1}} + \mu_{\max 2} \left(\frac{T}{300} \right)^{\gamma_{\max 2}} \quad (100)$$

Mnatsakanov *et al.*⁸⁶⁹ tackled the challenge of doping dependent temperature coefficients by separating impurity and lattice scattering and scaling each independently with temperature. Starting from Eq. (93) this led to the expressions shown in Eq. (101) and Eq. (102) with γ the temperature scaling factor of the impurity scattering contribution. For $T = T_0$ Eq. (101) collapses to Eq. (93). The authors claimed that this model is able to simultaneously describe the temperature behavior for low and very high doping.

$$\mu(N, T) = \mu_{\max}(T_0) \frac{B(N) \left(\frac{T}{T_0}\right)^\gamma}{1 + B(N) \left(\frac{T}{T_0}\right)^{\gamma + \gamma_{\max}}} \quad (101)$$

$$B(N) = \left[\frac{\mu_{\min} + \mu_{\max} \left(\frac{N_{\text{ref}}}{N}\right)^\delta}{\mu_{\max} - \mu_{\min}} \right] \Big|_{T=T_0} \quad (102)$$

Finally, Klaassen⁸⁷⁵ proposed a unified description of majority and minority charge carriers including screening effects, also called Philips model, which was recently used in conjunction with 4H-SiC⁸⁷³. Although this model is already included in state of the art simulation frameworks we did not consider it in our review, because we could not find explicit parameters for 4H-SiC.

2. High-Field Mobility

At high electric fields the charge carrier velocity approaches a maximum value, the so-called *saturation velocity*. Higher optical phonon scattering^{242,353,440} or elastic and nonelastic scattering rates owing to the increase in carrier energy¹⁴⁴ explain this behavior. According to Eq. (92) the velocity is proportional to the field strength, meaning that the mobility has to decrease. Caughey and Thomas⁸⁶¹ modeled this field dependency according to Eq. (103): μ_{low} denotes the low field mobility as described in the previous section and v_{sat} the saturation mobility (Kimoto and Cooper⁴³ calls the latter sound velocity). In some cases an additive factor α was introduced in various spots of this equation^{146,330,448}, but it was always set to 0, rendering it irrelevant. Chen *et al.*⁴⁴¹ used the hydrodynamic version of this equation, which we are not going to discuss in this review.

$$\mu = \frac{\mu_{\text{low}}}{\left[1 + \left(\frac{\mu_{\text{low}} F}{v_{\text{sat}}} \right)^\beta \right]^{\frac{1}{\beta}}} \quad (103)$$

The high field mobility is temperature dependent^{35,155,173} so Canali *et al.*⁸⁷⁶ suggested to scale the parameters β and v_{sat} with temperature as was shown for the low-field case in Eq. (95)^{141,144}.

This model is thus often called Canali model^{517,582}. Quay *et al.*⁸⁷⁷ proposed a very similar model of the form $v_{\text{sat}}/[(1 - A) + A(T/300)]$ for semiconductors in general, but we did not find a single application for 4H-SiC yet. In some occasions^{218,854} the temperature dependency of v_{sat} was modeled by the approach commonly used for Si (see Eq. (104))^{389,878}.

$$v_{\text{sat}} = \frac{v_{\text{max}}}{1 + d \exp\left(\frac{T}{600}\right)}. \quad (104)$$

Roschke and Schwierz³⁸ proposed an exponential and Bertilsson, Harris, and Nilsson⁸⁵⁴ a linear dependency of β with temperature. For a more concise presented we merged both in Eq. (105).

$$\beta = \beta_0 + a \exp\left(\frac{T - T_{\text{ref}}}{b}\right) + c T \quad (105)$$

Monte-Carlo simulations^{22,72,166,168,175,184,227,318,465,536,854,857} indicated a velocity peak, i.e., a negative differential mobility at fields near $1 \times 10^6 \text{ V/cm}$ ³⁸. Foutz, O’Leary, and Shur⁸⁷⁹ proposed a new model for wide band gap materials that covered this *overshoot* (see Eq. (106))⁸⁵⁷. This approach was used for GaN⁸⁸⁰ and lately also for 4H-SiC⁸⁵⁷ but is not yet available in TCAD tools. A simplified version ($\alpha = -\infty$) was denoted as transferred-electron model^{488,881}.

$$v(F) = \frac{\mu_0 F + \mu_1 F(F/F_0)^\alpha + v_{\text{sat}}(F/F_1)^\beta}{1 + (F/F_0)^\alpha + (F/F_1)^\beta} \quad (106)$$

Finally, Baliga¹⁷³ used the representation shown in Eq. (107) to describe the high field mobility. The parameters from Eq. (93) can be achieved by using $v_{\text{sat}} = A$ and $\mu_{\text{low}} = v_{\text{sat}}/B^{1/\beta}$.

$$\mu = \frac{A}{[B + F^\beta]^{1/\beta}} \quad (107)$$

3. Carrier-Carrier Scattering

This scattering process denotes interactions among the same type of charge carriers, e.g., electron-electron³⁵, or between electrons and holes⁴¹⁵, which decreases the mobility at high injection levels^{16,173,882}. In the literature it was either assumed negligible⁸⁸³ or described by the Conwell-Weisskopf equation (see Eq. (108))^{48,150,884,885}, which was also used in the past to describe silicon. For the latter, Lutz *et al.*⁴¹⁵ mentioned the possibility to cover carrier-carrier-scattering by including the free charge carriers in N of Eq. (93) but we did not encounter this approach for 4H-SiC.

$$\mu_{\text{ccs}} = \frac{D \left(\frac{T}{T_0}\right)^{\frac{3}{2}}}{\sqrt{np}} \left[\ln \left(1 + F \left(\frac{T}{T_0} \right)^2 (pn)^{-\frac{1}{3}} \right) \right]^{-1} \quad (108)$$

TCAD tools combine the carrier-carrier and the low/high field mobility with the Matthiessen rule (see Eq. (91)).

4. Hall Scattering Factor

The mobility can be experimentally extracted from conductivity measurements, delivering the so-called conductivity or drift mobility (see Eq. (90))³⁵. The main issue with this method is that the charge carriers concentrations have to be known as well. Instead, the simpler Hall measurements are often preferred that, however, deliver a slightly different mobility, the Hall mobility μ_H ¹³³. In general, it is said that the Hall mobility is easier to measure, while the conductivity mobility is easier to calculate³⁵.

The ratio of Hall and conductivity mobility is called Hall factor r_H (see Eq. (109))^{35,223,271,281,335,864}. To calculate r_H for holes one has to consider both light and heavy holes^{119,688}. The Hall factor must not be confused with the Hall coefficient R_H (see Eq.(110)), which is the value actually derived in Hall measurements. It depends on the Hall charge carrier count n_H ^{70,120,823,824,830} and is used to connect conductivity and mobility (see Eq. (111))^{8,173,310}. For further theoretical analyses and overviews on Hall mobilities and measurements the interested reader is referred to the dedicated literature^{22,118,341,690}.

$$r_H = \frac{\mu_H}{\mu_c} = \frac{n}{n_H} \quad (109)$$

$$R_H = \frac{1}{n_H e} = \frac{r_H}{n e} \quad (110)$$

$$\mu_H = \sigma R_H = \frac{1}{e n_H \rho} \quad (111)$$

Consequently, one can not use the Hall mobility directly in Eq. (90) to calculate the conductivity of a material. To properly handle proposed values it is, therefore, mandatory to consider the utilized characterization method.

5. Methods

Several approaches to determine the mobility were proposed in the literature. These include simulations such as Monte Carlo^{166,168,184,227,323,465,536,886}, full band monte carlo (FBMC)^{424,887}, empirical pseudo potentials (EPM)^{72,175,184}, monte carlo particle (MCP)¹⁶⁷, non equilibrium statistical ensemble formalism (NESEF)¹⁷⁶, linear augmented plane wave (LAPW)⁶⁸², density func-

tional theory (DFT)⁷⁰, extraction from the diffusion coefficient (DIFF)³³⁴, conductivity tensor calculations (COTE)^{223–225,284}, general calculations^{118,119,314} and fitting (FIT)^{38,93,141,144,517,672,812,857,888}. Nilsson *et al.*⁸⁸⁹ provided a comparison among several Monte-Carlo models.

Measurements include collected charge (CCh)⁸⁹⁰, nanosecond pulsed conductance (NPC)^{891–895}, resistance measurements (RES)^{671,679}, Schottky barrier diode I-V fitting (SBD-IV)⁸⁹⁶, Raman scattering (Raman)^{96,257,267}, low temperature photoluminescence (LTPL)⁷¹⁴, spectroscopic ellipsometry (SE)⁹⁴, optical detection of cyclotron resonance (ODCR)^{299,856}, diode I-V (DIV)^{471,896}, bipolar transistor I-V (BIV)²⁵ and Hall measurements^{7,8,34,69,120,133,271,281,282,309,345,356,392,398,454,477,673,678,683,699,814,824,826,828,834,863,864,868,897–903}.

The majority of publications provided

Hall^{7,8,69,118–120,224,225,281,282,284,314,392,673,678,699,814,824,828,834,863,864,898,900,903} and only few conductivity mobilities^{96,166,267,856,887}.

It is also possible to calculate the mobility from the charge carrier lifetime τ (cp. Section VIII) and the conductivity mass m_c^* (cp. Section V) according to Eq. (112)^{70,96,253,281,282,285}. Neimontas *et al.*³³⁴ calculated it from the diffusion coefficient using the Einstein relationship $\mu = De/k_B T$.

$$\mu = \frac{e\tau}{m_c^* m_0} \quad (112)$$

B. Results & Discussion

In the sequel we present the gathered results on mobility in 4H-SiC. We had to exclude publications that solely focused on channel or inversion layer mobilities^{129,137,411,517,892,904–909}, that did not clearly specify the SiC polytype^{114,210,462,574,910–912}, that dealt with mobility variations induced by irradiation defects⁹¹³ or that did not clearly specify the used equations, making a unique mapping of the parameter values impossible²²⁰. We also did not consider Wright²²⁶ that was superseded by Wright *et al.*¹⁷¹.

1. Hall Scattering Factor

We discussed in the last section that the results of Hall measurements have to be scaled by the Hall scattering factor r_H to obtain the conductivity mobility. In early investigations r_H was assumed approximately unity^{38,96,141,197,901,904} due to the lack of reliable data²⁷¹. Later it was shown that this is only the case for high magnetic fields⁶⁹⁰ and that the Hall scattering factors drops

with increasing doping concentration⁸²³. More thorough investigations revealed a dependency on the magnetic field^{690,830,914}, temperature^{7,8,70,119,120,223,335,351,688,690,826}, the anisotropy of the effective masses²²³ and the doping concentration^{70,351,823}, causing variations of r_H predominantly in the range of [0.5, 1.5]. The impact of compensation¹²⁰ as well as the anisotropy^{830,914} is still under investigation.

Both an increase²⁸² and a decrease^{223,823} of r_H with increasing temperature was observed in measurements, which may be explained by differing doping concentration²⁸². Pernot, Contreras, and Camassel¹¹⁹ provided a fit of the results by Pensl *et al.*³³⁵ (see Eq. (113)), which showed a rapid decline from 1.2 at 300 K to approx. 0.5 at 800 K. On the flip side, theoretical analyses predicted an increase of r_H with rising temperature^{120,223}.

$$r_H = 1.74823 - 6.22 \times 10^{-3} T + 1.36729 \times 10^{-5} T^2 - 1.44837 \times 10^{-8} T^3 + 5.86498 \times 10^{-12} T^4 \quad (113)$$

Tanaka *et al.*⁷⁰ obtained an analytic equation for temperature and doping dependent variations of r_H (see Eq. (114)). For this purpose the authors fitted the Hall and conductivity mobility with the model shown in Eq. (93). A division of these fits then led to the shown expression, which predicted a decrease up to a concentration of $3 \times 10^{19}/\text{cm}^3$, where a minimum of 0.74 (for $T = 300\text{K}$) was achieved.

$$r_H = 1.16 \left(\frac{T}{300\text{K}} \right)^{-0.9} \frac{1 + \left(\frac{T}{300\text{K}} \right)^{-1.5} \left(\frac{N_A}{1 \times 10^{19}/\text{cm}^3} \right)^{0.7}}{1 + \left(\frac{T}{300\text{K}} \right)^{-1.8} \left(\frac{N_A}{3 \times 10^{18}/\text{cm}^3} \right)^{0.6}} \quad (114)$$

An investigation of Hall and conductivity mobility in literature was published by Darmody and Goldsman¹⁹⁷. Due to the fact that the achieved results contradict commonly agreed values we want to discuss this publication in greater detail. At first, the ratio μ_c/μ_H , which is the definition of r_H , was introduced as the ratio of the free charge carriers and the doping concentration. This is based on the assumption that all dopants contribute to the conductivity mobility, i.e., are ionized, which is not the case in 4H-SiC (cp. Section IX). The Hall scattering coefficient itself was set to one in this analysis. In the sequel the authors showed two plots, one for the Hall and one for the conductivity mobility. The values of the latter were much lower, which resulted from the fact that the authors gathered the values from resistivity measurements, assuming that the amount of charge carriers was equal to the doping concentration. According to the definitions in the paper $r_H > 5$ was achieved, which is more than three times the biggest value we encountered in the remaining literature.

In summary, there exists no simple and unique translation between Hall and conductivity mobility. Consequently, we are going to present the values as they were published and denote their meaning with H (Hall) resp. C (conductivity) whenever possible, whereas the absence of both indicates that we were unable to classify the results.

2. Low-Field Mobility

The simplest way to describe the mobility is to use a constant value¹⁸. Although this approach is also applicable in TCAD tools it mainly serves the purpose of a rough and quick comparison among different materials. Consequently, often no information about doping concentration and temperature are provided. We found a wide range of values for the individual spatial directions and also combined to an effective mobility (see Fig. 49), which reflects range of dependencies, e.g., doping concentration, temperature and field strength. Nevertheless, it becomes clear that the mobility of electrons is almost one order of magnitude higher than to the mobility of holes.

The reference chain (see Fig. 50) shows that these values are not derived from a main source but from small clusters. This indicates that the authors assumed the mobilities as common knowledge, without the need to provide references.

In the data an anisotropy of the mobility in regard to the spatial direction is visible. Some authors argued that it is low enough such that just considering the mobility in the base plane is a reasonable approximation²¹⁸. However, Hatakeyama *et al.*³⁹² showed that not even within the basal plane the mobility is constant. The anisotropy of the mobility is most probably caused by the anisotropy of the effective masses^{69,144,176,223,225} (cp. Section V) and thus depends on additional parameters such as the temperature²⁸¹.

We found 14 investigations on the electron but only three on the hole mobility ratio, i.e., μ^\perp/μ^\parallel , whose results agree well (see Table XXVI). All but one fundamental investigation predicted for electrons a higher mobility parallel to the c-axis with $\mu_n^\perp/\mu_n^\parallel = 0.83 \pm 0.07$. Solely Harima, Nakashima, and Uemura⁹⁶ stated the exact opposite, i.e., $1/0.83 = 1.2$. Also various predominantly qualitative overview papers used $\mu_n^\perp > \mu_n^\parallel$ ^{26,179,180,221,234,239,244,250,251}, while others predicted no anisotropy at all^{128,130,132,164,459}.

Iwata, Itoh, and Pensl²²⁵ investigated the mobility in varying in-plane directions, revealing a maximum anisotropy factor for electrons of 0.7. Cheng and Vasileska⁸⁸⁷ stated that previous publications⁸⁶⁴ did not specify the exact perpendicular direction. Thus their values for $\mu_n^\parallel/\mu_n^\perp$ range

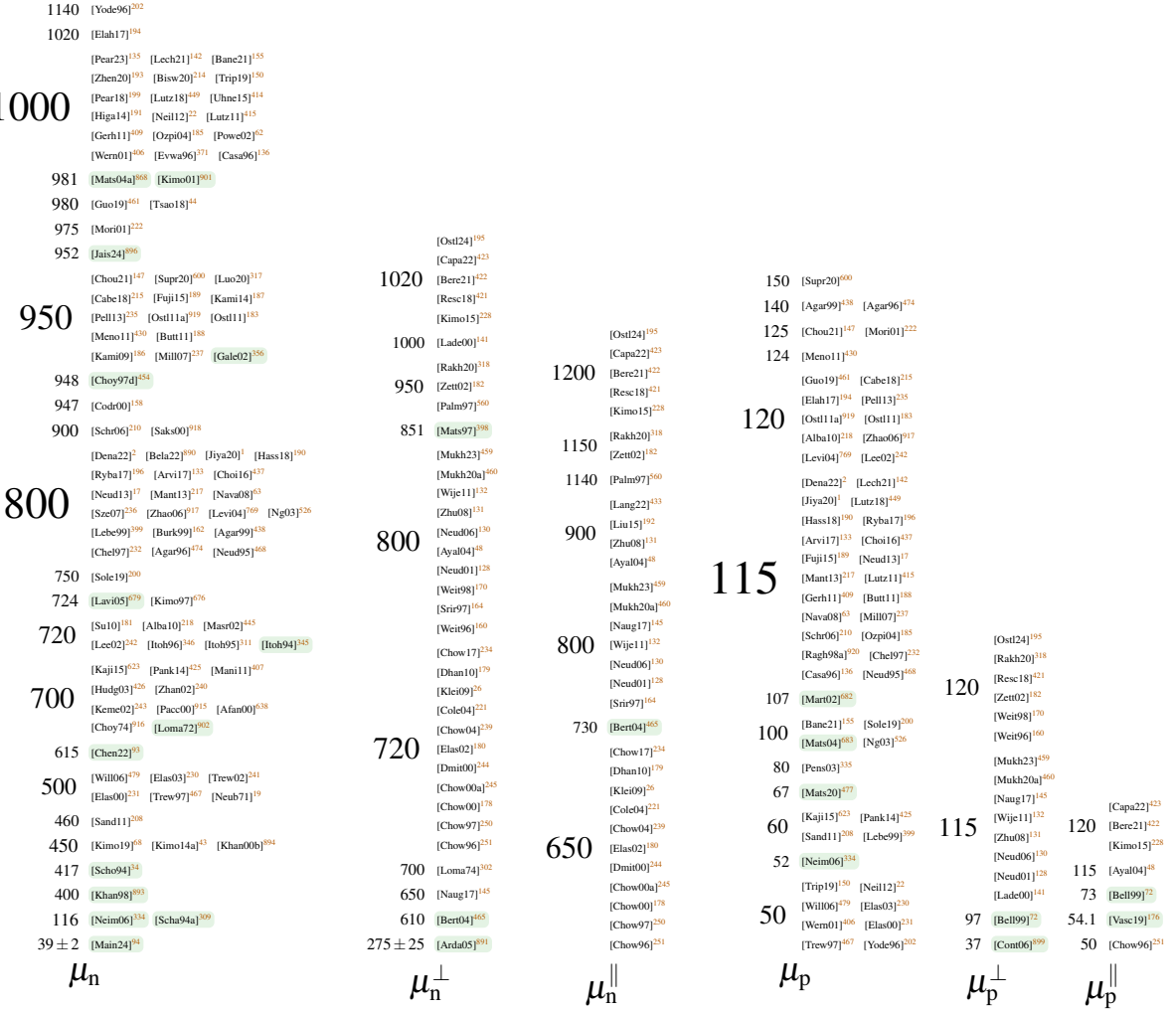


FIG. 49. Constant mobility values for 4H-SiC in directions relative to the c-axis.

between 1.25 and 1.75, compared to the previously achieved 1.2⁸⁶⁴. For holes all investigations predicted a ratio bigger than one with the most common values of 1.15 ± 0.04 . For electric fields $< 50\text{kV/cm}$ Vasconcelos, Rodrigues, and Luzzi¹⁷⁶ calculated a ratio > 10 , which drops below six for fields $\geq 200\text{kV/cm}$.

Ishikawa *et al.*^{69,281} utilized the resistivity ratio to achieve μ^\perp/μ^\parallel because in this way the Hall scattering factor cancels. We also found several investigations on temperature and doping concentration dependencies^{8,166,227,281,282,301,309,323,682,864}. Schadt *et al.*³⁰⁹ reported an increasing ratio (up to unity, see Fig. 51) with rising temperature but Schaffer *et al.*⁸⁶⁴ stated that the value of 0.83 did not change over temperature in homogeneous samples. Only for a wafer with an additional deep donor level a comparable tendency was observed in the range [0.83, 1] when varying the temperature within 100 – 600 K. Joshi³²³ showed a slight decrease from 0.78 to 0.73 within 100 –

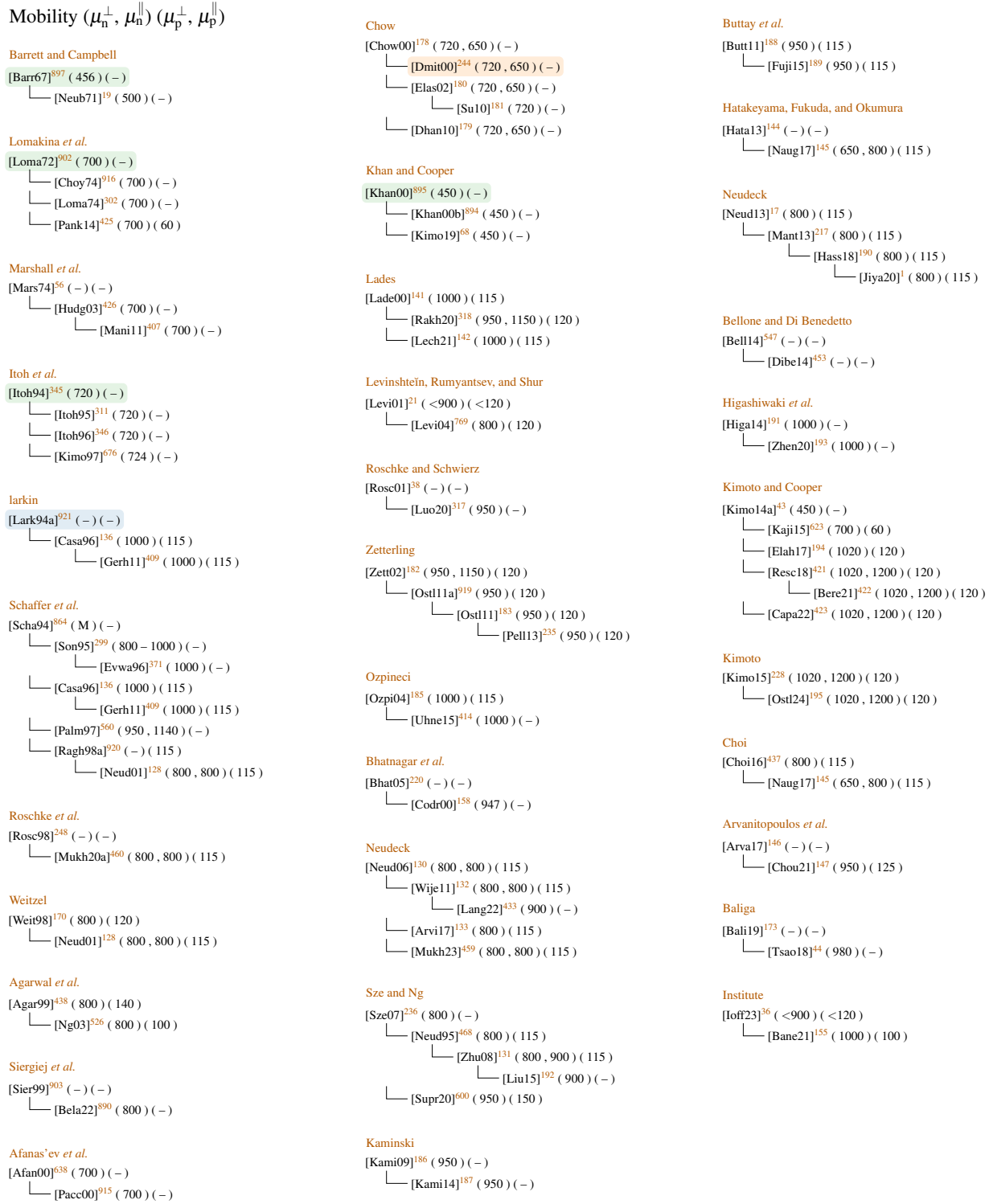


FIG. 50. Reference chain for constant mobility values in different spatial directions. If only a single value is shown the value denotes the effective value. are fundamental investigations, research not focused on 4H and references we inferred based on the used data.

TABLE XXVI. Fundamental investigations on the ratio of mobilities perpendicular (\perp) and parallel (\parallel) to the c-axis for electrons and holes.

ref.	$\mu_n^\perp / \mu_n^\parallel$	$\mu_p^\perp / \mu_p^\parallel$	T	type ^a	method
	[1]	[1]			
[Scha94a] ³⁰⁹	0.83 ± 0.03	–	300	H	Hall
[Scha94] ⁸⁶⁴	0.83	–	300	H	Hall
[Hari95] ⁹⁶	1.2 ± 0.3	–	–	C	Raman
[Josh95] ³²³	0.75	–	300	C	MC
[Son95] ²⁹⁹	0.7	–	2R6	C	ODCR
[Nils96] ²²⁷	0.82	–	300	C	MC
[Choy97d] ⁴⁵⁴	0.86	–	300	H	Hall
[Mats97] ³⁹⁸	$(1.2)^{-1}$	–	–	H	Hall
[Mick98] ¹⁶⁶	0.79	–	300	C	MC
[Bell99] ⁷²	–	1.33	–	C	EPM
[Iwat00] ²²⁵	0.7	–	–	H	COTE
[Bert01] ⁸⁸⁶	0.85	–	–	C	MC
[Hata03] ³⁹²	0.83	1.15	300	H	Hall
[Chen20] ⁸⁸⁷	$(1.75)^{-1} - (1.25)^{-1}$ ^b	–	–	C	FBMC
[Ishi21] ²⁸¹	$(1.17)^{-1}$	–	300	H	Hall
[Ishi24] ²⁸²	–	$(0.9)^{-1}$	300	H	Hall

^a type of mobility: Hall (H), conductivity (C)

^b ratio is lower for smaller doping concentrations and lower voltages

650 K, Nilsson, Sannemo, and Petersson²²⁷ various values with no clear tendency in [0.81, 0.84] within 100 – 500 K and Mickevičius and Zhao¹⁶⁶ as well as Ishikawa *et al.*²⁸¹ a slight decrease with rising temperature. The ratio of hole mobilities was reported constant with temperature²⁸².

Despite these various dependencies, which render constant values not well suited⁴⁶⁵, almost exclusively constant factors are used in literature. In accordance with the fundamental investigations shown earlier, the majority agrees upon $\mu_n^\perp < \mu_n^\parallel$ and $\mu_p^\perp > \mu_p^\parallel$ (see Fig. 52).

a. Doping Dependency The low-field mobility in regard to the doping concentration was heavily investigated^{7,8,118,119,224,225,284,314,392,673,678,699,814,834,864,898,903}

^{69,96,120,166,253,257,267,281,282,824,828,856,863,887,900,914}, which makes it impossible to show all gathered results in this review. Instead we focus on the models that were developed based on these

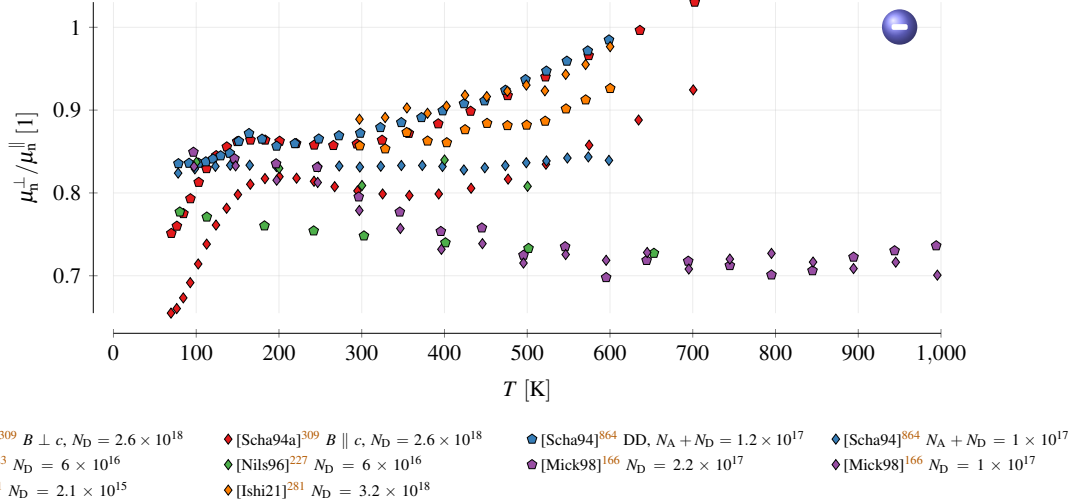


FIG. 51. Ratio of electron mobilities in the direction perpendicular (\perp) and parallel (\parallel) to the c-axis versus temperature. The entry “[Scha94] ⁸⁶⁴ DD” denotes the measurements including deep donor levels (see text).

data.

We found 26 investigations focused on the doping dependency of electrons in 4H-SiC based on Eq. (93) (see Table XXVII) over a time span of three decades. The maximum mobility varies within a range of $800 - 1240 \text{ cm}^2/(\text{Vs})$ while the reference doping concentration N_{ref} varies only slightly in the low $10^{17}/\text{cm}^3$ range. We also highlighted the deviating interpretations of the parameter N in the table, which underlines the large discrepancy in literature. The overview shows that different models share some of their values, which suggests that these were created by combining other ones or extending them by additional parameters. For N_{ref} the values $1.94 \times 10^{17}/\text{cm}^3$ and $2 \times 10^{17}/\text{cm}^3$ are used in 16 out of 28 models and for δ , 0.76 and 0.61 are used in 11 out of 28. The most prominent value for μ_{min} is $40 \text{ cm}^2/(\text{Vs})$ in 11 and $0 \text{ cm}^2/(\text{Vs})$ in 7 out of 28 while for μ_{max} $947 - 954 \text{ cm}^2/(\text{Vs})$ was chosen in 10 out of 28 investigations.

The models agree qualitatively (see Fig. 53). Exceptions are the ones by Ruff, Mitlehner, and Helbig ³⁶⁹, which was fitted to 6H, Pezzimenti, Della Corte, and Nipoti ¹³⁴, who predicted a very low maximum mobility, and Zhang and You ⁵⁶⁶, who used the model in Eq. (94) with the parameters in Table XXVIII to predict the decrease in mobility at higher doping densities. In the plot an additional reduction at doping densities around $10^{20}/\text{cm}^3$ is visible. Since the authors did not provide μ_{max} we picked $950 \text{ cm}^2/(\text{Vs})$. The remaining descriptions mainly differ in the value of μ_{max} .

We also found a more direct modeling of the mobility as shown in Eq. (115)^{172,173}. According

TABLE XXVII. Parameters for the Caughey-Thomas model in Eq. (93) used to describe the electron mobility.

ref.	dir	μ_{\min} [cm ² /(Vs)]	μ_{\max} [cm ² /(Vs)]	μ_0 [cm ² /(Vs)]	N_{ref} [1/cm ³]	δ [1]	γ_{\min} [1]	γ_{\max} [1]	γ_0 [1]	γ_{ref} [1]	γ_s [1]	γ_{NNref} [1]	N^a	K^b	method
[Ruff94] ³⁶⁹	—	20	—	380	4.50×10^{17}	0.45	—	—	-3	—	—	—	—	—	—
[Scha94] ⁸⁶⁴	⊥	—	947	—	1.94×10^{17}	0.61	—	-2.15 ^c	—	—	—	—	S	H	Hall
[Mick98] ¹⁶⁶	—	—	1071	—	1.94×10^{17}	0.4	—	—	—	—	—	—	S	C	MC
[Rosc98] ^{248d}	—	40	800	—	4×10^{17}	0.44	—	—	—	—	—	—	D	—	FIT
[Shah98] ²⁴⁷	—	—	947	—	1.94×10^{17}	0.61	—	—	—	—	—	—	—	—	—
[Wrig98] ^{171e}	—	88	—	970	1.43×10^{17}	1	-0.57	—	-2.7	2.55	—	—	I	—	—
[Levi01a] ^{775f}	—	79.8	855	—	2×10^{17}	1	—	—	—	—	—	—	D	—	FIT
[Mnat01] ^{888g}	—	30	880	—	2×10^{17}	0.67	—	—	—	—	—	—	D	C	FIT
[Mori01] ²²²		—	1141	—	1.94×10^{17}	0.61	—	—	—	—	—	—	S	C	DIV
[Rosc01] ^{38h}	⊥	40	950	—	2×10^{17}	0.76	-0.5	-2.4	—	1	—	—	D	—	FIT
[Hata03] ³⁹²	—	—	954	—	1.28×10^{17}	0.61	—	—	—	—	—	—	I	H	Hall
[Kaga04] ⁶⁷²ⁱ	—	—	977	—	1.17×10^{17}	0.49	—	—	—	—	—	—	S	H	Hall
[Adac05] ³⁵	—	—	1400	—	1×10^{17}	0.5	—	—	—	—	—	—	I	—	—
[Bala05] ³⁶²	—	40	950	—	2×10^{17}	0.73	—	-2.4	—	—	—	-0.76	—	—	—
[Werb07] ⁴⁷¹	—	33	771	—	2×10^{17}	0.76	—	—	—	—	—	—	D	C	DIV
[Cha08] ⁴⁴⁰	—	—	950	—	1.90×10^{17}	0.6	1	-2.15	—	—	—	0.05	D	—	—
[Pezz08] ¹³⁴	—	6	200	—	1×10^{16}	1	—	—	—	—	—	—	—	C	DIV
[Habi11] ^{351j}	—	40	—	910	2×10^{17}	0.76	-1.538	—	-2.397	0.75	0.722	—	S	—	FIT
[Hata13] ^{144k}	—	5	1010	—	1.25×10^{17}	0.65	-0.57	-2.6	—	2.4	-0.146	—	S	—	FIT
[Stef14] ¹⁵¹	⊥	28	950	—	1.94×10^{17}	0.61 ^m	—	-2.4	—	—	—	0.73	I	—	FIT
[Shar15] ⁵⁶⁵		40	947	—	1.94×10^{17}	0.61	-0.5	-2.9	—	—	—	2.4	S	C	DIV
[Arva17] ¹⁴⁶	—	40	950	—	1.94×10^{17}	0.61	-1.536	-2.4	—	—	—	—	D	—	—
[Vasi17] ⁸⁶³	—	20	950	—	2×10^{17}	0.8	—	—	—	—	—	—	D	H	Hall
[Ishi21] ²⁸¹	⊥	40	—	970	2.4×10^{17}	0.7	—	—	-2.58 ⁿ	—	—	—	D	H	Hall
		60	—	1120	2.3×10^{17}	0.74	—	—	-2.67 ⁿ	—	—	—	D	H	Hall
[Lech21] ¹⁴²		15.48	—	1415.4	1.80×10^{17}	0.560723	—	—	-2.5	—	—	—	—	—	—
[Rao22] ²⁰³	—	40	950	—	2×10^{17}	0.76	-0.5	-2.15	—	—	—	-0.76	I	—	—
[Ishi23] ⁶⁹	⊥	40	—	1000	2.2×10^{17}	0.68	-0.7	—	-2.9	—	—	-2.5	D	H	Hall
		20	—	1240	2×10^{17}	0.64	0.3	—	-3.2	—	—	-2.7	D	H	Hall

^a meaning of N: doping (D), ionized (I), sum of all dopants (S), intrinsic (N)

^b type of mobility: Hall (H), conductivity (C)

^c $T > 250\text{K}$ in $\langle 11\bar{2}0 \rangle$ direction ($\gamma_{\max} = -2.4$ towards $\langle 0001 \rangle$). $T < 250\text{K}$: $\gamma_{\max} = -1.18$ resp. -1.2

^d fitted to⁶

^e parameters referenced from Si based investigation⁸⁶² but not found there

^f fitted to^{117,864}

^g fitted to⁸⁶⁴ using dedicated Hall scattering factor⁸³⁰

^h fitted to^{166,284,323,864,922,923}

ⁱ fitted to^{271,314,398,834,864,922}

^j fitted to^{864,869,922,923}

^k fitted to³⁹⁸

^l fitted to^{119,120,284,363}

^m In the paper $\delta = -0.61$ was stated, which did not match the shown plots.¹⁴⁰

ⁿ $N_D = 2.1 \times 10^{15}/\text{cm}^3$, increases with doping concentration



FIG. 52. Constant values for the ratio of mobilities perpendicular (\perp) and parallel (\parallel) to the c-axis for electrons and holes.

TABLE XXVIII. Doping dependency parameters for the model in Eq. (94).

ref	mob.	μ_{\min}	$\mu_{\min2}$	N_{ref}	δ	μ_1	N_{ref2}	κ
		$[\text{cm}^2/(\text{Vs})]$	$[\text{cm}^2/(\text{Vs})]$	$[1/\text{cm}^3]$	[1]	$[\text{cm}^2/(\text{Vs})]$	$[1/\text{cm}^3]$	[1]
[Zhan18] ⁵⁶⁶	μ_n	88	0	5×10^{18}	1	43.4	3.43×10^{20}	2
	μ_p	44	0	5×10^{19}	1	29	6.1×10^{20}	2

to the authors these expressions are, however, based on Ruff, Mitlehner, and Helbig³⁶⁹ which only contains values on 6H-SiC. For the sake of comparison we added it to Fig. 53 as well.

$$\begin{aligned} \mu_n &= \frac{4.05 \times 10^{13} + 20N_D^{0.61}}{3.55 \times 10^{10} + N_D^{0.61}} \\ \mu_p &= \frac{4.05 \times 10^{13} + 10N_A^{0.65}}{3.3 \times 10^{11} + N_A^{0.65}} \end{aligned} \quad (115)$$

Similarly, Pernot *et al.*³¹⁴ fitted the Hall mobility to the free electron density n as shown in Eq. (116). In the plot we set $n = N$.

$$\mu_n = -39\,000 + 7436 \log(n) - 450.5 \log^2(n) + 8.81 \log^3(n) \quad (116)$$

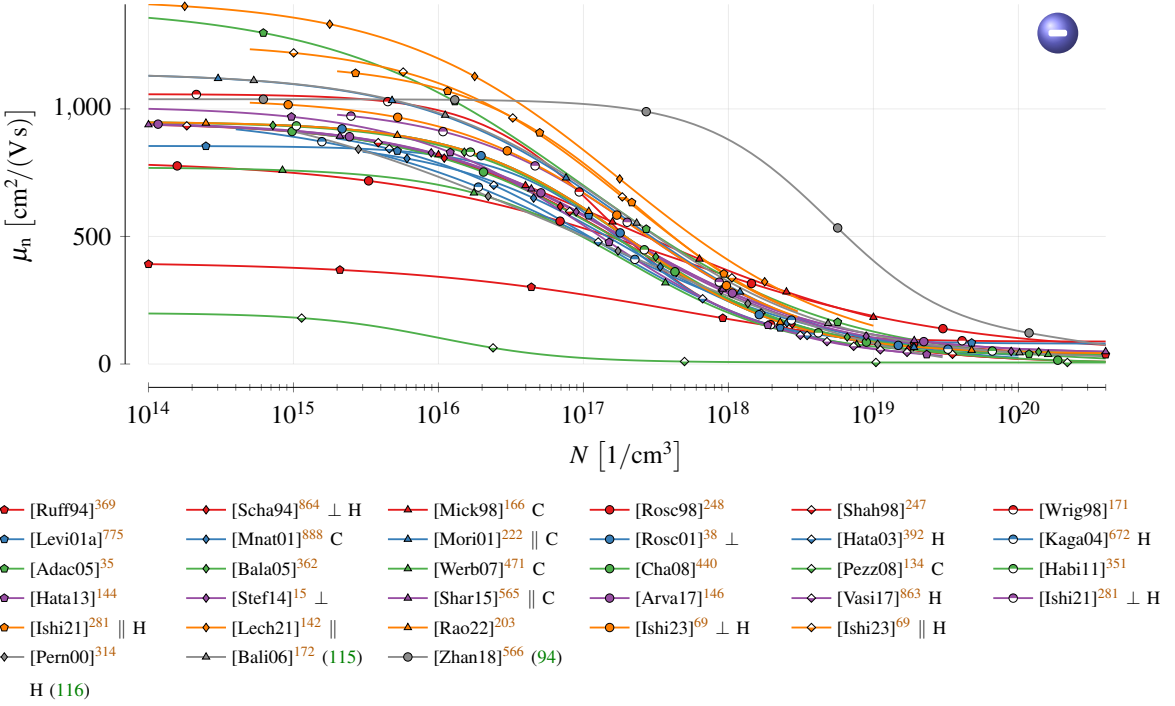


FIG. 53. Electron mobility approximations using the Caughey-Thomas model in Eq. (93) at $T = 300$ K. The models are only shown in the region used for characterization.

For the hole mobility less models were proposed with a larger spread in the respective parameters (see Table XXIX). Qualitatively, the decrease of the hole mobility, compared to the electron one, starts at higher doping densities (see Fig. 54), i.e., the maximum mobility can be maintained longer. In contrast to electrons we do not see a reuse of model parameters here, which might be an explanation for the big discrepancies: The models differ in the absolute mobility values at low and high doping concentrations, at which concentration and even at which rate the transition occurs. An outlier is again the model by Pezzimenti, Della Corte, and Nipoti¹³⁴, showing a very low mobility.

Negoro *et al.*⁸¹⁴ pointed out that the value $\mu_{\min} = 16$ cm²/(Vs) proposed by Hatakeyama *et al.*³⁹² was too high. Similarly Stefanakis and Zekentes¹⁵ argued that Schaffer *et al.*⁸⁶⁴ overestimated the hole mobility at high doping values, although the latest studies again indicated a value larger than zero. Exceptional in this regard is the large value of Wright *et al.*¹⁷¹ that even exceeded some values for μ_{\max} , which vary in the range of 75 – 140 cm²/(Vs).

We also added the model by Zhang and You⁵⁶⁶ to Fig. 54, who utilized Eq. (94) with the parameters in Table XXVIII. Since the authors did not define the maximum mobility we picked $\mu_{\max} = 80$ cm²/(Vs). This model shows the most delayed transition from high to low mobility

TABLE XXIX. Parameters for the Caughey-Thomas model in Eq. (93) used to describe the hole mobility.

ref.	dir	μ_{\min} [cm ² /(Vs)]	μ_{\max} [cm ² /(Vs)]	μ_0 [cm ² /(Vs)]	N_{ref} [1/cm ³]	δ [1]	γ_{\min} [1]	γ_{\max} [1]	γ_0 [1]	γ_{ref} [1]	γ_{δ} [1]	γ_{Nref} [1]	N^{a}	K^{b}	method
[Ruff94] ³⁶⁹	–	5	–	70	1×10^{19}	0.5	–	–	–3	–	–	–	–	–	–
[Scha94] ⁸⁶⁴	⊥	15.9	124	–	1.76×10^{19}	0.34	–	–	–	–	–	–	S	H	Hall
[Shah98] ²⁴⁷	–	25.9	128.1	–	1×10^{19}	0.24	–	–	–	–	–	–	–	–	–
[Wrig98] ^{171c}	–	74	–	43	1.43×10^{17}	1	–0.57	–	–2.7	2.55	–	–	I	–	–
[Levi01a] ^{775d}	–	65	114	–	5×10^{17}	1	–	–	–	–	–	–	D	–	FIT
[Mnat01] ^{888e}	–	33	117	–	1×10^{19}	0.5	–	–	–	–	–	–	D	C	FIT
[Hata03] ³⁹²	–	15.9	120	–	1.80×10^{18}	0.65	–	–	–	–	–	–	I	H	Hall
[Mats04] ⁶⁸³	–	37.6	106	–	2.97×10^{18}	0.356	–	–	–	–	–	–	S	H	Hall
[Bala05] ³⁶²	–	53.3	105.4	–	2.20×10^{18}	0.7	–	–2.1	–	–	–	–	–	–	–
[Werb07] ⁴⁷¹	–	10	–	81	1×10^{19}	0.5	–	–	–	–	–	–	D	C	DIV
[Cha08] ⁴⁴⁰	–	16	140	–	1.70×10^{19}	0.34	–1.6	–2.14	–	–	–	0.17	D	–	–
[Pezz08] ¹³⁴	–	2	20	–	1×10^{16}	1	–	–	–	–	–	–	–	C	DIV
[Koiz09] ^{120f}	–	–	114.1	–	5.38×10^{18}	0.66	–	–2.72	–	–	–0.35	2.44	D	H	Hall
[Habi11] ^{351g}	–	40	–	82	6.30×10^{18}	0.55	–1.538	–	–2.2397	0.75	0.722	–	S	–	FIT
[Hata13] ^{144h}	–	–	113.5	–	2.40×10^{18}	0.69	–0.57	–2.6	–	2.9	–0.2	–	S	–	FIT
[Liau15] ⁷¹⁴	–	–	75	–	2×10^{19}	0.7	–	–	–	–	–	–	D	C	LTPL
[Shar15] ⁵⁶⁵		15.9	124	–	1.76×10^{19}	0.34	–0.5	–2.9	–	–	–	2.3	S	C	DIV
[Tana18] ⁷⁰	–	–	110	–	3×10^{18}	0.6	–	–3	–	–	–	–1.8	D	H	DFT
–	–	95	–	–	1×10^{19}	0.7	–	–2.1	–	–	–	–1.5	D	C	DFT
[Lech21] ¹⁴²	–	2.529	–	469.42607	1.28×10^{19}	0.332645	–	–	–2	–	–	–	–	–	–
[Rao22] ²⁰³	–	15.9	125	–	1.76×10^{19}	0.76	–0.5	–2.15	–	–	–	–0.76	I	–	–
[Ishi24] ²⁸²	⊥	20	–	74	6.2×10^{18}	0.72	–2.2	–	–2.3	–	–	–0.9	D	H	Hall
	20	–	63	6.4×10^{18}	0.83	–2.2	–	–2.3	–	–	–0.9	D	H	Hall	

^a meaning of N: doping (D), ionized (I), sum of all dopants (S), intrinsic (N)

^b type of mobility: Hall (H), conductivity (C)

^c parameters referenced from Si based investigation⁸⁶² but not found there

^d fitted to^{117,864}

^e fitted to⁸⁶⁴ using dedicated Hall scattering factor⁸³⁰

^f fitting done by Stefanakis and Zekentes¹⁵

^g fitted to^{864,869,922,923}

^h fitted to³⁹⁸

in literature. In addition, we fitted the doping dependent parameters by Rambach, Bauer, and Ryssel⁸¹³ using a polynomial of degree two (see Eq. (117)). Although this fit solely used values in a doping range of $(0.5 - 5) \times 10^{19}/\text{cm}^3$ we extended the model in the plot, showing that it is also accurate well beyond these borders. Thereby we picked $\mu_{\min} = 15.9 \text{ cm}^2/(\text{Vs})$ and $\mu_{\max} =$

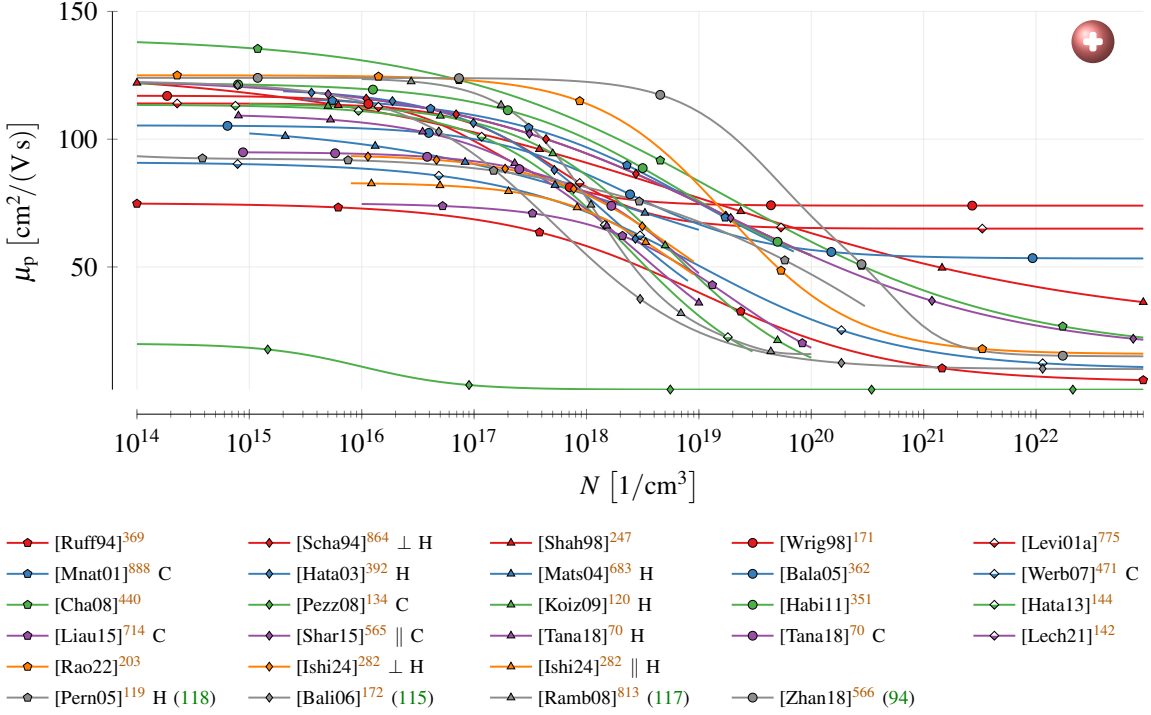


FIG. 54. Hole mobility approximations by the Caughey-Thomas model in Eq. (93) at $T = 300\text{K}$. The models are only shown in the region used for characterization.

$124\text{ cm}^2/(\text{V s})$.

$$\begin{aligned} \gamma_{\min}(N_A) &= \gamma_{\max}(N_A) = -1.24 + 5 \times 10^{-20} N_A - 4 \times 10^{-40} N_A^2 \\ \delta(N_A) &= 1.14 + 9.4 \times 10^{-21} N_A + 5.55 \times 10^{-40} N_A^2 \\ N_{\text{ref}}(N_A) &= 1.2 \times 10^{18} + 5.4 \times 10^{-2} N_A + 2 \times 10^{-21} N_A^2 \end{aligned} \quad (117)$$

Some authors also investigated the impact of compensation on the mobility. Pernot, Contreras, and Camassel ¹¹⁹ fitted the Hall mobility using the logarithmic doping concentration for non-compensated (see Eq. (118)) and weakly-compensated (see Eq. (119)) devices. In the graphical representation, where we used $N_A = N$, we only show the former case, since the latter results in negative mobility values.

$$\begin{aligned} \text{non-compensated: } \sigma R_H(292\text{K}) &= 2964.3 - 648.72 \log(N_A) + 53.393 \log^2(N_A) \\ &\quad - 1.8717 \log^3(N_A) + 0.002296 \log^4(N_A) \end{aligned} \quad (118)$$

$$\begin{aligned} \text{weakly-compensated: } \sigma R_H(292\text{K}) &= 24617 - 5982 \log(N_A) + 536.12 \log^2(N_A) \\ &\quad - 21.151 \log^3(N_A) + 0.30937 \log^4(N_A) \end{aligned} \quad (119)$$

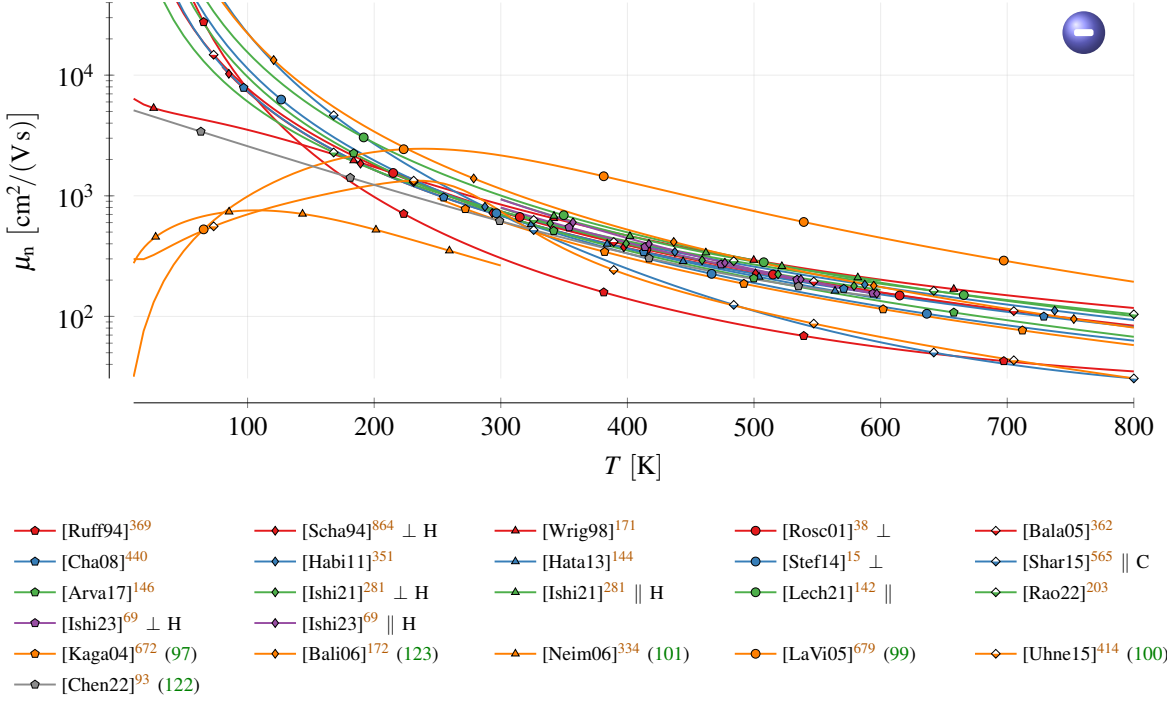


FIG. 55. Electron mobility models for varying temperature according to Eq. (93) for a doping of $4 \times 10^{16}/\text{cm}^3$.

b. Temperature Dependency In our review we encountered numerous investigations of the Hall^{69,120,133,223–225,271,281,282,284,345,351,398,672,673,676,678,688,824,868,873,899,901,902,7,8,34,70,118,119,314,334,477,683,699,826,828,834,864,869,914} and conductivity mobility^{323,671,679,682,714,856} variations with changing temperature.

The temperature scaling parameters of electrons in Eq. (93) (see Table XXVII) showed a consistent picture. We found 16 fits, which all agree on an increase of μ_{\min} , μ_{\max} and μ_0 for decreasing temperatures. An exception is μ_{\min} by Ishikawa *et al.*⁶⁹ parallel to the c-axis, but in this case the remaining temperature dependencies ensure the previously described behavior (see Fig. 55). The values for γ_δ and γ_{NNref} are less consistent; even positive and negative values were proposed. Nevertheless, due to the complicated interactions discussing parameters in isolation is not meaningful. Instead it is favorable to investigate the complete model at once.

For an in-detail comparison we plotted all models for $N = 4 \times 10^{16}/\text{cm}^3$ (see Fig. 55). As we discussed earlier, the mobility values change with doping concentration, so this plot serves as a qualitative comparison of the temperature dependency. In this regard the predictions by Eq. (99) are an exception, because the mobility always approaches zero for $T \rightarrow 0$, independent of the

TABLE XXX. Parameters for the model in Eq. (97) and Eq. (98).

ref	mob.	β_{\min}	β_{\max}	N_p	η	K	method
		[1]	[1]	[1/cm ³]	[1]		
[Kaga04] ⁶⁷²	μ_n	1.54	2.62	1.14×10^{17}	1.35	–	FIT
[Mats04] ⁶⁸³	μ_p	2.51	3.04	8.64×10^{17}	0.456	H	Hall

TABLE XXXI. Parameters for the model in Eq. (101) and Eq. (102).

ref	mob.	μ_{\min}	μ_{\max}	N_{ref}	δ	γ_{\max}	γ_l
		[cm ² /(Vs)]	[cm ² /(Vs)]	[1/cm ³]	[1]	[1]	[1]
[Neim06] ³³⁴	μ_n	100	320	2×10^{17}	0.67	2.6	0.5

doping concentration.

For low temperatures (< 200 K) almost all models agree on high mobilities (1000 cm²/(Vs)) that further increase with decreasing temperature. This includes the description according to Eq. (97), whose parameters are shown in Table XXX. However, such a tendency contradicts the increasing impact of impurity scattering, which is only covered by three models (four if we include the one by Hatakeyama, Fukuda, and Okumura¹⁴⁴ that is only plotted for $T > 300$ K): La Via *et al.*⁶⁷⁹ used Eq. (99) with the parameters shown in Eq. (120), whereat we picked suitable values for A and B . Izzo *et al.*⁶⁷¹, who also used this mode, derived $n = 3.06$.

$$n = 3, \quad A = 1, \quad B = 1 \times 10^{-11} \quad (120)$$

For the model in Eq. (101) we used the parameters provided by Neimontas *et al.*³³⁴ (see Table XXXI), whereat Mnatsakanov, Pomortseva, and Yurkov⁸⁸⁸ already proposed the values $\gamma_{\max} = 2.6$ and $\gamma_l = 0.5$ earlier. The predicted mobility values are lower than in other investigations, because the model described the electron mobility in heavily p-doped 4H-SiC, i.e., the minority carrier mobility.

For the model proposed by Uhnevionak⁴¹⁴ (cp. Eq. (100)) we used the parameters shown in Eq. (121) and the remaining ones according to Roschke and Schwierz³⁸. The increase of the mobility at low temperatures is thereby not automatically caused by splitting the maximum

mobility but relies on a careful selection of all parameters.

$$\begin{aligned} \mu_{\max 1} &= 500 \text{ cm}^2/(\text{Vs}), & \mu_{\max 2} &= 450 \text{ cm}^2/(\text{Vs}), & \gamma_{\max 1} &= -11.6 \\ & & & & \gamma_{\max 2} &= -2.74, & \gamma_{\text{NNref}} &= -12.5 \end{aligned} \quad (121)$$

At $T > 300$ K all models predict a decreasing mobility. Some observed a dependency of $T^{-2.1}$ to $T^{-2.5}$ instead of the expected $T^{-1.5}$ ^{398,477,868}. The temperature dependency even showed anisotropy. Schaffer *et al.*⁸⁶⁴ proposed a temperature scaling parallel to the c-axis of $T^{-2.4}$ and perpendicular of $T^{-2.15}$ above 200 K. Below that temperature they got $T^{-1.2}$ (parallel) and $T^{-1.18}$ (perpendicular). Ishikawa *et al.*²⁸¹ investigated the temperature dependency using a multiplicative factor $T^{-\beta}$ for three differing doping concentrations, observing an absolute decrease of β with increasing doping concentration and an anisotropy²⁸². In Fig. 55 we chose $\beta = -2.58$ perp. to the c-axis and $\beta = -2.67$ parallel to it which corresponds to measurements at a doping concentration of $N_D = 2.1 \times 10^{15} / \text{cm}^3$. Kagamihara *et al.*⁶⁷² stated that according to theoretical consideration the temperature parameters are 1.5 for low temperatures and 2.6 for high ones, which is close to $\beta_{\min} = 1.54$ and $\beta_{\max} = 2.62$ in their fit. Mitchel *et al.*⁸⁷⁴ used $\propto T^{-1.8}$, which is close to the expected $T^{-1.5}$ due to phonon scattering. Buono⁶⁶ pointed out that $\gamma_{\max} = -2.15$ for both charge carriers is smaller than the ideal factor of -1.5 that is expected from lattice scattering. This was believed to be due to non-polar optical-phonon scattering. Lades¹⁴¹ achieved $-1.8 \geq \gamma_{\max} \geq -2.2$, which lies between acoustical-mode phonon (-1.5) and optical-mode phonon (-2.5) scattering. Thus, the author assumed that other scattering factors contributed less to limit the mobility.

We also show the simplified models by Cheng, Yang, and Zheng⁹³, who fitted the expression shown in Eq. (122) to the measurements by Schaffer *et al.*⁸⁶⁴, and Baliga¹⁷², who fitted Eq. (123) to data by Koizumi, Suda, and Kimoto¹²⁰.

$$\mu_n(T) = 5422 \exp\left(-\frac{T}{128}\right) + 95 \quad (122)$$

$$\mu_n(T) = 1140 \left(\frac{T}{300}\right)^{-2.7} \quad (123)$$

The investigations of hole mobilities show the same tendencies for γ_{\min} , γ_{\max} and γ_0 and inconsistencies for γ_{δ} and γ_{NNref} that we observed for electrons. Although overall less investigations are available, the amount of temperature dependency studies is comparable (13 for holes, 16 for electrons). The main difference is that only one model, i.e., the one by Hatakeyama, Fukuda, and Okumura¹⁴⁴, was proposed that covers the decreasing mobility at low temperatures (see Fig. 56). For increasing temperature all models agree upon a continuous decrease of the mobility. The

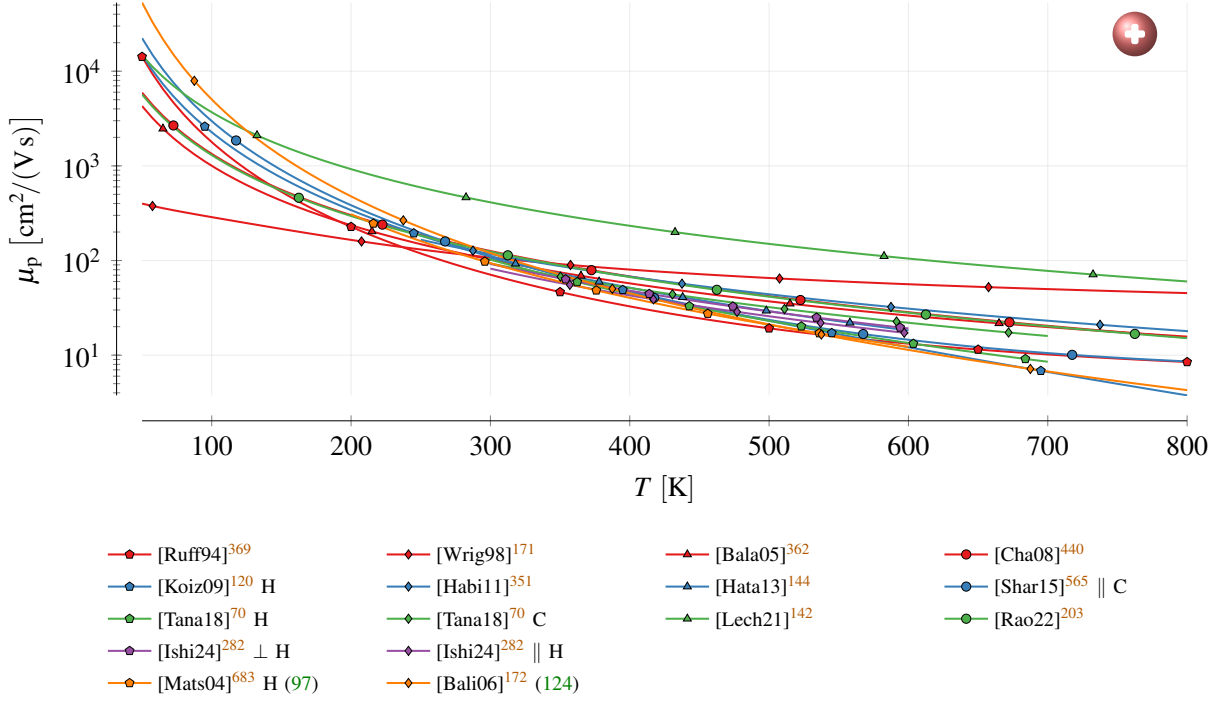


FIG. 56. Hole mobility models for varying temperature according to Eq. (93) for a doping of $4 \times 10^{16}/\text{cm}^3$.

parameters for the model by Matsuura *et al.*⁶⁸³ are shown in Table XXX and for the model by Baliga¹⁷² we used the parameters from Eq. (124).

$$\mu_p(T) = 120 \exp\left(\frac{T}{300}\right)^{-3.4} \quad (124)$$

c. Analysis It is common in literature to mix the parameters of different models, e.g., using the mobility values from one and the temperature scaling from another. We regularly encountered^{48,146,216,242,582} a combination of the models by Schaffer *et al.*⁸⁶⁴ and Roschke and Schwierz³⁸ (see Fig. 57). These are also the most influential publications, whereat newer studies were barely adopted in literature. On the positive side almost all references go back to one of the fundamental studies and almost exclusively 4H values are used. The only exception are the values by Ruff⁷⁵³ and Ruff, Mitlehner, and Helbig³⁶⁹ which were referenced three times.

For holes the majority of the values goes back to a single publication by Schaffer *et al.*⁸⁶⁴ (see Fig. 58), whereat, again, newer values were not widely adopted in the community. We are also unsure about the temperature scaling of the hole mobility in the publications citing Schaffer *et al.*⁸⁶⁴, because the latter stated $\gamma_{\max} = -2.15$ only for electrons. There were also multiple instances^{216,229,389,452,925,926} where μ_{\max} was interpreted as μ_0 , i.e., without subtracting μ_{\min} .

We were unable to retrace some values^{206,362,363,448} back to any scientific publication. In other

Electron (dir) (μ_{\min} , μ_{\max} , μ_0 , N_{ref} , δ) (γ_{\min} , γ_{\max} , γ_0 , γ_{ref} , γ_{δ} , $\gamma_{N_{\text{ref}}}$)

Ruff

[Ruff93]¹⁵³ (−) (−, −, −, −, −) (−, −, −, −, −, −)
 └─ [Bion12]¹³⁰ (−) (−, −, 870, 2×10^{17} , 0.55) (−, −, −, 2, −, −, −)

Ruff, Mittlehner, and Helbig

[Ruff94]¹⁶⁹ (−) (20, −, 380, 4.50×10^{17} , 0.45) (−, −, −3, −, −, −)
 └─ [Nall99]⁴³⁹ (−) (20, −, 700, 4.50×10^{17} , 0.45) (−, −, −3, −, −, −)
 └─ [Nall00]⁵²² (−) (20, −, 700, 4.50×10^{17} , 0.45) (−, −, −3, −, −, −)

Schaffer *et al.*

[Scha94]⁸⁶⁴ (⊥) (0, 947, −, 1.94×10^{17} , 0.61) (−, −2.15, −, −, −, −)
 └─ [Bako97]¹³⁹ (−) (0, −, 947, −, 1.94×10^{17} , 0.61) (−, −, −2.15, −, −, −)
 └─ [Codo00]¹⁵⁸ (−) (0, −, 947, −, 1.94×10^{17} , 0.61) (−, −, −2.15, −, −, −)
 └─ [Mcnu04]¹⁰¹ (−) (−, −, 947, −, 1.94×10^{17} , 0.61) (−, −, −2.15, −, −, −)
 └─ [Mcnu13]⁹²⁴ (−) (−, −, 947, −, 1.94×10^{17} , 0.61) (−, −, −2.15, −, −, −)
 └─ [Dibe14]⁴⁵³ (−) (−, −, −, −) (−, −, −2.15, −, −, −)
 └─ [Wang98]²²⁵ (−) (−, −, 947, −, 1.94×10^{17} , 0.61) (−, −, −2, −, −, −)
 └─ [Wang99]³⁸⁹ (−) (−, −, 947, −, 1.94×10^{17} , 0.61) (−, −, −2, −, −, −)
 └─ [Lade00]⁴¹ (−) (0, 947, −, 1.94×10^{17} , 0.61) (−, −, −, −, −, −)
 └─ [Chen01]⁸⁸⁷ (||) (0, 947, −, −, 1.94×10^{17} , 0.61) (−, −, −, −, −, −)
 └─ [Lee02]²⁴² (||/⊥) (0, −, 1136/947, −, 1.94×10^{17} , 0.61) (−2.4/−2.15, −, −, −, −)
 └─ [Li03]⁹⁰² (−) (−, −, 947, −, 1.94×10^{17} , 0.61) (−, −, −2, −, −, −)
 └─ [Zhao03]²⁹ (−) (−, −, 947, −, 1.94×10^{17} , 0.61) (−, −, −2, −, −, −)
 └─ [Das15]¹⁵³ (−) (0, −, 947, −, 1.94×10^{17} , 0.61) (−, −, −2, −, −, −)
 └─ [Ayalo04]⁴⁸ (⊥) (40, 950, −, 1.94×10^{17} , 0.61) (−0.5, −2.4, −, −, −, −)
 └─ [Max23]³¹³ (−) (40, 950, −, 1.94×10^{17} , 0.61) (−0.5, −2.4, −, −, −, −)
 └─ [Bros04]¹⁵⁶ (−) (0, 947, −, −, 1.94×10^{17} , 0.61) (0, −2.15, −, −, −, −)
 └─ [Schr06]²¹⁰ (−) (0, 947, −, −, 1.94×10^{17} , 0.61) (−, −, −, −, −, −)
 └─ [Zhan09]²⁶ (−) (−, −, 947, −, 1.94×10^{17} , 0.61) (−, −, −2, −, −, −)
 └─ [Khal12]³⁸⁶ (−) (−, −, 947, −, −, 1.94×10^{17} , 0.61) (−, −, −2, −, −, −)
 └─ [Zhan10]¹⁵² (−) (−, −, 947, −, 1.94×10^{17} , 0.61) (−, −, −2, −, −, −)
 └─ [Lutz11]⁴¹⁵ (−) (0, 947, −, −, 1.94×10^{17} , 0.61) (−, −2.15, −, −, −, −)
 └─ [Buon12]¹⁶ (−) (−, −, 950, −, 1.94×10^{17} , 0.61) (−, −, −2.15, −, −, −)
 └─ [Chen15]¹⁶ (||/⊥) (0, −, 1136/947, −, 1.94×10^{17} , 0.61) (−2.4/−2.15, −, −, −, −)
 └─ [Joha16]³⁹⁵ (−) (0, 947, −, −, 1.94×10^{17} , 0.61) (−, −2.15, −, −, −, −)
 └─ [Lutz18]¹⁴⁹ (−) (0, 947, −, −, 1.94×10^{17} , 0.61) (−, −2.15, −, −, −, −)
 └─ [Arva19]³⁸² (⊥) (40, 950, −, −, 1.94×10^{17} , 0.61) (−, −, −, −, −, −)
 └─ [Joha19]¹⁴⁷ (−) (−, −940, −, −, −) (−, −, −, −, −, −)
 └─ [Yang22]²¹³ (−) (−, −, −, −, −) (−, −, −, −, −, −)

Mickevičius and Zhao

[Micke98]¹⁶⁶ (−) (−, 1071, −, 1.94×10^{17} , 0.4) (−, −, −, −, −, −)
 └─ [Tila07]³¹⁵ (−) (−, 1071, −, −, 1.94×10^{17} , 0.4) (−, 2.4, −, −, −, −)

Wright *et al.*

[Wrig98]¹⁷¹ (−) (88, −, 970, 1.43×10^{17} , 1) (−0.57, −, −2.7, 2.55, −, −)
 └─ [Bali06]¹⁷² (−) (−, 1140, −, −, −) (−, −2.7, −, −, −, −)
 └─ [Bali19]¹⁷³ (−) (−, 1140, −, −, −) (−, −2.7, −, −, −, −)

Mnatsakanov, Pomortseva, and Yurkov

[Mnat01]⁸⁸⁸ (−) (30, 880, −, 2×10^{17} , 0.67) (−, −, −, −, −, −)
 └─ [Mnat02]⁸⁶⁹ (−) (30, 880, −, 2×10^{17} , 0.67) (−, −, −, −, −, −)

Roschke and Schwierz

[Ros01]³⁸ (⊥) (40, 950, −, 2×10^{17} , 0.76) (−0.5, −2.4, −, 1, −, −, −)
 └─ [Line03]⁸⁶⁵ (−) (40, 950, −, 2×10^{17} , 0.76) (−, −, −, −, −, −)
 └─ [Bert04]⁴⁶⁵ (⊥) (40, 950, −, 2×10^{17} , 0.76) (−, −2.4, −, −, −, −0.76)
 └─ [Bert04a]⁵⁵⁴ (⊥) (40, 950, −, 2×10^{17} , 0.76) (−, −2.4, −, −, −, −0.76)
 └─ [Lv04]³⁵⁷ (−) (40, 950, −, 2×10^{17} , 0.76) (−, −2.4, −, −, −, 1.05)
 └─ [Pere06]²³⁸ (−) (40, 950, −, 2×10^{17} , 0.76) (−, −2, −, −, −, −)
 └─ [Tama08a]³²⁴ (−) (−, 950, −, 2×10^{17} , 0.76) (−, −2.8, −, −, −, −)
 └─ [Song12]³²⁵ (−) (0, 950, −, 2×10^{17} , 0.76) (−, −2.8, −, −, −, −)
 └─ [Liu21]⁵⁰ (−) (−, 950, −, 2×10^{17} , 0.76) (−, −2.9, −, −, −, −)
 └─ [Alba10]³¹⁸ (−) (40, 950, −, 2×10^{17} , 0.76) (−0.5, −2.4, −, −, −, −0.76)
 └─ [Bell11]²⁰⁹ (−) (40, 950, −, 2×10^{17} , 0.76) (−0.5, −2.4, −, 1, 0, −)
 └─ [Neil12]²² (−) (40, 950, −, 2×10^{17} , 0.76) (−0.5, −2.4, −, 1, 0, −)
 └─ [Pezz13]²⁰⁷ (−) (40, 950, −, 2×10^{17} , 0.76) (−0.5, −2.4, −, −, −, −0.76)
 └─ [Megh15]³⁹⁰ (−) (40, 950, −, 2×10^{17} , 0.76) (−0.5, −2.4, −, −, −, −0.76)
 └─ [Zhou16]²²⁷ (−) (40, 950, −, 2×10^{17} , 1) (−, −, −, −, −, −)
 └─ [Megh18]¹⁵⁷ (−) (40, 950, −, −, −) (−, −, −, −, −, −)
 └─ [Megh18a]⁴⁰³ (−) (40, 950, −, 2×10^{17} , −) (−, −, −, −, −, −)
 └─ [Zegh19]⁴⁰⁴ (−) (40, 950, −, 2×10^{17} , 0.76) (−0.5, −2.4, −, −, −, −0.76)
 └─ [Zegh20]⁴⁰⁵ (−) (40, 950, −, 2×10^{17} , 0.76) (0.5, 2.4, −, −, −, 0.76)

Hatakeyama *et al.*

[Hata03]⁹⁹² (−) (0, 954, −, 1.28×10^{17} , 0.61) (−, −, −, −, −, −)
 └─ [Nipo16a]⁷⁹⁵ (−) (−, −, −, −, −) (−, −, −, −, −, −)

Balachandran, Chow, and Agarwal

[Bala05]⁶⁶² (−) (40, 950, −, 2×10^{17} , 0.73) (−, −2.4, −, −, −, −0.76)
 └─ [Nawa10]³⁶³ (−) (40, 950, −, 2×10^{17} , 0.73) (0, −2.4, −, −, −, −0.76)
 └─ [Usma14]³⁰⁶ (−) (40, 950, −, 2×10^{17} , 0.73) (0, −2.4, −, −, −, −0.76)

Habib, Wright, and Horsfall

[Habi11]³⁵¹ (−) (40, −, 910, 2×10^{17} , 0.76) (−1.538, −, −2.397, 0.75, 0.722, −)
 └─ [Loph18]³⁴⁸ (⊥/||) (40, 910/1100, −, 2×10^{17} , 0.76) (−1.536, −2.4, −, 0.75, 0.722, −)
 └─ [Rakh20]³¹⁸ (−) (−, 699.4, −, −, −) (−, −, −, −, −, −)

Hatakeyama, Fukuda, and Okumura

[Hata13]¹⁴⁴ (−) (5, 1010, −, 1.25×10^{17} , 0.65) (−0.57, −2.6, −, 2.4, −0.146, −)
 └─ [Naug17]⁴⁴⁵ (⊥) (5, 1010, −, 1.25×10^{17} , 0.65) (−0.57, −2.6, −, 2.4, −0.146, −)
 └─ [Jin24]⁴¹⁷ (−) (5, 1010, −, 1.25×10^{17} , 0.65) (−, −, −, −, −, −)

Kimoto and Cooper

[Kimo14a]¹³ (⊥) (−, 1020, −, 1.80×10^{17} , 0.6) (−, −1.8, −2.8, −, −, −, −)
 └─ [Fuji17]⁹⁰⁰ (−) (−, −, −, −, −) (−, −, −, −, −, −)
 └─ [Kimo19]⁶⁸ (⊥) (−, 1020, −, 1.80×10^{17} , 0.6) (−, −1.8, −2.8, −, −, −, −)

Stefanakis and Zekentes

[Stef14]¹⁵ (⊥) (28, 950, −, 1.94×10^{17} , 0.61) (0, −2.4, −, −, −, −0.73)
 └─ [Trip19]¹⁵⁰ (−) (28, 950, −, 1.94×10^{17} , 0.61) (0, −2.4, −, −, −, −0.73)

FIG. 57. Reference chain for low field electron mobility models. are fundamental investigations, research not focused on 4H and connections predicted from the used values.

occasions references were provided but the presented values could not be found therein^{142,448}. Some publications^{2,43,318} even present multiple models that contradict each other.

At last we want to discuss two previous reviews on mobility models, as we encountered problematic parameters. We begin with the analysis by Stefanakis and Zekentes¹⁵ who investigated six models and fitted a seventh to measurement results for holes. The model denoted as “Reggio



FIG. 58. Reference chain for low field hole mobility models. are fundamental investigations, connections implied by the values used in the publication.

“Calabria Uni.” was cited from Pezzimenti²⁰⁷ but goes back to Schaffer et al.⁸⁶⁴ for holes and Roschke and Schwierz³⁸ for electrons. In addition, the shown parameters for this model contain some flaws: δ of the electrons should be 0.76 instead of 0.34, while γ_{NNref} of the holes should be −0.34 instead of −0.76. A similar confusion occurred for the values of the model denoted as “Nawaz”³⁶³, which used for the electrons $\delta = 0.73$ instead of the stated 0.34 and $\gamma_{\text{NNref}} = -0.76$

instead of 0.73. For holes μ_{\min} should be $53.3 \text{ cm}^2/(\text{Vs})$ instead of the stated $15.3 \text{ cm}^2/(\text{Vs})$. The authors also fitted the measurements presented by Koizumi, Suda, and Kimoto¹²⁰ but extracted N_{ref} at a temperature of 400 K instead of 300 K. The value $\gamma_{\text{NNref}} = 2.44$ further inferred a decrease of N_{ref} with rising temperature, but the measurements showed the opposite. Finally, there is a typographical error in δ of the proposed model for electrons, which should be 0.61 instead of the proposed -0.61 .

The second overview paper was published by Tian *et al.*¹⁶. For the values cited from Nawaz³⁶³ δ of the electrons should be 0.73 instead of the stated 0.34 and $\gamma_{\text{NNref}} = -0.76$ instead of 0.73. For holes μ_{\min} should be $53.3 \text{ cm}^2/(\text{Vs})$ instead of $15.3 \text{ cm}^2/(\text{Vs})$. Surprisingly, these are the same discrepancies that we discovered for the review discussed in the last paragraph. Despite these variations, the values from Nawaz³⁶³ achieved the best results and was chosen for the simulations by the authors. For an other approach, the maximum mobility for electrons was changed from $950 \text{ cm}^2/(\text{Vs})$ ⁶⁶ to $947 \text{ cm}^2/(\text{Vs})$. The model proposed by Megherbi *et al.*⁴⁵⁷ was extended by a temperature scaling, which matched an earlier publication by the same authors³⁹⁰ with deviations for γ_{NNref} (0 instead of -0.76 for electrons and -0.34 for holes).

The models called “Bakowski” by Stefanakis and Zekentes¹⁵ and “Gustafsson” by Tian *et al.*¹⁶ share the same values, which were primarily adopted from Schaffer *et al.*⁸⁶⁴. However, the origin of $\mu_{\min} = 88 \text{ cm}^2/(\text{Vs})$ for electrons and $\mu_{\min} = 74 \text{ cm}^2/(\text{Vs})$ for holes is indeterminate. Both reviews denoted Bakowski, Gustafsson, and Lindefelt¹³⁹ as the model source, but we were unable to locate it there. In fact, Wright *et al.*¹⁷¹, Wright²²⁶ first proposed the stated values in the 1990s and provided as reference the publication by Arora, Hauser, and Roulston⁸⁶². In that investigation of silicon the authors stated for the electron mobility $\mu_{\min} = 88.3 \text{ cm}^2/(\text{Vs})$ at 300 K and $\mu_{\min} = 73.78 \text{ cm}^2/(\text{Vs})$ at 400 K, which seemingly got adapted by Wright *et al.*¹⁷¹. A comprehensive listing of all inconsistencies for the mobility can be found in Section A 7.

3. High-Field Mobility

Early publications on SiC had to rely on silicon parameters for the high-field mobility³⁶⁹, but starting from the year 1995 we identified 20 investigations of the electric field dependency of electron and hole velocities^{68,72,166–168,175,184,536,854,887,890–895}. For this purpose, simulations and measurements were used to the same extent. The achieved parameters for electrons (see Table XXXII) reveal saturation velocities in the range from a few 10^6 V/cm to a few 10^7 V/cm . Hjelm, Bertils-

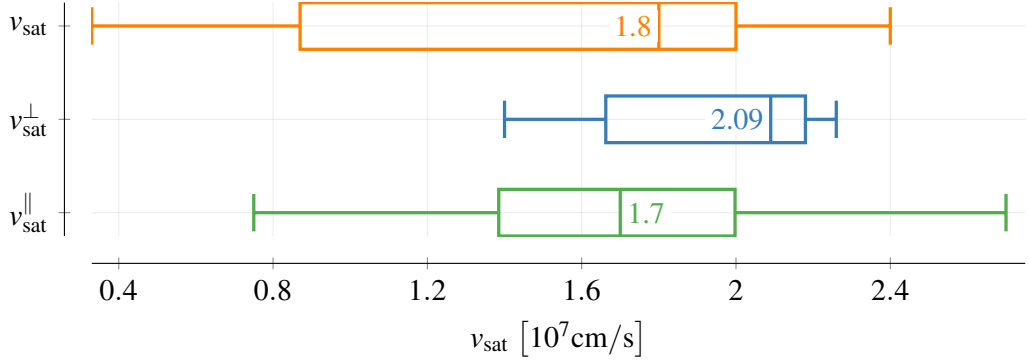


FIG. 59. Statistical evaluation of electron saturation velocity. Shown are the 0th, 25th, 50th, 75th and 100th quartile. The mean value is added in numerical form.

son, and Nilsson⁹²⁹ investigated the saturation velocity for varying field angle in respect to the steps in the interface, which reduced with increasing angle.

A statistical interpretation shows that the values parallel to the c-axis and those without direction information have a similar mean value (see Fig. 59) but also a considerable uncertainty. For the direction perpendicular to the c-axis the results agree better and indicate a higher velocity. Exceptions are the investigations by Mickevičius and Zhao¹⁶⁶ and Joshi³²³, whose parallel values were larger than their perpendicular ones. Hatakeyama *et al.*⁵¹⁴ estimated the anisotropy based on impact ionization coefficients, which are also higher for the perpendicular direction (see Section IX) and Hjelm, Bertilsson, and Nilsson⁹²⁹ explained it by the anisotropy in the band structure. Hatakeyama, Fukuda, and Okumura¹⁴⁴ obtained a ratio of $v_{\text{sat}}^{\parallel}/v_{\text{sat}}^{\perp} = 0.6$.

The hole saturation velocity is lower than the electron one but $v_{\text{sat}}^{\perp} > v_{\text{sat}}^{\parallel}$ is still satisfied (see Table XXXIII). Hatakeyama, Fukuda, and Okumura¹⁴⁴ calculated a ratio of $v_{\text{sat}}^{\parallel}/v_{\text{sat}}^{\perp} = 0.8$. The key difference to electrons is the amount of conducted investigations. We only found six publications focusing on holes starting in the year 2000, whereat the latest was published a decade ago. In consequence, the value of the hole saturation velocity is often just assumed^{43,146} or set equal to the electron one^{146,207,248,318,369,389}. Vasconcelos, Rodrigues, and Luzzi¹⁷⁶ calculated the field dependency but only up to $F = 200 \text{kV/cm}$, where they obtained $v_{\perp} \approx 5 \times 10^6 \text{cm/s}$ and $v_{\parallel} \approx 1 \times 10^6 \text{cm/s}$. A fit of Guo *et al.*⁹²⁸ to these values predicted $v_{\text{sat}} = 1 \times 10^7 \text{cm/s}$.

We mentioned in the introduction that Monte-Carlo simulations revealed a maximum in the charge carrier velocity, followed by a decrease with increasing field strengths^{22,72,166,168,175,184,227,424,465,536,854,857}. Lv *et al.*⁸⁵⁷ used the model introduced in Eq. (106)

TABLE XXXII. High field mobility parameters in Eq. (103) for electrons.

ref.	v_{sat} [cm/s]	v_{sat}^{\perp} [cm/s]	$v_{\text{sat}}^{\parallel}$ [cm/s]	β [1]	γ_{sat} [1]	γ_{β} [1]	T [K]	K^a	method
[Ruff94] ^{369b}	2×10^7	–	–	2	–	–	–	–	–
[Josh95] ³²³	–	2.10×10^7	2.70×10^7	–	–	–	300	C	MC
[Nils96] ²²⁷	–	2.10×10^7	1.80×10^7	–	–	–	300	C	MC
[Khan98] ⁸⁹³	–	2.08×10^7 ^c	–	0.825	–	–	300	C	NPC
[Mick98] ¹⁶⁶	–	2×10^7	2.50×10^7	1	–	–	300	C	MC
[Khan00] ⁸⁹⁵	–	2.2×10^7	–	1.2	–	–	296	C	NPC
–	1.6×10^7	–	2.2	–	–	–	593	C	NPC
[Lade00] ^{141d}	–	2.20×10^7	–	1.2	–0.44	1	–	–	FIT
[Nils00] ⁵³⁶	–	2.26×10^7	1.64×10^7	–	–	–	–	C	MC
[Sank00] ⁹³⁰	3.30×10^6	–	–	–	–	–	–	C	BIV
[Vass00] ⁹³¹	–	–	8×10^6	–	–	–	300	C	DIV
–	–	7.5×10^6	–	–	–	–	460	C	DIV
[Zhao00] ¹⁶⁷	–	–	1.83×10^7	–	–	–	–	C	MCP
[Bert01] ⁸⁸⁶	–	2.10×10^7	1.70×10^7	0.84/1.1 ^e	–	–	–	C	MC
[Rosc01] ^{38f}	2.40×10^7	–	–	0.85	– ^g	– ^g	300	–	FIT
[Hjel03] ¹⁸⁴	–	2.12×10^7	1.58×10^7	–	–	–	–	C	EPM
[Bert04a] ^{854h}	–	2×10^7	1.70×10^7	0.9/1.1 ^e	– ^f	– ^f	300	–	FIT
[Arda05] ⁸⁹¹	–	1.40×10^7	–	–	–	–	293	C	NPC
[Aktu09] ¹⁶⁸	1.60×10^7	–	–	–	–	–	300	C	MC DFT-DOS
[Donn09] ²¹⁹	–	1.85×10^7	–	–	–	–	296	C	MC
–	1.5×10^7	–	–	–	–	–	593	C	MC
[Sun10] ⁹³²	1.80×10^7	–	–	–	–	–	300	C	MC
[Hata13] ¹⁴⁴ⁱ	–	2.20×10^7	–	1.2	–0.46	0.88	–	–	FIT
[Das15] ³⁵³	2×10^7	–	–	1	0.87	0.66	–	–	–
[Bela22] ⁸⁹⁰	8.70×10^6	–	–	2	–	–	–	C	CCh
[Jais24] ⁸⁹⁶	2×10^7	–	–	–	–	–	–	C	DIV
[Tana24] ⁴²⁴	–	1.40×10^7	–	–	–	–	300	–	–

^a type of mobility: Hall (H), conductivity (C)

^b β taken from Silicon

^c Value extrapolated. Highest measured velocity was 1.5×10^7 cm/s.

^d fitted to⁸⁹⁵

^e values of $\beta \perp / \parallel$ to c-axis

^f fitted to⁸⁹⁵

^g temperature scaling according to Eq. (104)

^h fitted to²²⁷

ⁱ fitted to^{141,895}

TABLE XXXIII. High field mobility parameters in Eq. (103) for holes.

ref.	v_{sat} [cm/s]	v_{sat}^{\perp} [cm/s]	$v_{\text{sat}}^{\parallel}$ [cm/s]	β [1]	γ_{sat} [1]	γ_{β} [1]	T [K]	K^a	method
[Ruff94] ^{369b}	2×10^7	–	–	–	–	–	–	–	–
[Nils00] ⁵³⁶	–	1.10×10^7	6.50×10^6	–	–	–	–	C	MC
[Zhao00] ¹⁶⁷	–	–	8.60×10^6	–	–	–	–	C	MCP
[Hjel03] ¹⁸⁴	–	1.08×10^7	7.30×10^6	–	–	–	–	C	EPM
[Aktu09] ¹⁶⁸	1×10^7	–	–	–	–	–	–	C	MC DFT-DOS
[Kimo14a] ^{43c}	1.30×10^7	–	–	–	–	–	–	–	–
[Das15] ³⁵³	2×10^7	–	–	1.213	0.52	0.17	–	–	–
[Guo25] ^{928d}	1×10^7	–	–	1.2	–	–	–	–	FIT

^a type of mobility: Hall (H), conductivity (C)

^b v_{sat} set equal to electron saturation velocity

^c values estimated

^d fitted to^{176,895,933}

with the parameter shown in Eq. (125) to model this “overshoot”^{22,318,857}.

$$\begin{aligned} \mu_0 &= 0.17\mu_1, \alpha = -1.95, \beta = 3 \\ F_0 &= 3.05 \times 10^4 \text{ V/cm}, F_1 = 2.8 \times 10^5 \text{ V/cm}, v_{\text{max}} = 4.8 \times 10^7 \text{ cm/s} \end{aligned} \quad (125)$$

Interestingly, none of the publications that presented these decreasing velocities used the term “overshoot”. Instead, the peak value, i.e., the maximum, was denoted as the saturation velocity. The question remains whether the decrease in velocity is real or just a simulation artifact, also because this effect has yet to be seen in experiments³¹⁸. Nilsson, Sannemo, and Petersson²²⁷ explained the pronounced peak in the velocity due to band bending at the zone boundaries, which decreases the energy gradient there and Tanaka, Kimoto, and Mori⁵³⁸ named Bloch oscillations as the main reason⁴²⁴. Mickevičius and Zhao¹⁶⁶ stated that, within their simplified analytical band model, the velocity decreased at high electric fields due to conduction band non-parabolicity at higher energies. The authors then showed on 3C-SiC that impact ionization cools the electrons down, which effectively increased their velocity, resulting in a constant velocity at high fields. However, later studies that also took impact ionization into account still observed a velocity decrease^{536,929}. In the majority of cases the decrease is simply not commented, although the velocity can decrease up to one order of magnitude^{167,854,886,932}. Exceptional are the results presented by

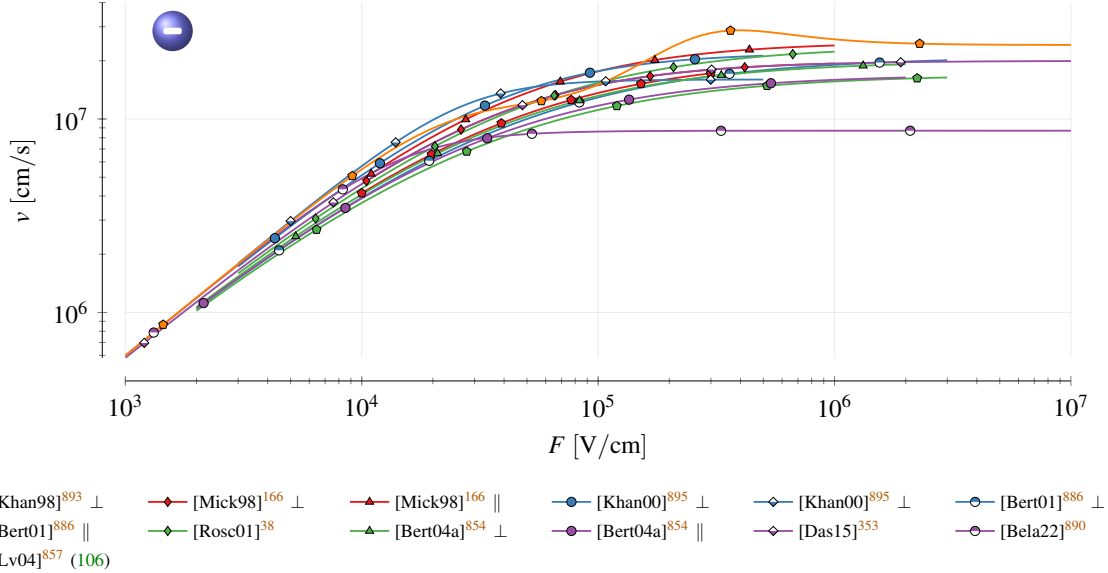


FIG. 60. Electron carrier velocity with varying field for $\mu_{\text{low}} = 400 \text{ cm}^2/(\text{Vs})$. The models are only plotted in the range used for the characterization.

Akturk *et al.*¹⁶⁸, whose electron velocity stabilized at $7 \times 10^6 \text{ cm/s}$ after passing the peak value of $1.6 \times 10^7 \text{ cm/s}$. The predicted hole velocity passes a saddle point, i.e., it further increased for high fields.

The models show a good agreement for varying field strengths (see Fig. 60). The first deviations among the model are visible already at a few kV/cm, whereat considerable deviations from the low field mobility are detectable around 10 kV/cm¹⁷³. This is significantly smaller than the 200 kV/cm proposed by Lophitis *et al.*⁴⁴⁸. We were unable to recreate the plots shown by Lv *et al.*⁸⁵⁷ with the provided parameters (see Eq. (125)). In the paper a continuously decreasing derivative of v is visible with increasing field strength, with a peak at $F = E_1$ and a value of $v = 1 \times 10^7 \text{ cm/s}$ at $F = 2 \times 10^6 \text{ V/cm}$. We do not explicitly show the results for holes as we only found a single model in literature.

The temperature dependency of the high-field velocity was measured by Khan and Cooper^{893,893,895} and investigated by simulations^{227,465,854}. With increasing temperature the velocity decreases (see Fig. 61). Later these results were numerically fitted^{141,144}. Lades¹⁴¹ used a linear fit for the exponent β such that the value published by Khan and Cooper⁸⁹⁵ for 620 K could not be perfectly matched (2.2 vs. 2.4). The values published by Das and Duttagupta³⁵³ predict a steep increase of the velocity with temperature also for holes. Since this is the only fit for holes we found, further comments about its accuracy are impossible. We did not include the results by

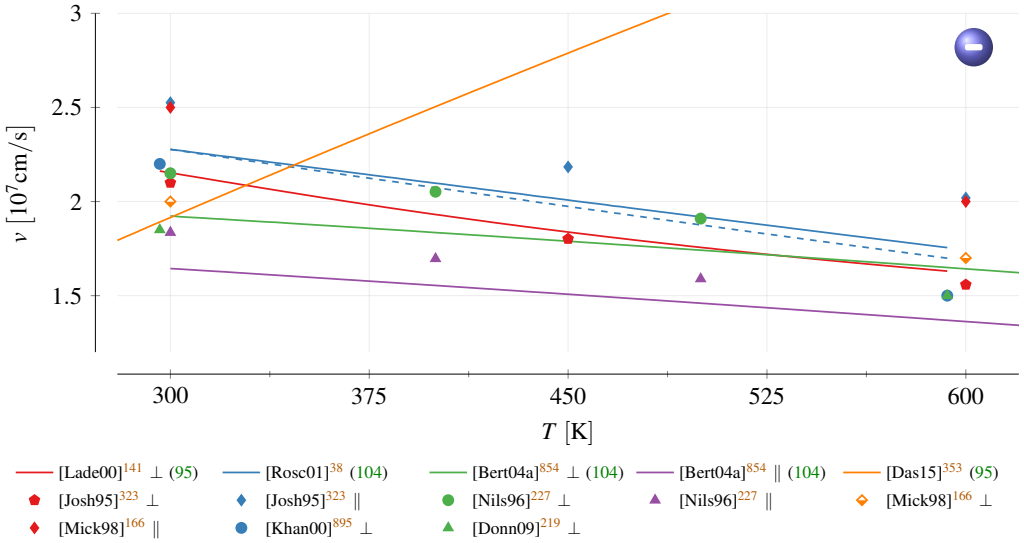


FIG. 61. Temperature dependency of electron velocity for $F = 10^6 \text{ V/cm}$ and $\mu_{\text{low}} = 450 \text{ cm}^2/(\text{V s})$. The dashed line shows the model by Roschke and Schwierz³⁸ with $d = 0.8$ and $v_{\text{max}} = 5.56 \times 10^7 \text{ cm/s}$ in Eq. (104).

TABLE XXXIV. Model parameters for temperature dependent carrier velocity in Eq. (104) and Eq. (105).

ref.	dir	v_{max}	d	β_0	T_{ref}	a	b	c
		[cm/s]	[1]	[1]	[K]	[1]	[K]	[1/K]
[Rosc01] ^{38a}	-	4.77×10^7	0.6	0.816	327	4.27×10^{-2}	98.4	0
[Bert04a] ^{854b}	\perp	2.77×10^7	0.23	0.6	0	0	∞	10^{-3}
	\parallel	2.55×10^7	0.3	1.01	0	0	∞	3×10^{-4}

^a fitted to^{227,895}

^b fitted to simulations by Nilsson, Sannemo, and Petersson²²⁷

Hatakeyama, Fukuda, and Okumura¹⁴⁴ in the plot for improved readability due to a high similarity with Lades¹⁴¹.

Roschke and Schwierz³⁸ and Bertilsson, Harris, and Nilsson⁸⁵⁴ used the models in Eq. (104) and Eq. (105) with the parameters shown in Table XXXIV. Multiple investigations^{22,218,389,547} later reused these values. For Eq. (104) we regularly found $d = 0.8$ ^{369,389,488}, which we could trace back to the publication by Jacoboni *et al.*⁸⁷⁸. Another popular value, $d = 0.6$ ^{22,38,857}, was referenced from an early edition of Sze and Ng²³⁶, but the version we used in this review also stated $d = 0.8$. This indicates that $d = 0.6$ is outdated.

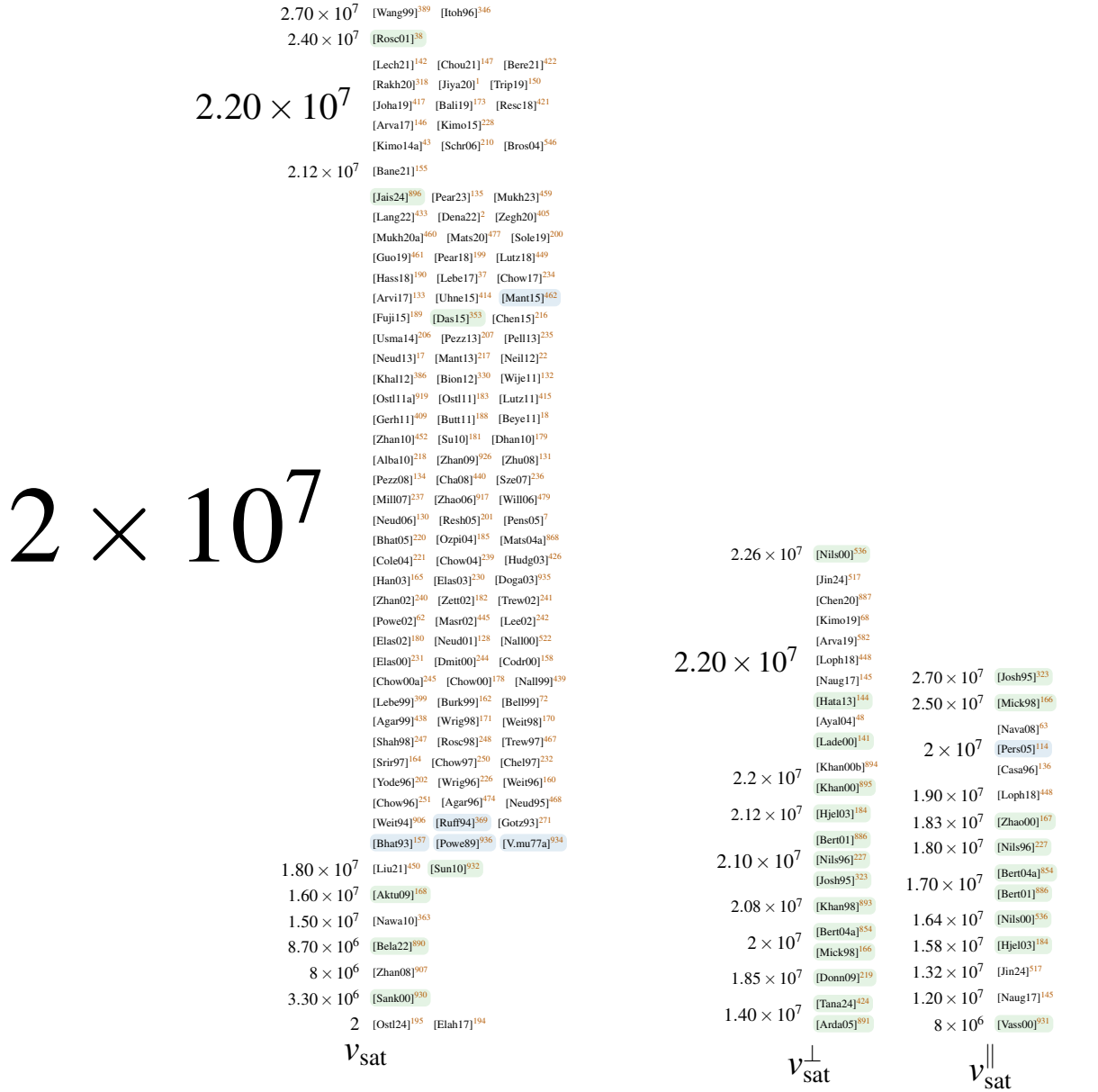


FIG. 62. Electron saturation velocity values used in literature. are fundamental investigations and research not focused on 4H.

In simple overviews the electron saturation velocity is dominantly denoted as 2×10^7 cm/s (see Fig. 62). This popular value was already reported by V. Muench and Pettenpaul⁹³⁴ for 6H, as pointed out by Khan and Cooper⁸⁹³, and then reused for 4H. Three investigations^{166,353,896} achieved the same value also for 4H. Slightly lower/higher values are also available but are cited not nearly as prominently.

For holes very similar values were proposed (see Fig. 63) but, again, in less amount. The fact

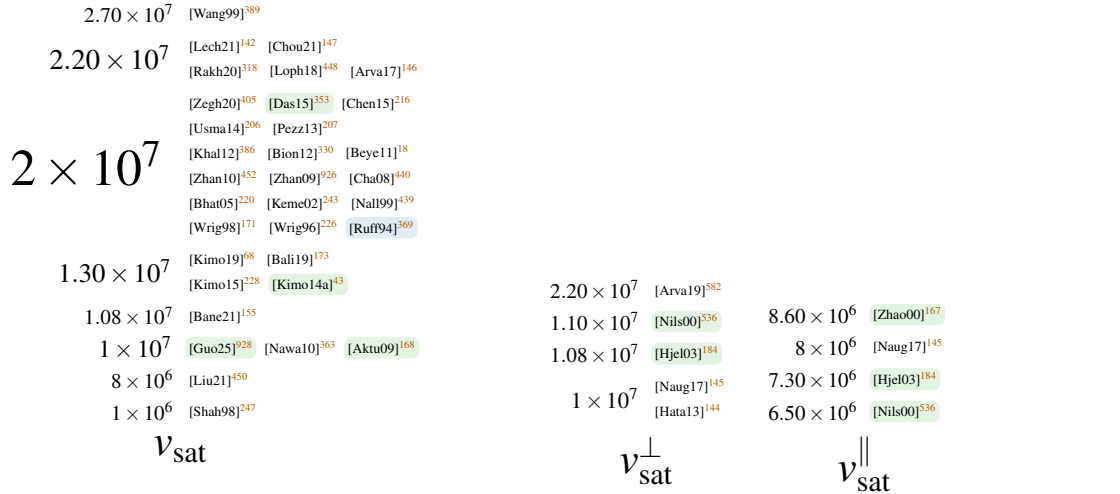


FIG. 63. Hole saturation velocity values used in literature. ■ are fundamental investigations and □ research not focused on 4H.

that the most popular value is equal to electrons indicates that this value was reused for holes as well. Considering the high impact ionization coefficient of holes and its importance for a wide range of devices, more data will be required for the high-field behavior of holes in the future.

The reference chain for electrons (see Fig. 64) confirms our earlier intuition. The value $v_{\text{sat}} = 2 \times 10^7$ cm/s could not be traced back to any 4H based publication. Instead, it is mentioned often without proper references. The analysis shows, similar to the low-field mobility, that small clusters are formed, especially for the most prominent values. This is a sign that the respective values are commonly accepted within the community. On the bright side eight fundamental investigations were referenced at least once.

The reference chain for holes (see Fig. 65) paints a similar picture. Small clusters for the most prominent values are formed, but also four out of the seven fundamental investigations directly referenced. In addition, we see for many entries blank lines, which indicates that the cited publication did not state any values. This shows that values were misused, e.g., by using the electron saturation velocity for holes³¹⁸.

4. Carrier-Carrier Scattering

The only investigation of carrier-carrier scattering in 4H-SiC we found was conducted by Lades¹⁴¹, who started from the parameters of Eq. (108) for silicon and scaled them until the

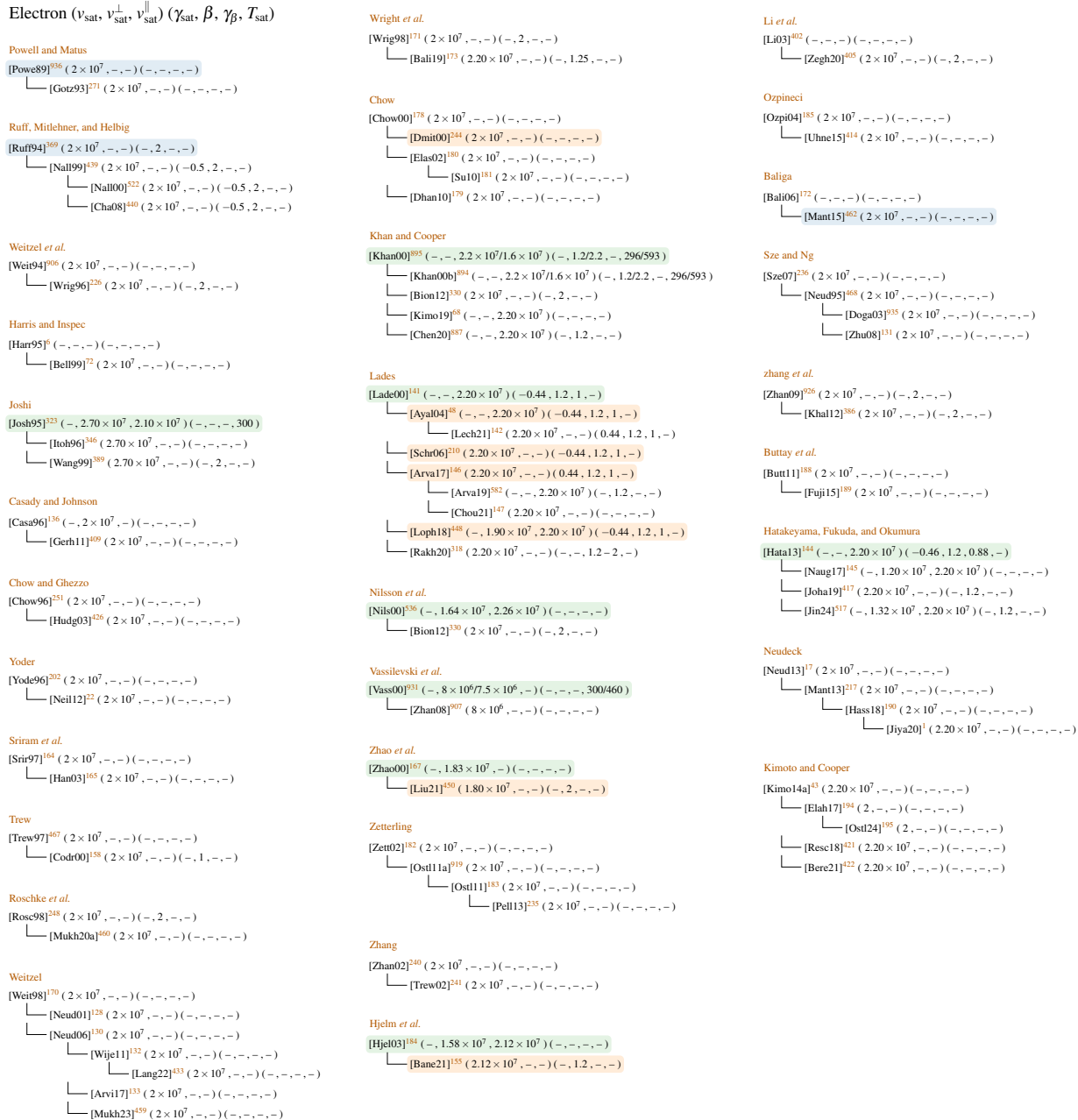


FIG. 64. High-field mobility reference chain for electrons.

results fit to 4H-SiC measurements. In this fashion the values shown in Eq. (126) were achieved, which are already reused at various occasions^{48,150,210}

$$D = 6.9 \times 10^{20} / (\text{cm V s}), F = 7.452 \times 10^{13} / \text{cm}^2 \quad (126)$$

We found further sources that were not suited for this review: Onoda *et al.*⁸⁸⁵ proposed values for 6H and Bhatnagar *et al.*²²⁰ separate values for electrons and holes but used an equation that

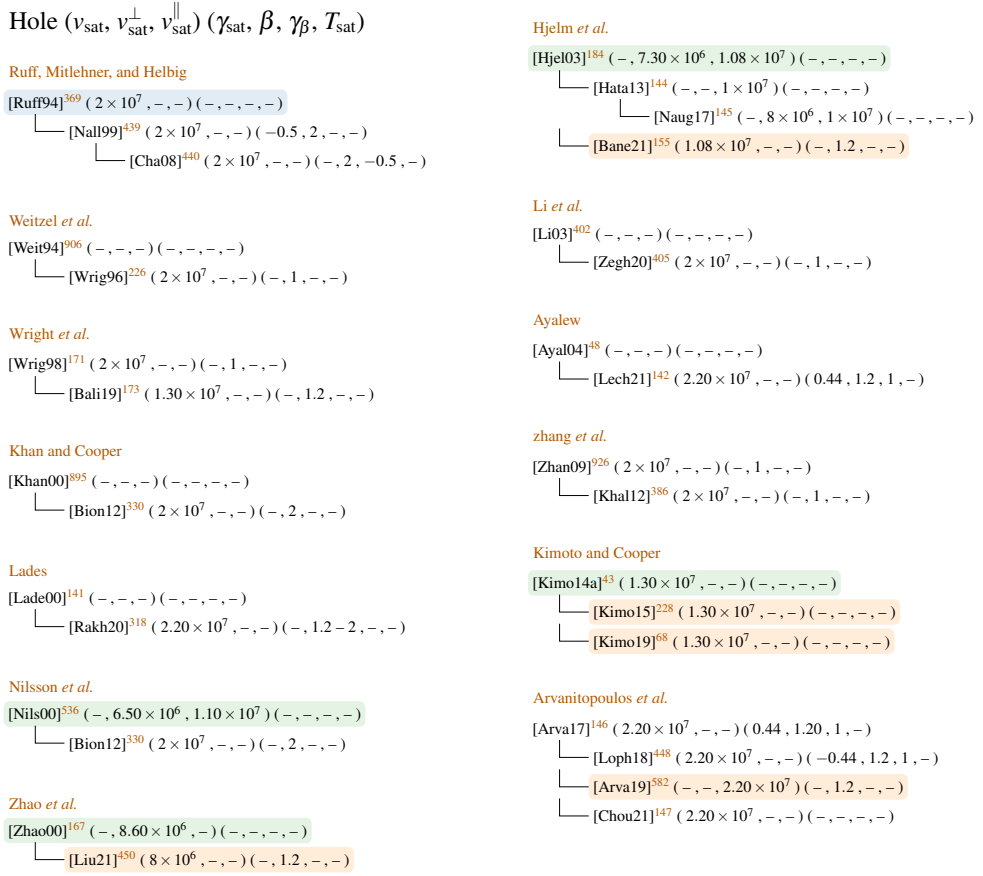


FIG. 65. High-field mobility reference chain for holes.

was developed by Dorkel and Leturcq⁸⁸² for impurity scattering. Finally, Lechner¹⁴² referenced the values by Fletcher⁹³⁷, which were fitted for silicon.

XI. CONCLUSION

The models and parameters we found for each of the covered properties were propagated but also changed and misinterpreted within the community. We were able to show, among others, that (i) the majority of permittivity values are based on a single publication from the year 1970 that focused on a different SiC polytype, (ii) the increase of the hole density-of-states mass by 100 % between 0 and 300 K is rarely considered, (iii) the most common band gap values at room temperature are based on a lower energy gap at zero Kelvin, (iv) impact ionization data perpendicular to the c-axis, where electrons and holes behave similarly, are almost non-existent, and (v) reliable data on the hole saturation velocity and velocity overshoots at high electric fields are missing.

Despite our extensive analyses this work is unable to provide a common material parameter set

that matches every device. Instead we experienced in our daily business that each physical object is unique, i.e., simulations always have to be calibrated. However, we are confident that the provided overview improves the initial parameter values and decreases the required effort. The achieved results are not limited to TCAD simulation but applicable to any task that requires knowledge of the physical properties of 4H-SiC, e.g., in material science.

For future research we envision a critical evaluation of the current knowledge base within the scientific community. In detail, further characterizations (measurements, calculations, simulations) will be required to obliterate the shortcomings we discovered.

ACKNOWLEDGMENTS

This work was supported by the Austrian Research Promotion Agency (FFG) in the project RadHardDetSim (895291).

The authors would like to thank Christa Bay from the library at TU Wien, who helped to acquire countless publications.

AUTHOR DECLARATIONS

Conflict of Interest

The authors have no conflicts to disclose.

Author Contributions

Jürgen Burin: Conceptualization (lead), Data curation (lead), Investigation (lead), Methodology (lead), Resources (lead), Validation (lead), Visualization (lead), Writing - original draft (lead), Writing - review & editing (equal). **Philipp Gaggl:** Conceptualization (supporting), Data curation (equal), Resources (equal), Validation (supporting), Visualization (supporting), Writing - original draft (equal), Writing - review & editing (equal). **Simon Waid:** Conceptualization (supporting), Methodology (supporting), Visualization (supporting), Writing - review & editing (equal). **Andreas Gsponer:** Conceptualization (supporting), Methodology (supporting), Validation (supporting), Visualization (supporting), Writing - review & editing (equal). **Thomas Bergauer:** Funding acquisition (lead), Project administration (lead).

DATA AVAILABILITY STATEMENT

The data, evaluation scripts and figures of this study are openly available in the repository [Data of 4H SiC TCAD Parameter Review³⁹](#).

Appendix A: Inaccuracies

In this section we list inaccuracies we encountered throughout our review. The purpose of this listing is not to blame any of the authors or suggest any wrongdoing. Instead, we think that mistakes are unavoidable (there are definitely a lot of them also in this review) and that it is important to highlight them in order to prevent a further spread. If not further specified the described actions were done by the authors of the respective publication.

1. Permittivity

- [Acha17]¹⁵⁴: We could not find the value $\epsilon_s = 8.5884$ in the referenced paper³⁶. Even using the available values and calculating the effective relative permittivity did not yield the desired result.
- [Arpa06]¹⁴³: Changed $\epsilon_s^{\parallel} = 10.03^{81}$ to $\epsilon_s = 10$.
- [Arva17]¹⁴⁶: Changed $\epsilon_s^{\perp} = 9.66^{81}$ to $\epsilon_s = 9.66$.
- [Chen94]¹¹³: The second column in Table II denotes 4H but is labeled 2H.
- [Choi05]¹²⁹: Changed $\epsilon_s^{\perp} = 9.66^6$ to $\epsilon_s = 9.7$.
- [Darm19]¹⁹⁷: Changed $\epsilon_s^{\perp} = 9.76^{43}$ to $\epsilon_s = 9.76$.
- [Egil99]¹⁴⁰: Changed $\epsilon_s^{\perp} = 9.66^{81}$ to $\epsilon_s = 9.7$.
- [Elah17]¹⁹⁴: Changed $\epsilon_s = 9.94^{43}$ to $\epsilon_s = 10$.
- [Hari98]¹⁶³: Changed $\epsilon_{\infty}^{\parallel} = 6.78^{96}$ to $\epsilon_{\infty} = 6.8$.
- [Harr95]⁶: Changed $\epsilon_s^{\parallel} = 10.03^{81}$ to $\epsilon_s^{\parallel} = 10.3$.
- [Huan98]¹³⁷: Changed $\epsilon_s = 9.66^{136}$ to $\epsilon_s = 9.7$.

[Kimo19]⁶⁸: Used $\epsilon_s^{\parallel} = 10.32$ instead of $\epsilon_s^{\parallel} = 9.98$ specified in the referenced publication⁹².

[Klah20]¹⁵¹: Changed $\epsilon_s^{\parallel} = 10.03^{81}$ to $\epsilon_s = 10$.

[Kova20]¹⁵²: Changed $\epsilon_s^{\perp} = 9.66^{81}$ to $\epsilon_s = 9.67$.

[Micc19]¹⁴⁹: Changed $\epsilon_s^{\perp} = 9.66^{81}$ to $\epsilon_s = 9.66$.

[Neil12]²²: The used $\epsilon_s = 9.72$ is actually a 3C value⁸¹.

[Neud01]¹²⁸: Changed $\epsilon_s^{\perp} = 9.66^6$ to $\epsilon_s = 9.7$.

[Neud06]¹³⁰: Changed $\epsilon_s^{\perp} = 9.66^6$ to $\epsilon_s = 9.7$.

[Ozpi04]¹⁸⁵: Changed $\epsilon_s = 10.007^{107}$ to $\epsilon_s = 10.1$.

[Pear23]¹³⁵: Changed $\epsilon_s^{\perp} = 9.66^6$ to $\epsilon_s = 9.7$.

[Ryba17]¹⁹⁶: Changed $\epsilon_s^{\perp} = 9.76^{43}$ to $\epsilon_s = 9.7$.

[Scho94]³⁴: The specified reference [77Pan] could not be found in the reference list. The similar reference [75Pan]⁹³⁸ did also not contain the desired values.

[Torp01]²⁵⁴: Used $\epsilon_s = 6.7$, which is, however, a value for the high-frequency one. It is unclear whether the wrong value was picked from the reference or the textual description is flawed.

[Trip19]¹⁵⁰: Changed $\epsilon_s^{\perp} = 9.66^{81}$ to $\epsilon_s = 9.66$.

[Wije11]¹³²: Changed $\epsilon_s = 9.7^{130}$ to $\epsilon_s = 10$.

[Yosh18]¹⁴⁸: Changed $\epsilon_s^{\perp} = 9.66^{81}$ to $\epsilon_s^{\perp} = 9.7$.

[Zatk21]¹⁵³: Changed $\epsilon_s^{\perp} = 9.66^{81}$ to $\epsilon_s = 9.66$.

[Zipp11]¹⁶⁹: Changed $\epsilon_s^{\perp} = 9.76^{10}$ to $\epsilon_s = 9.76$.

2. DOS Mass

[Arpa06]¹⁴³: Changed $m_{de}^* = 0.19^{271}$ to 0.2.

[Fang05]³²⁰: Referenced $m_{de}^* = 0.4m_0$ ³¹⁹ but that publication is focused on GaAs and we could not find the respective values.

[Flor03]³³³: Present values for the hole effective masses but the labels $m_{M\Gamma}$ and m_{ML} refer to electron effective masses.

[Gale98]³²⁷: Changed $m_{TM}^* = 4.23$ ²⁹⁰ to 4.2.

[Harr95]⁶: Changed $m_{de\perp}^* = 0.21$ ³⁰¹ to 0.24, $m_{de\perp}^* = 0.176$ ²⁷¹ to 0.18 and $m_{de\parallel}^* = 0.224$ ²⁷¹ to $m_{de\parallel}^* = 0.22$.

[Hemm97]²⁷⁴: Calculated $m_{de}^* = 0.37$ but it is actually 0.39.

[Itoh95]³¹¹: Changed $m_{de}^* = 0.19$ ²⁷¹ to 0.2.

[Kim24]¹⁵⁶: Changed $m_{de}^* = 0.39$ ³²⁹ to 0.2.

[Lind98]¹¹⁷: We could not retrace the values for the hole masses in the referenced publication⁴⁸⁴.

[Penn01]²⁹⁶: Only used the transversal masses to calculate the DOS masses.

[Penn04]³⁰⁶: Changed $m_{MK}^* = 0.28$ ²⁹⁴ to 0.29 and $m_{ML}^* = 0.31$ ²⁹⁴ to 0.33. Only used the transversal masses to calculate the DOS masses.

[Pens93]³¹⁰: In the definition $m_{de}^* = (m_{de\perp}^* m_{de\parallel}^*)^{(1/3)}$ the square for $m_{de\perp}^*$ is missing. Changed $m_{de\perp}^* = 0.176$ ²⁷¹ to 0.17 and $m_{de\parallel}^* = 0.224$ ²⁷¹ to 0.22.

[Pere06]²³⁸: The origin of the used values is unclear, because the cited publication⁶ corresponds to hole effective masses of 3C and 6H.

[Pern05]¹¹⁹: Calculated $m_{dh}^* = 2.66$ but our calculations resulted in $m_{dh}^* = 2.64$.

[Pers98a]²⁷⁷: We were not able to confirm $m_{dh}^* = 0.88$ based on the referenced data¹²⁵. Instead we achieved $m_{dh}^* = 0.78$. Similarly, instead of $m_{de}^* = 0.45$ we got $m_{de}^* = 0.44$.

[Resh05]²⁰¹: Changed $m_{M\Gamma}^* = 0.57$ ¹²⁵ to 0.58.

[Rodr21]¹⁷⁷: Changed $m_{de\perp}^* = 0.176$, $m_{de\parallel}^* = 0.224$ ²⁷¹ to $m_{de\perp}^* = 0.18$, $m_{de\parallel}^* = 0.22$.

[Scha94a]³⁰⁹: Changed $m_{de\perp}^* = 0.176$ ²⁷¹ to 0.17 and $m_{de\parallel}^* = 0.224$ ²⁷¹ to 0.22.

[Scho94]³⁴: Changed $m_{de\perp}^* = 0.176$ ²⁷¹ to 0.18 and $m_{de\parallel}^* = 0.224$ ²⁷¹ to 0.22. Assumed $m_{dh}^* = 1$, $g_A = 4$ and $g_D = 2$.

- [Sozz19]²⁰⁴: Changed $m_{\text{de}}^* = 0.394$ ²⁶² to 0.4.
- [Yang19]³²⁶: Calculated $m_{\text{de}}^* = 0.36$, but we achieved $m_{\text{de}}^* = 0.37$.

3. Band Gap

- [Alba10]²¹⁸: In the doping dependency factor ΔE_{ga} the exponent for the prefactor 1.57×10^{-2} should be $1/4$ instead of $1/3$ and the factor 1.54×10^{-2} should be 1.54×10^{-3} . In addition, factor 1.7×10^{-2} in ΔE_{gd} is actually 1.17×10^{-2} .
- [Back94]³⁷⁷: Stated that the band gap energies by Choyke, Hamilton, and Patrick³³⁶ suffer from an inaccuracy in the order of 0.015 eV. This value, however, refers to the non-measured values. The correct inaccuracy is 0.003 eV.
- [Bade20]⁴¹¹: Changed $E_g = 3.26 \text{ eV}$ ²³⁴ to $E_g = 3.3 \text{ eV}$.
- [Baie19]⁴¹⁰: The value $E_g = 3.268 \text{ eV}$ does not match $E_g = 3.26 \text{ eV}$ ²²⁸ and $E_{\text{gx}} = 3.263 \text{ eV}$ ⁴¹⁶ from the provided references.
- [Bako97]¹³⁹: The temperature dependency $\alpha = -3.3 \times 10^{-3} \text{ eV/K}$ is stated, but it should be $\alpha = -3.3 \times 10^{-4} \text{ eV/K}$ ³⁷⁰.
- [Bane21]¹⁵⁵: Used the value $E_g(300) = 3.23 \text{ eV}$ ³⁶ but interpreted it as $E_g(0)$. Consequently the authors end up with $E_g(300) = 3.1934 \text{ eV}$.
- [Bech04]⁴²⁷: Changed $E_g = 3.265 \text{ eV}$ ³⁴⁴ to $E_g = 3.27 \text{ eV}$.
- [Bell99]⁷²: Changed $E_{\text{gx}} = 3.263 \text{ eV}$ ⁴¹² to $E_g = 3.26 \text{ eV}$.
- [Bere21]⁴²²: Changed $E_{\text{gx}} = 3.265 \text{ eV}$ ⁴³ to $E_g = 3.26 \text{ eV}$.
- [Bion12]³³⁰: Changed $E_{\text{gx}} = 3.263 \text{ eV}$ ⁴¹² to $E_g = 3.26 \text{ eV}$.
- [Buon12]⁶⁶: Eq. (2.41) denotes ΔE_v instead of ΔE_c . The respective parameters need to be positive and the exponent of the first summand is $1/4$ not $1/3$.
- [Cama08]²⁸⁶: Changed E_{gx} ³³⁶ to E_g .
- [Capa22]⁴²³: Changed $E_{\text{gx}} = 3.265 \text{ eV}$ ⁴³ to $E_g = 3.26 \text{ eV}$.

[Casa96]¹³⁶: Changed $E_{gx} = 3.265 \text{ eV}$ ³⁴⁴ to $E_g = 3.26 \text{ eV}$.

[Cha08]⁴⁴⁰: States $E_g(300) = 3.25 \text{ eV}$ but the respective reference⁴³⁹ denotes it as the band gap at 0 K.

[Choi05]¹²⁹: Changed $E_{gx} = 3.263 \text{ eV}$ ⁴¹² to $E_g = 3.26 \text{ eV}$.

[Dena22]²: According to the presented equation for the temperature induced band gap narrowing α has to be negative to fit the description in the text.
Changed $\beta = 1.8 \times 10^3$ ⁴³ to 1.3×10^3 .
Changed $E_{gx} = 3.265 \text{ eV}$ ⁴³ to $E_g = 3.26 \text{ eV}$.

[Dhan20]¹⁷⁹: Changed $E_g = 3.26 \text{ eV}$ ¹⁷⁸ to $E_g = 3.3 \text{ eV}$.

[Donn12]³⁹⁴: Lists a range of values for $E_g(300)$ but in one⁹⁶ of the provided references only $E_g(4)$ is available. The value $E_g(300) = 3.03 \text{ eV}$ was taken from Sandeep and Komaragiri²⁰⁸ instead of Galeckas *et al.*⁷⁸⁵, as stated in the paper. The origin of the remaining value $E_g(4) = 3.28 \text{ eV}$ could not be retraced.

[Egil99]¹⁴⁰: Changed exciton band gap energy E_{gx} from 3.266 eV ²⁸⁵ to 3.265 eV .

[Elah17]¹⁹⁴: Changed $E_{gx} = 3.265 \text{ eV}$ ⁴³ to $E_g = 3.2 \text{ eV}$.

[Feng04a]²⁰: Changed $E_{gx} = 3.265 \text{ eV}$ ⁵³ to $E_{gx} = 3.26 \text{ eV}$.

[Gale97]³²⁷: Changed $E_{gx} = 3.265 \text{ eV}$ ³⁴⁶ to $E_g = 3.275 \text{ eV}$.

[Gale02]³⁵⁶: According to the provided definition of the temperature dependency using dE_g/dT the parameter should be $2.4 \times 10^{-4} \text{ eV/K}$ instead of $-2.4 \times 10^{-4} \text{ eV/K}$. Otherwise the band gap would increase with increasing temperature.

[Griv07]³⁶⁰: The values from Itoh, Kimoto, and Matsunami³⁴⁶ were displayed in a plot but got shifted by 2 meV to compensate for differing band gap energies at 0 K.
It is unclear how the phonon dispersion $\Delta = 0.29$ was derived, as it leads to $p = 3.59$. The stated $p = 2.9$ would, in contrast, result in $\Delta = 0.37$.

[Huan98]¹³⁷: Changed $E_{gx} = 3.265 \text{ eV}$ ³⁴⁴ to $E_g = 3.26 \text{ eV}$.

[Hudg03]⁴²⁶: It is unclear to us how $E_g(300) = 3.25 \text{ eV}$ was derived based upon $E_{gx}(4.2) = 3.265 \text{ eV}$ ⁵⁶.

[Ioff23]³⁶: All Lindefelt parameters have negative values, however, only the ones impacting the conduction band should be < 0 . The exponent $1/4$ with parameters A_{nv} and A_{pc} were changed to $1/3$.

The authors state that the values from Dubrovskii and Lepneva³⁸¹ denote the exciton band gap energy E_{gx} instead of E_g .

[Joha19]⁴¹⁷: Changed $E_{gx} = 3.265 \text{ eV}$ ¹⁴¹ to $E_g = 3.26 \text{ eV}$.

[Khal12]³⁸⁶: Referenced an investigation on GaN⁹³⁹ that only contains the model. The origin of the shown values is for us unclear.

Proposed $\alpha = -2.206 \times 10^{-2}$, which leads to an increasing band gap with temperature. This contradicts the presented reference⁹³⁹.

[Kimo19]⁶⁸: It is unclear how the value $E_g(0) = 3.292 \text{ eV}$ was derived.

[Kohl03]²⁷³: Changed $E_{gx} = 3.263 \text{ eV}$ ⁴¹² to $E_g = 3.26 \text{ eV}$.

[Kwas14]³⁴⁰: Changed E_{gx} ³³⁷ to E_g .

[Lade00]¹⁴¹: The values $E_x = 40 \text{ meV}$ was picked as average value from $10 - 80 \text{ meV}$ ¹³, which we could, however, not retrace. The only value that is stated for 4H by Devaty and Choyke¹³ is $E_x = 20 \text{ meV}$ ³⁴⁸.

[Lebe99]³⁹⁹: Changed $E_g = 3.26 \text{ eV}$ ³⁹⁸ to $E_g = 3.2 \text{ eV}$.

[Lech21]¹⁴²: Changed $E_{gx} = 3.265 \text{ eV}$ ¹⁴¹ to $E_g = 3.265 \text{ eV}$.

[Levc11]³⁹¹: Changed $E_{gx} = 3.267 \text{ eV}$ ³⁶⁰ to $E_g = 3.267 \text{ eV}$.

[Lutz11]⁴¹⁵: Used $\alpha = 6.5 \times 10^4 \text{ eV/K}$ instead of $6.5 \times 10^{-4} \text{ eV/K}$.

[Lutz18]⁴⁴⁹: Used $\alpha = 6.5 \times 10^4 \text{ eV/K}$ instead of $6.5 \times 10^{-4} \text{ eV/K}$.

[Made91]¹²³: Changed E_g ³⁸¹ to E_{gx} .

[Maxi23]³¹³: The value $E_g = 3.23 \text{ eV}$ could not be found in the provided references. We achieved this value only by using the 2H band gap from Persson and Lindefelt¹²⁵ and scaling it with temperature.

[Mcnu04]⁴⁰¹: Stated $\alpha = 3.3 \times 10^{-3} \text{ eV/K}$, which should be $\alpha = 3.3 \times 10^{-4} \text{ eV/K}$.

[Megh18a]⁴⁰³: Changed $E_g = 3.26 \text{ eV}$ ⁴⁰² to $E_g = 3.2 \text{ eV}$.

[Mill00]³⁷⁵: For reasonable results an exponent of -1 had to be added to the term $(\exp(\theta_E/T) - 1)$ in Eq. (2).

[Ozpi04]¹⁸⁵: Changed $E_g = 3.25\text{ eV}$ ⁴³⁸ to $E_g = 3.26\text{ eV}$.

[Pear23]¹³⁵: Changed $E_{gx} = 3.263\text{ eV}$ ⁴¹² to $E_g = 3.26\text{ eV}$.

[Pers97]¹²⁵: The stated value $E_g = 3.29\text{ eV}$ appeared in the referenced publication⁶ only in the context of 2H- and 3C-SiC.

[Pers99]¹²⁶: Changed $E_g = 3.285\text{ eV}$ ²⁵⁶ to 3.29 eV .

[Rayn10]²⁷⁶: Changed E_g ⁴¹² to E_{gx} .

[Resc18]⁴²¹: Changed $E_{gx} = 3.265\text{ eV}$ ⁴³ to $E_g = 3.26\text{ eV}$.

[Resh05]²⁰¹: We could not find the stated value $E_g = 3.26\text{ eV}$ in the referenced publication¹²⁵.

[Scho94]³⁴: We did not find the specified reference [77Pan] from the reference list. The similar reference [75Pan]⁹³⁸ did also not contain the desired values.

[Sole19]²⁰⁰: Changed $E_g = 3.25\text{ eV}$ ¹⁹⁹ to $E_g = 3.2\text{ eV}$.

[Son12]⁶⁹³: We were unable to locate the specified values in the provided reference¹³⁶ but the same values were used by Tamaki *et al.*³²⁴ four years earlier.

[Stef14]¹⁵: In the Lindefelt model the dopants should be N_D^+ for the n-type and N_A^- for the p-type semiconductor. The exponents for A_{nv} and A_{pv} should be $1/4$ instead of $1/3$.

In Table 1 the band gap for the “Vienna Uni.” model is $E_{gx} = 3.265\text{ eV}$ at 0 K ⁴⁸ instead of the stated $E_g = 3.265\text{ eV}$ at 300 K .

In the Slotboom model the logarithmic term in the quadratic root was only applied to the fraction N/N_0 and not to the term $+C$ as well.

The parameters for the Pssler (sic!) model are referenced from Grivickas *et al.*³⁶⁰ and not the specified Pässler³⁶¹. For the latter $E_{gx} = 3.267\text{ eV}$ got changed to $E_g = 3.27\text{ eV}$.

[Tama08a]³²⁴: We could not find the shown values in the provided reference¹³⁶.

[Tann07]⁴¹³: Changed $E_{gx} = 3.263\text{ eV}$ ⁴¹² to $E_g = 3.26\text{ eV}$.

- [Trof98]¹⁰: Changed $E_{gx} = 3.263 \text{ eV}$ ⁵³ to $E_g = 3.265 \text{ eV}$.
- [Uhne15]⁴¹⁴: Changed $E_{gx} = 3.263 \text{ eV}$ ⁴¹² to $E_g = 3.26 \text{ eV}$.
- [Usma14]²⁰⁶: Changed band gap energy E_g from 3.26 eV ³⁶³ to 3.24 eV .
- [Wrig98]¹⁷¹: The second term in the temperature dependent band gap, i.e., $T^2/(T + \beta)$ should be preceded by a minus sign.
- [Yosh18]¹⁴⁸: Changed $E_{gx} = 3.265 \text{ eV}$ ³⁰⁸ to $E_g = 3.26 \text{ eV}$.
- [Zipp11]¹⁶⁹: Changed $E_{gx} = 3.263 \text{ eV}$ ⁴¹² to $E_g = 3.26 \text{ eV}$.

4. Impact Ionization

- [Aktu08]⁵⁷⁵: We were unable to confirm the electron parameters for Model 3. In fact the used values $a_n = 2.5 \times 10^5 \text{ /cm}$ and $E_c^n = 1.84 \times 10^7 \text{ V/cm}$ match very well the impact ionization parameters for holes in 6H-SiC by Raghunathan and Baliga⁵⁶⁹, i.e., $a_p = (2.5 \pm 0.1) \times 10^6 \text{ /cm}$ and $b_p = (1.48 \pm 0.10) \times 10^7 \text{ V/cm}$, if we consider a small typographical error for the latter.
Switched parameters γ_n and γ_p for model 2⁵²⁶.
- [Arva19]⁵⁸²: Turned coefficients parallel to c-axis from Niwa, Suda, and Kimoto²⁵² to perpendicular ones.
- [Ayal04]⁴⁸: Seemingly changed parameter b for the electrons in 6H from $2.58 \times 10^6 \text{ V/cm}$ ¹³⁹ to $2.58 \times 10^7 \text{ V/cm}$. This value presumably then got the default value in simulation tools and got reused¹⁵⁰.
- [Bako97]¹³⁹: Defined $\alpha_\perp = \beta/3.5$, which we assume should be $\alpha/3.5$.
- [Bane21]¹⁵⁵: In Table 1 on page 159 the range of the field for 4H-SiC should be $(10 - 100) \times 10^7 \text{ V/m}$.
- [Bert04]⁴⁶⁵: Changed $\beta_p \perp$ from $2.5 \times 10^7 \text{ V/cm}$ to $1.8 \times 10^7 \text{ V/cm}$.

[Bion12]³³⁰: In Eq. (21) the temperature scaling in the exponent is flawed. Instead of $1 + DT - 300$ it should be $1 + D(T - 300)$. In Eq. (21) B and C should be switched.

We changed m from 2 to 1 and n from 1 to 0 to fit the results shown in the paper.

[Bros12]⁵⁴⁶: The value $b_n = 1.67 \times 10^5 \text{ V/cm}$ leads to unrealistic results. We changed it to $b_n = 1.67 \times 10^7 \text{ V/cm}$.

[Buon12]⁶⁶: Changed $a_n = 2.1 \times 10^7 \text{ /cm}^{514}$ to $a_n = 2.1 \times 10^8 \text{ /cm}$.

[Chea21]⁵³²: a and b were presumably stated in $1/\text{m}$ and MV/m in the paper, although they are denoted as $1/\text{cm}$ and MV/cm .

[Gree12]⁵³¹: Stated that for electrons and $F > 2.5 \text{ MV/cm}$ the parameters proposed by Ng *et al.*⁵²⁶ ($a = 1.98 \times 10^6 \text{ /cm}$, $b = 9.46 \text{ MV/cm}$, $m = 1.42$) were used, but the presented values slightly differ ($a = 1.878 \times 10^6 \text{ /cm}$, $b = 9.134 \text{ MV/cm}$, $m = 1.459$).

The exponent of the Ocuto-Crowell models in Eqs. (8) to (10) have to be pulled inside the squared brackets.

We changed $a_p = 6 \times 10^4 \text{ /cm}$ to $6 \times 10^6 \text{ /cm}$ and $b_p = 1.387 \times 10^6 \text{ V/cm}$ to $1.387 \times 10^7 \text{ V/cm}$ to fit the shown plots.

[Hata09]⁵¹⁶: Changed $a_n = 2.1 \times 10^7 \text{ /cm}^{514}$ to $a_n = 2.1 \times 10^8 \text{ /cm}$ and $a_p = 2.96 \times 10^7 \text{ /cm}^{514}$ to $a_p = 2.96 \times 10^8 \text{ /cm}$.

[Khal12]³⁸⁶: Eqs. (19) and (20) both denote a_n . While the references for the parameters in Eq. (19) are clear^{330,514}, the sources for a and b in Eq. (20) could not be retraced by us.

Changed $a_p = 29.6 \times 10^6 \text{ /cm}^{514}$ to $29 \times 10^6 \text{ /cm}$ and $b_p = 16 \times 10^6 \text{ V/cm}^{514}$ to $14 \times 10^6 \text{ V/cm}$.

[Kimo19]⁶⁸: Changed parallel $a_p = 3.14 \times 10^6 \text{ /cm}$ to $a_p = 3.12 \times 10^6 \text{ /cm}$.

[Kons97]⁴⁹⁴: The factor $3E_p$ of Eq. (40) is not shown for β in the paper. We assume a typographical error as the division sign is visible.

[Loh09]⁵⁶⁴: The exponent c in Eq. (2) has to be pulled inside the exponential function.

We changed $b_p = 8.9 \times 10^6 - 4.95 \times 10^3 T$ to $b_p = 8.9 \times 10^6 + 4.95 \times 10^3 T$ to better match the results in the paper.

- [Megh15]³⁹⁰: Changed parallel $a_p = 3.41 \times 10^8 / \text{cm}$ to $a_p = 2.41 \times 10^8 / \text{cm}$.
- [Nall99]⁴³⁹: Used for the electron and hole impact ionization coefficient the 6H parameters for holes published by Raghunathan and Baliga⁵⁶⁹.
- [Nall00]⁵²²: The values for a and b could not be found in the provided reference⁴³⁹.
- [Niwa15]²⁵²: Once a_p is specified as $3.12 \times 10^6 / \text{cm}$ and once as $3.14 \times 10^6 / \text{cm}$.
- [Pezz13]²⁰⁷: The used values $a_n = 2.5 \times 10^5 / \text{cm}$ and $n = 1.84 \times 10^7 \text{ V/cm}$ match the impact ionization parameters for holes in 6H-SiC by Raghunathan and Baliga⁵⁶⁹, i.e., $a_p = (2.5 \pm 0.1) \times 10^6 / \text{cm}$ and $b_p = (1.48 \pm 0.10) \times 10^7 \text{ V/cm}$, if we consider a small typographical error for the latter. These are the same errors as done by Akturk *et al.*⁵⁷⁵, although no direct connection could be found between these publications.
- [Rayn09]²³: Referred to intermediate results by Konstantinov *et al.*⁴⁹⁴ for a comparison.
- [Rayn10]²⁷⁶: Turned $a_n = 0.408 \times 10^6 / \text{cm}$ ⁵⁴⁶ to $0.41 \times 10^6 / \text{cm}$.
- [Sher00]⁵⁴⁵: Fitted to Konstantinov *et al.*⁴⁹⁴, but only the holes. Interestingly the achieved results are equal to those presented in³⁶⁹, whereat these were based on 6H-SiC measurements.
- [Stef21]²⁴: The hole parameters presented for “Nguyen”⁵²⁸ ($a_p = 4 \times 10^7 / \text{cm}$, $b_p = 1.89 \times 10^7 \text{ V/cm}$) could not be retraced.
The parameter b_p for “Loh Power”⁵²⁵ should be $0.35 \times 10^7 \text{ V/cm}$ instead of $0.035 \times 10^7 \text{ V/cm}$.
 c_n and c_p for entry “Akturk Power” were transferred correctly from the cited publication⁵⁷⁵ but there the values got switched. Thus, it should be $c_n = 1.42$ and $c_p = 1.06$ ⁵²⁶. Consequently, the fitting for the hole impact ionization coefficient is more than one order of magnitude lower than the other models.
The value $a_p = 8.5 \times 10^6 / \text{cm}$ for entry “Raghunathan” could not be found in the provided reference⁵⁶⁹. The only explanation we found was that the authors misinterpreted $(3.5 \pm 0.5) \times 10^6 / \text{cm}$ with $(3.5 \pm 5.0) \times 10^6 / \text{cm}$.

[Stei23]⁵⁶⁸: In Fig. 6 the high temperature plots should refer to 470 K instead of 470 °C for a good fit of the describing model.
 For the fitting to Niwa, Suda, and Kimoto²⁵² we had to change $d_n = -0.72 \times 10^{-3} / \text{K}$ to $d_n = -0.72 \times 10^{-6} / \text{K}$ to achieve reasonable results.

[Trip19]¹⁵⁰: It is safe to assume that the value of b_n is an order of magnitude too high and stems from a 6H-SiC sample (see the analysis of Ayalew⁴⁸ in this section).

[Wang22a]⁵⁷⁹: The used parameters match the values by Loh *et al.*⁵²⁵ with the exception that the exponent m in the Ocuto-Crowell model was not considered. This causes an implicit change of $m = 1.37$ for electrons and $m = 1.09$ to 1.

[Zhao19]⁵³⁰: The proposed $c_p = 6.19 \times 10^{-3} / \text{K}$ and $d_p = 1.15 \times 10^{-3} / \text{K}$ cause β to increase in the range 150 – 300 K. This was not observed with other models.

5. Charge Carrier Recombination

[Adit15]⁴⁸⁵: The referenced lifetime values could not be found in provided references.

[Alba10]²¹⁸: Used n_i instead of n_1 and p_1 in the SRH lifetime model.

[Arva17]¹⁴⁶: The value of $\tau_p = 0.5 \mu\text{s}$ could not be found in the provided reference⁴⁸⁵, where $\tau_p = 0.6 \mu\text{s}$ was proposed. The used $\tau_n = 1 \text{ ns}$ also does not match $\tau_n = 2.5 \mu\text{s}$ in the reference.

[Ayal04]⁴⁸: Used the Auger coefficients from 6H⁷⁹¹.

[Bell11]²⁰⁹: Changed $\tau_n = \tau_p = 15 \text{ ns}$ ²¹⁸ in the bipolar transistor base to $\tau_n = \tau_p = 16 \text{ ns}$.

[Bion12]³³⁰: The expression for n_1 and p_1 in Eq. (18) are flawed. n_i^2 should be n_i and the exponent for n_1 is actually negative.
 Used the sum $C_n + C_p$ ³²⁷ as C_n and C_p .

[Choi05]¹²⁹: The provided Scharfetter parameters could not be found in the provided references⁶.

[Das15]³⁵³: The Auger coefficient C_p was taken from Ruff, Mitlehner, and Helbig³⁶⁹ which is based on Silicon values.

[Gao22a]⁹¹: In the temperature dependent Auger recombination coefficient the first part of the product scales with $T^{-1.5} = T^{-3/2}$ ⁵⁸⁹ but a value of $T^{-2/3}$ was used instead.

[Kaka20]⁷⁹²: For the temperature dependency of the SRH lifetime values determined for Si⁷²⁷ were used.

[Khal12]³⁸⁶: Used the sum $C_n + C_p$ ³²⁷ as C_n and C_p .

[Lech21]¹⁴²: Used 6H values for Auger coefficients⁴⁸.

[Levi01b]²⁹: Changed $B = 5 \times 10^{-12} \text{ cm}^3/\text{s}$ ³²⁷ to $B = 1 \times 10^{-12} \text{ cm}^3/\text{s}$.
Turned $\tau_n = 600 \text{ ns}$ ⁷²⁰ into $\tau_n = \tau_p = 300 \text{ ns}$. Since the measurements were done under high injection levels this might be reasonable.

[Liu21]⁴⁵⁰: Change $\gamma = 0.3$ ²⁰⁶ to $\gamma = 1$.

[Megh15]³⁹⁰: Changed $\tau_p = 12 \text{ ns}$ ³⁹⁴ to $\tau_n = 10 \text{ ns}$.

[Megh18a]⁴⁰³: Referenced a very high value of $N_{\text{ref}} = 1 \times 10^{30} / \text{cm}^3$ ^{139,748}.

[Nall99]⁴³⁹: Proposed value of $\tau_n = \tau_p = 50 \text{ ns}$ could not be found in the stated reference³²⁷.
The temperature dependency is presented in a ambiguous fashion, because it is not clear that the term $(\frac{T}{300} - 1)$ belongs to *Coeff* in the exponential.

[Rao22]²⁰³: The term n_i^2 in the definition of n_1 and p_1 should be n_i .

[Scho94]³⁴: Denoted in Eqs. (5.21) and (5.22) a decrease of the SRH lifetime with increasing temperature, which may go back to an error in the sign of the exponential (is negative, should be positive).

[Usma14]²⁰⁶: Changed the Auger coefficients by one order of magnitude³²⁷ to $C_n = 5 \times 10^{-32} \text{ cm}^6/\text{s}$ and $C_p = 2 \times 10^{-32} \text{ cm}^6/\text{s}$.
In the text a value of the Scharfetter parameter $\alpha = 1.72$ was stated but in the overall parameter listing $\alpha = 5$.

[Tama08]⁷²⁸: Changed the activation energy from $E_{\text{act}} = 0.11 \text{ eV}$ ⁷²² to $E_{\text{act}} = 0.105 \text{ eV}$.

[Zegh20]⁴⁰⁵: The value $C_n = 5 \times 10^{31} \text{ cm}^6/\text{s}$ was provided for the Auger coefficient but it should be $5 \times 10^{-31} \text{ cm}^6/\text{s}$.

[Zhan18]⁵⁶⁶: Unit of Auger coefficients stated as $1/(\text{cm}^3 \text{ s})$ but should be cm^6/s .

6. Incomplete Ionization

[Arva17]¹⁴⁶: Referenced a Nitrogen ionization energy of 71 meV³⁹⁹ but only 81 meV for 6H-SiC was provided.

[Darm19]¹⁹⁷: Equation (18), i.e., $\frac{p}{N_A} = \beta \frac{p^v}{N_A} + (1 - \beta)$ could not be retraced given the expressions $p = p^v + p^i$ (Eq. (14)) and $p^i = (1 - \beta)N_A^0$ (Eq. (16)).

[Dona18]⁸⁰²: We were unable to confirm the used ionization energies for Phosphorous (hexagonal: 55 meV, cubic: 102 meV).
For Nitrogen the ionization energies (hexagonal: 70 meV, cubic: 120 meV) are presumably based on the values by Ikeda, Matsunami, and Tanaka⁹⁵ (hexagonal: 66 meV, cubic: 124 meV).

[Feng04a]²⁰: Changed for Nitrogen the ionization energy on the cubic lattice site from 91.8 meV²⁷¹ to 92 meV and on the hexagonal site from 52.1 meV²⁷¹ to 52 meV.

[Huh06]⁶⁶⁹: Used 6H values⁶⁹⁵ and changed the ionization energy for Boron from 270 meV to 300 meV.

[Ivan05]⁴³⁶: The values for cubic and hexagonal site of Phosphorous were switched. These incorrect results were later copied¹⁴ and implicitly corrected³³.

[Khal12]³⁸⁶: Changed the value of the donor energy level from 67 meV³²⁵ to 650 meV.
The ionized acceptors are denoted as N_D^- instead of N_A^- .

[Kuzn95]³²¹: In the conclusion the cross section of Aluminum was stated as $8 \times 10^{-3} (300/T)^3 \text{ cm}^2$ but the first term should be 8×10^{-13} as noted earlier in the paper.

[Lebe99]³⁹⁹: Changed the ionization energy of Nitrogen on the cubic lattice site from 91.8 meV²⁷¹ to 92 meV and on the hexagonal site from 52.1 meV²⁷¹ to 52 meV.

[Lech21]¹⁴²: The used values for Aluminum seem to go back to Arvinte¹³³ but the parameter α to describe the doping dependency was 1.8×10^{-5} meV cm instead of 2.8×10^{-5} meV cm.

[Levi01]²¹: Changed the ionization energy of Aluminum from 191 meV⁹⁵ to 190 meV and for Boron from 647 meV⁹⁵ to 650 meV.

[Lu21]²⁹¹: Changed the ionization energy of Aluminum from 230 meV³⁹⁹ to 220 meV.

[Maxi23]³¹³: In equations (6a) and (6b), corresponding to Eq. (79), N_C and N_V were added as multiplicative factor to the exponential in the denominator.

[Nipo18]⁸⁰³: Presumably used the ionization energies by Ivanov, Henry, and Janzén⁴³⁶ but changed the value for the hexagonal lattice site from 197.9 meV to 198 meV and the value for the cubic from 201.3 meV to 210 meV.

Changed the ionization energy for Phosphorous on the hexagonal site from 60.7 meV⁴³⁶ to 60 meV.

[Pank14]⁴²⁵: Referenced 90 meV for the ionization energy of the cubic lattice site of Nitrogen from Hagen, Van Kemenade, and Van Der Does De Bye⁴⁵⁵, but there only 90 meV for the hexagonal or 130 meV for the cubic lattice site were proposed.

[Pens93]³¹⁰: Changed the ionization energy of Nitrogen on the cubic lattice site from 91.8 meV²⁷¹ to 91.4 meV and on the hexagonal site from 52.1 meV²⁷¹ to 51.8 meV, which can be explained by the fact that the reference was not yet published when the values were taken.

[Pers05]¹¹⁴: Changed the ionization energy of Nitrogen on the cubic lattice site from 91.8 meV²⁷¹ to 92 meV and on the hexagonal site from 52.1 meV²⁷¹ to 52 meV.

[Rakh20]³¹⁸: Referenced a 6H source⁸⁵³ for the energy levels of Boron, Vanadium and Nitrogen but the values could not be found there.

[Scab11a]³³: In the derivation of Eq. (83) on page 22 an expression for n^{270} was presented that (i) is not required for the calculation and (ii) we were unable to retrace in the original publication. We solely achieved the shown result if we calculated $1/n$ and used in one occasion the wrong parameter.

[Song12]³²⁵: Changed the donor ionization energy from 66 meV³²⁴ to 67 meV and the acceptor one from 191 meV³²⁴ to 19 meV.

[Sozz19]²⁰⁴: Interpreted the maximum ionization energy of Nitrogen on the hexagonal lattice site of 50 meV⁶⁷⁴ as the effective value.

[Tian20]¹⁶: Used the ionization energy 201.3 meV⁴³⁶ of Aluminum on a cubic lattice site as the effective value.

[Yang19]³²⁶: Changed the ionization energy of Nitrogen on a hexagonal lattice site from (61.4 ± 0.5) meV¹¹¹ to an effective value of 61 meV.

[Yosh18]¹⁴⁸: Changed the ionization energy of Aluminum from 191 meV⁹⁵ to 190 meV.

[Zett02]¹⁸²: Changed the ionization energy of Nitrogen on the cubic lattice site from 91.8 meV²⁷¹ to 92 meV and on the hexagonal site from 52.1 meV²⁷¹ to 50 meV.

[Zhan18]⁵⁶⁶: Used in equations (13) and (14), corresponding to Eq. (79), instead of the donor (E_D) and acceptor (E_A) energy level the conduction and valence band energies.

[Zhu08]¹³¹: Changed the ionization energy of Nitrogen on the cubic lattice site from 91.8 meV²⁷¹ to 92 meV and on the hexagonal site from 52.1 meV²⁷¹ to 50 meV.

Changed the ionization energy of Phosphorous on the hexagonal lattice site from 53 meV⁶⁵⁰ to 54 meV.

7. Mobility

[Aktu09]¹⁶⁸: Changed the following electron saturation velocities: $2.12 \times 10^7 \text{ cm/s}$ ⁹²⁹ to $2 \times 10^7 \text{ cm/s}$, $1.58 \times 10^7 \text{ cm/s}$ ⁹²⁹ to $1.6 \times 10^7 \text{ cm/s}$, $2.5 \times 10^7 \text{ cm/s}$ ¹⁶⁶ to $2.4 \times 10^7 \text{ cm/s}$ and $1.83 \times 10^7 \text{ cm/s}$ ¹⁶⁷ to $2 \times 10^7 \text{ cm/s}$.

[Alba10]²¹⁸: Changed μ_{\max} of holes from $124 \text{ cm}^2/(\text{Vs})$ ⁸⁶⁴ to $125 \text{ cm}^2/(\text{Vs})$.

[Arda05]⁸⁹¹: Changed the electron low field mobility from $720 \text{ cm}^2/(\text{Vs})$ ⁴⁴⁵ to $730 \text{ cm}^2/(\text{Vs})$.

[Arva17]¹⁴⁶: Changed γ_{sat} for electrons from -0.44 ¹⁴¹ to 0.44 .

[Arva19]⁵⁸²: Rounded μ_{\min} for holes from $15.9 \text{ cm}^2/(\text{Vs})$ ⁸⁶⁴ to $16 \text{ cm}^2/(\text{Vs})$.

[Ayal04]⁴⁸: Changed μ_{\max} of holes from $124 \text{ cm}^2/(\text{Vs})$ ⁸⁶⁴ to $125 \text{ cm}^2/(\text{Vs})$.

[Bane21]¹⁵⁵: In equation (10), describing the carrier velocity at high fields, the exponent $1/\kappa$ should be only applied to the denominator and not also to the dominator.

[Bela22]⁸⁹⁰: The unit of the saturation velocity is stated as $\text{cm}^2/(\text{Vs})$ instead of cm/s .

[Bell11]²⁰⁹: Changed μ_{\max} of holes from $124 \text{ cm}^2/(\text{Vs})$ ⁸⁶⁴ to $125 \text{ cm}^2/(\text{Vs})$.

[Bhat05]²²⁰: The saturation velocity is stated as $2 \times 10^{17} \text{ cm/s}$ instead of $2 \times 10^7 \text{ cm/s}$.
Only the parameters are shown but not the corresponding equations.
Therefore, it is not possible to uniquely identify the correct values.

[Buon12]⁶⁶: Dismissed the leading μ_{\min} from Eq. (93).
Changed μ_{\max} of electrons from $947 \text{ cm}^2/(\text{Vs})$ ⁸⁶⁴ to $950 \text{ cm}^2/(\text{Vs})$.

[Capa22]⁴²³: Rounded the hole mobility from $118 \text{ cm}^2/(\text{Vs})$ ⁴³ to $120 \text{ cm}^2/(\text{Vs})$.

[Chen22]⁹³: Referenced the electron mobility parallel to the c-axis from¹⁴¹ but there it is actually stated perpendicular to the c-axis.

[Das15]³⁵³: In equation (4), describing the carrier velocity at high fields, the exponent $1/\beta 1$ should be only applied to the denominator and not also to the dominator.

[Elah17]¹⁹⁴: v_{sat} was stated as 2 cm/s . We assume that $2 \times 10^7 \text{ cm/s}$ was intended.

[Gotz93]²⁷¹: Took saturation velocity from literature⁹³⁶, where the investigated material is only specified as α -SiC. So it is not clear whether 4H-SiC was meant.

[Huan98]¹³⁷: Referenced values for β from Ruff, Mitlehner, and Helbig³⁶⁹, who used Silicon values only.

[Joha19]⁴¹⁷: We were unable to locate the stated maximum hole mobility $\mu_{\max} = 20 \text{ cm}^2/(\text{Vs})$ in the specified reference. We assumed a typographical mistake and it should be $120 \text{ cm}^2/(\text{Vs})$ (rounded from $124 \text{ cm}^2/(\text{Vs})$ ⁸⁶⁴).

Changed μ_{\max} of electrons from $947 \text{ cm}^2/(\text{Vs})$ ⁸⁶⁴ to $940 \text{ cm}^2/(\text{Vs})$.

[Josh95]³²³: In the text the value of the saturation velocity is provided in m/s but as unit cm/s was specified.

Changed μ_{\max} of electrons from $947 \text{ cm}^2/(\text{Vs})$ ⁸⁶⁴ to $940 \text{ cm}^2/(\text{Vs})$.

[Kimo97]⁶⁷⁶: Turned $\mu_n = 720 \text{ cm}^2/(\text{Vs})$ ³⁴⁵ to $\mu_n = 724 \text{ cm}^2/(\text{Vs})$.

[Lade00]¹⁴¹: For parameter F of the carrier-carrier scattering the wrong unit was specified. It should be $1/\text{cm}^2$ instead of $\text{cm}^{2/3}$.

[Lang22]⁴³³: In the referenced publication¹³² the electron mobility was denoted as $900 \text{ cm}^2/(\text{Vs})$ not $800 \text{ cm}^2/(\text{Vs})$.

[Lech21]¹⁴²: We were unable to locate the used mobility values in the stated reference⁴⁸.

[Liu21]⁴⁵⁰: Changed γ_{\max} for electrons from -2.9 ³²⁴ to -2.8 .

Turned μ_{\max} for holes from $124 \text{ cm}^2/(\text{Vs})$ ³²⁴ to $125 \text{ cm}^2/(\text{Vs})$ and the reference doping concentration N_{ref} from $1.76 \times 10^{19} / \text{cm}^3$ ³²⁴ to $1.76 \times 10^{17} / \text{cm}^3$.

Used as hole saturation velocity the electron saturation velocity⁹⁰⁷.

In the high field equations in Table 1 (cp. Eq. (103)) β is defined over the whole sum in the denominator and the exponent outside the brackets should be $-1/\beta$ instead of $-\beta$.

[Lv04]⁸⁵⁷: We were not able to recreate the high field velocity curves shown in Fig. 2 of the paper with the presented parameters.

[Mcnu04]⁴⁰¹: Turned μ_{\max} for holes from $108.1 \text{ cm}^2/(\text{Vs})$ ¹³⁹ to $108.9 \text{ cm}^2/(\text{Vs})$.

[Megh18]⁴⁵⁷: Turned μ_{\max} for holes from $124 \text{ cm}^2/(\text{Vs})$ ⁴⁰² to $125 \text{ cm}^2/(\text{Vs})$.

[Neud01]¹²⁸: We could not find the stated electron mobility parallel to the c-axis ($800 \text{ cm}^2/(\text{V s})$) in the mentioned reference⁸⁵⁵.

[Ostl24]¹⁹⁵: v_{sat} was stated as 2 cm/s . We assumed that $2 \times 10^7 \text{ cm/s}$ was intended.

[Palm97]⁵⁶⁰: Changed μ_{max} of electrons from $947 \text{ cm}^2/(\text{V s})$ ⁸⁶⁴ to $950 \text{ cm}^2/(\text{V s})$.

[Pere06]²³⁸: Changed $\gamma_{\text{max}} = -2.4$ ³⁸ for electrons to -2 .

[Pezz08]¹³⁴: The unit of the velocity saturation was stated in cm^2/s but should be cm/s .

[Powe02]⁶²: The unit of the saturation velocity was stated in m/s but the value indicates cm/s .

[Rakh20]³¹⁸: Changed μ_{max} of electrons from $947 \text{ cm}^2/(\text{V s})$ ¹⁴¹ to $950 \text{ cm}^2/(\text{V s})$.
Changed μ_{max} of holes from $124 \text{ cm}^2/(\text{V s})$ ⁸⁶⁴ to $120 \text{ cm}^2/(\text{V s})$.
The velocity saturation for holes was extracted from¹⁴¹ but there this value denotes the electron saturation velocity.

[Sand11]²⁰⁸: It is reasonable to assume that in Table II the columns for 4H and 6H got exchanged, especially because of the deviating band gap values.

[Shah98]²⁴⁷: References Schaffer *et al.*⁸⁶⁴ regarding the hole mobility but all parameters are different.

[Shar15]⁵⁶⁵: In the Caughey-Thomas equation (cp. Eq. (93)) μ_{min} also shows up in the denominator.

[Sole19]²⁰⁰: We were unable to locate the presented values in the provided reference¹⁹⁹.

[Stef14]¹⁵: See detailed analysis in Section X.

[Tama08a]³²⁴: The charge carrier mobility was referenced from Ruff, Mitlehner, and Helbig³⁶⁹ but the values fit the models by Schaffer *et al.*⁸⁶⁴ resp. Roschke and Schwierz³⁸ better.

[Tian20]¹⁶: See detailed analysis in Section X.

[Tila07]³¹⁵: We could not find $\gamma_{\text{max}} = 2.4$ in the provided reference¹⁶⁶. Also the value contradicts many others.

[Trip19]¹⁵⁰: Corrected the wrong value of $\delta = -0.61$ ¹⁵ to $\delta = 0.61$.

The value of $N_{\text{ref}} = 1 \times 10^{16} / \text{cm}^3$ could not be found in the reference¹⁵.

Overall, using this parameter set is risky, as pointed out in Section X.

[Vasc19]¹⁷⁶: In the overview table 2 the minimum instead of the maximum mobility was used from Arvanitopoulos *et al.*⁵⁸². The value for Contreras *et al.*⁸⁹⁹ should be $45.2 \text{ cm}^2 / (\text{Vs})$ instead of $37 \text{ cm}^2 / (\text{Vs})$. For Stefanakis and Zekentes¹⁵ a value was stated $116.1 \text{ cm}^2 / (\text{Vs})$, but the authors used $\mu_{\text{max}} = 114 \text{ cm}^2 / (\text{Vs})$.

[Wang98]⁹²⁵: Changed $\gamma_{\text{max}} = -2.15$ ⁸⁶⁴ to $\gamma_{\text{max}} = -2$.

[Wang99]³⁸⁹: In the description of the high-field mobility (Eq. (4)) only the saturation velocity was squared instead of the whole fraction $F\mu_n/v_{\text{sat}}$ (cp. Eq. (103)).
Changed $\gamma_{\text{max}} = -2.15$ ⁸⁶⁴ to $\gamma_{\text{max}} = -2$.

[Wrig98]¹⁷¹: Used for carrier-carrier scattering an equation that was proposed to describe the impurity scattering in Silicon by Dorkel and Leturcq⁸⁸².

[Zegh19]⁴⁰⁴: Changed μ_{max} of holes from $124 \text{ cm}^2 / (\text{Vs})$ ⁸⁶⁴ to $125 \text{ cm}^2 / (\text{Vs})$.

[Zegh20]⁴⁰⁵: All temperature dependency parameters γ are positive, which leads to $\mu(0) = 0$ and a continuously increasing mobility with temperature.

[Zhan18]⁵⁶⁶: In Eq. (2) we presumed that C_S should be replaced by T and N_i by T_0 .
In Eq. (4) β is defined by using β .

[Zhou16]⁹²⁷: Rounded $\delta = 0.76$ ³⁸ to 1.

REFERENCES

¹I. N. Jiya and R. Gouws, *Micromachines* **11**, 1116 (2020).

²M. De Napoli, *Frontiers in Physics* **10**, 898833 (2022).

³F. Bechstedt, P. Käckell, A. Zywietz, K. Karch, B. Adolph, K. Tenelsen, and J. Furthmüller, *physica status solidi (b)* **202**, 35 (1997).

⁴F. Bechstedt, *Materials Science Forum* **264–268**, 265 (1998).

⁵W. M. Chen, N. T. Son, E. Janzén, D. M. Hofmann, and B. K. Meyer, *physica status solidi (a)* **162**, 79 (1997).

⁶G. L. Harris and Inspec, eds., *Properties of Silicon Carbide*, EMIS Datareviews Series No. 13 (INSPEC, the Inst. of Electrical Engineers, London, 1995).

⁷G. Pensl, F. Ciobanu, T. Frank, M. Krieger, S. Reshanov, F. Schmid, and M. Weidner, *International Journal of High Speed Electronics and Systems* **15**, 705 (2005).

⁸M. Schadt, *Transporteigenschaften von Elektronen Und Löchern in Siliciumkarbid*, Ph.D. thesis, FriedrichAlexander-Universität (1997).

⁹Y. M. Tairov and Y. A. Vodakov, in *Electroluminescence*, Vol. 17, edited by J. I. Pankove (Springer Berlin Heidelberg, Berlin, Heidelberg, 1977) pp. 31–61.

¹⁰T. Troffer, *Elektrische und optische Charakterisierung Bauelementrelevanter Dotierstoffe in Siliciumkarbid*, Ph.D. thesis, FriedrichAlexander-Universität (1998).

¹¹K. Takahashi, A. Yoshikawa, and A. Sandhu, eds., *Wide Bandgap Semiconductors* (Springer Berlin Heidelberg, Berlin, Heidelberg, 2007).

¹²M. Shur, S. L. Rumyantsev, and M. E. Levinshtein, eds., *SiC Materials and Devices*, Selected Topics in Electronics and Systems No. v. 40 (World Scientific, New Jersey ; London, 2006).

¹³R. P. Devaty and W. J. Choyke, *physica status solidi (a)* **162**, 5 (1997).

¹⁴E. Janzén, A. Gali, A. Henry, I. G. Ivanov, B. Magnusson, and N. T. Son, in *Defects in Microelectronic Materials and Devices* (CRC Press, 2008) pp. 615–669.

¹⁵D. Stefanakis and K. Zekentes, *Microelectronic Engineering* **116**, 65 (2014).

¹⁶K. Tian, J. Xia, K. Elgammal, A. Schöner, W. Kaplan, R. Karhu, J. Ul-Hassan, and A. Hallén, *Materials Science in Semiconductor Processing* **115**, 105097 (2020).

¹⁷P. G. Neudeck, in *Extreme Environment Electronics* (CRC Press, Taylor & Francis Group, 2013) pp. 225–232.

¹⁸F. C. Beyer, *Deep Levels in SiC*, Ph.D. thesis, Linköping University (2011).

¹⁹M. Neuberger, *Handbook of Electronic Materials* (Springer US, Boston, MA, 1971).

²⁰Z. C. Feng and J. H. Zhao, eds., *Silicon Carbide: Materials, Processing, and Devices*, Opto-electronic Properties of Semiconductors and Superlattices No. v. 20 (Taylor & Francis, New York, 2004).

²¹M. E. Levinshtein, S. L. Rumyantsev, and M. Shur, eds., *Properties of Advanced Semiconductor Materials: GaN, AlN, InN, BN, SiC, SiGe* (Wiley, New York, 2001).

²²I. Neila Inglesias, “APPLYING NUMERICAL SIMULATION TO MODELS SiC SEMICONDUCTOR DEVICES,” (2012).

²³C. Raynaud, D.-M. Nguyen, N. Dheilly, D. Tournier, P. Brosselard, M. Lazar, and D. Planson, *physica status solidi (a)* **206**, 2273 (2009).

²⁴D. Stefanakis, N. Makris, K. Zekentes, and D. Tassis, *IEEE Transactions on Electron Devices* **68**, 2582 (2021).

²⁵V. I. Sankin, *Semiconductors* **36**, 717 (2002).

²⁶P. B. Klein, *physica status solidi (a)* **206**, 2257 (2009).

²⁷M. J. Marinella, D. K. Schroder, G. Chung, M. J. Loboda, T. Isaacs-Smith, and J. R. Williams, *IEEE Transactions on Electron Devices* **57**, 1910 (2010).

²⁸R. Wang, Y. Huang, D. Yang, and X. Pi, *Applied Physics Letters* **122**, 180501 (2023).

²⁹M. E. Levenshtein, T. T. Mnatsakanov, P. A. Ivanov, A. K. Agarwal, J. W. Palmour, S. L. Rumyantsev, A. G. Tandoev, and S. N. Yurkov, *Solid-State Electronics* **45**, 453 (2001).

³⁰V. Heera, D. Panknin, and W. Skorupa, *Applied Surface Science* **184**, 307 (2001).

³¹J. M. Bluet, J. Pernot, J. Camassel, S. Contreras, J. L. Robert, J. F. Michaud, and T. Billon, *Journal of Applied Physics* **88**, 1971 (2000).

³²I. G. Atabaev, Kh. N. Juraev, and M. U. Hajiev, *Journal of Spectroscopy* **2018**, 1 (2018).

³³R. Scaburri, *The Incomplete Ionization of Substitutional Dopants in Silicon Carbide*, Ph.D. thesis, Università di Bologna, Bologna (2011).

³⁴A. Schöner, *Elektrische Charakterisierung von Flächen Und Tiefen Störstellen in 4H-, 6H- Und 15R-Siliziumkarbid*, Ph.D. thesis, FriedrichAlexander-Universität (1994).

³⁵S. Adachi, *Properties of Group-IV, III-V and II-VI Semiconductors* (John Wiley, Chichester, England, 2005).

³⁶I. Institute, “Silicon Carbide,” <http://www.ioffe.ru/SVA/NSM/Semicond/SiC/index.html> (2023).

³⁷A. A. Lebedev, *Radiation Effects in Silicon Carbide*, Materials Research Foundations No. volume 6 (2017) (Materials Research Forum LLC, Millersville, PA, USA, 2017).

³⁸M. Roschke and F. Schwierz, *IEEE Transactions on Electron Devices* **48**, 1442 (2001).

³⁹J. Burin, “Data of 4H SiC TCAD Parameter Review,” https://gitlab.com/dd-hephy/HiBPM/review_4HSiC (2025).

⁴⁰K. Hess, *Monte Carlo Device Simulation: Full Band and Beyond* (Springer US, Boston, MA, 1991).

⁴¹P. Friedrichs, T. Kimoto, L. Ley, and G. Pensl, eds., *Silicon Carbide: Volume 1: Growth, Defects, and Novel Applications*, 1st ed. (Wiley, 2009).

⁴²J. J. Berzelius, *Annalen der Physik* **77**, 169 (1824).

⁴³T. Kimoto and J. A. Cooper, *Fundamentals of Silicon Carbide Technology: Growth, Characterization, Devices, and Applications*, 1st ed. (Wiley, 2014).

⁴⁴J. Y. Tsao, S. Chowdhury, M. A. Hollis, D. Jena, N. M. Johnson, K. A. Jones, R. J. Kaplar, S. Rajan, C. G. Van De Walle, E. Bellotti, C. L. Chua, R. Collazo, M. E. Coltrin, J. A. Cooper, K. R. Evans, S. Graham, T. A. Grotjohn, E. R. Heller, M. Higashiwaki, M. S. Islam, P. W. Juodawlkis, M. A. Khan, A. D. Koehler, J. H. Leach, U. K. Mishra, R. J. Nemanich, R. C. N. Pilawa-Podgurski, J. B. Shealy, Z. Sitar, M. J. Tadjer, A. F. Witulski, M. Wraback, and J. A. Simmons, *Advanced Electronic Materials* **4**, 1600501 (2018).

⁴⁵Z. C. Feng, ed., *Handbook of Silicon Carbide Materials and Devices*, first edition ed., Series in Materials Science & Engineering (CRC Press, Boca Raton, 2023).

⁴⁶V. Švárna and M. Frivaldský, in *2024 ELEKTRO (ELEKTRO)* (IEEE, Zakopane, Poland, 2024) pp. 1–5.

⁴⁷E. G. Acheson, British Patent: 17911 (1982).

⁴⁸T. Ayalew, *SiC Semiconductor Devices Technology, Modeling, and Simulation*, Ph.D. thesis, TU Wien (2004).

⁴⁹H. J. Round, in *Semiconductor Devices: Pioneering Papers* (WORLD SCIENTIFIC, 1907) pp. 879–879.

⁵⁰H. Moissan, in *Les Comptes Rendus de l'Académie Des Sciences* (1905) pp. 405–406.

⁵¹A. Lely, *Darstellung von Einkristallen von Siliciumcarbid Und Beherrschung von Art Und Menge Der Eingebackten Verunreinigungen*, Laboratoria N.V. Philips' Gloeilampenfabrieken (N.V. Philips' Gloeilampenfabrieken, 1955).

⁵²A. Lely, United States Patent: 2854364 (1958).

⁵³W. Choyke, in *Silicon Carbide–1968* (Elsevier, 1969) pp. S141–S152.

⁵⁴M. Di Paolo Emilio, ed., *SiC Technology: Materials, Manufacturing, Devices and Design for Power Conversion* (Springer Nature Switzerland, Cham, 2024).

⁵⁵J. O'Connor, J. Smiltens, and A. F. C. R. L. U. S. . E. R. Directorate, *Silicon Carbide, a High Temperature Semiconductor: Proceedings*, Proceedings of the Conference on Silicon Carbide, Boston, Mass. April 2-3, 1959 (Symposium Publications Division, Pergamon Press, 1960).

⁵⁶R. C. Marshall, J. W. Faust, C. E. Ryan, A. F. C. R. L. (U.S.), and University of South Carolina, eds., *Silicon Carbide–1973: Proceedings*, 1st ed. (University of South Carolina Press, Columbia, 1974).

⁵⁷J. A. Powell, P. Pirouz, and W. J. Choyke, in *Semiconductor Interfaces, Microstructures and Devices : Properties and Applications* (Institute of Physics Publishing, Bristol, 1993) pp. 257–293.

⁵⁸Yu.M. Tairov and V. Tsvetkov, *Journal of Crystal Growth* **43**, 209 (1978).

⁵⁹Yu.M. Tairov and V. Tsvetkov, *Journal of Crystal Growth* **52**, 146 (1981).

⁶⁰D. Barrett, R. Seidensticker, W. Gaida, R. Hopkins, and W. Choyke, *Journal of Crystal Growth* **109**, 17 (1991).

⁶¹Davis, R. F. and Carter, C. H. and Hunter, C. E., United States Patent: RE34861 (1995).

⁶²A. Powell and L. Rowland, *Proceedings of the IEEE* **90**, 942 (2002).

⁶³F. Nava, G. Bertuccio, A. Cavallini, and E. Vittone, *Measurement Science and Technology* **19**, 102001 (2008).

⁶⁴G. R. Fisher and P. Barnes, *Philosophical Magazine B* **61**, 217 (1990).

⁶⁵P. Käckell, *Siliziumkarbid - Strukturelle und elektronische Eigenschaften verschiedener Polytypen*, Ph.D. thesis, Friedrich-Schiller-Universität Jena (1996).

⁶⁶B. Buono, *Simulation and Characterization of Silicon Carbide Power Bipolar Junction Transistors*, Ph.D. thesis, KTH Royal Institute of Technology (2012).

⁶⁷A. R. West, *Basic Solid State Chemistry*, second ed. repr ed. (Wiley, Chichester Weinheim, 2012).

⁶⁸T. Kimoto, in *Wide Bandgap Semiconductor Power Devices* (Elsevier, 2019) pp. 21–42.

⁶⁹R. Ishikawa, H. Tanaka, M. Kaneko, and T. Kimoto, *physica status solidi (b)* **260**, 2300275 (2023).

⁷⁰H. Tanaka, S. Asada, T. Kimoto, and J. Suda, *Journal of Applied Physics* **123**, 245704 (2018).

⁷¹X. Wang, J. Zhao, Z. Xu, F. Djurabekova, M. Rommel, Y. Song, and F. Fang, *Nanotechnology and Precision Engineering* **3**, 211 (2020).

⁷²E. Bellotti, *Advanced Modeling of Wide Band Gap Semiconductor Materials and Devices*, Ph.D. thesis, Georgia Institute of Technology (1999).

⁷³V. Komarov, S. Wang, and J. Tang, in *Encyclopedia of RF and Microwave Engineering*, edited by K. Chang (Wiley, 2005) 1st ed.

⁷⁴S. M. Sze and M. K. Lee, *Semiconductor Devices, Physics and Technology*, 3rd ed. (Wiley, Hoboken, N.J, 2012).

⁷⁵M. Naftaly, J. F. Molloy, B. Magnusson, Y. M. Andreev, and G. V. Lanskii, *Optics Express* **24**, 2590 (2016).

⁷⁶A. T. Tarekegne, B. Zhou, K. Kaltenecker, K. Iwaszczuk, S. Clark, and P. U. Jepsen, *Optics Express* **27**, 3618 (2019).

⁷⁷L. Li, S. Reyes, M. J. Asadi, X. Wang, G. Fabi, E. Ozdemir, W. Wu, P. Fay, and J. C. M. Hwang, in *2023 100th ARFTG Microwave Measurement Conference (ARFTG)* (IEEE, Las Vegas, NV, USA, 2023) pp. 1–4.

⁷⁸J. G. Hartnett, D. Mouneyrac, J. Krupka, J.-M. Le Floch, M. E. Tobar, and D. Cros, *Journal of Applied Physics* **109**, 064107 (2011).

⁷⁹J. Olivares, M. DeMiguel-Ramos, E. Iborra, M. Clement, T. Mirea, M. Moreira, and I. Katardiev, in *2013 Joint European Frequency and Time Forum & International Frequency Control Symposium (EFTF/IFC)* (IEEE, Prague, Czech Republic, 2013) pp. 118–121.

⁸⁰W. Ching, Y.-N. Xu, P. Rulis, and L. Ouyang, *Materials Science and Engineering: A* **422**, 147 (2006).

⁸¹L. Patrick and W. J. Choyke, *Physical Review B* **2**, 2255 (1970).

⁸²R. H. Lyddane, R. G. Sachs, and E. Teller, *Physical Review* **59**, 673 (1941).

⁸³K. Karch, F. Bechstedt, P. Pavone, and D. Strauch, *Physical Review B* **53**, 13400 (1996).

⁸⁴G. Wellenhofer, K. Karch, P. Pavone, U. Rössler, and D. Strauch, *Physical Review B* **53**, 6071 (1996).

⁸⁵B. Adolph, K. Tenelsen, V. I. Gavrilenko, and F. Bechstedt, *Physical Review B* **55**, 1422 (1997).

⁸⁶R. Ahuja, A. Ferreira Da Silva, C. Persson, J. M. Osorio-Guillén, I. Pepe, K. Järrendahl, O. P. A. Lindquist, N. V. Edwards, Q. Wahab, and B. Johansson, *Journal of Applied Physics* **91**, 2099 (2002).

⁸⁷X. Peng-Shou, X. Chang-Kun, P. Hai-Bin, and X. Fa-Qiang, *Chinese Physics* **13**, 2126 (2004).

⁸⁸J. Coutinho, V. J. B. Torres, K. Demmouche, and S. Öberg, *Physical Review B* **96**, 174105 (2017).

⁸⁹I. G. Ivanov, A. Stelmach, M. Kleverman, and E. Janzén, *Physical Review B* **73**, 045205 (2006).

⁹⁰C. R. Jones, J. Dutta, G. Yu, and Y. Gao, *Journal of Infrared, Millimeter, and Terahertz Waves* **32**, 838 (2011).

⁹¹M.-m. Gao, L.-y. Fan, X.-y. Gong, J.-l. You, and Z.-z. Chen, *Journal of Applied Physics* **132**, 135702 (2022).

⁹²S. Ninomiya and S. Adachi, *Japanese Journal of Applied Physics* **33**, 2479 (1994).

⁹³L. Cheng, J.-Y. Yang, and W. Zheng, *ACS Applied Electronic Materials* **4**, 4140 (2022).

⁹⁴M. K. Mainali, P. Dulal, B. Shrestha, E. Amonette, A. Shan, and N. J. Podraza, *Surface Science Spectra* **31**, 026003 (2024).

⁹⁵M. Ikeda, H. Matsunami, and T. Tanaka, *Physical Review B* **22**, 2842 (1980).

⁹⁶H. Harima, S.-i. Nakashima, and T. Uemura, *Journal of Applied Physics* **78**, 1996 (1995).

⁹⁷Q. Yang, Q. Liu, W. Xu, D. Zhou, F. Ren, R. Zhang, Y. Zheng, and H. Lu, *Solid-State Electronics* **187**, 108196 (2022).

⁹⁸J. M. Dutta, G. Yu, and C. R. Jones, in *2006 Joint 31st International Conference on Infrared Millimeter Waves and 14th International Conference on Terahertz Electronics* (IEEE, Shanghai, China, 2006) pp. 411–411.

⁹⁹S. Chen, M. Afsar, and D. Sakdatorn, *IEEE Transactions on Instrumentation and Measurement* **57**, 706 (2008).

¹⁰⁰L. Li, S. Reyes, M. J. Asadi, P. Fay, and J. C. M. Hwang, *Applied Physics Letters* **123**, 012105 (2023).

¹⁰¹T. Li, L. Li, X. Wang, J. C. M. Hwang, S. Yanagimoto, and Y. Yanagimoto, *IEEE Journal of Microwaves* , 1 (2024).

¹⁰²M. Afsar, Shu Chen, Yong Wang, and D. Sakdatorn, in *2005 IEEE Instrumentation and Measurement Technology Conference Proceedings*, Vol. 3 (IEEE, Ottawa, ON, Canada, 2005) pp. 1975–1978.

¹⁰³Y. Yanagimoto, S. Yanagimoto, T. Li, and J. C. M. Hwang, in *2024 103rd ARFTG Microwave Measurement Conference (ARFTG)* (IEEE, Washington, DC, USA, 2024) pp. 1–4.

¹⁰⁴A. Schöner, in *Silicon Carbide*, edited by W. J. Choyke, H. Matsunami, and G. Pensl (Springer Berlin Heidelberg, Berlin, Heidelberg, 2004) pp. 229–250.

¹⁰⁵I. Polaert, N. Benamara, J. Tao, T.-H. Vuong, M. Ferrato, and L. Estel, *Chemical Engineering and Processing: Process Intensification* **122**, 339 (2017).

¹⁰⁶D. Hofman, J. Lely, and J. Volger, *Physica* **23**, 236 (1957).

¹⁰⁷A. Agarwal, S.-H. Ryu, and J. Palmour, in *Silicon Carbide*, edited by W. J. Choyke, H. Matsunami, and G. Pensl (Springer Berlin Heidelberg, Berlin, Heidelberg, 2004) pp. 785–811.

¹⁰⁸T. A. Baeraky, *Egypt. J. Sol.* **25**, 263 (2002).

¹⁰⁹H.-J. Yang, J. Yuan, Y. Li, Z.-L. Hou, H.-B. Jin, X.-Y. Fang, and M.-S. Cao, *Solid State Communications* **163**, 1 (2013).

¹¹⁰I. G. Ivanov, B. Magnusson, and E. Janzén, *Physical Review B* **67**, 165211 (2003).

¹¹¹I. G. Ivanov, B. Magnusson, and E. Janzén, *Physical Review B* **67**, 165212 (2003).

¹¹²D. Bimberg, ed., *Numerical data and functional relationships in science and technology. Teilbd. a: Gruppe 3: Kristall- und Festkörperphysik = Group 3: @Crystal and solid state physics Bd. 17. Halbleiter Physik der Elemente der IV. Gruppe und der III - V Verbindungen*, Vol. 17 (Springer, Berlin Heidelberg, 1982).

¹¹³J. Chen, Z. H. Levine, and J. W. Wilkins, *Physical Review B* **50**, 11514 (1994).

¹¹⁴C. Persson and A. Ferreira Da Silva, in *Optoelectronic Devices: III Nitrides* (Elsevier, 2005) pp. 479–559.

¹¹⁵N. W. Thibault, American Mineralogist **29**, 327 (1944), <https://pubs.geoscienceworld.org/msa/ammin/article-pdf/29/9-10/327/4243453/am-1944-327.pdf>.

¹¹⁶P. T. B. Shaffer, *Applied Optics* **10**, 1034 (1971).

¹¹⁷U. Lindefelt, *Journal of Applied Physics* **84**, 2628 (1998).

¹¹⁸J. Pernot, W. Zawadzki, S. Contreras, J. L. Robert, E. Neyret, and L. Di Cioccio, *Journal of Applied Physics* **90**, 1869 (2001).

¹¹⁹J. Pernot, S. Contreras, and J. Camassel, *Journal of Applied Physics* **98**, 023706 (2005).

¹²⁰A. Koizumi, J. Suda, and T. Kimoto, *Journal of Applied Physics* **106**, 013716 (2009).

¹²¹S. Zollner, J. G. Chen, E. Duda, T. Wetteroth, S. R. Wilson, and J. N. Hilfiker, *Journal of Applied Physics* **85**, 8353 (1999).

¹²²W. Choyke and Edward. D. Palik, in *Handbook of Optical Constants of Solids* (Elsevier, 1997) pp. 587–595.

¹²³O. Madelung and R. Poerschke, eds., *Semiconductors: Group IV Elements and III-V Compounds*, Data in Science and Technology (Springer Berlin Heidelberg, Berlin, Heidelberg, 1991).

¹²⁴B. Wenzien, P. Käckell, F. Bechstedt, and G. Cappellini, *Physical Review B* **52**, 10897 (1995).

¹²⁵C. Persson and U. Lindefelt, *Journal of Applied Physics* **82**, 5496 (1997).

¹²⁶C. Persson, U. Lindefelt, and B. E. Sernelius, *Journal of Applied Physics* **86**, 4419 (1999).

¹²⁷N. T. Son, C. Persson, U. Lindefelt, W. M. Chen, B. K. Meyer, D. M. Hofmann, and E. Janzén, in *Silicon Carbide*, edited by W. J. Choyke, H. Matsunami, and G. Pensl (Springer Berlin Heidelberg, Berlin, Heidelberg, 2004) pp. 437–460.

¹²⁸P. Neudeck, in *Encyclopedia of Materials: Science and Technology* (Elsevier, 2001) pp. 8508–8519.

¹²⁹Y. Choi, H.-Y. Cha, L. Eastman, and M. Spencer, *IEEE Transactions on Electron Devices* **52**, 1940 (2005).

¹³⁰P. G. Neudeck (CRC Press, 2006).

¹³¹X. Zhu, *ALTERNATIVE GROWTH AND INTERFACE PASSIVATION TECHNIQUES FOR SiO₂ ON 4H-SiC*, Ph.D. thesis, Auburn University (2008).

¹³²M. B. Wijesundara and R. Azevedo, *Silicon Carbide Microsystems for Harsh Environments*, MEMS Reference Shelf, Vol. 22 (Springer New York, New York, NY, 2011).

¹³³I.-R. Arvinte, *Investigation of Dopant Incorporation in Silicon Carbide Epilayers Grown by Chemical Vapor Deposition*, Ph.D. thesis, Universite Cote d'Azur (2017).

¹³⁴F. Pezzimenti, F. G. Della Corte, and R. Nipoti, *Microelectronics Journal* **39**, 1594 (2008).

¹³⁵S. J. Pearton, X. Xia, F. Ren, M. A. J. Rasel, S. Stepanoff, N. Al-Mamun, A. Haque, and D. E. Wolfe, *Journal of Vacuum Science & Technology B* **41**, 030802 (2023).

¹³⁶J. Casady and R. Johnson, *Solid-State Electronics* **39**, 1409 (1996).

¹³⁷M. Huang, N. Goldsman, C.-H. Chang, I. Mayergoyz, J. M. McGarrity, and D. Woolard, *Journal of Applied Physics* **84**, 2065 (1998).

¹³⁸O. Madelung, ed., *Semiconductors — Basic Data* (Springer Berlin Heidelberg, Berlin, Heidelberg, 1996).

¹³⁹M. Bakowski, U. Gustafsson, and U. Lindefelt, *physica status solidi (a)* **162**, 421 (1997).

¹⁴⁰T. Egilsson, J. P. Bergman, I. G. Ivanov, A. Henry, and E. Janzén, *Physical Review B* **59**, 1956 (1999).

¹⁴¹M. Lades, *Modeling and Simulation of Wide Bandgap Semiconductor Devices: 4H/6H-SiC*, Ph.D. thesis, Technische Universität München (2000).

¹⁴²B. Lechner, *Behaviour of 4H-SiC Power Semiconductor Devices under Extreme Operating Conditions*, Ph.D. thesis, Technische Universität München (2021).

¹⁴³N. Arpatzhanis, A. Tsormpatzoglou, C. A. Dimitriadis, K. Zekentes, N. Camara, and M. Godlewski, *physica status solidi (a)* **203**, 2551 (2006).

¹⁴⁴T. Hatakeyama, K. Fukuda, and H. Okumura, *IEEE Transactions on Electron Devices* **60**, 613 (2013).

¹⁴⁵A. Naugarhiya, P. Wakhradkar, P. N. Kondekar, G. C. Patil, and R. M. Patrikar, *Journal of Computational Electronics* **16**, 190 (2017).

¹⁴⁶A. Arvanitopoulos, N. Lophitis, S. Perkins, K. N. Gyftakis, M. Belanche Guadas, and M. Antoniou, in *2017 IEEE 11th International Symposium on Diagnostics for Electrical Machines*,

Power Electronics and Drives (SDEMPED) (IEEE, Tinos, Greece, 2017) pp. 565–571.

¹⁴⁷R. Choudhary, M. Mehta, R. Singh Shekhawat, S. Singh, and D. Singh, *Materials Today: Proceedings* **46**, 5889 (2021).

¹⁴⁸H. Yoshioka and K. Hirata, *AIP Advances* **8**, 045217 (2018).

¹⁴⁹C. Miccoli and F. Iucolano, *Materials Science in Semiconductor Processing* **97**, 40 (2019).

¹⁵⁰S. Tripathi, C. Upadhyay, C. Nagaraj, A. Venkatesan, and K. Devan, *Nuclear Instruments and Methods in Physics Research Section A: Accelerators, Spectrometers, Detectors and Associated Equipment* **916**, 246 (2019).

¹⁵¹W. M. Klahold, W. J. Choyke, and R. P. Devaty, *Physical Review B* **102**, 205203 (2020).

¹⁵²A. Kovalchuk, J. Wozny, Z. Lisik, J. Podgorski, L. Ruta, A. Kubiak, and A. Boiadzhian, *Journal of Physics: Conference Series* **1534**, 012006 (2020).

¹⁵³B. Zaťko, L. Hrubčín, A. Šagátová, J. Osvald, P. Boháček, E. Kováčová, Y. Halahovets, S. V. Rozov, and V. Sandukovskij, *Applied Surface Science* **536**, 147801 (2021).

¹⁵⁴A. Acharyya, *Applied Physics A* **123**, 629 (2017).

¹⁵⁵S. Banerjee, in *Advances in Terahertz Technology and Its Applications*, edited by S. Das, N. Anvesh Kumar, J. Dutta, and A. Biswas (Springer Singapore, Singapore, 2021) pp. 153–172.

¹⁵⁶H. Kim, *Transactions on Electrical and Electronic Materials* **25**, 141 (2024).

¹⁵⁷M. Bhatnagar and B. Baliga, *IEEE Transactions on Electron Devices* **40**, 645 (1993).

¹⁵⁸C. Codreanu, M. Avram, E. Carbunescu, and E. Iliescu, *Materials Science in Semiconductor Processing* **3**, 137 (2000).

¹⁵⁹T. Chow and R. Tyagi, in *[1993] Proceedings of the 5th International Symposium on Power Semiconductor Devices and ICs* (IEEE, Monterey, CA, USA, 1993) pp. 84–88.

¹⁶⁰C. Weitzel, J. Palmour, C. Carter, K. Moore, K. Nordquist, S. Allen, C. Thero, and M. Bhatnagar, *IEEE Transactions on Electron Devices* **43**, 1732 (1996).

¹⁶¹H. Morkoç, S. Strite, G. B. Gao, M. E. Lin, B. Sverdlov, and M. Burns, *Journal of Applied Physics* **76**, 1363 (1994).

¹⁶²A. Burk, M. O'Loughlin, R. Siergiej, A. Agarwal, S. Sriram, R. Clarke, M. MacMillan, V. Balakrishna, and C. Brandt, *Solid-State Electronics* **43**, 1459 (1999).

¹⁶³H. Harima, T. Hosoda, and S. Nakashima, *Materials Science Forum* **264–268**, 449 (1998).

¹⁶⁴S. Sriram, R. R. Siergiej, R. C. Clarke, A. K. Agarwal, and C. D. Brandt, *physica status solidi (a)* **162**, 441 (1997).

¹⁶⁵R. Han, X. Xu, X. Hu, N. Yu, J. Wang, Y. Tian, and W. Huang, *Optical Materials* **23**, 415 (2003).

¹⁶⁶R. Mickevičius and J. H. Zhao, *Journal of Applied Physics* **83**, 3161 (1998).

¹⁶⁷J. H. Zhao, V. Gruzinskis, Y. Luo, M. Weiner, M. Pan, P. Shiktorov, and E. Starikov, *Semiconductor Science and Technology* **15**, 1093 (2000).

¹⁶⁸A. Akturk, N. Goldsman, S. Potbhare, and A. Lelis, *Journal of Applied Physics* **105**, 033703 (2009).

¹⁶⁹B. Zippelius, *Elektrische Charakterisierung Bauelement-relevanter Defekte in 3C- Und 4H-Siliziumkarbid*, Ph.D. thesis, Friedrich-Alexander-Universität, Erlangen-Nürnberg (2011).

¹⁷⁰C. Weitzel, *Materials Science Forum* **264–268**, 907 (1998).

¹⁷¹N. G. Wright, D. Morrison, C. M. Johnson, and A. G. O'Neill, *Materials Science Forum* **264–268**, 917 (1998).

¹⁷²B. J. Baliga, *Silicon Carbide Power Devices* (WORLD SCIENTIFIC, 2006).

¹⁷³B. J. Baliga, *Fundamentals of Power Semiconductor Devices* (Springer International Publishing, Cham, 2019).

¹⁷⁴H.-E. Nilsson, E. Bellotti, M. Hjelm, K. F. Brennan, and C. Petersson, **Proceedings of the IMACS Conference, Sofia, Bulgaria, June 1999** (1999).

¹⁷⁵E. Bellotti, H.-E. Nilsson, K. F. Brennan, P. P. Ruden, and R. Trew, *Journal of Applied Physics* **87**, 3864 (2000).

¹⁷⁶J. L. Vasconcelos, C. G. Rodrigues, and R. Luzzi, *Materials Science and Engineering: B* **249**, 114426 (2019).

¹⁷⁷C. G. Rodrigues, *Semiconductors* **55**, 625 (2021).

¹⁷⁸T. P. Chow, *Materials Science Forum* **338–342**, 1155 (2000).

¹⁷⁹G. Dhanaraj, K. Byrappa, V. Prasad, and M. Dudley, eds., *Springer Handbook of Crystal Growth* (Springer Berlin Heidelberg, Berlin, Heidelberg, 2010).

¹⁸⁰A. Elasser and T. Chow, *Proceedings of the IEEE* **90**, 969 (2002).

¹⁸¹M. Su, *Power Devices and Integrated Circuits Based on 4H-SiC Lateral JFETs*, Ph.D. thesis, New Brunswick Rutgers, New Jersey (2010).

¹⁸²C.-M. Zetterling, ed., *Process Technology for Silicon Carbide Devices*, EMIS Processing Series No. 2 (Institution of Electrical Engineers, London, 2002).

¹⁸³M. Östling, *Science China Information Sciences* **54**, 1087 (2011).

¹⁸⁴M. Hjelm, H.-E. Nilsson, A. Martinez, K. F. Brennan, and E. Bellotti, *Journal of Applied Physics* **93**, 1099 (2003).

¹⁸⁵B. Ozpineci, “Comparison of Wide-Bandgap Semiconductors for Power Electronics Applications,” Tech. Rep. ORNL/TM-2003/257, 885849 (Oak Ridge National Laboratory, 2004).

¹⁸⁶N. Kaminski, 2009 13th European Conference on Power Electronics and Applications **8** (2009).

¹⁸⁷N. Kaminski and O. Hilt, *IET Circuits, Devices & Systems* **8**, 227 (2014).

¹⁸⁸C. Buttay, D. Planson, B. Allard, D. Bergogne, P. Bevilacqua, C. Joubert, M. Lazar, C. Martin, H. Morel, D. Tournier, and C. Raynaud, *Materials Science and Engineering: B* **176**, 283 (2011).

¹⁸⁹S. Fujita, *Japanese Journal of Applied Physics* **54**, 030101 (2015).

¹⁹⁰A. Hassan, Y. Savaria, and M. Sawan, *IEEE Access* **6**, 78790 (2018).

¹⁹¹M. Higashiwaki, K. Sasaki, A. Kuramata, T. Masui, and S. Yamakoshi, *physica status solidi (a)* **211**, 21 (2014).

¹⁹²G. Liu, B. R. Tuttle, and S. Dhar, *Applied Physics Reviews* **2**, 021307 (2015).

¹⁹³X.-Q. Zheng and P. X.-L. Feng, in *Wide Bandgap Semiconductor-Based Electronics*, 2053-2563 (IOP Publishing, 2020) pp. 3–1 to 3–18.

¹⁹⁴H. Elahipanah, *Design Optimization and Realization of 4H-SiC Bipolar Junction Transistors*, Ph.D. thesis, KTH, Electronics / KTH, Electronics (2017).

¹⁹⁵M. Östling, *IEEE Electron Devices Magazine* **2**, 30 (2024).

¹⁹⁶S. Rybalka, E. Yu. Krayushkina, A. Demidov, O. Shishkina, and B. Surin, *International Journal of Physical Research* **5**, 11 (2017).

¹⁹⁷C. Darmody and N. Goldsman, *Journal of Applied Physics* **126**, 145701 (2019).

¹⁹⁸V. J. B. Torres, I. Capan, and J. Coutinho, *Physical Review B* **106**, 224112 (2022).

¹⁹⁹S. J. Pearton, J. Yang, P. H. Cary, F. Ren, J. Kim, M. J. Tadjer, and M. A. Mastro, *Applied Physics Reviews* **5**, 011301 (2018).

²⁰⁰V. Soler, *Design and Process Developments towards an Optimal 6.5 kV SiC Power MOSFET*, Ph.D. thesis, Universitat Politecnica de Catalunya (2019).

²⁰¹S. Reshanov, *Device-relevant defect centers and minority carrier lifetime in 3C-, 4H- and 6H-SiC*, Ph.D. thesis, Friedrich-Alexander-Universität, Erlangen-Nürnberg (2005).

²⁰²M. Yoder, *IEEE Transactions on Electron Devices* **43**, 1633 (1996).

²⁰³S. Rao, E. D. Mallemace, and F. G. Della Corte, *Electronics* **11**, 1839 (2022).

²⁰⁴G. Sozzi, M. Puzzanghera, R. Menozzi, and R. Nipoti, *IEEE Transactions on Electron Devices* **66**, 3028 (2019).

²⁰⁵R. Nipoti, G. Sozzi, M. Puzzanghera, and R. Menozzi, *MRS Advances* **1**, 3637 (2016).

²⁰⁶M. Usman and M. Nawaz, *Solid-State Electronics* **92**, 5 (2014).

²⁰⁷F. Pezzimenti, *IEEE Transactions on Electron Devices* **60**, 1404 (2013).

²⁰⁸S. Sandeep and R. Komaragiri, in *India International Conference on Power Electronics 2010 (IICPE2010)* (IEEE, New Delhi, India, 2011) pp. 1–5.

²⁰⁹S. Bellone, F. G. Della Corte, L. F. Albanese, and F. Pezzimenti, *IEEE Transactions on Power Electronics* **26**, 2835 (2011).

²¹⁰D. Schröder, *Leistungselektronische Bauelemente* (Springer Berlin Heidelberg, Berlin, Heidelberg, 2006).

²¹¹X. Dong, M. Huang, Y. Ma, C. Fu, M. He, Z. Yang, Y. Li, and M. Gong, *IEEE Transactions on Nuclear Science* , 1 (2024).

²¹²T. Yang, C. Fu, W. Song, Y. Tan, S. Xiao, C. Wang, K. Liu, X. Zhang, and X. Shi, *Nuclear Instruments and Methods in Physics Research Section A: Accelerators, Spectrometers, Detectors and Associated Equipment* **1056**, 168677 (2023).

²¹³T. Yang, Y. Tan, C. Wang, X. Zhang, and X. Shi, “Simulation of the 4H-SiC Low Gain Avalanche Diode,” (2022), [arXiv:2206.10191 \[physics\]](https://arxiv.org/abs/2206.10191).

²¹⁴M. Biswas and E. Ahmadi, in *Wide Bandgap Semiconductor-Based Electronics*, 2053-2563 (IOP Publishing, 2020) pp. 4–1 to 4–24.

²¹⁵M. Cabello, V. Soler, G. Rius, J. Montserrat, J. Rebollo, and P. Godignon, *Materials Science in Semiconductor Processing* **78**, 22 (2018).

²¹⁶Q. Chen, L. Yang, S. Wang, Y. Zhang, Y. Dai, and Y. Hao, *Applied Physics A* **118**, 1219 (2015).

²¹⁷H. A. Mantooth, in *Extreme Environment Electronics* (CRC Press, Taylor & Francis Group, 2013) pp. 243–252.

²¹⁸L. F. Albanese, *Characterization, Modeling and Simulation of 4H-SiC Power Diodes*, Ph.D. thesis, UniversitàdegliStudidiSalerno (2010).

²¹⁹G. Donnarumma, J. Woźny, and Z. Lisik, *Materials Science and Engineering: B* **165**, 47 (2009).

²²⁰P. Bhatnagar, A. B. Horsfall, N. G. Wright, C. M. Johnson, K. V. Vassilevski, and A. G. O'Neill, *Solid-State Electronics* **49**, 453 (2005).

²²¹M. W. Cole and P. Joshi, in *Silicon Carbide*, edited by Z. C. Feng and J. H. Zhao (Springer Berlin Heidelberg, Berlin, Heidelberg, 2004) pp. 517–536.

²²²D. T. Morisette, *Development of Robust Power Schottky Barrier Diodes in Silicon Carbide*, Ph.D. thesis, Purdue University (2001).

²²³H. Iwata and K. M. Itoh, *Journal of Applied Physics* **89**, 6228 (2001).

²²⁴H. Iwata and K. M. Itoh, *Materials Science Forum* **338–342**, 729 (2000).

²²⁵H. Iwata, K. M. Itoh, and G. Pensl, *Journal of Applied Physics* **88**, 1956 (2000).

²²⁶N. Wright, in *IEE Colloquium on New Developments in Power Semiconductor Devices*, Vol. 1996 (IEE, London, UK, 1996) pp. 6–6.

²²⁷H.-E. Nilsson, U. Sannemo, and C. S. Petersson, *Journal of Applied Physics* **80**, 3365 (1996).

²²⁸T. Kimoto, *Japanese Journal of Applied Physics* **54**, 040103 (2015).

²²⁹J. Zhao, X. Li, K. Tone, P. Alexandrov, M. Pan, and M. Weiner, *Solid-State Electronics* **47**, 377 (2003).

²³⁰A. Elasser, M. Kheraluwala, M. Ghezzo, R. Steigerwald, N. Evers, J. Kretchmer, and T. Chow, *IEEE Transactions on Industry Applications* **39**, 915 (2003).

²³¹A. Elasser, M. Ghezzo, N. Krishnamurthy, J. Kretchmer, A. Clock, D. Brown, and T. Chow, *Solid-State Electronics* **44**, 317 (2000).

²³²V. Chelnokov and A. Syrkin, *Materials Science and Engineering: B* **46**, 248 (1997).

²³³F. L. L. Nouketcha, Y. Cui, A. Lelis, R. Green, C. Darmody, J. Schuster, and N. Goldsman, *IEEE Transactions on Electron Devices* **67**, 3999 (2020).

²³⁴T. P. Chow, I. Omura, M. Higashiwaki, H. Kawarada, and V. Pala, *IEEE Transactions on Electron Devices* **64**, 856 (2017).

²³⁵J. A. Pellish and L. M. Cohn, in *Extreme Environment Electronics* (CRC Press, Taylor & Francis Group, 2013) pp. 49–58.

²³⁶S. M. Sze and K. K. Ng, *Physics of Semiconductor Devices*, 3rd ed. (Wiley-Interscience, Hoboken, N.J, 2007).

²³⁷J. Millán, *IET Circuits, Devices & Systems* **1**, 372 (2007).

²³⁸A. Pérez-Tomás, P. Brosselard, P. Godignon, J. Millán, N. Mestres, M. R. Jennings, J. A. Covington, and P. A. Mawby, *Journal of Applied Physics* **100**, 114508 (2006).

²³⁹T. P. Chow, N. Ramungul, J. Fedison, and Y. Tang, in *Silicon Carbide*, edited by W. J. Choyke, H. Matsunami, and G. Pensl (Springer Berlin Heidelberg, Berlin, Heidelberg, 2004) pp. 737–767.

²⁴⁰N. Zhang, *High Voltage GaN HEMTs with Low On-Resistance for Switching Applications*, Ph.D. thesis, UNIVERSITY of CALIFORNIA, Santa Barbara (2002).

²⁴¹R. Trew, *Proceedings of the IEEE* **90**, 1032 (2002).

²⁴²S. K. Lee, *Processing and Characterization of Silicon Carbide (6H-SiC and 4H-SiC) Contacts for High Power and h...* (Mikroelektronik och informationsteknik, Kista, 2002).

²⁴³R. Kemerley, H. Wallace, and M. Yoder, *Proceedings of the IEEE* **90**, 1059 (2002).

²⁴⁴V. Dmitriev, T. P. Chow, S. P. DenBaars, M. S. Shur, and M. G. Spencer, “*High-Temperature Electronics in Europe:*,” Tech. Rep. (Defense Technical Information Center, Fort Belvoir, VA, 2000).

²⁴⁵T. Chow, V. Khemka, J. Fedison, N. Ramungul, K. Matocha, Y. Tang, and R. Gutmann, *Solid-State Electronics* **44**, 277 (2000).

²⁴⁶C. M. Zetterling, M. Östling, C. I. Harris, N. Nordell, K. Wongchotigul, and M. G. Spencer, *Materials Science Forum* **264–268**, 877 (1998).

²⁴⁷P. B. Shah and K. A. Jones, *Journal of Applied Physics* **84**, 4625 (1998).

²⁴⁸M. Roschke, F. Schwierz, G. Paasch, and D. Schipanski, *Materials Science Forum* **264–268**, 965 (1998).

²⁴⁹E. Danielsson, C. I. Harris, C. M. Zetterling, and M. Östling, *Materials Science Forum* **264–268**, 805 (1998).

²⁵⁰T. P. Chow, N. Ramungul, and M. Ghezzo, *MRS Proceedings* **483**, 89 (1997).

²⁵¹T. P. Chow and M. Ghezzo, *MRS Proceedings* **423**, 9 (1996).

²⁵²H. Niwa, J. Suda, and T. Kimoto, *IEEE Transactions on Electron Devices* **62**, 3326 (2015).

²⁵³T. E. Tiwald, J. A. Woollam, S. Zollner, J. Christiansen, R. B. Gregory, T. Wetteroth, S. R. Wilson, and A. R. Powell, *Physical Review B* **60**, 11464 (1999).

²⁵⁴L. Torpo, M. Marlo, T. E. M. Staab, and R. M. Nieminen, *Journal of Physics: Condensed Matter* **13**, 6203 (2001).

²⁵⁵D. W. Feldman, J. H. Parker, W. J. Choyke, and L. Patrick, *Physical Review* **173**, 787 (1968).

²⁵⁶J. A. Freitas, in *Properties of Silicon Carbide*, EMIS Datareviews Series No. 13, edited by G. L. Harris and Inspec (INSPEC, the Inst. of Electrical Engineers, London, 1995) pp. 29–41.

²⁵⁷G.-S. Sun, X.-F. Liu, H.-L. Wu, G.-G. Yan, L. Dong, L. Zheng, W.-S. Zhao, L. Wang, Y.-P. Zeng, X.-G. Li, and Z.-G. Wang, *Chinese Physics B* **20**, 033301 (2011).

²⁵⁸Q. Zheng, C. Li, A. Rai, J. H. Leach, D. A. Broido, and D. G. Cahill, *Physical Review Materials* **3**, 014601 (2019).

²⁵⁹R. Mickevičius and J. H. Zhao, *Materials Science Forum* **264–268**, 291 (1998).

²⁶⁰K. Adachi, *Simulation and Modelling of Power Devices Based on 4H Silicon Carbide*, Ph.D. thesis, University of Newcastle (2003).

²⁶¹N. T. Son, P. N. Hai, W. M. Chen, C. Hallin, B. Monemar, and E. Janzén, *Physical Review B* **61**, R10544 (2000).

²⁶²G. Wellenhofer and U. Rössler, *physica status solidi (b)* **202**, 107 (1997).

²⁶³C. Persson and U. Lindefelt, *Physical Review B* **54**, 10257 (1996).

²⁶⁴K. Karch, G. Wellenhofer, P. Pavone, U. Rössler, and D. Strauch, “Structural and electronic properties of SiC polytypes,” (1995).

²⁶⁵J. Dong and A.-B. Chen, in *SiC Power Materials*, Vol. 73, edited by R. Hull, R. M. Osgood, J. Parisi, H. Warlimont, and Z. C. Feng (Springer Berlin Heidelberg, Berlin, Heidelberg, 2004) pp. 63–87.

²⁶⁶H. P. Iwata, U. Lindefelt, S. Öberg, and P. R. Briddon, *Physical Review B* **68**, 245309 (2003).

²⁶⁷S. Nakashima and H. Harima, *physica status solidi (a)* **162**, 39 (1997).

²⁶⁸Y. Kuroiwa, Y.-i. Matsushita, K. Harada, and F. Oba, *Applied Physics Letters* **115**, 112102 (2019).

²⁶⁹W. Lambrecht, S. Limpijumnong, S. Rashkeev, and B. Segall, *physica status solidi (b)* **202**, 5 (1997).

²⁷⁰J. Blakemore, *Semiconductor Statistics* (Elsevier, 1962).

²⁷¹W. Götz, A. Schöner, G. Pensl, W. Sutrop, W. J. Choyke, R. Stein, and S. Leibenzeder, *Journal of Applied Physics* **73**, 3332 (1993).

²⁷²W. Sutrop, *Aluminium, Bor und Stickstoff als Dotierstoffe in einkristallinem Siliziumkarbid SiC(6H)*, Ph.D. thesis, Friedrich-Alexander-Universität, Erlangen-Nürnberg (1991).

²⁷³J. Kohlscheen, Y. N. Emirov, M. M. Beerbom, J. T. Wolan, S. E. Saddow, G. Chung, M. F. MacMillan, and R. Schlaf, *Journal of Applied Physics* **94**, 3931 (2003).

²⁷⁴C. Hemmingsson, N. T. Son, O. Kordina, J. P. Bergman, E. Janzén, J. L. Lindström, S. Savage, and N. Nordell, *Journal of Applied Physics* **81**, 6155 (1997).

²⁷⁵P. Ščajev, M. Karaliūnas, E. Kuokštis, and K. Jarašiūnas, *Journal of Luminescence* **134**, 588 (2013).

²⁷⁶C. Raynaud, D. Tournier, H. Morel, and D. Planson, *Diamond and Related Materials* **19**, 1 (2010).

²⁷⁷C. Persson and U. Lindefelt, *Journal of Applied Physics* **83**, 266 (1998).

²⁷⁸V. K. Khanna, *Extreme-Temperature and Harsh-Environment Electronics: Physics, Technology and Applications*, second edition ed. (IOP Publishing, Bristol [England] (Temple Circus, Temple Way, Bristol BS1 6HG, UK), 2023).

²⁷⁹J. E. Lang, F. L. Madarasz, and P. M. Hemenger, *Journal of Applied Physics* **54**, 3612 (1983).

²⁸⁰C. Persson, U. Lindefelt, and B. E. Sernelius, *Physical Review B* **60**, 16479 (1999).

²⁸¹R. Ishikawa, M. Hara, H. Tanaka, M. Kaneko, and T. Kimoto, *Applied Physics Express* **14**, 061005 (2021).

²⁸²R. Ishikawa, H. Tanaka, M. Kaneko, and T. Kimoto, *Journal of Applied Physics* **135**, 075704 (2024).

²⁸³H. P. Iwata, *Applied Physics Letters* **82**, 598 (2003).

²⁸⁴T. Kinoshita, K. M. Itoh, J. Muto, M. Schadt, G. Pensl, and K. Takeda, *Materials Science Forum* **264–268**, 295 (1998).

²⁸⁵O. Kordina, A. Henry, J. P. Bergman, N. T. Son, W. M. Chen, C. Hallin, and E. Janzén, *Applied Physics Letters* **66**, 1373 (1995).

²⁸⁶J. Camassel and S. Juillaguet, *physica status solidi (b)* **245**, 1337 (2008).

²⁸⁷J. T. Devreese, in *Digital Encyclopedia of Applied Physics*, edited by Wiley-VCH Verlag GmbH & Co. KGaA (Wiley, 2003) 1st ed.

²⁸⁸G. D. Mahan, *Many-Particle Physics* (Springer US, Boston, MA, 1990).

²⁸⁹H. Fröhlich, *Advances in Physics* **3**, 325 (1954).

²⁹⁰P. Käckell, B. Wenzien, and F. Bechstedt, *Physical Review B* **50**, 10761 (1994).

²⁹¹L. Lu, H. Zhang, X. Wu, J. Shi, and Y.-Y. Sun, *Chinese Physics B* **30**, 096806 (2021).

²⁹²C. Persson and U. Lindefelt, *Journal of Applied Physics* **86**, 5036 (1999).

²⁹³G. L. Zhao and D. Bagayoko, *New Journal of Physics* **2**, 16 (2000).

²⁹⁴W. R. L. Lambrecht and B. Segall, *Physical Review B* **52**, R2249 (1995).

²⁹⁵A.-B. Chen and P. Srichaikul, *physica status solidi (b)* **202**, 81 (1997).

²⁹⁶G. Pennington and N. Goldsman, *Physical Review B* **64**, 045104 (2001).

²⁹⁷G. Ng, *Computational Studies of 4H and 6H Silicon Carbide*, Ph.D. thesis, Arizona State University (2010).

²⁹⁸G. Ng, D. Vasileska, and D. Schroder, *Superlattices and Microstructures* **49**, 109 (2011).

²⁹⁹N. T. Son, W. M. Chen, O. Kordina, A. O. Konstantinov, B. Monemar, E. Janzén, D. M. Hofman, D. Volm, M. Drechsler, and B. K. Meyer, *Applied Physics Letters* **66**, 1074 (1995).

³⁰⁰K. Mikami, M. Kaneko, and T. Kimoto, *IEEE Electron Device Letters* , 1 (2024).

³⁰¹G. Lomakina and Y. A. Vodakov, *Sov. Phys. Solid State* **15**, 83 (1973).

³⁰²G. Lomakina, in *In: Silicon Carbide-1973; Proceedings of the Third International Conference* (1974) pp. 520–526.

³⁰³N. T. Son, P. Hai, W. Chen, C. Hallin, B. Monemar, and E. Janzén, *Materials Science Forum* **338–342**, 563 (2000).

³⁰⁴D. Volm, B. K. Meyer, D. M. Hofmann, W. M. Chen, N. T. Son, C. Persson, U. Lindefelt, O. Kordina, E. Sörman, A. O. Konstantinov, B. Monemar, and E. Janzén, *Physical Review B* **53**, 15409 (1996).

³⁰⁵G. Bosch, *Journal of Physics and Chemistry of Solids* **27**, 795 (1966).

³⁰⁶G. Pennington and N. Goldsman, *Journal of Applied Physics* **95**, 4223 (2004).

³⁰⁷M. Goano, E. Bellotti, K. F. Brennan, and G. Ghione, in *11th III–V Semiconductor Device Simulation Workshop, IEMN Villeneuve d'Ascq* (1999).

³⁰⁸L. Patrick, W. J. Choyke, and D. R. Hamilton, *Physical Review* **137**, A1515 (1965).

³⁰⁹M. Schadt, G. Pensl, R. P. Devaty, W. J. Choyke, R. Stein, and D. Stephani, *Applied Physics Letters* **65**, 3120 (1994).

³¹⁰G. Pensl and W. Choyke, *Physica B: Condensed Matter* **185**, 264 (1993).

³¹¹A. Itoh, T. Kimoto, and H. Matsunami, *IEEE Electron Device Letters* **16**, 280 (1995).

³¹²P. A. Ivanov, M. E. Levenshtein, J. W. Palmour, S. L. Rumyantsev, and R. Singh, *Semiconductor Science and Technology* **15**, 908 (2000).

³¹³S. I. Maximenko, *AIP Advances* **13**, 105021 (2023).

³¹⁴J. Pernot, S. Contreras, J. Camassel, J. L. Robert, W. Zawadzki, E. Neyret, and L. Di Cioccio, *Applied Physics Letters* **77**, 4359 (2000).

³¹⁵V. Tilak, K. Matocha, and G. Dunne, *IEEE Transactions on Electron Devices* **54**, 2823 (2007).

³¹⁶R. A. Faulkner, *Physical Review* **184**, 713 (1969).

³¹⁷P. Luo and S. N. E. Madathil, *IEEE Transactions on Electron Devices* **67**, 5621 (2020).

³¹⁸S. Rakheja, L. Huang, S. Hau-Riege, S. E. Harrison, L. F. Voss, and A. M. Conway, *IEEE Journal of the Electron Devices Society* **8**, 1118 (2020).

³¹⁹D. C. Look, in *Semiconductors and Semimetals*, Vol. 19 (Elsevier, 1983) pp. 75–170.

³²⁰Z. Q. Fang, B. Claflin, D. C. Look, L. Polenta, and W. C. Mitchel, *Journal of Electronic Materials* **34**, 336 (2005).

³²¹N. Kuznetsov and A. Zubrilov, *Materials Science and Engineering: B* **29**, 181 (1995).

³²²N. T. Son, O. Kordina, A. O. Konstantinov, W. M. Chen, E. Sörman, B. Monemar, and E. Janzén, *Applied Physics Letters* **65**, 3209 (1994).

³²³R. P. Joshi, *Journal of Applied Physics* **78**, 5518 (1995).

³²⁴T. Tamaki, G. G. Walden, Y. Sui, and J. A. Cooper, *IEEE Transactions on Electron Devices* **55**, 1920 (2008).

³²⁵Q.-W. Song, Y.-M. Zhang, Y.-M. Zhang, and X.-Y. Tang, *Diamond and Related Materials* **22**, 42 (2012).

³²⁶A. Yang, K. Murata, T. Miyazawa, T. Tawara, and H. Tsuchida, *Journal of Applied Physics* **126**, 055103 (2019).

³²⁷A. Galeckas, J. Linnros, V. Grivickas, U. Lindefelt, and C. Hallin, *Applied Physics Letters* **71**, 3269 (1997).

³²⁸C. Q. Chen, J. Zeman, F. Engelbrecht, C. Peppermüller, R. Helbig, Z. H. Chen, and G. Martinez, *Journal of Applied Physics* **87**, 3800 (2000).

³²⁹Y. Negoro, K. Katsumoto, T. Kimoto, and H. Matsunami, *Journal of Applied Physics* **96**, 224 (2004).

³³⁰S. Biondo, W. Vervisch, L. Ottaviani, and O. Palais, *Journal of Applied Physics* **111**, 024506 (2012).

³³¹S. G. Sridhara, L. L. Clemen, R. P. Devaty, W. J. Choyke, D. J. Larkin, H. S. Kong, T. Troffer, and G. Pensl, *Journal of Applied Physics* **83**, 7909 (1998).

³³²H. Van Daal, W. Knippenberg, and J. Wasscher, *Journal of Physics and Chemistry of Solids* **24**, 109 (1963).

³³³M. Flores, F. Maia, V. Freire, J. Da Costa, and E. Da Silva, *Microelectronics Journal* **34**, 717 (2003).

³³⁴K. Neimontas, T. Malinauskas, R. Aleksiejūnas, M. Sūdžius, K. Jarašiūnas, L. Storasta, J. P. Bergman, and E. Janzen, *Semiconductor Science and Technology* **21**, 952 (2006).

³³⁵G. Pensl, F. Schmid, F. Ciobanu, M. Laube, S. A. Reshanov, N. Schulze, K. Semmelroth, A. Schöner, G. Wagner, and H. Nagasawa, *Materials Science Forum* **433–436**, 365 (2003).

³³⁶W. J. Choyke, D. R. Hamilton, and L. Patrick, *Physical Review* **133**, A1163 (1964).

³³⁷W. J. Choyke, L. Patrick, and D. Hamilton, 7th in conference on semicond. physics paris 1964, **7**, 751 (1964).

³³⁸G. Zanmarchi, 7th in conference on semicond. physics paris 1964, **7**, 57 (1964).

³³⁹A. Gsponer, M. Knopf, P. Gaggl, J. Burin, S. Waid, and T. Bergauer, *Nuclear Instruments and Methods in Physics Research Section A: Accelerators, Spectrometers, Detectors and Associated Equipment* **1064**, 169412 (2024).

³⁴⁰P. Kwasnicki, *Evaluation of Doping in 4H-SiC by Optical Spectroscopies*, Ph.D. thesis, UNIVERSITE MONTPELLIER II (2014).

³⁴¹D. K. Schroder, *Semiconductor Material and Device Characterization*, 1st ed. (Wiley, 2005).

³⁴²J. P. Wolfe and A. Mysyrowicz, *Scientific American* **250**, 98 (1984), [24969326](#).

³⁴³R. J. Elliott, *Physical Review* **108**, 1384 (1957).

³⁴⁴Ch. Haberstroh, R. Helbig, and R. A. Stein, *Journal of Applied Physics* **76**, 509 (1994).

³⁴⁵A. Itoh, H. Akita, T. Kimoto, and H. Matsunami, *Applied Physics Letters* **65**, 1400 (1994).

³⁴⁶A. Itoh, T. Kimoto, and H. M. Matsunami, *Japanese Journal of Applied Physics* **35**, 4373 (1996).

³⁴⁷M. Ikeda and H. Matsunami, *Physica Status Solidi (a)* **58**, 657 (1980).

³⁴⁸G. B. Dubrovskii and V. I. Sankin, *Sov. Phys. Solid State* **17**, 1847 (1975).

³⁴⁹W. J. Choyke, H. Matsunami, and G. Pensl, eds., *Silicon Carbide: Recent Major Advances*, Advanced Texts in Physics (Springer Berlin Heidelberg, Berlin, Heidelberg, 2004).

³⁵⁰R. Freer, ed., *The Physics and Chemistry of Carbides, Nitrides and Borides* (Springer Netherlands, Dordrecht, 1990).

³⁵¹H. Habib, N. G. Wright, and A. B. Horsfall, *Advanced Materials Research* **413**, 229 (2011).

³⁵²H. Y. Fan, *Physical Review* **82**, 900 (1951).

³⁵³A. Das and S. P. Duttagupta, *Radiation Protection Dosimetry* **167**, 443 (2015).

³⁵⁴R. Pässler, *physica status solidi (b)* **200**, 155 (1997).

³⁵⁵R. Pässler, *Journal of Applied Physics* **83**, 3356 (1998).

³⁵⁶A. Galeckas, P. Grivickas, V. Grivickas, V. Bikabajevas, and J. Linnros, *physica status solidi (a)* **191**, 613 (2002).

³⁵⁷R. Pässler, *Physical Review B* **66**, 085201 (2002).

³⁵⁸K. P. O'Donnell and X. Chen, *Applied Physics Letters* **58**, 2924 (1991).

³⁵⁹Y. P. Varshni, *Physica* **34**, 149 (1967).

³⁶⁰P. Grivickas, V. Grivickas, J. Linnros, and A. Galeckas, *Journal of Applied Physics* **101**, 123521 (2007).

³⁶¹R. Pässler, *physica status solidi (b)* **216**, 975 (1999).

³⁶²S. Balachandran, T. P. Chow, and A. K. Agarwal, *Materials Science Forum* **483–485**, 909 (2005).

³⁶³M. Nawaz, *Microelectronics Journal* **41**, 801 (2010).

³⁶⁴P. Ščajev and K. Jarašiūnas, *Journal of Physics D: Applied Physics* **42**, 055413 (2009).

³⁶⁵L. Viña, S. Logothetidis, and M. Cardona, *Physical Review B* **30**, 1979 (1984).

³⁶⁶R. Pässler, *physica status solidi (b)* **236**, 710 (2003).

³⁶⁷E. F. Schubert, *Doping in III-V Semiconductors*, Cambridge Studies in Semiconductor Physics and Microelectronic Engineering No. 1 (Cambridge University Press, Cambridge [England] ; New York, NY, USA, 1993).

³⁶⁸S. Jain and D. Roulston, *Solid-State Electronics* **34**, 453 (1991).

³⁶⁹M. Ruff, H. Mitlehner, and R. Helbig, *IEEE Transactions on Electron Devices* **41**, 1040 (1994).

³⁷⁰W. J. Choyke and L. Patrick, *Physical Review* **105**, 1721 (1957).

³⁷¹A. O. Ewvaraye, S. R. Smith, and W. C. Mitchel, *Journal of Applied Physics* **79**, 7726 (1996).

³⁷²I. G. Ivanov, U. Lindefelt, A. Henry, O. Kordina, C. Hallin, M. Aroyo, T. Egilsson, and E. Janzén, *Physical Review B* **58**, 13634 (1998).

³⁷³I. G. Ivanov, J. Zhang, L. Storasta, and E. Janzén, *Materials Science Forum* **389–393**, 613 (2002).

³⁷⁴Y. Fang, X. Wu, J. Yang, G. Chen, Y. Chen, Q. Wu, and Y. Song, *Applied Physics Letters* **112**, 201904 (2018).

³⁷⁵K. Miller, Q. Zhou, J. Chen, M. O. Manasreh, Z. C. Feng, and I. Ferguson, *MRS Proceedings* **640**, H5.23 (2000).

³⁷⁶S. Sridhara, S. Bai, O. Shigiltchoff, R. P. Devaty, and W. J. Choyke, *Materials Science Forum* **338–342**, 567 (2000).

³⁷⁷W. H. Backes, P. A. Bobbert, and W. Van Haeringen, *Physical Review B* **49**, 7564 (1994).

³⁷⁸H.-g. Junginger and W. Van Haeringen, *physica status solidi (b)* **37**, 709 (1970).

³⁷⁹W. Van Haeringen, P. Bobbert, and W. Backes, *physica status solidi (b)* **202**, 63 (1997).

³⁸⁰K. Yamaguchi, D. Kobayashi, T. Yamamoto, and K. Hirose, *Physica B: Condensed Matter* **532**, 99 (2018).

³⁸¹G. B. Dubrovskii and A. A. Lepneva, *Sov. Phys. Solid State* **19**, 729 (1977).

³⁸²V. I. Gavrilenko, A. V. Postnikov, N. I. Klyui, and V. G. Litovchenko, *physica status solidi (b)* **162**, 477 (1990).

³⁸³C. H. Park, B.-H. Cheong, K.-H. Lee, and K. J. Chang, *Physical Review B* **49**, 4485 (1994).

³⁸⁴W. J. Choyke and L. Patrick, *Physical Review* **127**, 1868 (1962).

³⁸⁵I. Shalish, I. B. Altfeder, and V. Narayanamurti, *Physical Review B* **65**, 073104 (2002).

³⁸⁶M. Khalid, S. Riaz, and S. Naseem, *Communications in Theoretical Physics* **58**, 577 (2012).

³⁸⁷Y. Huang, R. Wang, Y. Zhang, D. Yang, and X. Pi, *Journal of Applied Physics* **131**, 185703 (2022).

³⁸⁸S. G. Sridhara, R. P. Devaty, and W. J. Choyke, *Journal of Applied Physics* **84**, 2963 (1998).

³⁸⁹J. Wang and B. W. Williams, *Semiconductor Science and Technology* **14**, 1088 (1999).

³⁹⁰M. L. Megherbi, L. Dehimi, W. terghini, F. Pezzimenti, and F. G. Della Corte, *Courrier du Savoir* **19**, 71 (2015).

³⁹¹S. Levcenco, D. Dumcenco, Y. Huang, E. Arushanov, V. Tezlevan, K. Tiong, and C. Du, *Journal of Alloys and Compounds* **509**, 4924 (2011).

³⁹²T. Hatakeyama, T. Watanabe, M. Kushibe, K. Kojima, S. Imai, T. Suzuki, T. Shinohe, T. Tanaka, and K. Arai, *Materials Science Forum* **433–436**, 443 (2003).

³⁹³R. Weingärtner, P. J. Wellmann, M. Bickermann, D. Hofmann, T. L. Straubinger, and A. Winnacker, *Applied Physics Letters* **80**, 70 (2002).

³⁹⁴G. Donnarumma, V. Palankovski, and S. Selberherr, in *Proceedings of the International Conference on Simulation of Semiconductor Processes and Devices (SISPAD)* (2012) pp. 125–128.

³⁹⁵D. Johannesson and M. Nawaz, *IEEE Transactions on Power Electronics* **31**, 4517 (2016).

³⁹⁶H. Lanyon and R. Tuft, *IEEE Transactions on Electron Devices* **26**, 1014 (1979).

³⁹⁷V. V. Afanas'ev, M. Bassler, G. Pensl, M. J. Schulz, and E. Stein Von Kamienski, *Journal of Applied Physics* **79**, 3108 (1996).

³⁹⁸H. Matsunami and T. Kimoto, *Materials Science and Engineering: R: Reports* **20**, 125 (1997).

³⁹⁹A. A. Lebedev, *Semiconductors* **33**, 107 (1999).

⁴⁰⁰A. Hefner, R. Singh, Jih-Sheg Lai, D. Berning, S. Bouche, and C. Chapuy, *IEEE Transactions on Power Electronics* **16**, 273 (2001).

⁴⁰¹T. McNutt, A. Hefner, H. Mantooth, J. Duliere, D. Berning, and R. Singh, *IEEE Transactions on Power Electronics* **19**, 573 (2004).

⁴⁰²X. Li, Y. Luo, L. Fursin, J. Zhao, M. Pan, P. Alexandrov, and M. Weiner, *Solid-State Electronics* **47**, 233 (2003).

⁴⁰³M. L. Megherbi, F. Pezzimenti, L. Dehimi, A. Saadoune, and F. G. Della Corte, *Journal of Electronic Materials* **47**, 1414 (2018).

⁴⁰⁴K. Zeghdar, L. Dehimi, F. Pezzimenti, S. Rao, and F. G. Della Corte, *Japanese Journal of Applied Physics* **58**, 014002 (2019).

⁴⁰⁵K. Zeghdar, L. Dehimi, F. Pezzimenti, M. L. Megherbi, and F. G. Della Corte, *Journal of Electronic Materials* **49**, 1322 (2020).

⁴⁰⁶M. Werner and W. Fahrner, *IEEE Transactions on Industrial Electronics* **48**, 249 (2001).

⁴⁰⁷V. R. Manikam and Kuan Yew Cheong, *IEEE Transactions on Components, Packaging and Manufacturing Technology* **1**, 457 (2011).

⁴⁰⁸M. Philip and A. O'Neill, in *2006 Conference on Optoelectronic and Microelectronic Materials and Devices* (IEEE, Perth, Australia, 2006) pp. 137–140.

⁴⁰⁹R. Gerhardt, ed., *Properties and Applications of Silicon Carbide* (IntechOpen, 2011).

⁴¹⁰D. Baierhofer, in *ESSDERC 2019 - 49th European Solid-State Device Research Conference (ESSDERC)* (IEEE, Cracow, Poland, 2019) pp. 31–34.

⁴¹¹S. J. Bader, H. Lee, R. Chaudhuri, S. Huang, A. Hickman, A. Molnar, H. G. Xing, D. Jena, H. W. Then, N. Chowdhury, and T. Palacios, *IEEE Transactions on Electron Devices* **67**, 4010 (2020).

⁴¹²S. Yoshida, in *Properties of Silicon Carbide*, EMIS Datareviews Series No. 13, edited by G. L. Harris and Inspec (INSPEC, the Inst. of Electrical Engineers, London, 1995) pp. 29–41.

⁴¹³C. M. Tanner, J. Choi, and J. P. Chang, *Journal of Applied Physics* **101**, 034108 (2007).

⁴¹⁴V. Uhnevionak, *Simulation and Modeling of Silicon-Carbide Devices*, Ph.D. thesis, Friedrich-Alexander-Universität (2015).

⁴¹⁵J. Lutz, H. Schlangenotto, U. Scheuermann, and R. De Doncker, *Semiconductor Power Devices: Physics, Characteristics, Reliability* (Springer Berlin Heidelberg, Berlin, Heidelberg, 2011).

⁴¹⁶J. Fan and P. K. Chu, “General Properties of Bulk SiC,” in *Silicon Carbide Nanostructures* (Springer International Publishing, Cham, 2014) pp. 7–114.

⁴¹⁷D. Johannesson, M. Nawaz, and H. P. Nee, *Materials Science Forum* **963**, 670 (2019).

⁴¹⁸A. Suzuki, H. Matsunami, and T. Tanaka, *Journal of The Electrochemical Society* **124**, 241 (1977).

⁴¹⁹L. I. Berger, *Semiconductor Materials*, 1st ed. (CRC Press, 1996).

⁴²⁰T. Egilsson, I. G. Ivanov, N. T. Son, G. Henry, A., J. P. Bergman, and E. Janzén, in *Silicon Carbide*, edited by Z. C. Feng and J. H. Zhao (Springer Berlin Heidelberg, Berlin, Heidelberg, 2004) pp. 517–536.

⁴²¹G. Rescher, *Behavior of SiC-MOSFETs under Temperature and Voltage Stress*, Ph.D. thesis, TU Wien (2018).

⁴²²J. V. Berens, *Carrier Mobility and Reliability of 4H-SiC Trench MOSFETs*, Ph.D. thesis, TU Wien (2021).

⁴²³I. Capan, *Electronics* **11**, 532 (2022).

⁴²⁴K. Tanaka and M. Kato, *Japanese Journal of Applied Physics* **63**, 011002 (2024).

⁴²⁵J. I. Pankove, ed., *Electroluminescence*, softcover reprint of the original 1st ed. 1977 ed. (Springer Berlin, Berlin, 2014).

⁴²⁶J. Hudgins, G. Simin, E. Santi, and M. Khan, *IEEE Transactions on Power Electronics* **18**, 907 (2003).

⁴²⁷F. Bechstedt, J. Furthmüller, U. Grossner, and C. Raffy, in *Silicon Carbide*, edited by W. J. Choyke, H. Matsunami, and G. Pensl (Springer Berlin Heidelberg, Berlin, Heidelberg, 2004) pp. 3–25.

⁴²⁸T. R. Garcia, A. Kumar, B. Reinke, T. E. Blue, and W. Windl, *Applied Physics Letters* **103**, 152108 (2013).

⁴²⁹M. Jiménez-Ramos, A. García Osuna, M. Rodriguez-Ramos, E. Viezzer, G. Pellegrini, P. Godignon, J. Rafí, G. Rius, and J. García López, *Radiation Physics and Chemistry* **214**, 111283 (2024).

⁴³⁰K. G. Menon, A. Nakajima, L. Ngwendson, and E. M. Sankara Narayanan, *IEEE Electron Device Letters* **32**, 1272 (2011).

⁴³¹M. B. J. Wijesundara and R. G. Azevedo, “System Integration,” in *Silicon Carbide Microsystems for Harsh Environments*, Vol. 22 (Springer New York, New York, NY, 2011) pp. 189–230.

⁴³²M. B. J. Wijesundara and R. G. Azevedo, “Introduction,” in *Silicon Carbide Microsystems for Harsh Environments*, Vol. 22 (Springer New York, New York, NY, 2011) pp. 1–32.

⁴³³C. Langpoklakpam, A.-C. Liu, K.-H. Chu, L.-H. Hsu, W.-C. Lee, S.-C. Chen, C.-W. Sun, M.-H. Shih, K.-Y. Lee, and H.-C. Kuo, *Crystals* **12**, 245 (2022).

⁴³⁴J. D. Cressler and H. A. Mantooth, *Extreme Environment Electronics* (CRC Press, Taylor & Francis Group, Boca Raton, 2013).

⁴³⁵G. Wolfowicz, C. P. Anderson, A. L. Yeats, S. J. Whiteley, J. Niklas, O. G. Poluektov, F. J. Heremans, and D. D. Awschalom, *Nature Communications* **8**, 1876 (2017).

⁴³⁶I. G. Ivanov, A. Henry, and E. Janzén, *Physical Review B* **71**, 241201 (2005).

⁴³⁷H. Choi, “Overview of Silicon Carbide Power Devices,” (2016).

⁴³⁸A. Agarwal, S. Seshadri, J. Casady, S. Mani, M. MacMillan, N. Saks, A. Burk, G. Augustine, V. Balakrishna, P. Sanger, C. Brandt, and R. Rodrigues, *Diamond and Related Materials* **8**, 295 (1999).

⁴³⁹F. Nallet, D. Planson, K. Isoird, M. Locatelli, and J. Chante, in *CAS '99 Proceedings. 1999 International Semiconductor Conference (Cat. No.99TH8389)*, Vol. 1 (IEEE, Sinaia, Romania, 1999) pp. 195–198.

⁴⁴⁰H.-Y. Cha and P. M. Sandvik, *Japanese Journal of Applied Physics* **47**, 5423 (2008).

⁴⁴¹B. Chen, Y. Yang, X. Xie, N. Wang, Z. Ma, K. Song, and X. Zhang, *Chinese Science Bulletin* **57**, 4427 (2012).

⁴⁴²B. Nedzvetskii, B. V. Novikov, N. K. Prokof'eva, and M. B. Reifman, *Sov. Phys. Solid State* **2**, 914 (1969).

⁴⁴³V. I. Sankin, *Sov. Phys. Solid State* **17**, 1191 (1975).

⁴⁴⁴H. Matsunami, A. Suzuki, and T. Tanaka, in *In: Silicon Carbide-1973; Proceedings of the Third International Conference* (1974) pp. 618–625.

⁴⁴⁵P. Masri, *Surface Science Reports* **48**, 1 (2002).

⁴⁴⁶P. Ščajev, V. Gudelis, K. Jarašiūnas, and P. B. Klein, *Journal of Applied Physics* **108**, 023705 (2010).

⁴⁴⁷L. Di Benedetto, N. Rinaldi, G. D. Licciardo, R. Liguori, A. Rubino, A. May, and M. Rommel, in *2024 International Semiconductor Conference (CAS)* (IEEE, Sinaia, Romania, 2024) pp. 23–28.

⁴⁴⁸N. Lophitis, A. Arvanitopoulos, S. Perkins, and M. Antoniou, in *Disruptive Wide Bandgap Semiconductors, Related Technologies, and Their Applications*, edited by Y. K. Sharma (In-Tech, 2018).

⁴⁴⁹J. Lutz, U. Scheuermann, H. Schlangenotto, and R. De Doncker, “Power Semiconductor Devices—Key Components for Efficient Electrical Energy Conversion Systems,” in *Semiconductor Power Devices* (Springer International Publishing, Cham, 2018) pp. 1–20.

⁴⁵⁰H. Liu, J. Wang, S. Liang, H. Yu, and W. Deng, *Semiconductor Science and Technology* **36**, 025009 (2021).

⁴⁵¹P. Wellmann, S. Bushevoy, and R. Weingärtner, *Materials Science and Engineering: B* **80**, 352 (2001).

⁴⁵²Y.-R. Zhang, B. Zhang, Z.-J. Li, and X.-C. Deng, *Chinese Physics B* **19**, 067102 (2010).

⁴⁵³L. Di Benedetto, G. D. Licciardo, R. Nipoti, and S. Bellone, *IEEE Electron Device Letters* **35**, 244 (2014).

⁴⁵⁴W. Choyke and G. Pensl, *MRS Bulletin* **22**, 25 (1997).

⁴⁵⁵S. Hagen, A. Van Kemenade, and J. Van Der Does De Bye, *Journal of Luminescence* **8**, 18 (1973).

⁴⁵⁶G. Rescher, G. Pobegen, T. Aichinger, and T. Grasser, *IEEE Transactions on Electron Devices* **65**, 1419 (2018).

⁴⁵⁷M. L. Megherbi, F. Pezzimenti, L. Dehimi, M. A. Saadoune, and F. G. Della Corte, *IEEE Transactions on Electron Devices* **65**, 3371 (2018).

⁴⁵⁸K. C. Mandal, P. G. Muzykov, R. M. Krishna, and J. R. Terry, *IEEE Transactions on Nuclear Science* **59**, 1591 (2012).

⁴⁵⁹D. Mukherjee and M. Neto, *Recent Advances in SiC/Diamond Composite Devices* (IOP Publishing, 2023).

⁴⁶⁰D. Mukherjee, M. Neto, F. J. Oliveira, R. F. Silva, L. Pereira, S. Rotter, and J. C. Mendes, in *Wide Bandgap Semiconductor-Based Electronics*, 2053-2563 (IOP Publishing, 2020) pp. 21–1 to 21–40.

⁴⁶¹X. Guo, Q. Xun, Z. Li, and S. Du, *Micromachines* **10**, 406 (2019).

⁴⁶²H. A. Mantooth, K. Peng, E. Santi, and J. L. Hudgins, *IEEE Transactions on Electron Devices* **62**, 423 (2015).

⁴⁶³V. Cimalla, J. Pezoldt, and O. Ambacher, *Journal of Physics D: Applied Physics* **40**, S19 (2007).

⁴⁶⁴M. J. Kumar and V. Parihar, *Microelectronic Engineering* **81**, 90 (2005).

⁴⁶⁵K. Bertilsson, *Simulation and Optimization of SiC Field Effect Transistors*, Ph.D. thesis, Mikroelektronik och informationsteknik / KTH, Microelectronics and Information Technology, IMIT / KTH, Microelectronics and Information Technology, IMIT (2004).

⁴⁶⁶Y. Gao, S. I. Soloviev, T. S. Sudarshan, and C.-C. Tin, *Journal of Applied Physics* **90**, 5647 (2001).

⁴⁶⁷R. J. Trew, *physica status solidi (a)* **162**, 409 (1997).

⁴⁶⁸P. G. Neudeck, *Journal of Electronic Materials* **24**, 283 (1995).

⁴⁶⁹R. Karsthof, M. E. Batten, A. Galekas, and L. Vines, *Physical Review B* **102**, 184111 (2020).

⁴⁷⁰G. Lioliou, M. Mazzillo, A. Sciuto, and A. Barnett, *Optics Express* **23**, 21657 (2015).

⁴⁷¹D. Werber, P. Borthen, and G. Wachutka, *Materials Science Forum* **556–557**, 905 (2007).

⁴⁷²B. Ng, J. David, D. Massey, R. Tozer, G. Rees, F. Yan, J. H. Zhao, and M. Weiner, *Materials Science Forum* **457–460**, 1069 (2004).

⁴⁷³J. Shenoy, J. Cooper, and M. Melloch, *IEEE Electron Device Letters* **18**, 93 (1997).

⁴⁷⁴A. Agarwal, G. Augustine, V. Balakrishna, C. Brandt, A. Burk, Li-Shu Chen, R. Clarke, P. Esker, H. Hobgood, R. Hopkins, A. Morse, L. Rowland, S. Seshadri, R. Siergiej, T. Smith, and S. Sriram, in *International Electron Devices Meeting. Technical Digest* (IEEE, San Francisco, CA, USA, 1996) pp. 225–230.

⁴⁷⁵Wolfspeed, “Silicon Carbide and Nitride Materials Catalog,” (2023).

⁴⁷⁶W. Xi, Z. Chao, P. Hongbin, L. Yao, H. Jichao, X. Jianning, and Q. Mingxuan, *AIP Advances* **12**, 125008 (2022).

⁴⁷⁷H. Matsunami, *Proceedings of the Japan Academy, Series B* **96**, 235 (2020).

⁴⁷⁸S. Chowdhury, C. Hitchcock, R. Dahal, I. B. Bhat, and T. P. Chow, in *2015 IEEE 27th International Symposium on Power Semiconductor Devices & IC's (ISPSD)* (IEEE, Hong Kong, China, 2015) pp. 353–356.

⁴⁷⁹M. Willander, M. Friesel, Q.-u. Wahab, and B. Straumal, *Journal of Materials Science: Materials in Electronics* **17**, 1 (2006).

⁴⁸⁰T. P. Chow, *Microelectronic Engineering* **83**, 112 (2006).

⁴⁸¹S. Dhar, Y. W. Song, L. C. Feldman, T. Isaacs-Smith, C. C. Tin, J. R. Williams, G. Chung, T. Nishimura, D. Starodub, T. Gustafsson, and E. Garfunkel, *Applied Physics Letters* **84**, 1498 (2004).

⁴⁸²M. V. Rao, J. B. Tucker, M. C. Ridgway, O. W. Holland, N. Papanicolaou, and J. Mittereder, *Journal of Applied Physics* **86**, 752 (1999).

⁴⁸³J. W. Kleppinger, S. K. Chaudhuri, O. Karadavut, and K. C. Mandal, *Journal of Applied Physics* **129**, 244501 (2021).

⁴⁸⁴C. Persson and U. Lindefelt, *Materials Science Forum* **264–268**, 275 (1998).

⁴⁸⁵A. Aditya, S. Khandelwal, C. Mukherjee, A. Khan, S. Panda, and B. Maji, in *2015 International Conference on Recent Developments in Control, Automation and Power Engineering (RDCAPE)* (IEEE, Noida, India, 2015) pp. 61–65.

⁴⁸⁶L. Patrick, D. R. Hamilton, and W. J. Choyke, *Physical Review* **143**, 526 (1966).

⁴⁸⁷F. Capasso, in *Semiconductors and Semimetals*, Vol. 22 (Elsevier, 1985) pp. 1–172.

⁴⁸⁸S. Selberherr, *Analysis and Simulation of Semiconductor Devices* (Springer Vienna, Vienna, 1984).

⁴⁸⁹A. G. Chynoweth, *Physical Review* **109**, 1537 (1958).

⁴⁹⁰A. G. Chynoweth, *Journal of Applied Physics* **31**, 1161 (1960).

⁴⁹¹R. Van Overstraeten and H. De Man, *Solid-State Electronics* **13**, 583 (1970).

⁴⁹²P. A. Wolff, *Physical Review* **95**, 1415 (1954).

⁴⁹³W. Shockley, *Solid-State Electronics* **2**, 35 (1961).

⁴⁹⁴A. O. Konstantinov, Q. Wahab, N. Nordell, and U. Lindefelt, *Applied Physics Letters* **71**, 90 (1997).

⁴⁹⁵T. Lackner, *Solid-State Electronics* **34**, 33 (1991).

⁴⁹⁶G. A. Baraff, *Physical Review* **128**, 2507 (1962).

⁴⁹⁷K. K. Thornber, *Journal of Applied Physics* **52**, 279 (1981).

⁴⁹⁸S. K. Chaudhuri, K. J. Zavalla, and K. C. Mandal, *Nuclear Instruments and Methods in Physics Research Section A: Accelerators, Spectrometers, Detectors and Associated Equipment* **728**, 97 (2013).

⁴⁹⁹M. V. S. Chandrashekhar, C. I. Thomas, and M. G. Spencer, *Applied Physics Letters* **89**, 042113 (2006).

⁵⁰⁰A. Lo Giudice, F. Fizzotti, C. Manfredotti, E. Vittone, and F. Nava, *Applied Physics Letters* **87**, 222105 (2005).

⁵⁰¹B. Phlips, K. Hobart, F. Kub, R. Stahlbush, M. Das, B. Hull, G. De Geronimo, and P. O'Connor, in *IEEE Nuclear Science Symposium Conference Record, 2005*, Vol. 3 (IEEE, Wyndham El Conquistador Resort, Puerto Rico, 2005) pp. 1236–1239.

⁵⁰²A. A. Lebedev, *Semiconductors* **38**, 125 (2004).

⁵⁰³A. M. Ivanov, E. V. Kalinina, A. O. Konstantinov, G. A. Onushkin, N. B. Strokan, G. F. Kholuyanov, and A. Hallén, *Technical Physics Letters* **30**, 575 (2004).

⁵⁰⁴G. Bertuccio and R. Casiraghi, *IEEE Transactions on Nuclear Science* **50**, 175 (2003).

⁵⁰⁵A. S. Kyuregyan, *Semiconductors* **50**, 289 (2016).

⁵⁰⁶Y. Okuto and C. R. Crowell, *Physical Review B* **6**, 3076 (1972).

⁵⁰⁷Y. Okuto and C. Crowell, *Solid-State Electronics* **18**, 161 (1975).

⁵⁰⁸W. Bartsch, R. Schörner, and K. O. Dohnke, *Materials Science Forum* **645–648**, 909 (2010).

⁵⁰⁹Z. Stum, Y. Tang, H. Naik, and T. P. Chow, *Materials Science Forum* **778–780**, 467 (2014).

⁵¹⁰A. Acharyya and J. P. Banerjee, *Journal of Computational Electronics* **13**, 917 (2014).

⁵¹¹M. Valdinoci, D. Ventura, M. Vecchi, M. Rudan, G. Baccarani, F. Illien, A. Stricker, and L. Zullino, in *1999 International Conference on Simulation of Semiconductor Processes and Devices. SISPAD'99 (IEEE Cat. No.99TH8387)* (Japan Soc. Appl. Phys, Kyoto, Japan, 1999) pp. 27–30.

⁵¹²T. Kitawaki, X. Chi, M. Kaneko, and T. Kimoto, *Japanese Journal of Applied Physics* **63**, 118004 (2024).

⁵¹³S.-i. Nakamura, H. Kumagai, T. Kimoto, and H. Matsunami, *Applied Physics Letters* **80**, 3355 (2002).

⁵¹⁴T. Hatakeyama, T. Watanabe, T. Shinohe, K. Kojima, K. Arai, and N. Sano, *Applied Physics Letters* **85**, 1380 (2004).

⁵¹⁵P. N. S. Bhargav and V. K. Gurugubelli, in *2024 IEEE 11th Workshop on Wide Bandgap Power Devices & Applications (WiPDA)* (IEEE, Dayton, OH, USA, 2024) pp. 1–4.

⁵¹⁶T. Hatakeyama, *physica status solidi (a)* **206**, 2284 (2009).

⁵¹⁷S. Jin, K. Lee, W. Choi, C. Park, S. Yi, H. Fujii, J. Yoo, Y. Park, J. Jeong, and D. S. Kim, *IEEE Transactions on Electron Devices*, 1 (2024).

⁵¹⁸S. Nida and U. Grossner, *IEEE Transactions on Electron Devices* **66**, 1899 (2019).

⁵¹⁹H. Niwa, J. Suda, and T. Kimoto, *Materials Science Forum* **778–780**, 461 (2014).

⁵²⁰H. Hamad, C. Raynaud, P. Bevilacqua, S. Scharnholz, and D. Planson, *Materials Science Forum* **821–823**, 223 (2015).

⁵²¹C. R. Crowell and S. M. Sze, *Applied Physics Letters* **9**, 242 (1966).

⁵²²F. Nallet, A. Senes, D. Planson, M. Locatelli, J. Chante, and J. Taboy, in *Proceedings IPEMC 2000. Third International Power Electronics and Motion Control Conference (IEEE Cat. No.00EX435)*, Vol. 1 (Int. Acad. Publishers, Beijing, China, 2000) pp. 396–401.

⁵²³R. Raghunathan and B. Baliga, *Solid-State Electronics* **43**, 199 (1999).

⁵²⁴A. O. Konstantinov, Q. Wahab, N. Nordell, and U. Lindefelt, *Journal of Electronic Materials* **27**, 335 (1998).

⁵²⁵W. S. Loh, B. K. Ng, J. S. Ng, S. I. Soloviev, H.-Y. Cha, P. M. Sandvik, C. M. Johnson, and J. P. R. David, *IEEE Transactions on Electron Devices* **55**, 1984 (2008).

⁵²⁶B. Ng, J. David, R. Tozer, G. Rees, Feng Yan, Jian H. Zhao, and M. Weiner, *IEEE Transactions on Electron Devices* **50**, 1724 (2003).

⁵²⁷D. Nguyen, C. Raynaud, N. Dheilly, M. Lazar, D. Tournier, P. Brosselard, and D. Planson, *Diamond and Related Materials* **20**, 395 (2011).

⁵²⁸D. Nguyen, C. Raynaud, M. Lazar, G. Pâques, S. Scharnholz, N. Dheilly, D. Tournier, and D. Planson, *Materials Science Forum* **717–720**, 545 (2012).

⁵²⁹D. Stefanakis, X. Chi, T. Maeda, M. Kaneko, and T. Kimoto, *IEEE Transactions on Electron Devices* **67**, 3740 (2020).

⁵³⁰Y. Zhao, H. Niwa, and T. Kimoto, *Japanese Journal of Applied Physics* **58**, 018001 (2019).

⁵³¹J. E. Green, W. S. Loh, A. R. J. Marshall, B. K. Ng, R. C. Tozer, J. P. R. David, S. I. Soloviev, and P. M. Sandvik, *IEEE Transactions on Electron Devices* **59**, 1030 (2012).

⁵³²P. L. Cheang, E. K. Wong, and L. L. Teo, *Journal of Electronic Materials* **50**, 5259 (2021).

⁵³³C. Sun, A. You, and E. Wong, *The European Physical Journal Applied Physics* **60**, 10204 (2012).

⁵³⁴K. Brennan, E. Bellotti, M. Farahmand, H.-E. Nilsson, P. Ruden, and Yumin Zhang, *IEEE Transactions on Electron Devices* **47**, 1882 (2000).

⁵³⁵R. Fujita, K. Konaga, Y. Ueoka, Y. Kamakura, N. Mori, and T. Kotani, in *2017 International Conference on Simulation of Semiconductor Processes and Devices (SISPAD)* (IEEE, Kamakura, Japan, 2017) pp. 289–292.

⁵³⁶H.-E. Nilsson, E. Bellotti, K. Brennan, and M. Hjelm, *Materials Science Forum* **338–342**, 765 (2000).

⁵³⁷C. C. Sun, A. H. You, and E. K. Wong, in *MALAYSIA ANNUAL PHYSICS CONFERENCE 2010 (PERFIK-2010)* (Damai Laut, (Malaysia), 2011) pp. 277–280.

⁵³⁸H. Tanaka, T. Kimoto, and N. Mori, *Journal of Applied Physics* **131**, 225701 (2022).

⁵³⁹L. Zhu, P. A. Losee, T. P. Chow, K. A. Jones, C. Scozzie, M. H. Ervin, P. B. Shah, M. A. Derenge, R. Vispute, T. Venkatesan, and A. K. Agarwal, *Materials Science Forum* **527–529**, 1367 (2006).

⁵⁴⁰A. Concannon, F. Piccinini, A. Mathewson, and C. Lombardi, in *Proceedings of International Electron Devices Meeting* (IEEE, Washington, DC, USA, 1995) pp. 289–292.

⁵⁴¹K. Katayama and T. Toyabe, in *International Technical Digest on Electron Devices Meeting* (IEEE, Washington, DC, USA, 1989) pp. 135–138.

⁵⁴²R. Raghunathan and B. J. Baliga, *Applied Physics Letters* **72**, 3196 (1998).

⁵⁴³P. Mukherjee, S. K. R. Hossain, A. Acharyya, and A. Biswas, *Applied Physics A* **126**, 127 (2020).

⁵⁴⁴P. Mukherjee, D. Chatterjee, and A. Acharyya, *Journal of Computational Electronics* **16**, 503 (2017).

⁵⁴⁵D. C. Sheridan, G. Niu, J. Merrett, J. D. Cressler, C. Ellis, and C.-C. Tin, *Solid-State Electronics* **44**, 1367 (2000).

⁵⁴⁶D. Brosselard, Pierre ; Planson, *Conception, Réalisation et Caractérisation d'interrupteurs (Thyristors et JFETs) Haute Tension (5kV) En Carbure de Silicium*, Ph.D. thesis, Université

de Lyon, Lyon (2004).

⁵⁴⁷S. Bellone and L. Di Benedetto, *IEEE Transactions on Power Electronics* **29**, 2174 (2014).

⁵⁴⁸K. Bertilsson, H.-E. Nilsson, and C. Petersson, in *COMPEL 2000. 7th Workshop on Computers in Power Electronics. Proceedings (Cat. No.00TH8535)* (IEEE, Blacksburg, VA, USA, 2000) pp. 118–120.

⁵⁴⁹C. Banc, E. Bano, T. Ouisse, O. Noblanc, and C. Brylinski, *Materials Science Forum* **389–393**, 1371 (2002).

⁵⁵⁰A. Kyuregyan and S. Yurkov, *Sov. Phys. Solid State* **23**, 1126 (1989).

⁵⁵¹K. Y. Cheong, S. Dimitrijev, and Jisheng Han, *IEEE Transactions on Electron Devices* **50**, 1433 (2003).

⁵⁵²J. S. Cheong, M. M. Hayat, Xinxin Zhou, and J. P. R. David, *IEEE Transactions on Electron Devices* **62**, 1946 (2015).

⁵⁵³T. Kimoto, M. Kaneko, K. Tachiki, K. Ito, R. Ishikawa, X. Chi, D. Stefanakis, T. Kobayashi, and H. Tanaka, in *2021 IEEE International Electron Devices Meeting (IEDM)* (IEEE, San Francisco, CA, USA, 2021) pp. 36.1.1–36.1.4.

⁵⁵⁴A. O. Konstantinov, N. Nordell, Q. Wahab, and U. Lindefelt, *Applied Physics Letters* **73**, 1850 (1998).

⁵⁵⁵J. W. Palmour, C. H. Carter, C. E. Weitzel, and K. J. Nordquist, *MRS Proceedings* **339**, 133 (1994).

⁵⁵⁶P. G. Neudeck and C. Fazi, , 5 (1999).

⁵⁵⁷G. Wei, Y. C. Liang, and G. S. Samudra, in *8th International Conference on Power Electronics - ECCE Asia* (IEEE, Jeju, Korea (South), 2011) pp. 1464–1468.

⁵⁵⁸P. G. Neudeck, *Journal of Electronic Materials* **27**, 317 (1998).

⁵⁵⁹T. Kimoto, H. Niwa, T. Okuda, E. Saito, Y. Zhao, S. Asada, and J. Suda, *Journal of Physics D: Applied Physics* **51**, 363001 (2018).

⁵⁶⁰J. Palmour, R. Singh, R. Glass, O. Kordina, and C. Carter, in *Proceedings of 9th International Symposium on Power Semiconductor Devices and IC's* (IEEE, Weimar, Germany, 1997) pp. 25–32.

⁵⁶¹D. Peters, P. Friedrichs, H. Mitlehner, R. Schoerner, U. Weinert, B. Weis, and D. Stephani, in *12th International Symposium on Power Semiconductor Devices & ICs. Proceedings (Cat. No.00CH37094)* (IEEE, Toulouse, France, 2000) pp. 241–244.

⁵⁶²R. Singh, J. Cooper, M. Melloch, T. Chow, and J. Palmour, *IEEE Transactions on Electron Devices* **49**, 665 (2002).

⁵⁶³O. Slobodyan, J. Flicker, J. Dickerson, J. Shoemaker, A. Binder, T. Smith, S. Goodnick, R. Kaplar, and M. Hollis, *Journal of Materials Research* **37**, 849 (2022).

⁵⁶⁴W. Loh, J. David, B. Ng, S. I. Soloviev, P. M. Sandvik, J. Ng, and C. M. Johnson, *Materials Science Forum* **615–617**, 311 (2009).

⁵⁶⁵R. K. Sharma, P. Hazdra, and S. Popelka, *IEEE Transactions on Nuclear Science* **62**, 534 (2015).

⁵⁶⁶X. Zhang and N. You, in *2018 IEEE 3rd International Conference on Integrated Circuits and Microsystems (ICICM)* (IEEE, Shanghai, 2018) pp. 60–63.

⁵⁶⁷H.-Y. Cha, S. Soloviev, S. Zelakiewicz, P. Waldrab, and P. M. Sandvik, *IEEE Sensors Journal* **8**, 233 (2008).

⁵⁶⁸P. Steinmann, B. Hull, I.-H. Ji, D. Lichtenwalner, and E. Van Brunt, *Journal of Applied Physics* **133**, 235705 (2023).

⁵⁶⁹R. Raghunathan and B. Baliga, in *Proceedings of 9th International Symposium on Power Semiconductor Devices and IC's* (IEEE, Weimar, Germany, 1997) pp. 173–176.

⁵⁷⁰H.-E. Nilsson, A. Martinez, U. Sannemo, M. Hjelm, E. Bellotti, and K. Brennan, *Physica B: Condensed Matter* **314**, 68 (2002).

⁵⁷¹P. P. Ruden, E. Bellotti, H.-E. Nilsson, and K. F. Brennan, *Journal of Applied Physics* **88**, 1488 (2000).

⁵⁷²B. Ng, F. Yan, J. David, R. Tozer, G. Rees, C. Qin, and J. Zhao, *IEEE Photonics Technology Letters* **14**, 1342 (2002).

⁵⁷³X. Guo, A. Beck, Xiaowei Li, J. Campbell, D. Emerson, and J. Sumakeris, *IEEE Journal of Quantum Electronics* **41**, 562 (2005).

⁵⁷⁴R. Trew, J.-B. Yan, and P. Mock, *Proceedings of the IEEE* **79**, 598 (1991).

⁵⁷⁵A. Akturk, N. Goldsman, S. Aslam, J. Sigwarth, and F. Herrero, *Journal of Applied Physics* **104**, 026101 (2008).

⁵⁷⁶T. Hatakeyama, T. Watanabe, K. Kojima, N. Sano, T. Shinohe, and K. Arai, *MRS Proceedings* **815**, J9.3 (2004).

⁵⁷⁷T. Hatakeyama, J. Nishio, C. Ota, and T. Shinohe, in *2005 International Conference On Simulation of Semiconductor Processes and Devices* (IEEE, Tokyo, Japan, 2005) pp. 171–174.

⁵⁷⁸C. Wang, X. Li, L. Li, X. Deng, W. Zhang, L. Zheng, Y. Zou, W. Qian, Z. Li, and B. Zhang, [IEEE Electron Device Letters **43**, 2025 \(2022\)](#).

⁵⁷⁹Y. Wang, J.-c. Zhou, M. Lin, X.-j. Li, J.-Q. Yang, and F. Cao, [IEEE Journal of the Electron Devices Society **10**, 373 \(2022\)](#).

⁵⁸⁰C. C. Sun, A. H. You, and E. K. Wong, in [2012 10th IEEE International Conference on Semiconductor Electronics \(ICSE\)](#) (IEEE, Kuala Lumpur, Malaysia, 2012) pp. 366–369.

⁵⁸¹J. Hasegawa, L. Pace, L. V. Phung, M. Hatano, and D. Planson, [IEEE Transactions on Electron Devices **64**, 1203 \(2017\)](#).

⁵⁸²A. E. Arvanitopoulos, M. Antoniou, S. Perkins, M. Jennings, M. B. Guadas, K. N. Gyftakis, and N. Lophitis, [IEEE Transactions on Industry Applications **55**, 4080 \(2019\)](#).

⁵⁸³W. Loh, C. M. Johnson, J. Ng, P. M. Sandvik, S. Arthur, S. I. Soloviev, and J. David, [Materials Science Forum **556–557**, 339 \(2007\)](#).

⁵⁸⁴W. S. Loh, E. Z. J. Goh, K. Vassilevski, I. Nikitina, J. P. R. David, N. G. Wright, and C. M. Johnson, [MRS Proceedings **1069**, 1069 \(2008\)](#).

⁵⁸⁵A. Ivanov, M. Mynbaeva, A. Sadokhin, N. Strokan, and A. Lebedev, [Nuclear Instruments and Methods in Physics Research Section A: Accelerators, Spectrometers, Detectors and Associated Equipment **606**, 605 \(2009\)](#).

⁵⁸⁶J. A. McPherson, C. W. Hitchcock, T. Paul Chow, W. Ji, and A. A. Woodworth, [IEEE Transactions on Nuclear Science **68**, 651 \(2021\)](#).

⁵⁸⁷T. Hayashi, K. Asano, J. Suda, and T. Kimoto, [Journal of Applied Physics **109**, 114502 \(2011\)](#).

⁵⁸⁸T. Hayashi, K. Asano, J. Suda, and T. Kimoto, [Journal of Applied Physics **109**, 014505 \(2011\)](#).

⁵⁸⁹P. Ščajev and K. Jarašiūnas, [Journal of Physics D: Applied Physics **46**, 265304 \(2013\)](#).

⁵⁹⁰W. Mao, C. Cui, H. Xiong, N. Zhang, S. Liu, M. Dou, L. Song, D. Yang, and X. Pi, [Semiconductor Science and Technology **38**, 073001 \(2023\)](#).

⁵⁹¹D. Schroder, [IEEE Transactions on Electron Devices **29**, 1336 \(1982\)](#).

⁵⁹²Y. Arafat, F. M. Mohammedy, and M. M. Shahidul Hassan, [International Journal of Optoelectronic Engineering **2**, 5 \(2012\)](#).

⁵⁹³K. Nagaya, T. Hirayama, T. Tawara, K. Murata, H. Tsuchida, A. Miyasaka, K. Kojima, T. Kato, H. Okumura, and M. Kato, [Journal of Applied Physics **128**, 105702 \(2020\)](#).

⁵⁹⁴P. T. Landsberg, [Recombination in Semiconductors](#), 1st ed. (Cambridge University Press, 1992).

⁵⁹⁵A. Hangleiter, [Physical Review B **37**, 2594 \(1988\)](#).

⁵⁹⁶W. Shockley and W. T. Read, [Physical Review **87**, 835 \(1952\)](#).

⁵⁹⁷I. D. Booker, *Carrier Lifetime Relevant Deep Levels in SiC*, Linköping Studies in Science and Technology. Dissertations, Vol. 1714 (Linköping University Electronic Press, Linköping, 2015).

⁵⁹⁸H. C. De Graaff and F. M. Klaassen, *Compact Transistor Modelling for Circuit Design*, edited by S. Selberherr, Computational Microelectronics (Springer Vienna, Vienna, 1990).

⁵⁹⁹V. N. Abakumov, V. I. Perel, and I. N. Yassievich, SOVIET PHYSICS SEMICONDUCTORS-USSR **12**, 1 (1978).

⁶⁰⁰M. Suproniuk, M. Wierzbowski, and P. Paziewski, *Scientific Reports* **10**, 11865 (2020).

⁶⁰¹J. Fossum and D. Lee, *Solid-State Electronics* **25**, 741 (1982).

⁶⁰²T. Mori, M. Kato, H. Watanabe, M. Ichimura, E. Arai, S. Sumie, and H. Hashizume, *Japanese Journal of Applied Physics* **44**, 8333 (2005).

⁶⁰³H. M. Ayedh, R. Nipoti, A. Hallén, and B. G. Svensson, *Journal of Applied Physics* **122**, 025701 (2017).

⁶⁰⁴Y. Cui, J. Li, K. Zhou, X. Zhang, and G. Sun, *Diamond and Related Materials* **92**, 25 (2019).

⁶⁰⁵J. Erlekampf, B. Kallinger, J. Weiße, M. Rommel, P. Berwian, J. Friedrich, and T. Erlbacher, *Journal of Applied Physics* **126**, 045701 (2019).

⁶⁰⁶J. Erlekampf, M. Rommel, K. Rosshirt-Lilla, B. Kallinger, P. Berwian, J. Friedrich, and T. Erlbacher, *Journal of Crystal Growth* **560–561**, 126033 (2021).

⁶⁰⁷A. Galeckas, V. Grivickas, J. Linnros, H. Bleichner, and C. Hallin, *Journal of Applied Physics* **81**, 3522 (1997).

⁶⁰⁸A. Galeckas, J. Linnros, M. Frischholz, K. Rottner, N. Nordell, S. Karlsson, and V. Grivickas, *Materials Science and Engineering: B* **61–62**, 239 (1999).

⁶⁰⁹A. Galeckas, J. Linnros, M. Frischholz, and V. Grivickas, *Applied Physics Letters* **79**, 365 (2001).

⁶¹⁰M. Kato, M. Kawai, T. Mori, M. Ichimura, S. Sumie, and H. Hashizume, *Japanese Journal of Applied Physics* **46**, 5057 (2007).

⁶¹¹P. B. Klein, *Journal of Applied Physics* **103**, 033702 (2008).

⁶¹²O. Kordina, J. P. Bergman, C. Hallin, and E. Janzén, *Applied Physics Letters* **69**, 679 (1996).

⁶¹³L. Lilja, I. D. Booker, J. U. Hassan, E. Janzén, and J. P. Bergman, *Journal of Crystal Growth* **381**, 43 (2013).

⁶¹⁴J. Hassan and J. P. Bergman, *Journal of Applied Physics* **105**, 123518 (2009).

⁶¹⁵H. Tsuchida, I. Kamata, T. Miyazawa, M. Ito, X. Zhang, and M. Nagano, *Materials Science in Semiconductor Processing* **78**, 2 (2018).

⁶¹⁶R. Zhang, R. Hong, J. Han, H. Ting, X. Li, J. Cai, X. Chen, D. Fu, D. Lin, M. Zhang, S. Wu, Y. Zhang, Z. Wu, and F. Zhang, *Chinese Physics B* **32**, 067205 (2023).

⁶¹⁷K. Murata, T. Tawara, A. Yang, R. Takanashi, T. Miyazawa, and H. Tsuchida, *Journal of Applied Physics* **126**, 045711 (2019).

⁶¹⁸N. A. Mahadik, R. E. Stahlbush, P. B. Klein, A. Khachatrian, S. Buchner, and S. G. Block, *Applied Physics Letters* **111**, 221904 (2017).

⁶¹⁹J. R. Jenny, D. P. Malta, V. F. Tsvetkov, M. K. Das, H. McD. Hobgood, C. H. Carter, R. J. Kumar, J. M. Borrego, R. J. Gutmann, and R. Aavikko, *Journal of Applied Physics* **100**, 113710 (2006).

⁶²⁰P. Grivickas, A. Galeckas, J. Linnros, M. Syväjärvi, R. Yakimova, V. Grivickas, and J. Tellefsen, *Materials Science in Semiconductor Processing* **4**, 191 (2001).

⁶²¹T. Hayashi, K. Asano, J. Suda, and T. Kimoto, *Journal of Applied Physics* **112**, 064503 (2012).

⁶²²S. Ichikawa, K. Kawahara, J. Suda, and T. Kimoto, *Applied Physics Express* **5**, 101301 (2012).

⁶²³N. Kaji, H. Niwa, J. Suda, and T. Kimoto, *IEEE Transactions on Electron Devices* **62**, 374 (2015).

⁶²⁴K. Kawahara, J. Suda, and T. Kimoto, *Journal of Applied Physics* **111**, 053710 (2012).

⁶²⁵T. Kimoto, K. Danno, and J. Suda, *physica status solidi (b)* **245**, 1327 (2008).

⁶²⁶T. Kimoto, T. Hiyoshi, T. Hayashi, and J. Suda, *Journal of Applied Physics* **108**, 083721 (2010).

⁶²⁷T. Miyazawa and H. Tsuchida, *Journal of Applied Physics* **113**, 083714 (2013).

⁶²⁸T. Okuda, T. Kimoto, and J. Suda, *Applied Physics Express* **6**, 121301 (2013).

⁶²⁹T. Okuda, T. Miyazawa, H. Tsuchida, T. Kimoto, and J. Suda, *Applied Physics Express* **7**, 085501 (2014).

⁶³⁰L. Storasta and H. Tsuchida, *Applied Physics Letters* **90**, 062116 (2007).

⁶³¹L. Storasta, H. Tsuchida, T. Miyazawa, and T. Ohshima, *Journal of Applied Physics* **103**, 013705 (2008).

⁶³²T. Tawara, T. Miyazawa, M. Ryo, M. Miyazato, T. Fujimoto, K. Takenaka, S. Matsunaga, M. Miyajima, A. Otsuki, Y. Yonezawa, T. Kato, H. Okumura, T. Kimoto, and H. Tsuchida, *Journal of Applied Physics* **120**, 115101 (2016).

⁶³³M. Wang, M. Yang, W. Liu, S. Yang, J. Liu, C. Han, L. Geng, and Y. Hao, *Applied Physics Express* **13**, 111002 (2020).

⁶³⁴T. Hiyoshi and T. Kimoto, *Applied Physics Express* **2**, 041101 (2009).

⁶³⁵G. Yan, X. Liu, W. Zhao, L. Wang, Z. Fu, Q. Zhang, C. Xiao, Q. Yin, G. Sun, and Y. Zeng, in *2024 21st China International Forum on Solid State Lighting & 2024 10th International Forum on Wide Bandgap Semiconductors (SSLCHINA: IFWS)* (IEEE, Suzhou, China, 2024) pp. 37–40.

⁶³⁶V. Khemka, R. Patel, N. Ramungul, T. P. Chow, M. Ghezzo, and J. Kretchmer, *Journal of Electronic Materials* **28**, 167 (1999).

⁶³⁷D. Åberg, A. Hallén, and B. Svensson, *Physica B: Condensed Matter* **273–274**, 672 (1999).

⁶³⁸V. V. Afanas'ev, A. Stesmans, M. Bassler, G. Pensl, and M. J. Schulz, *Applied Physics Letters* **76**, 336 (2000).

⁶³⁹G. Alfieri, E. V. Monakhov, B. G. Svensson, and M. K. Linnarsson, *Journal of Applied Physics* **98**, 043518 (2005).

⁶⁴⁰G. Alfieri and A. Mihaila, *Journal of Physics: Condensed Matter* **32**, 465703 (2020).

⁶⁴¹M. Anikin, A. A. Lebedev, A. Syrkin, and A. Suvorov, *Sov. Phys. Semicond.* **19**, 1847 (1985).

⁶⁴²T. Ayalew, T. Grasser, H. Kosina, and S. Selberherr, *Materials Science Forum* **483–485**, 845 (2005).

⁶⁴³H. M. Ayedh, V. Bobal, R. Nipoti, A. Hallén, and B. G. Svensson, *Materials Science Forum* **858**, 331 (2016).

⁶⁴⁴M. E. Bathen, A. Galeckas, J. Müting, H. M. Ayedh, U. Grossner, J. Coutinho, Y. K. Frodason, and L. Vines, *npj Quantum Information* **5**, 111 (2019).

⁶⁴⁵J. P. Bergman, O. Kordina, and E. Janzén, *physica status solidi (a)* **162**, 65 (1997).

⁶⁴⁶I. D. Booker, E. Janzén, N. T. Son, J. Hassan, P. Stenberg, and E. Ö. Sveinbjörnsson, *Journal of Applied Physics* **119**, 235703 (2016).

⁶⁴⁷T. Brodar, L. Bakrač, I. Capan, T. Ohshima, L. Snoj, V. Radulović, and Ž. Pastuović, *Crystals* **10**, 845 (2020).

⁶⁴⁸I. Capan, T. Brodar, J. Coutinho, T. Ohshima, V. P. Markevich, and A. R. Peaker, *Journal of Applied Physics* **124**, 245701 (2018).

⁶⁴⁹I. Capan, T. Brodar, Ž. Pastuović, R. Siegele, T. Ohshima, S.-i. Sato, T. Makino, L. Snoj, V. Radulović, J. Coutinho, V. J. B. Torres, and K. Demmouche, *Journal of Applied Physics* **123**, 161597 (2018).

⁶⁵⁰M. A. Capano, J. A. Cooper, M. R. Melloch, A. Saxler, and W. C. Mitchel, *Journal of Applied Physics* **87**, 8773 (2000).

⁶⁵¹A. Castaldini, A. Cavallini, L. Rigutti, and F. Nava, *Applied Physics Letters* **85**, 3780 (2004).

⁶⁵²S. K. Chaudhuri, O. Karadavut, J. W. Kleppinger, and K. C. Mandal, *Journal of Applied Physics* **130**, 074501 (2021).

⁶⁵³C. J. Cochrane, P. M. Lenahan, and A. J. Lelis, *Applied Physics Letters* **90**, 123501 (2007).

⁶⁵⁴C. J. Cochrane, P. M. Lenahan, and A. J. Lelis, *Journal of Applied Physics* **105**, 064502 (2009).

⁶⁵⁵T. Dalibor, G. Pensl, T. Kimoto, H. Matsunami, S. Sridhara, R. P. Devaty, and W. J. Choyke, *Diamond and Related Materials* **6**, 1333 (1997).

⁶⁵⁶T. Dalibor and M. Schulz, eds., *Numerical Data and Functional Relationships in Science and Technology. Subvol. A2: Gruppe 3: Kristall- Und Festkörperphysik = Group 3: @Crystal and Solid State Physics Vol. 41, Semiconductors Impurities and Defects in Group IV Elements, IV-IV and III-V Compounds. Part Beta: Group IV-IV and III-V Compounds / Ed. by M. Schulz; Authors: T. Dalibor*, Vol. 41 (Springer, Berlin Heidelberg, 2003).

⁶⁵⁷K. Danno, D. Nakamura, and T. Kimoto, *Applied Physics Letters* **90**, 202109 (2007).

⁶⁵⁸K. Danno and T. Kimoto, *Journal of Applied Physics* **100**, 113728 (2006).

⁶⁵⁹M. L. David, G. Alfieri, E. M. Monakhov, A. Hallén, C. Blanchard, B. G. Svensson, and J. F. Barbot, *Journal of Applied Physics* **95**, 4728 (2004).

⁶⁶⁰J. Doyle, M. Aboelfotoh, B. Svensson, A. Schöner, and N. Nordell, *Diamond and Related Materials* **6**, 1388 (1997).

⁶⁶¹S. Greulich-Weber, *physica status solidi (a)* **162**, 95 (1997).

⁶⁶²P. Hazdra and S. Popelka, *Materials Science Forum* **897**, 463 (2017).

⁶⁶³P. Hazdra, P. Smrkovsky, J. Vobecky, and A. Mihaila, *IEEE Transactions on Electron Devices* **68**, 202 (2021).

⁶⁶⁴C. G. Hemmingsson, N. T. Son, A. Ellison, J. Zhang, and E. Janzén, *Physical Review B* **58**, R10119 (1998).

⁶⁶⁵H. K. Henisch and R. Roy, *Silicon Carbide—1968: Proceedings of the International Conference on Silicon Carbide, University Park, Pennsylvania, October 20-23, 1968* (Elsevier, 2013).

⁶⁶⁶T. Hornos, A. Gali, and B. G. Svensson, *Materials Science Forum* **679–680**, 261 (2011).

⁶⁶⁷Y. Huang, R. Wang, Y. Zhang, D. Yang, and X. Pi, *Chinese Physics B* **31**, 056108 (2022).

⁶⁶⁸Y. Huang, R. Wang, Y. Qian, Y. Zhang, D. Yang, and X. Pi, *Chinese Physics B* **31**, 046104 (2022).

⁶⁶⁹S. W. Huh, J. J. Sumakeris, A. Polyakov, M. Skowronski, P. B. Klein, B. Shanabrook, and M. J. O'Loughlin, *Materials Science Forum* **527–529**, 493 (2006).

⁶⁷⁰H. Itoh, T. Troffer, and G. Pensl, *Materials Science Forum* **264–268**, 685 (1998).

⁶⁷¹G. Izzo, G. Litrico, L. Calcagno, G. Foti, and F. La Via, *Journal of Applied Physics* **104**, 093711 (2008).

⁶⁷²S. Kagamihara, H. Matsuura, T. Hatakeyama, T. Watanabe, M. Kushibe, T. Shinohe, and K. Arai, *Journal of Applied Physics* **96**, 5601 (2004).

⁶⁷³L. Kasamakova-Kolaklieva, L. Storasta, I. G. Ivanov, B. Magnusson, S. Contreras, C. Consejo, J. Pernot, M. Zielinski, and E. Janzén, *Materials Science Forum* **457–460**, 677 (2004).

⁶⁷⁴T. Kimoto, A. Itoh, H. Matsunami, S. Sridhara, L. L. Clemen, R. P. Devaty, W. J. Choyke, T. Dalibor, C. Peppermüller, and G. Pensl, *Applied Physics Letters* **67**, 2833 (1995).

⁶⁷⁵T. Kimoto, K. Hashimoto, and H. Matsunami, *Japanese Journal of Applied Physics* **42**, 7294 (2003).

⁶⁷⁶T. Kimoto, A. Itoh, and H. Matsunami, *physica status solidi (b)* **202**, 247 (1997).

⁶⁷⁷P. B. Klein, B. V. Shanabrook, S. W. Huh, A. Y. Polyakov, M. Skowronski, J. J. Sumakeris, and M. J. O’Loughlin, *Applied Physics Letters* **88**, 052110 (2006).

⁶⁷⁸M. Laube, F. Schmid, K. Semmelroth, G. Pensl, R. P. Devaty, W. J. Choyke, G. Wagner, and M. Maier, in *Silicon Carbide*, edited by W. J. Choyke, H. Matsunami, and G. Pensl (Springer Berlin Heidelberg, Berlin, Heidelberg, 2004) pp. 493–515.

⁶⁷⁹F. La Via, G. Galvagno, F. Roccaforte, A. Ruggiero, and L. Calcagno, *Applied Physics Letters* **87**, 142105 (2005).

⁶⁸⁰D. J. Lichtenwalner, J. H. Park, S. Rogers, H. Dixit, A. Scholtze, S. Bubel, and S. H. Ryu, *Materials Science Forum* **1089**, 3 (2023).

⁶⁸¹K. C. Mandal, J. W. Kleppinger, and S. K. Chaudhuri, *Micromachines* **11**, 254 (2020).

⁶⁸²A. Martinez, U. Lindefelt, M. Hjelm, and H.-E. Nilsson, *Journal of Applied Physics* **91**, 1359 (2002).

⁶⁸³H. Matsuura, M. Komeda, S. Kagamihara, H. Iwata, R. Ishihara, T. Hatakeyama, T. Watanabe, K. Kojima, T. Shinohe, and K. Arai, *Journal of Applied Physics* **96**, 2708 (2004).

⁶⁸⁴H. Matsuura, T. K. Tsunenobu Kimoto, and H. M. Hiroyuki Matsunami, *Japanese Journal of Applied Physics* **38**, 4013 (1999).

⁶⁸⁵P. G. Muzykov, R. M. Krishna, and K. C. Mandal, *Journal of Applied Physics* **111**, 014910 (2012).

⁶⁸⁶Y. Negoro, T. Kimoto, and H. Matsunami, *Electronics and Communications in Japan (Part II: Electronics)* **86**, 44 (2003).

⁶⁸⁷K. V. Nguyen, M. A. Mannan, and K. C. Mandal, *IEEE Transactions on Nuclear Science* **62**, 3199 (2015).

⁶⁸⁸A. Parisini and R. Nipoti, *Journal of Applied Physics* **114**, 243703 (2013).

⁶⁸⁹Ž. Pastuović, R. Siegele, I. Capan, T. Brodar, S.-i. Sato, and T. Ohshima, *Journal of Physics: Condensed Matter* **29**, 475701 (2017).

⁶⁹⁰F. Schmid, M. Krieger, M. Laube, G. Pensl, and G. Wagner, in *Silicon Carbide*, edited by W. J. Choyke, H. Matsunami, and G. Pensl (Springer Berlin Heidelberg, Berlin, Heidelberg, 2004) pp. 517–536.

⁶⁹¹S. R. Smith, A. O. Evwaraye, W. C. Mitchel, and M. A. Capano, *Journal of Electronic Materials* **28**, 190 (1999).

⁶⁹²N. T. Son, Mt. Wagner, C. G. Hemmingsson, L. Storasta, B. Magnusson, W. M. Chen, S. Greulich-Weber, J.-M. Spaeth, and E. Janzén, in *Silicon Carbide*, edited by W. J. Choyke, H. Matsunami, and G. Pensl (Springer Berlin Heidelberg, Berlin, Heidelberg, 2004) pp. 461–492.

⁶⁹³N. T. Son, X. T. Trinh, L. S. Løvlie, B. G. Svensson, K. Kawahara, J. Suda, T. Kimoto, T. Umeda, J. Isoya, T. Makino, T. Ohshima, and E. Janzén, *Physical Review Letters* **109**, 187603 (2012).

⁶⁹⁴L. Storasta, J. P. Bergman, E. Janzén, A. Henry, and J. Lu, *Journal of Applied Physics* **96**, 4909 (2004).

⁶⁹⁵L. Storasta, P. Bergman, E. Janzén, and C. Hallin, *Materials Science Forum* **389–393**, 549 (2002).

⁶⁹⁶A. Suzuki, H. Matsunami, and T. Tanaka, *Japanese Journal of Applied Physics* **12**, 1083 (1973).

⁶⁹⁷Y. Tanaka, N. Kobayashi, H. Okumura, R. Suzuki, T. Ohdaira, M. Hasegawa, M. Ogura, S. Yoshida, and H. Tanoue, *Materials Science Forum* **338–342**, 909 (2000).

⁶⁹⁸T. Tawara, H. Tsuchida, S. Izumi, I. Kamata, and K. Izumi, *Materials Science Forum* **457–460**, 565 (2004).

⁶⁹⁹P. Terziyska, C. Blanc, J. Pernot, H. Peyre, S. Contreras, G. Bastide, J. L. Robert, J. Camassel, E. Morvan, C. Dua, and C. C. Brylinski, *physica status solidi (a)* **195**, 243 (2003).

⁷⁰⁰T. Troffer, M. Schadt, T. Frank, H. Itoh, G. Pensl, J. Heindl, H. P. Strunk, and M. Maier, *physica status solidi (a)* **162**, 277 (1997).

⁷⁰¹X. Xu, L. Zhang, L. Li, Z. Li, J. Li, J. Zhang, and P. Dong, *Discover Nano* **18**, 128 (2023).

⁷⁰²X. Yan, P. Li, L. Kang, S.-H. Wei, and B. Huang, *Journal of Applied Physics* **127**, 085702 (2020).

⁷⁰³J. Zhang, L. Storasta, J. P. Bergman, N. T. Son, and E. Janzén, *Journal of Applied Physics* **93**, 4708 (2003).

⁷⁰⁴B. Zippelius, J. Suda, and T. Kimoto, *Journal of Applied Physics* **111**, 033515 (2012).

⁷⁰⁵P. Gaggl, J. Burin, A. Gsponer, S.-E. Waid, R. Thalmeier, and T. Bergauer, *Nuclear Instruments and Methods in Physics Research Section A: Accelerators, Spectrometers, Detectors and Associated Equipment* **1070**, 170015 (2025).

⁷⁰⁶S. Yamashita and T. Kimoto, *Applied Physics Express* **13**, 011006 (2020).

⁷⁰⁷M. Kato, A. Ogawa, L. Han, and T. Kato, *Materials Science in Semiconductor Processing* **170**, 107980 (2024).

⁷⁰⁸R. N. Hall, *Physical Review* **87**, 387 (1952).

⁷⁰⁹L. Lilja, I. Farkas, I. Booker, J. Ul Hassan, E. Janzén, and J. P. Bergman, *Materials Science Forum* **897**, 238 (2017).

⁷¹⁰D. Scharfetter and R. Johnston, *IEEE Transactions on Electron Devices* **14**, 634 (1967).

⁷¹¹D. Roulston, N. Arora, and S. Chamberlain, *IEEE Transactions on Electron Devices* **29**, 284 (1982).

⁷¹²M. Law, E. Solley, M. Liang, and D. Burk, *IEEE Electron Device Letters* **12**, 401 (1991).

⁷¹³M. Tyagi and R. Van Overstraeten, *Solid-State Electronics* **26**, 577 (1983).

⁷¹⁴G. Liaugaudas, D. Dargis, P. Kwasnicki, H. Peyre, R. Arvinte, S. Juillaguet, M. Zielinski, and K. Jarašiūnas, *Materials Science Forum* **821–823**, 249 (2015).

⁷¹⁵H. Shao, X. Yang, D. Wang, X. Li, X. Chen, G. Hu, H. Li, X. Xiong, X. Xie, X. Hu, and X. Xu, *Journal of Electronic Materials* **53**, 2429 (2024).

⁷¹⁶S. Sapienza, G. Sozzi, D. Santoro, P. Cova, N. Delmonte, G. Verrini, and G. Chiorboli, *Microelectronics Reliability* **113**, 113937 (2020).

⁷¹⁷V. Meyers, D. Mauch, J. Dickens, and A. Neuber, *Journal of Applied Physics* **121**, 115703 (2017).

⁷¹⁸P. B. Klein, R. Myers-Ward, K.-K. Lew, B. L. VanMil, C. R. Eddy, D. K. Gaskill, A. Shrivastava, and T. S. Sudarshan, *Journal of Applied Physics* **108**, 033713 (2010).

⁷¹⁹M. E. Levenshtein, P. A. Ivanov, M. S. Boltovets, V. A. Krivutsa, J. W. Palmour, M. K. Das, and B. A. Hull, *Solid-State Electronics* **49**, 1228 (2005).

720 A. K. Agarwal, P. A. Ivanov, M. E. Levenshtein, J. W. Palmour, S. L. Rumyantsev, and S.-H. Ryu, *Semiconductor Science and Technology* **16**, 260 (2001).

721 P. Ivanov, M. Levenshtein, K. Irvine, O. Kordina, J. Palmour, S. Rumyantsev, and R. Singh, *Electronics Letters* **35**, 1382 (1999).

722 P. Ivanov, M. Levenshtein, A. Agarwal, S. Krishnaswami, and J. Palmour, *IEEE Transactions on Electron Devices* **53**, 1245 (2006).

723 A. Udal and E. Velmre, *Materials Science Forum* **556–557**, 375 (2007).

724 R. Wu and A. Peaker, *Solid-State Electronics* **25**, 643 (1982).

725 H. Goebel and K. Hoffmann, in *Proceedings of the 4th International Symposium on Power Semiconductor Devices and Ics* (IEEE, Tokyo, Japan, 1992) pp. 130–135.

726 D. Klaassen, *Solid-State Electronics* **35**, 961 (1992).

727 A. Schenk, *Solid-State Electronics* **35**, 1585 (1992).

728 T. Tamaki, G. G. Walden, Y. Sui, and J. A. Cooper, *IEEE Transactions on Electron Devices* **55**, 1928 (2008).

729 K. Gulbinas, V. Grivickas, H. P. Mahabadi, M. Usman, and A. Hallén, *Materials Science* **17**, 119 (2011).

730 M. Kato, A. Yoshida, and M. Ichimura, *Japanese Journal of Applied Physics* **51**, 02BP12 (2012).

731 M. Kato, Z. Xinchi, K. Kohama, S. Fukaya, and M. Ichimura, *Journal of Applied Physics* **127**, 195702 (2020).

732 Y. Mori, M. Kato, and M. Ichimura, *Journal of Physics D: Applied Physics* **47**, 335102 (2014).

733 G. Y. Chung, M. J. Loboda, M. Marinella, D. Schroder, T. Isaacs-Smith, and J. R. Williams, *Materials Science Forum* **615–617**, 283 (2009).

734 S. Asada, J. Suda, and T. Kimoto, *IEEE Transactions on Electron Devices* **65**, 4786 (2018).

735 T. Hayashi, T. Okuda, J. Suda, and T. Kimoto, *Japanese Journal of Applied Physics* **53**, 111301 (2014).

736 Y. Ichikawa, M. Ichimura, T. Kimoto, and M. Kato, *ECS Journal of Solid State Science and Technology* **7**, Q127 (2018).

737 T. Kimoto, Y. Nanen, T. Hayashi, and J. Suda, *Applied Physics Express* **3**, 121201 (2010).

738 K. Nonaka, A. Horiuchi, Y. Negoro, K. Iwanaga, S. Yokoyama, H. Hashimoto, M. Sato, Y. Maeyama, M. Shimizu, and H. Iwakuro, *physica status solidi (a)* **206**, 2457 (2009).

⁷³⁹M. S. Boltovets, V. V. Basanets, N. Camara, V. A. Krivutsa, and K. Zekentes, *Materials Science Forum* **527–529**, 1375 (2006).

⁷⁴⁰B. Buono, R. Ghandi, M. Domeij, B. G. Malm, C.-M. Zetterling, and M. Ostling, *IEEE Transactions on Electron Devices* **57**, 704 (2010).

⁷⁴¹V. V. Afanasev, M. Bassler, G. Pensl, and M. Schulz, *physica status solidi (a)* **162**, 321 (1997).

⁷⁴²D. Fitzgerald and A. Grove, *Surface Science* **9**, 347 (1968).

⁷⁴³E. Yablonovitch, D. L. Allara, C. C. Chang, T. Gmitter, and T. B. Bright, *Physical Review Letters* **57**, 249 (1986).

⁷⁴⁴K. Murata, T. Tawara, A. Yang, R. Takanashi, T. Miyazawa, and H. Tsuchida, *Journal of Applied Physics* **129**, 025702 (2021).

⁷⁴⁵J. Fossum, R. Mertens, D. Lee, and J. Nijs, *Solid-State Electronics* **26**, 569 (1983).

⁷⁴⁶J. Linnros, *Journal of Applied Physics* **84**, 275 (1998).

⁷⁴⁷K. Tanaka, K. Nagaya, and M. Kato, *Japanese Journal of Applied Physics* **62**, SC1017 (2023).

⁷⁴⁸P. T. Landsberg and G. S. Kousik, *Journal of Applied Physics* **56**, 1696 (1984).

⁷⁴⁹M. Takeshima, *Physical Review B* **23**, 6625 (1981).

⁷⁵⁰J. Dziewior and W. Schmid, *Applied Physics Letters* **31**, 346 (1977).

⁷⁵¹A. Hangleiter, *Physical Review B* **35**, 9149 (1987).

⁷⁵²G. Y. Chung, M. J. Loboda, M. Marinella, D. Schroder, P. B. Klein, T. Isaacs-Smith, and J. Williams, *Materials Science Forum* **600–603**, 485 (2008).

⁷⁵³M. Ruff, *Elektronische Bauelemente Aus Siliziumkarbid (SiC) : Physikalische Grundlagen Und Numerische Simulation*, Ph.D. thesis, Friedrich-Alexander-Universität, Erlangen-Nürnberg (1993).

⁷⁵⁴S. S. Suvanam, K. Gulbinas, M. Usman, M. K. Linnarson, D. M. Martin, J. Linnros, V. Grivickas, and A. Hallén, *Journal of Applied Physics* **117**, 105309 (2015).

⁷⁵⁵K. Tanaka and M. Kato, *AIP Advances* **13**, 085220 (2023).

⁷⁵⁶H. Tsuchida, I. Kamata, M. Ito, T. Miyazawa, H. Uehigashi, K. Fukada, H. Fujibayashi, M. Naitou, K. Hara, H. Osawa, T. Sugiura, and T. Kozawa, *Materials Science Forum* **858**, 119 (2016).

⁷⁵⁷A. Meli, A. Muoio, R. Reitano, A. Trotta, M. Parisi, L. Meda, and F. La Via, *Materials Science Forum* **1062**, 278 (2022).

⁷⁵⁸A. Meli, A. Muoio, R. Reitano, E. Sangregorio, L. Calcagno, A. Trotta, M. Parisi, L. Meda, and F. La Via, *Micromachines* **13**, 1042 (2022).

⁷⁵⁹C. Hettler, C. James, J. Dickens, and A. Neuber, in *2010 IEEE International Power Modulator and High Voltage Conference* (IEEE, Atlanta, GA, USA, 2010) pp. 34–37.

⁷⁶⁰C. Hettler, W. W. Sullivan Iii, and J. Dickens, *Materials Science Forum* **717–720**, 301 (2012).

⁷⁶¹T. Miyazawa, M. Ito, and H. Tsuchida, *Applied Physics Letters* **97**, 202106 (2010).

⁷⁶²T. Okuda, T. Kobayashi, T. Kimoto, and J. Suda, *Applied Physics Express* **9**, 051301 (2016).

⁷⁶³E. Saito, J. Suda, and T. Kimoto, *Applied Physics Express* **9**, 061303 (2016).

⁷⁶⁴T. Hirayama, K. Nagaya, A. Miyasaka, K. Kojima, T. Kato, H. Okumura, and M. Kato, *Review of Scientific Instruments* **91**, 123902 (2020).

⁷⁶⁵T. Kimoto, N. Miyamoto, and H. Matsunami, *Materials Science and Engineering: B* **61–62**, 349 (1999).

⁷⁶⁶A. Udal and E. Velmre, *Materials Science Forum* **338–342**, 781 (2000).

⁷⁶⁷S. A. Reshanov, W. Bartsch, B. Zippelius, and G. Pensl, *Materials Science Forum* **615–617**, 699 (2009).

⁷⁶⁸P. A. Ivanov, M. E. Levenshtein, J. W. Palmour, M. K. Das, and B. A. Hull, *Solid-State Electronics* **50**, 1368 (2006).

⁷⁶⁹M. E. Levenshtein, T. T. Mnatsakanov, P. A. Ivanov, R. Singh, J. W. Palmour, and S. N. Yurkov, *Solid-State Electronics* **48**, 807 (2004).

⁷⁷⁰G. Sozzi, S. Sapienza, G. Chiorboli, L. Vines, A. Hallén, and R. Nipoti, *IEEE Access* , 1 (2024).

⁷⁷¹M. Puzzanghera and R. Nipoti, *Materials Science Forum* **858**, 773 (2016).

⁷⁷²M. Domeij, E. Danielsson, W. Liu, U. Zimmermann, C.-M. Zetterling, and M. Ostling, in *ISPSD '03. 2003 IEEE 15th International Symposium on Power Semiconductor Devices and ICs, 2003. Proceedings.* (IEEE, Cambridge, UK, 2003) pp. 375–378.

⁷⁷³A. Koyama, M. Sometani, K. Takenaka, K. Nakayama, A. Miyasaka, K. Kojima, K. Eto, T. Kato, J. Senzaki, Y. Yonezawa, and H. Okumura, *Japanese Journal of Applied Physics* **59**, SGGD14 (2020).

⁷⁷⁴M. Kato, Y. Mori, and M. Ichimura, *Materials Science Forum* **778–780**, 293 (2014).

⁷⁷⁵M. Levenshtein, T. Mnatsakanov, P. Ivanov, J. Palmour, S. Rumyantsev, R. Singh, and S. Yurkov, *IEEE Transactions on Electron Devices* **48**, 1703 (2001).

⁷⁷⁶M. Kato, S. Katahira, Y. Ichikawa, S. Harada, and T. Kimoto, *Journal of Applied Physics* **124**, 095702 (2018).

⁷⁷⁷A. K. Tiwari, M. Antoniou, N. Lophitis, S. Perkin, T. Trajkovic, and F. Udrea, *IEEE Transactions on Electron Devices* **66**, 3066 (2019).

⁷⁷⁸S. Bellone, L. F. Albanese, and G.-D. Licciardo, *IEEE Transactions on Electron Devices* **56**, 2902 (2009).

⁷⁷⁹M. Usman, B. Buono, and A. Hallen, *IEEE Transactions on Electron Devices* **59**, 3371 (2012).

⁷⁸⁰K. Jarašiūnas, P. Ščajev, V. Gudelis, P. B. Klein, and M. Kato, *Materials Science Forum* **645–648**, 215 (2010).

⁷⁸¹A. M. Strel'chuk, B. Berenguier, E. B. Yakimov, and L. Ottaviani, *Materials Science Forum* **858**, 345 (2016).

⁷⁸²S.-H. Ryu, C. Capell, L. Cheng, C. Jonas, A. Gupta, M. Donofrio, J. Clayton, M. O'Loughlin, A. Burk, D. Grider, A. Agarwal, J. Palmour, A. Hefner, and S. Bhattacharya, in *2012 IEEE Energy Conversion Congress and Exposition (ECCE)* (IEEE, Raleigh, NC, USA, 2012) pp. 3603–3608.

⁷⁸³T. Kimoto, K. Yamada, H. Niwa, and J. Suda, *Energies* **9**, 908 (2016).

⁷⁸⁴K. Naydenov, N. Donato, and F. Udrea, *Engineering Research Express* **3**, 035008 (2021).

⁷⁸⁵A. Galeckas, J. Linnros, V. Grivickas, U. Lindefelt, and C. Hallin, *Materials Science Forum* **264–268**, 533 (1998).

⁷⁸⁶T. Grasser, B. Kaczer, W. Goes, Th. Aichinger, Ph. Hehenberger, and M. Nelhiebel, in *2009 IEEE International Reliability Physics Symposium* (IEEE, Montreal, QC, Canada, 2009) pp. 33–44.

⁷⁸⁷S. I. Maximenko, J. A. Freitas, R. L. Myers-Ward, K.-K. Lew, B. L. VanMil, C. R. Eddy, D. K. Gaskill, P. G. Muzykov, and T. S. Sudarshan, *Journal of Applied Physics* **108**, 013708 (2010).

⁷⁸⁸H. Pourbagheri Mahabadi, *Optical Studies of Surface Recombination Velocity in 4H-SiC Epitaxial Layer*, Master's thesis, KTH, School of Information and Communication Technology (ICT) / KTH, School of Information and Communication Technology (ICT) (2011).

⁷⁸⁹A. Xiang, *IEEE Transactions on Nanotechnology* **20**, 28 (2021).

⁷⁹⁰T. Kimoto, N. Miyamoto, and H. Matsunami, *IEEE Transactions on Electron Devices* **46**, 471 (1999).

⁷⁹¹N. Ramungul, V. Khemka, T. P. Chow, M. Ghezzo, and J. W. Kretchmer, *Materials Science Forum* **264–268**, 1065 (1998).

⁷⁹²B. Kakarla, A. Tsibizov, R. Stark, I. K. Badstuber, and U. Grossner, in *2020 32nd International Symposium on Power Semiconductor Devices and ICs (ISPSD)* (IEEE, Vienna, Austria,

2020) pp. 234–237.

⁷⁹³S. Asada, T. Miyazawa, and H. Tsuchida, *IEEE Transactions on Electron Devices* **68**, 3468 (2021).

⁷⁹⁴A. Galeckas, J. Linnros, and B. Breitholtz, *Applied Physics Letters* **74**, 3398 (1999).

⁷⁹⁵R. Nipoti, A. Parisini, G. Sozzi, M. Puzzanghera, A. Parisini, and A. Carnera, *ECS Journal of Solid State Science and Technology* **5**, P621 (2016).

⁷⁹⁶M. Miyata, Y. Higashiguchi, and Y. Hayafuji, *Journal of Applied Physics* **104**, 123702 (2008).

⁷⁹⁷J. Senzaki, K. Fukuda, Y. Ishida, Y. Tanaka, H. Tanoue, N. Kobayashi, T. Tanaka, and K. Arai, *MRS Proceedings* **622**, T6.7.1 (2000).

⁷⁹⁸T. Troffer, G. Pensl, A. Schöner, A. Henry, C. Hallin, Kordina, and E. Janzén, *Materials Science Forum* **264–268** (1998), 10.4028/www.scientific.net/MSF.264-268.557.

⁷⁹⁹M. Krieger, M. Rühl, T. Sledziewski, G. Ellrott, T. Palm, H. B. Weber, and M. Bockstedte, *Materials Science Forum* **858**, 301 (2016).

⁸⁰⁰E. M. Handy, M. V. Rao, O. W. Holland, K. A. Jones, M. A. Derenge, and N. Papanicolaou, *Journal of Applied Physics* **88**, 5630 (2000).

⁸⁰¹G. Xiao, J. Lee, J. Liou, and A. Ortiz-Conde, *Microelectronics Reliability* **39**, 1299 (1999).

⁸⁰²N. Donato and F. Udrea, *IEEE Transactions on Electron Devices* **65**, 4469 (2018).

⁸⁰³R. Nipoti, H. M. Ayedh, and B. G. Svensson, *Materials Science in Semiconductor Processing* **78**, 13 (2018).

⁸⁰⁴Q. Chen, W. He, C. Cheng, and Y. Xue, *Journal of Physics: Conference Series* **1649**, 012048 (2020).

⁸⁰⁵H. Matsuura, *Materials Science Forum* **389–393**, 679 (2002).

⁸⁰⁶G. L. Pearson and J. Bardeen, *Physical Review* **75**, 865 (1949).

⁸⁰⁷BI. Shklovskii and AL. Efros, **14**, 351 (1980).

⁸⁰⁸T. F. Lee and T. C. McGill, *Journal of Applied Physics* **46**, 373 (1975).

⁸⁰⁹R. Scaburri, A. Desalvo, and R. Nipoti, *Materials Science Forum* **679–680**, 397 (2011).

⁸¹⁰P. Achatz, J. Pernot, C. Marcenat, J. Kacmarcik, G. Ferro, and E. Bustarret, *Applied Physics Letters* **92**, 072103 (2008).

⁸¹¹J. Weiße, M. Hauck, T. Sledziewski, M. Tschiesche, M. Krieger, A. J. Bauer, H. Mitlehner, L. Frey, and T. Erlbacher, *Materials Science Forum* **924**, 184 (2018).

⁸¹²Y. Kajikawa, *Journal of Electronic Materials* **50**, 1247 (2021).

⁸¹³M. Rambach, A. J. Bauer, and H. Ryssel, *physica status solidi (b)* **245**, 1315 (2008).

⁸¹⁴Y. Negoro, T. Kimoto, H. Matsunami, F. Schmid, and G. Pensl, *Journal of Applied Physics* **96**, 4916 (2004).

⁸¹⁵P. P. Altermatt, A. Schenk, and G. Heiser, *Journal of Applied Physics* **100**, 113714 (2006).

⁸¹⁶P. P. Altermatt, A. Schenk, B. Schmithüsen, and G. Heiser, *Journal of Applied Physics* **100**, 113715 (2006).

⁸¹⁷P. T. Landsberg, *physica status solidi (b)* **41**, 457 (1970).

⁸¹⁸B. K. Ridley, *Journal of Physics C: Solid State Physics* **11**, 2323 (1978).

⁸¹⁹M. Lades, W. Kaindl, N. Kaminski, E. Niemann, and G. Wachutka, *IEEE Transactions on Electron Devices* **46**, 598 (1999).

⁸²⁰W. Kaindl, M. Lades, N. Kaminski, E. Niemann, and G. Wachutka, *Journal of Electronic Materials* **28**, 154 (1999).

⁸²¹M. Lax, *Physical Review* **119**, 1502 (1960).

⁸²²V. N. Abakumov, V. I. Perel, and I. N. Yassievich, *Nonradiative Recombination in Semiconductors*, Modern Problems in Condensed Matter Sciences No. v. 33 (North-Holland ; Sole distributors for the USA and Canada, Elsevier Science Pub. Co, Amsterdam ; New York : New York, NY, USA, 1991).

⁸²³S. Asada, T. Okuda, T. Kimoto, and J. Suda, *Applied Physics Express* **9**, 041301 (2016).

⁸²⁴S. Contreras, L. Konczewicz, P. Kwasnicki, R. Arvinte, H. Peyre, T. Chassagne, M. Zielinski, M. Kayambaki, S. Juillaguet, and K. Zekentes, *Materials Science Forum* **858**, 249 (2016).

⁸²⁵C. Hitchcock, R. Ghandi, P. Deeb, S. Kennerly, M. Torky, and T. P. Chow, *Materials Science Forum* **1062**, 422 (2022).

⁸²⁶R. Nipoti, R. Scaburri, A. Hallén, and A. Parisini, *Journal of Materials Research* **28**, 17 (2013).

⁸²⁷M. Obernhofer, M. Krieger, F. Schmid, H. B. Weber, G. Pensl, and A. Schöner, *Materials Science Forum* **556–557**, 343 (2007).

⁸²⁸M. Rambach, L. Frey, A. J. Bauer, and H. Ryssel, *Materials Science Forum* **527–529**, 827 (2006).

⁸²⁹S. Rao, T. P. Chow, and I. Bhat, *Materials Science Forum* **527–529**, 597 (2006).

⁸³⁰G. Rutsch, R. P. Devaty, W. J. Choyke, D. W. Langer, and L. B. Rowland, *Journal of Applied Physics* **84**, 2062 (1998).

⁸³¹N. S. Saks, A. K. Agarwal, S.-H. Ryu, and J. W. Palmour, *Journal of Applied Physics* **90**, 2796 (2001).

⁸³²N. S. Saks, A. V. Suvorov, and D. C. Capell, *Applied Physics Letters* **84**, 5195 (2004).

⁸³³F. Schmid, M. Laube, G. Pensl, G. Wagner, and M. Maier, *Journal of Applied Physics* **91**, 9182 (2002).

⁸³⁴A. Schöner, S. Karlsson, T. Schmitt, N. Nordell, M. Linnarsson, and K. Rottner, *Materials Science and Engineering: B* **61–62**, 389 (1999).

⁸³⁵G. Wagner, W. Leitenberger, K. Irmscher, F. Schmid, M. Laube, and G. Pensl, *Materials Science Forum* **389–393**, 207 (2002).

⁸³⁶R. Wang, I. B. Bhat, and T. P. Chow, *Journal of Applied Physics* **92**, 7587 (2002).

⁸³⁷S. Y. Ji, K. Kojima, Y. Ishida, H. Tsuchida, S. Yoshida, and H. Okumura, *Materials Science Forum* **740–742**, 181 (2013).

⁸³⁸H. Matsuura, K. Aso, S. Kagamihara, H. Iwata, T. Ishida, and K. Nishikawa, *Applied Physics Letters* **83**, 4981 (2003).

⁸³⁹S. Smith, A. Evwaraye, and W. Mitchel, *MRS Proceedings* **510**, 193 (1998).

⁸⁴⁰K. Kawahara, H. Watanabe, N. Miura, S. Nakata, and S. Yamakawa, *Materials Science Forum* **821–823**, 403 (2015).

⁸⁴¹S. Beljakowa, S. A. Reshanov, B. Zippelius, M. Krieger, G. Pensl, K. Danno, T. Kimoto, S. Onoda, T. Ohshima, F. Yan, R. P. Devaty, and W. J. Choyke, *Materials Science Forum* **645–648**, 427 (2010).

⁸⁴²C. Kisielowski, K. Maier, J. Schneider, and V. Oding, *Materials Science Forum* **83–87**, 1171 (1992).

⁸⁴³M. Kato, J. Di, Y. Ohkouchi, T. Mizuno, M. Ichimura, and K. Kojima, *Materials Today Communications* **31**, 103648 (2022).

⁸⁴⁴N. T. Son, A. Henry, J. Isoya, M. Katagiri, T. Umeda, A. Gali, and E. Janzén, *Physical Review B* **73**, 075201 (2006).

⁸⁴⁵M. Laube, F. Schmid, G. Pensl, G. Wagner, M. Linnarsson, and M. Maier, *Journal of Applied Physics* **92**, 549 (2002).

⁸⁴⁶F. Pezzimenti, L. F. Albanese, S. Bellone, and F. G. D. Corte, in *2009 IEEE Bipolar/BiCMOS Circuits and Technology Meeting* (IEEE, Capri, Italy, 2009) pp. 214–217.

⁸⁴⁷Z. Lv, J. Li, L. Dong, and J. Zang, in *2023 International Conference on Telecommunications, Electronics and Informatics (ICTEI)* (IEEE, Lisbon, Portugal, 2023) pp. 269–273.

⁸⁴⁸A. Gali, P. Deák, R. P. Devaty, and W. J. Choyke, *Physical Review B* **60**, 10620 (1999).

⁸⁴⁹P. Deák, B. Aradi, A. Gali, and U. Gerstmann, *physica status solidi (b)* **235**, 139 (2003).

⁸⁵⁰M. Bockstedte, A. Mattausch, and O. Pankratov, *Applied Physics Letters* **85**, 58 (2004).

85¹I. S. Gorban, A. P. Krokhmal', V. I. Levin, A. S. Skirda, Yu. M. Tairov, and V. F. Tsetkov, Sov. Phys. Semiconductors **21**, 119 (1987).

85²A. K. Tiwari, F. Udrea, N. Lophitis, and M. Antoniou, in *2019 31st International Symposium on Power Semiconductor Devices and ICs (ISPSD)* (IEEE, Shanghai, China, 2019) pp. 175–178.

85³J. Sullivan and J. Stanley, IEEE Transactions on Plasma Science **36**, 2528 (2008).

85⁴K. Bertilsson, C. Harris, and H.-E. Nilsson, Solid-State Electronics **48**, 2103 (2004).

85⁵G. Pensl, ed., *Silicon Carbide, III-nitrides and Related Materials: Proceedings of the 7th International Conference on Silicon Carbide, III-Nitrides and Related Materials, Stockholm, Sweden, September 1997*, Materials Science Forum No. 264/268 (1998).

85⁶B. K. Meyer, D. M. Hofmann, D. Volm, W. M. Chen, N. T. Son, and E. Janzén, Physical Review B **61**, 4844 (2000).

85⁷H. Lv, Y. Zhang, Y. Zhang, and L.-A. Yang, IEEE Transactions on Electron Devices **51**, 1065 (2004).

85⁸A. L. Efros, N. V. Lien, and B. I. Shklovskii, Journal of Physics C: Solid State Physics **12**, 1869 (1979).

85⁹H. Matsuura, A. Takeshita, T. Imamura, K. Takano, K. Okuda, A. Hidaka, S. Ji, K. Eto, K. Kojima, T. Kato, S. Yoshida, and H. Okumura, Applied Physics Express **11**, 101302 (2018).

86⁰H. Matsuura, A. Takeshita, A. Hidaka, S. Ji, K. Eto, T. Mitani, K. Kojima, T. Kato, S. Yoshida, and H. Okumura, Japanese Journal of Applied Physics **59**, 051004 (2020).

86¹D. Caughey and R. Thomas, Proceedings of the IEEE **55**, 2192 (1967).

86²N. Arora, J. Hauser, and D. Roulston, IEEE Transactions on Electron Devices **29**, 292 (1982).

86³K. Vasilevskiy, S. K. Roy, N. Wood, A. B. Horsfall, and N. G. Wright, Materials Science Forum **897**, 254 (2017).

86⁴W. J. Schaffer, G. H. Negley, K. G. Irvine, and J. W. Palmour, MRS Proceedings **339**, 595 (1994).

86⁵H. Linewih, S. Dimitrijev, and K. Y. Cheong, Microelectronics Reliability **43**, 405 (2003).

86⁶G. Masetti, M. Severi, and S. Solmi, IEEE Transactions on Electron Devices **30**, 764 (1983).

86⁷C. Lombardi, S. Manzini, A. Saporito, and M. Vanzi, IEEE Transactions on Computer-Aided Design of Integrated Circuits and Systems **7**, 1164 (1988).

86⁸H. Matsunami, Japanese Journal of Applied Physics **43**, 6835 (2004).

86⁹T. T. Mnatsakanov, M. E. Levenshtein, L. I. Pomortseva, and S. N. Yurkov, Semiconductor Science and Technology **17**, 974 (2002).

870 P. Brosselard, D. Planson, L. D. Cioccio, T. Billon, S. Scharnholz, M. Lazar, C. Raynaud, E. Spahn, and J.-P. Chante, in *Actes Electronique de Puissance Du Futur 2004* (Toulouse, France, 2004).

871 S. N. Mohammad, A. V. Bemis, R. L. Carter, and R. B. Renbeck, *Solid-State Electronics* **36**, 1677 (1993).

872 M. Sotoodeh, A. H. Khalid, and A. A. Rezazadeh, *Journal of Applied Physics* **87**, 2890 (2000).

873 H. Dixit, D. J. Lichtenwalner, A. Scholtze, J. H. Park, S. Rogers, S. Bubel, and S. H. Ryu, *Materials Science Forum* **1090**, 153 (2023).

874 W. C. Mitchel, W. D. Mitchell, G. Landis, H. E. Smith, W. Lee, and M. E. Zvanut, *Journal of Applied Physics* **101**, 013707 (2007).

875 D. Klaassen, *Solid-State Electronics* **35**, 953 (1992).

876 C. Canali, G. Majni, R. Minder, and G. Ottaviani, *IEEE Transactions on Electron Devices* **22**, 1045 (1975).

877 R. Quay, C. Moglestue, V. Palankovski, and S. Selberherr, *Materials Science in Semiconductor Processing* **3**, 149 (2000).

878 C. Jacoboni, C. Canali, G. Ottaviani, and A. Alberigi Quaranta, *Solid-State Electronics* **20**, 77 (1977).

879 B. Foutz, S. O'Leary, and M. Shur, in *High Power, Broadband, Linear, Solid State Amplifier* (Cornell University, 1998) p. 57.

880 V. Polyakov and F. Schwierz, *IEEE Transactions on Electron Devices* **48**, 512 (2001).

881 V. O. Turin, *Solid-State Electronics* **49**, 1678 (2005).

882 J. Dorkel and Ph. Leturcq, *Solid-State Electronics* **24**, 821 (1981).

883 D. Werber, M. Aigner, D. Denoth, F. Wittmann, and G. Wachutka, *Materials Science Forum* **600–603**, 493 (2008).

884 S. C. Choo, *IEEE Transactions on Electron Devices* **19**, 954 (1972).

885 S. Onoda, T. Ohshima, T. Hirao, K. Mishima, S. Hishiki, N. Iwamoto, and K. Kawano, *IEEE Transactions on Nuclear Science* **54**, 2706 (2007).

886 K. Bertilsson, H.-E. Nilsson, M. Hjelm, C. Petersson, P. Käckell, and C. Persson, *Solid-State Electronics* **45**, 645 (2001).

887 C.-Y. Cheng and D. Vasileska, *Journal of Applied Physics* **127**, 155702 (2020).

888 T. T. Mnatsakanov, L. I. Pomortseva, and S. N. Yurkov, *Semiconductors* **35**, 394 (2001).

88⁹ H.-E. Nilsson, E. Bellotti, M. Hjelm, and K. Brennan, *Mathematics and Computers in Simulation* **55**, 199 (2001).

89⁰ E. Belas, M. Betušiak, R. Grill, P. Praus, M. Brynza, J. Pipek, and P. Moravec, *Journal of Alloys and Compounds* **904**, 164078 (2022).

89¹ L. Ardaravičius, A. Matulionis, O. Kiprijanovic, J. Liberis, H.-Y. Cha, L. F. Eastman, and M. G. Spencer, *Applied Physics Letters* **86**, 022107 (2005).

89² H.-Y. Cha, Y. C. Choi, L. F. Eastman, M. G. Spencer, L. Ardaravicius, A. Matulionis, and O. Kiprijanovic, *Journal of Electronic Materials* **34**, 330 (2005).

89³ I. Khan and J. A. Cooper, *Materials Science Forum* **264–268**, 509 (1998).

89⁴ I. Khan and J. A. Cooper, *Materials Science Forum* **338–342**, 761 (2000).

89⁵ I. Khan and J. Cooper, *IEEE Transactions on Electron Devices* **47**, 269 (2000).

89⁶ V. Jaiswal and P. Vigneshwara Raja, *IEEE Transactions on Nuclear Science* , 1 (2024).

89⁷ D. L. Barrett and R. B. Campbell, *Journal of Applied Physics* **38**, 53 (1967).

89⁸ A. A. Burk, M. J. O'Loughlin, and S. Mani, *Materials Science Forum* **264–268**, 83 (1998).

89⁹ S. Contreras, M. Zielinski, L. Konczewicz, C. Blanc, S. Juillaguet, R. Müller, U. Künecke, P. J. Wellmann, and J. Camassel, *Materials Science Forum* **527–529**, 633 (2006).

90⁰ H. Fujihara, J. Suda, and T. Kimoto, *Japanese Journal of Applied Physics* **56**, 070306 (2017).

90¹ T. Kimoto, S. Nakazawa, K. Hashimoto, and H. Matsunami, *Applied Physics Letters* **79**, 2761 (2001).

90² G. Lomakina, G. F. Kholuyanov, R. Verenehikova, E. Mokhov, and Y. A. Vodakov, *Sov. Phys. Semiconductors* **6**, 988 (1972).

90³ R. Siergiej, R. Clarke, S. Sriram, A. Agarwal, R. Bojko, A. Morse, V. Balakrishna, M. MacMilian, A. Burk, Jr, and C. Brandt, *Materials Science and Engineering: B* **61–62**, 9 (1999).

90⁴ M. Noguchi, T. Iwamatsu, H. Amishiro, H. Watanabe, K. Kita, and S. Yamakawa, in *2017 IEEE International Electron Devices Meeting (IEDM)* (IEEE, San Francisco, CA, USA, 2017) pp. 9.3.1–9.3.4.

90⁵ H. Tanaka and N. Mori, in *2024 International VLSI Symposium on Technology, Systems and Applications (VLSI TSA)* (IEEE, HsinChu, Taiwan, 2024) pp. 1–2.

90⁶ C. Weitzel, J. Palmour, C. Carter, and K. Nordquist, *IEEE Electron Device Letters* **15**, 406 (1994).

90⁷ Q. Zhang, A. Q. Huang, J. Wang, C. Jonas, R. Callanan, J. J. Sumakeris, S.-H. Ryu, M. Das, A. Agarwal, and J. Palmour, *IEEE Transactions on Electron Devices* **55**, 1912 (2008).

908 P. Friedrichs, T. Kimoto, L. Ley, and G. Pensl, eds., *Silicon Carbide: Volume 2: Power Devices and Sensors*, 1st ed. (Wiley, 2009).

909 A. Poggi, F. Moscatelli, S. Solmi, A. Armigliato, L. Belsito, and R. Nipoti, *Journal of Applied Physics* **107**, 044506 (2010).

910 S. Murray and K. Roenker, *Solid-State Electronics* **46**, 1495 (2002).

911 D. K. Ferry, *Physical Review B* **12**, 2361 (1975).

912 J. Vuillod, in *Proceedings of International Conference on Microelectronics*, Vol. 1 (IEEE, Nis, Serbia, 1995) pp. 101–106.

913 J. Vobecky, P. Hazdra, S. Popelka, and R. K. Sharma, *IEEE Transactions on Electron Devices* **62**, 1964 (2015).

914 G. Rutsch, R. P. Devaty, W. J. Choyke, D. Langer, L. Rowland, E. Niemann, and F. Wischmeyer, *Materials Science Forum* **338–342**, 733 (2000).

915 G. Pacchioni, L. Skuja, and D. L. Griscom, eds., *Defects in SiO₂ and Related Dielectrics: Science and Technology* (Springer Netherlands, Dordrecht, 2000).

916 W.J. Choyke and L. Patrick, in *In: Silicon Carbide-1973; Proceedings of the Third International Conference* (1974) pp. 261–283.

917 J. H. Zhao, K. Sheng, and R. C. Lebron-Velilla, “SILICON CARBIDE SCHOTTKY BAR-RIER DIODE,” in *Sic Materials and Devices*, Vol. 40 (WORLD SCIENTIFIC, 2006) pp. 117–162.

918 N. S. Saks, S. S. Mani, and A. K. Agarwal, *Applied Physics Letters* **76**, 2250 (2000).

919 M. Ostling, R. Ghandi, and C.-M. Zetterling, in *2011 IEEE 23rd International Symposium on Power Semiconductor Devices and ICs* (IEEE, San Diego, CA, USA, 2011) pp. 10–15.

920 R. Raghunathan and B. Baliga, *IEEE Electron Device Letters* **19**, 71 (1998).

921 . larkin, “D. J. Larkin, P. G. Neudeck, J. A. Powell and L. G. Matus, Inst. Phys. Conf. Ser. 137, 51 (1994).” (1994).

922 C. Carter, Jr., V. Tsvetkov, R. Glass, D. Henshall, M. Brady, St.G. Müller, O. Kordina, K. Irvine, J. Edmond, H.-S. Kong, R. Singh, S. Allen, and J. Palmour, *Materials Science and Engineering: B* **61–62**, 1 (1999).

923 S. Nakashima and H. Harima, *SILICON CARBIDE AND RELATED MATERIALS 1995* **142**, 269 (1996).

924 T. R. McNutt, in *Extreme Environment Electronics* (CRC Press, Taylor & Francis Group, 2013) pp. 409–416.

925 J. Wang and B. W. Williams, *Semiconductor Science and Technology* **13**, 806 (1998).

926 Y.-R. Zhang, B. Zhang, Z.-J. Li, X.-C. Deng, and X.-L. Liu, *Chinese Physics B* **18**, 3995 (2009).

927 Y. Zhou, Y. Li, and B. Wang, in *2016 IEEE 4th Workshop on Wide Bandgap Power Devices and Applications (WiPDA)* (IEEE, Fayetteville, AR, 2016) pp. 1–7.

928 D. Guo, X. Tang, J. Guo, Y. Zhou, L. Sun, Y. Zhang, Y. Zhang, and Q. Song, *IEEE Transactions on Plasma Science* , 1 (2025).

929 M. Hjelm, K. Bertilsson, and H.-E. Nilsson, *Applied Surface Science* **184**, 194 (2001).

930 V. I. Sankin and A. A. Lepneva, *Materials Science Forum* **338–342**, 769 (2000).

931 K. Vassilevski, K. Zekentes, A. Zorenko, and L. Romanov, *IEEE Electron Device Letters* **21**, 485 (2000).

932 C. C. Sun, A. H. You, E. K. Wong, A. K. Yahya, and S. Alam, in *PROGRESS OF PHYSICS RESEARCH IN MALAYSIA: PERFIK2009* (Malacca (Malaysia), 2010) pp. 281–284.

933 H. Tanaka, T. Kimoto, and N. Mori, *Materials Science in Semiconductor Processing* **173**, 108126 (2024).

934 W. V. Muench and E. Pettenpaul, *Journal of Applied Physics* **48**, 4823 (1977).

935 S. Doğan, F. Yun, C. Roberts, J. Parish, D. Huang, R. E. Myers, M. Smith, S. E. Saddow, B. Ganguly, and H. Morkoç, *MRS Proceedings* **764**, C7.2 (2003).

936 J. A. Powell and L. G. Matus, in *Amorphous and Crystalline Silicon Carbide II*, Vol. 43, edited by H. K. V. Lotsch, M. M. Rahman, C. Y.-W. Yang, and G. L. Harris (Springer Berlin Heidelberg, Berlin, Heidelberg, 1989) pp. 14–19.

937 N. Fletcher, *Proceedings of the IRE* **45**, 862 (1957).

938 S. T. Pantelides, in *Festkörperprobleme 15*, Vol. 15, edited by H. J. Queisser (Springer Berlin Heidelberg, Berlin, Heidelberg, 1975) pp. 149–181.

939 K. Baik, Y. Irokawa, F. Ren, S. Pearton, S. Park, and Y. Park, *Solid-State Electronics* **47**, 1533 (2003).